Spatially coherent solutions of damped-driven nonlinear evolution equations and reaction-diffusion systems

NV Alexeeva

University of Cape Town

Thesis presented for the Degree of

DOCTOR OF PHILOSOPHY

Department of Mathematics and Applied Mathematics

University of Cape Town

June, 2001

University of Cape Town

Abstract

The thesis is devoted to the study of localized solutions of dispersive and dissipative nonlinear evolution equations. First, we consider the parametrically driven, damped nonlinear Schrödinger (NLS) equation. Soliton solutions of this NLS equation may become unstable due to a resonance of two internal oscillation modes. The objective of our study is to follow the nonlinear development of this oscillatory instability and describe supercritical dynamical regimes of the solitons. Our treatment is based on the reduced amplitude equation for the soliton's perturbation which we derive using an asymptotic multi-scale expansion technique. This fourth-order dynamical system is the normal form of the oscillatory instability bifurcation, in the same way as the complex Landau equation is the normal form of the Hopf bifurcation. The conclusion of our analysis is that no temporally-periodic solutions are possible in the undamped case. However, adding even a small damping gives rise to a stable periodic orbit of the four-dimensional dynamical system and thereby, to a stably oscillating soliton of the parametrically driven, damped NLS equation. In agreement with the predictions of the amplitude equation, direct numerical simulations of the full, nonreduced partial differential equation reveal no stably oscillating solitons in the undamped regime. Instead, all localized initial conditions evolve into a radiating soliton with slowly growing amplitude or a small-amplitude slowly decaying breather, or possibly into a couple of counter-propagating solitons of small amplitude.

Next, we utilize our results on stability of the damped-driven NLS solitons to propose a possible mechanism for the experimentally observed phenomenon of the suppression of chaos by means of impurities. We consider a parametrically driven chain of damped pendula, all identical except the central one, which can be longer or shorter than the rest of the chain. We show that the amplitude of the small-amplitude breather arising in the continuum limit, satisfies the parametrically driven damped NLS equation with an additional δ-function term. The possibility of spontaneous nucleation of solitons pinned on a long (attractive) impurity is predicted theoretically and corroborated by numerical simulations. It is demonstrated that the introduction of an attractive impurity enlarges the *stability* region of solitons. Although short impurities enhance *instability* of the pinned solitons, this instability will not generally set in as solitons are repelled by short impurities. We conclude that a random distribution of short and long defects will have a stabilizing net effect on the long chain. This will occur both due to the pinning of solitons on attrac-

University of Cape Town

tive impurities, and due to the effective partitioning of the chain into shorter subintervals (which do not support long-wavelength unstable modes) — by repulsive impurities.

As a prototype dissipative system, we consider a reaction-diffusion model of the $NO + CO \to \frac{1}{2}N_2 + CO_2$ catalytic chemical reaction on ring-shaped platinum surfaces. We study, numerically, the shape of the dispersion curves of single-pulse solutions, i.e. the dependencies of the pulse velocity on the spatial interval length. On the basis of this numerical analysis, regions of existence of pulses decaying to different homogeneous backgrounds are identified on the control parameter plane. The *normal* dispersion gives rise to the repulsion between pulses and, consequently, to the stability of equidistant pairs of pulses on finite rings. The *anomalous* dispersion leads to the attraction between pulses. In the latter case an equidistant pair is unstable against the merger of two pulses into one. Nonequidistant bound states of pulses can bifurcate off the maxima of the dispersion curve of a single pulse via the period-doubling mechanism. For some values of the control parameters the nonequidistant bound states of pulses are stable on small rings but loose their stability via the Hopf bifurcation on larger rings.

University of Cape Town

Acknowledgments

I would like to thank my supervisor, Prof. I.V. Barashenkov, for his guidance during my work on this thesis, and my co-supervisor Prof. B.M. Herbst for useful discussions. I am grateful to Dr. M. Bär, Dr. M. Or-Guil, Dr. D.E. Pelinovsky and Prof. G.P. Tsironis for sharing with me their insights and knowledge during our collaboration over three projects summarized in this thesis. I would also like to thank Prof. T.L. Boyadjiev, Mr. L. Brusch, Prof. N. Flytzanis, Prof. F. Mertens, Prof. I.V. Puzynin, Dr. V.S. Shchesnovich, and Dr. E.V. Zemlyanaya for their help and discussions. I am indebted to Prof. D.S. Butterworth and Prof. B.D. Hahn for providing me with financial support in the form of a temporary lectureship. Last but not least, I want to thank the whole Department of Maths and Applied Maths for its pleasant friendly atmosphere.

The financial assistance of the National Research Foundation towards this research is hereby acknowledged. Opinions expressed in this work, or conclusions arrived at, are those of the author and are not necessarily to be attributed to the National Research Foundation. I thank the University Research Council of UCT for awarding me the Research Associateship. I also thank the Max-Planck-Institut für Physik komplexer Systeme (Dresden, Germany), the University of Crete (Heraklion, Greece) and the Joint Institute for Nuclear Research (Dubna, Russia) for partial financial support during my visits to these institutions.

Finally, I wish to thank all the examiners of this thesis for their valuable remarks and suggestions.

University of Cape Town

University of Cape Town

Contents

University of Cape Town

University of Cape Town

University of Cape Town

University of Cape Town

Chapter 1

Introduction

University of Cape Town

The concept of a solitary wave was introduced in 1834 by Scott-Russell who observed a propagation of a localized hump of water without changing of its shape and speed over a considerable distance. The word "soliton" was coined by Zabusky and Kruskal [282] who carried out numerical simulations of solitary waves in plasma modelled by the Korteweg-de Vries equation and discovered that the solitary waves would emerge from collisions with the same amplitudes and velocities. Owing to this remarkable property, for many years soliton was defined as a solitary wave which asymptotically preserves its shape and velocity upon collision with other solitary waves. It turned out that this property is a manifestation of a hidden symmetry which allows to solve the underlying nonlinear equation using essentially linear techniques, namely the inverse scattering method. However, the notion of soliton has gradually broadened and nowadays soliton refers to any spatially localized solution to a nonlinear dispersive equation. Apart from the next section of the Introduction, we will be using the latter definition.

The simplest possible example of the soliton is given by a pulse-like travelling wave

$$u(x,t) = u_s(\xi), \quad \xi = x \pm ct \tag{1.1}$$

of the D'Alembert equation

$$u_{tt} - c^2 u_{xx} = 0. \tag{1.2}$$

In (1.1) $u_s(\xi)$ is any localised function of its argument: $u_s(\xi) \to 0$ as $|\xi| \to \infty$. An important characteristic of this (and any other) linear equation is its dispersion relation. This is the relation between the frequency ω and the wavenumber k of the harmonic wave solution $u(t,x) = \exp[i(kx - \omega t)]$. For equation (1.2), the dispersion formula is $\omega = \pm ck$. The quantities that are important for the analysis of the propagation of waves, are the phase velocity $v_p = \omega/k = \pm c$ and the group velocity $v_g = d\omega/dk = \pm c$.

The phase velocity describes the motion of surfaces of constant phase while the group velocity measures the velocity of propagation of wavepackets. Systems with the real-valued group velocity v_g depending on the wavenumber k are said to be *dispersive*. The D'Alembert equation provides an example of a *dispersionless* system. All wavepackets governed by equation (1.2) propagate with the same group velocity $\pm c$, and this is what makes the travelling-wave solution (1.1) possible. The introduction of dispersion without introducing nonlinearity destroys the solitary wave as different Fourier harmonics start propagating at different group velocities. On the other hand, introducing nonlinearity without dispersion also prevents the formation of solitary waves because the pulse energy is continually pumped into higher-frequency modes. (This usually leads to the formation of discontinuities and shock waves.) However, if both dispersion and nonlinearity are present, solitary waves can be sustained. Therefore, the solitary wave can be qualitatively understood as a product of the balance between the effect of nonlinearity and that of dispersion.

Another important class of wave equations are the *nonconservative* systems. The nonconservative systems are characterized by complex dispersion relations $\omega(k) = \omega_R + i\omega_I$. If $\omega_I > 0$, the amplitude of the linear waves will grow exponentially and therefore the system is unstable. When $\omega_I < 0$ the amplitude of the linear waves will decay exponentially. These systems are called *dissipative*. Similarly to the dispersion, dissipation can also give rise to solitary waves when combined with nonlinearity. In this case the balance is reached between the release of the energy "stored" by the nonlinearity and its diffusion by the propagating disturbance.

The three simplest, and at the same time most important, nonlinear equations that are solvable via the inverse scattering method, are the Korteweg-de Vries (KdV), sine-Gordon (SG), and nonlinear Schrödinger (NLS) equation. We will discuss some of their fundamental properties in the next section, 1.1. Next, in spite of the paramount importance of integrable equations one often has to consider their modifications obtained by adding extra terms which destroy the integrability. The nearly-integrable equations are reviewed in sec.1.2. Finally, in sec.1.3 of the Introduction, we consider the dissipative reaction-diffusion systems. Thus the Introduction contains a survey of results available in literature. The original results of our work are presented in Chapters 2, 3 and 4 of this thesis. In Chapter 2, we study the oscillatory instability of parametrically driven, damped NLS solitons and their supercritical dynamics. In Chapter 3, we introduce a point-like impurity in the system which allows to use it as a model of a the counter-intuitive phenomenon of taming chaos with disorder. The excitable reaction-diffusion

University of Cape Town

system discussed in Chapter 4, serves as a model of a chemical reaction in which the crucial role is played by localized waves of concentration of the reactants. Chapter 5 contains our concluding remarks and is followed by the bibliography.

1.1 Solitons in integrable systems

1.1.1 The Korteweg-de Vries equation

The equation

$$\hat{\mathrm{K}}u \equiv u_t + 6uu_x + u_{xxx} = 0 \tag{1.3}$$

was introduced by Korteweg and de Vries for the description of the lossless propagation of shallow water waves [143, 72, 178]. The equation takes into account nonlinear and dispersive effects but ignores the dissipation. The KdV turned out to be a useful approximation in variety of fields including ion-acoustic [74, 271, 254]-[256] and magnetohydrodynamic [118, 123, 192, 252] waves in plasma; the anharmonic lattices [283, 285, 286]; longitudinal dispersive waves in elastic rods [194]; pressure waves in liquid-gas bubble mixture [263]; rotating flow down a tube [155] and thermally excited phonon packets in low-temperature nonlinear crystals [253]. In general, it has been shown that a rather large class of nearly-hyperbolic, weakly dispersive, weakly nonlinear systems can be reduced to the KdV [248, 156].

We are not going to use the KdV equation in any of the further chapters of this thesis. However, it is useful to consider some of its fundamental properties for the reason of completeness. Apart from producing the exact soliton solution, we will review the construction of an infinite series of conservation laws and obtaining of exact two-soliton solutions using the Hirota method. For the sake of completeness we touch upon the generalized KdV and write an important modification of the KdV in two dimensions.

The KdV equation (1.3) can be derived from the Lagrangian density [275]

$$\mathcal{L} = \frac{1}{2}\theta_t\,\theta_x - \theta_x^3 + \theta_x\,\psi_x + \frac{1}{2}\psi^2,$$

where $\theta_x = u$ and $\psi = \theta_{xx}$. Korteweg and de Vries showed that eq.(1.3) has a solitary wave solution of the form [143]:

$$u(x,\,t) = \frac{1}{2}a^2\,\mathrm{sech}^2\left[\frac{1}{2}a\,(x - x_0 - a^2\,t)\right], \tag{1.4}$$

where a and x_0 are arbitrary constants. This formula illustrates some basic properties of the KdV. First, the amplitude of a KdV soliton in not independent of its velocity; instead,

University of Cape Town

larger solitons move faster. Second, KdV solitons are unidirectional, i.e. they propagate only to the right.

Conservation laws

In 1965 Zabusky and Kruskal published seminal numerical results describing the formation of solitons and their elastic scattering [282, 283]. They have derived the KdV equation as a continuous limit of the Fermi-Pasta-Ulam model. (The Fermi-Pasta-Ulam model consists of a lattice of linear oscillators with quadratic coupling to the nearest neighbours:

$$\ddot{Q}_n = f(Q_{n+1} - Q_n) - f(Q_n - Q_{n-1}), \quad f = \gamma Q + \alpha Q^2.$$

Here α and γ are constants.) Zabusky and Kruskal suggested that the reason for the elasticity of collision could be the fact that the KdV has an infinite number of conservation laws. The first four of them were found by Miura [189]. A conservation law is an equation of the form

$$T_t + X_x = 0,$$

where T is the conserved density and X the associated flux. Here T and X are polynomial in u and its spatial derivatives. The KdV equation itself can be written as such a conservation law:

$$u_t + [3u^2 + u_{xx}]_x = 0.$$

The next two conserved densities and their associated fluxes are given by

$$T_2 = u^2, \qquad X_2 = 4u^3 + 2uu_{xx} - u_x^2;$$

$$T_3 = u^3 - \frac{1}{2}u_x^2, \qquad X_3 = 18\frac{u^4}{4} + u^2u_{xx} - u_xu_{xxx} - 2uu_x^2 + \frac{u_{xx}^2}{2}.$$

If in the Fermi-Pasta-Ulam model the quadratic interaction is replaced by a cubic one, $f(Q) = \gamma Q + \alpha Q^3$, the long waves propagating from left to right satisfy the *modified* KdV equation:

$$\hat{\mathrm{M}}v \equiv v_t - 6v^2v_x + v_{xxx} = 0. \tag{1.5}$$

The modified KdV equation also has an infinite number of polynomial conservation laws, while other equations of the form

$$u_t - 6u^pu_x + u_{xxx} = 0, \quad p = 3,\ 4,\ 5\ldots,$$

University of Cape Town

have only three polynomial conservation laws each. Studying conservation laws of the KdV and modified KdV, Miura found a transformation between their solutions [187]. Namely, if v is a solution to the modified KdV equation, then

$$u = -(v^2 + v_x) \tag{1.6}$$

solves the KdV equation. This can be written as

$$\hat{\mathrm{K}}u = -\left(2v + \frac{\partial}{\partial x}\right)\hat{\mathrm{M}}v.$$

Making use of this transformation, it can be demonstrated [188] that the KdV equation has *infinitely many* conservation laws. Indeed, if w satisfies the Gardner equation

$$\hat{\mathrm{R}}w \equiv w_t - 6(w + \varepsilon^2 w^2)w_x + w_{xxx} = 0,$$

then

$$u = -(w + \varepsilon w_x + \varepsilon^2 w^2) \tag{1.7}$$

satisfies the KdV, i.e.

$$\hat{\mathrm{K}}u = -\left(1 + \varepsilon\frac{\partial}{\partial x} + 2\varepsilon^2 w\right)\hat{\mathrm{R}}w = 0. \tag{1.8}$$

Since u does not depend on ε but only on x and t while w depends on ε, x and t, it is possible to expand the solution w of (1.7) in a formal power series in ε and express it via u and its derivatives:

$$w(x, t; \varepsilon) = w_0 + \varepsilon w_1 + \varepsilon^2 w_2 + \ldots = -u + \varepsilon u_x - \varepsilon^2(u_{xx} + u^2) + \ldots \tag{1.9}$$

If we substitute the expansion (1.9) into the transformation (1.8) and equate to zero coefficients of equal powers of ε, we will obtain an infinite number of conservation laws for the KdV equation. The conservation laws arise in front of even powers of the parameter ε while coefficients in front of odd powers vanish.

Multi-soliton solutions

We now turn to solitons. It is possible to obtain two-soliton solutions to the KdV equation using the Cole-Hopf transformation. This technique was generalized by Hirota [98] to the N-soliton case.

The transformation $u = w_x$ transforms the KdV to the "potential" form:

$$w_t + 3w_x^2 + w_{xxx} = 0.$$

University of Cape Town

If we then apply the Cole-Hopf transformation $w = 2(\ln f)_x$, we obtain an equation which is bilinear in f and its derivatives:

$$f\, f_{xxxx} - 4 f_x\, f_{xxx} + 3 f_{xx}^2 + f\, f_{xt} - f_x\, f_t = 0.$$

One can check that $f = 1 + exp(\theta_i)$ with $\theta_i = a_i x - a_i^3 t$, gives the soliton solution. Guided by this observation, Hirota proposed to seek for solutions f of the form

$$f = 1 + \sum_{n=1}^{N} \varepsilon^n f^{(n)},$$

where ε is a formal expansion parameter. Equating to zero coefficients of like powers of ε, we obtain

$$\begin{aligned}
\varepsilon: \quad & f^{(1)}_{xxxx} + f^{(1)}_{xt} = 0, \\
\varepsilon^2: \quad & f^{(2)}_{xxxx} + f^{(2)}_{xt} = -\Big[f^{(1)} f^{(1)}_{xxxx} - 4 f^{(1)}_x f^{(1)}_{xxx} + \\
& \qquad + 3\left(f^{(1)}_{xx}\right)^2 + f^{(1)} f^{(1)}_{xt} - f^{(1)}_x f^{(1)}_t\Big], \\
\varepsilon^3: \quad & f^{(3)}_{xxxx} + f^{(3)}_{xt} = -\Big[f^{(1)} f^{(2)}_{xxxx} - 4 f^{(1)}_x f^{(2)}_{xxx} + 6 f^{(1)}_{xx} f^{(2)}_{xx} + f^{(1)} f^{(2)}_{xt} - \\
& \qquad - f^{(1)}_x f^{(2)}_t + f^{(2)} f^{(1)}_{xxxx} - 4 f^{(2)}_x f^{(1)}_{xxx} + f^{(2)} f^{(1)}_{xt} - f^{(2)}_x f^{(1)}_t\Big],
\end{aligned}$$

and so on. The ε-equation is linear and we can choose its solution in the form

$$f^{(1)} = \mathrm{e}^{a_1 x - a_1^3 t} + \mathrm{e}^{a_2 x - a_2^3 t} \equiv \mathrm{e}^{\theta_1} + \mathrm{e}^{\theta_2}. \tag{1.10}$$

Substituting (1.10) in the right-hand-side of the equation for $f^{(2)}$, we obtain

$$f^{(2)}_{xxxx} + f^{(2)}_{xt} = 3 a_1\, a_2\, (a_1 - a_2)^2\, \mathrm{e}^{\theta_1 + \theta_2}.$$

The solution to this equation is

$$f^{(2)} = \left(\frac{a_1 - a_2}{a_1 + a_2}\right)^2 \mathrm{e}^{\theta_1 + \theta_2}.$$

One could have expected the iteration process to continue indefinitely, but in the actual fact, if we substitute $f^{(1)}$ and $f^{(2)}$ in the right-hand-side of the equation for $f^{(3)}$, we get a linear equation again:

$$f^{(3)}_{xxxx} + f^{(3)}_{xt} = 0.$$

It can be shown that if we choose $f^{(3)} \equiv 0$, then all higher order terms will be also equal to zero. Thus we have found an exact solution:

$$u = 2\frac{\partial^2}{\partial x^2} \ln f, \quad f = 1 + \mathrm{e}^{\theta_1} + \mathrm{e}^{\theta_2} + \left(\frac{a_1 - a_2}{a_1 + a_2}\right)^2 \mathrm{e}^{\theta_1 + \theta_2}. \tag{1.11}$$

It is not difficult to verify that it indeed describes an interaction of two solitons.

University of Cape Town

Generalizations

A generalized KdV equation is

$$u_t + \alpha u^p u_x + (\partial/\partial x)^{2r+1} u = 0,$$

where α is a real constant and p and r are nonnegative integers.

If $r = 2a$, where a is a nonnegative integer, the lagrangian density can be written as:

$$\mathcal{L} = \frac{1}{2}\theta_t\theta_x + \frac{\alpha}{(p+1)(p+2)}\theta_x^p + 2 + \theta_x(\psi_{2a})_x + \psi_{2a}\psi_1 +$$

$$+(\psi_{2a-1})_x(\psi_1)_x + \psi_{2a-1}\psi_2 + \ldots + \psi_{a+1}\psi_a + \frac{1}{2}[(\psi_a)_x]^2,$$

where again $\theta_x = u$ and $\psi_i = \partial^{2i}u/\partial x^{2i}$ for $i = 1, 2$.

If $r = 2b - 1$, where b is a positive integer, the Lagrangian density is given by:

$$\mathcal{L} = \frac{1}{2}\theta_t\theta_x + \frac{\alpha}{(p+1)(p+2)}\theta_x^p + 2 + \theta_x(\psi_{2b-1})_x +$$

$$+\psi_{2b-1}\psi_1 + (\psi_{2b-2})_x(\psi_1)_x + \ldots + (\psi_b)_x(\psi_{b-1})_x + \frac{1}{2}\psi_b^2.$$

The two-dimensional generalization of the KdV is known as the Kadomtsev-Petviashvili (KP) equation :

$$(U_t + 6UU_x + U_{xxx})_x = -\sigma U_{yy}, \quad \sigma = \pm 1. \tag{1.12}$$

The KP equation describes the propagation of weakly nonlinear, weakly dispersive, quasi one-dimensional waves. The equation (1.12) is written in the reference frame moving in the x-direction. The variation of the wave form in the y-direction is assumed to be weak.

University of Cape Town

1.1.2 The sine-Gordon equation

The sine-Gordon equation is

$$\phi_{xx} - \phi_{tt} = \sin\phi. \tag{1.13}$$

This equation can be derived from the Lagrangian density

$$\mathcal{L} = \frac{1}{2}\phi_x^2 - \frac{1}{2}\phi_t^2 - \cos\phi.$$

Using the Lagrangian one can easily construct the conserved energy:

$$H = \int_{-\infty}^{\infty} \left\{ \frac{1}{2}(\phi_x^2 + \phi_t^2) + (1 - \cos\phi) \right\} dx. \tag{1.14}$$

One of the most important applications is in the theory of long Josephson junctions [107, 146, 154, 232, 233, 235, 22, 161]. In this case $\phi(t,x)$ stands for the magnetic flux measured in units of the flux quantum $\Phi_0/2\pi = h/4\pi e$. Magnetic flux can penetrate along the insulating barrier of the junction and this flux can propagate in the longitudinal x-direction. There are two possible orientations for the flux. A quantum of flux in one direction is called a "fluxon" and in the other direction an "antifluxon". Mathematically, the fluxon and the antifluxon are described by the kink and antikink solutions of eq.(1.13) (see equation (1.16) below). Kinks play an important role in the dynamical theory of the long junctions [77]. The theory of magnetism is another important area of application. In particular, the dynamics of domain walls in quasi-one-dimensional ferromagnets with easy-plane anisotropy can be described using SG kinks [63, 183, 135, 27]. The dynamics of weak antiferromagnets is also described by the SG [292, 26, 25]. In magnetic applications $\phi(t,x)$ is interpreted as the angle of the local orientation of the magnetization vector lying in the easy-plane. Another application of the SG is in the theory of charge-density-waves systems [226, 76, 71, 90]. The SG equation is used in studies of liquid crystals [159, 160, 110, 168, 169, 44]; self-induced transparency of a two-level medium in nonlinear optics [167, 150], and hydrodynamics [82, 191, 51]. The SG equation was used to describe propagation of crystal dislocations [73]; propagation of a "splay wave" along a lipid membrane [68]. It also arises in theory of elementary particles [229, 242, 243]. In chapter 3 we will use the fact that the SG equation is the continuous limit of the Frenkel-Kontorova model (the chain of diffusively coupled pendula). The first mechanical model of this kind was constructed by Scott [234].

We also note that by the change of variables $\xi = x$, , $\eta = (x+t)/2$, the SG equation can be cast into the form

$$\phi_{\xi\xi} + \phi_{\xi\eta} = \sin\phi,$$

which was used in studies of equations of self-induced transparency [11, 12, 13, 60, 100, 150, 151]. After the transformation to the light-cone variables, $\xi = (x+t)/2$, $\eta = (x-t)/2$, the SG equation acquires the form

$$\phi_{\xi\eta} = \sin\phi. \tag{1.15}$$

The SG equation in this form was studied in connection with the theory of pseudospherical surfaces.

In this subsection we will review soliton solutions of the sine-Gordon equation and Bäcklund transformations which allow to construct exact N-soliton solutions.

University of Cape Town

Kinks and breathers

The simplest type of solitary wave solutions of the SG equation have the form:

$$\phi_k = 4 \arctan \left[\exp \left(\pm \frac{x - vt}{\sqrt{1 - v^2}} \right) \right]. \tag{1.16}$$

The solution corresponding to "+" is usually referred to as the *kink*, while the solution corresponding to "–" is called *antikink*. The kink can be considered as a positive rotation by 2π in ϕ, as x goes from $-\infty$ to $+\infty$, and the antikink as a negative rotation. Since the total rotation must be conserved, the difference between number of kinks and the number of antikinks must be conserved in any collision. Therefore kinks and antikinks are created and destroyed in pairs. This property and the Lorentz invariance of the SG equation makes kink solutions alike to elementary particles. In [221] the analytic expressions for "kink-kink" and "kink-antikink" collisions are found. The "kink-kink" collision is described by

$$\phi_{kk} = 4 \arctan \left[\frac{v \sinh \left(x/\sqrt{1 - v^2} \right)}{\cosh \left(vt/\sqrt{1 - v^2} \right)} \right] \tag{1.17}$$

and the "kink-antikink" collision is given by

$$\phi_{ka} = 4 \arctan \left[\frac{\sinh \left(vt/\sqrt{1 - v^2} \right)}{v \cosh \left(x/\sqrt{1 - v^2} \right)} \right]. \tag{1.18}$$

It is interesting and important to notice that according to the latter formula, a kink and antikink can pass though each other without mutual destruction even through such destruction would not violate the conservation of total rotation.

One of the most important properties of the kink is that its energy is finite. If we integrate the Hamiltonian density (1.14), it turns out that the energy $E_k = 8/\sqrt{1 - v^2}$, i.e. the energy exhibits relativistic dependence on the kink's velocity. This result shows that in order to create even a static kink, the energy of the system should be at least 8 (units). From this point of view more appealing is another solution of the SG equation, known as the "breather". This solution is given by

$$\phi_b = 4 \arctan \left\{ \frac{\sqrt{1 - \omega^2}}{\omega} \sin (\omega t) \operatorname{sech} \left(\sqrt{1 - \omega^2} x \right) \right\}. \tag{1.19}$$

The energy of the breather is

$$E_b = 16\sqrt{1 - \omega^2}.$$

University of Cape Town

As $\omega \to 1$, it decreases from 16, the energy of two static kinks, to zero. Therefore, even a small amount of energy is sufficient to produce a breather. The breather (1.19) can be obtained from the "kink-antikink" solution by substituting, formally,

$$v = \frac{i\omega}{\sqrt{1-\omega^2}}.$$

Bäcklund transformation

Similarly to the KdV, it is possible to obtain an explicit two-soliton solution to the SG equation. Here it is convenient to work with the light-cone formulation of the equation (1.15). Let us consider the Klein-Gordon equation with a general nonlinearity:

$$\phi_{\xi\eta} = F(\phi). \tag{1.20}$$

Let ϕ and ψ be two independent solutions of (1.20), and write

$$u = \frac{\phi+\psi}{2}, \quad v = \frac{\phi-\psi}{2}.$$

Assume that it is possible to determine a relation between u and v as a system of two first-order equations:

$$u_\xi = f(v), \quad v_\eta = g(u). \tag{1.21}$$

We will specify the form of F, g and f so as to separate the partial derivatives with respect to ξ and η into two different equations. Differentiating the first equation in (1.21) with respect to η and the second one with respect to ξ, we obtain

$$u_{\xi\eta} = g(u)\, f_v(v), \tag{1.22}$$

$$v_{\xi\eta} = g_u(u)\, f(v). \tag{1.23}$$

Although eqs.(1.22)-(1.23) have similar form to eq.(1.20), u or v independently are not solutions to the Klein-Gordon equation because (1.22)-(1.23) contain derivatives with respect to v and u, respectively. However, if we add and subtract them, we obtain

$$(u+v)_{\xi\eta} = g(u)\, f_v(v) + g_u(u)\, f(v), \tag{1.24}$$

$$(u-v)_{\xi\eta} = g(u)\, f_v(v) - g_u(u)\, f(v). \tag{1.25}$$

Since ϕ and ψ are solutions to the Klein-Gordon equation, we can write that

$$F(u+v) = g(u)\, f_v(v) + g_u(u)\, f(v), \tag{1.26}$$

$$F(u-v) = g(u)\, f_v(v) - g_u(u)\, f(v). \tag{1.27}$$

University of Cape Town

Differentiating the first equation with respect to u and the second one with respect to v, and then combining them, we obtain

$$\frac{g''(u)}{g(u)} = \frac{f''(v)}{f(v)} = -\lambda. \tag{1.28}$$

Since the first fraction is a function only of u and the second one is a function only of v, λ must be a constant. Therefore we have

$$g'' + \lambda g = 0, \quad f'' + \lambda f = 0.$$

Choosing $\lambda = 1$, gives

$$g(u) = \beta \sin u, \quad f(v) = \alpha \sin v.$$

If we substitute these f and g back into (1.26) and (1.27), we obtain

$$F(\phi) = \sin \phi, \quad \beta = \frac{1}{\alpha},$$

and the equations for ϕ and ψ now read

$$\frac{1}{2}(\phi + \psi)_\xi = \alpha \sin\left(\frac{\phi - \psi}{2}\right), \tag{1.29}$$

$$\frac{1}{2}(\phi - \psi)_\eta = \frac{1}{\alpha} \sin\left(\frac{\phi + \psi}{2}\right). \tag{1.30}$$

In this way we have obtained two equations linking two particular solutions of the sine-Gordon equation. These equations are called the Bäcklund transformations. If we had chosen $\lambda = -1$, we would have obtained the sinh-Gordon equation. Therefore the only Klein-Gordon equations that have Bäcklund transformations of this type are the sine- and sinh-Gordon equations.

If ϕ is a solution to the SG equation, we can obtain from the Bäcklund transformations (1.29)-(1.30) a two-parameter family of solutions. The simplest possibility is to start with $\phi = 0$. Then we obtain for ψ

$$\psi = 4 \arctan\left[\exp\left(a\xi + \frac{\eta}{a} + \xi_0\right)\right], \quad a = -\alpha.$$

This is the kink solution in the light-cone variables. There is a simple geometric way of constructing new solutions starting form the kink solution. It uses the fact that two Bäcklund transformations are commutative as illustrated by the diagram in fig.1.1. Starting from the $\phi_0 = 0$, we construct two kink solutions, ϕ_1 and ϕ_2, for different values of the parameter α. Then we construct the third solution ϕ_3 using the above diagram. Consider pairs

University of Cape Town

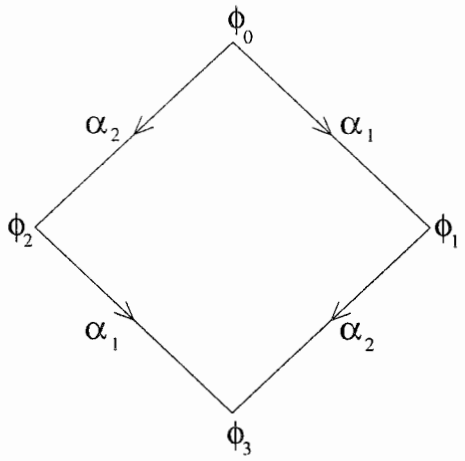

Figure 1.1: The commutativity diagram.

of solutions (ϕ_0, ϕ_1), (ϕ_1, ϕ_3), (ϕ_2, ϕ_3), (ϕ_0, ϕ_2). If we add the first and the third pair and subtract the second and the fourth ones, we obtain

$$\alpha_1 \sin\left(\frac{\phi_0 - \phi_1 + \phi_2 - \phi_3}{4}\right) = \alpha_2 \sin\left(\frac{\phi_1 - \phi_3 + \phi_0 - \phi_2}{4}\right).$$

This can be rewritten as

$$\tan\frac{\phi_0 - \phi_3}{4} = \frac{a_1 + a_2}{a_2 - a_1} \tan\frac{\phi_2 - \phi_1}{4}.$$

If we take $\phi_0 = 0$, then

$$\phi_3 = 4 \arctan\left[\left(\frac{a_1 + a_2}{a_1 - a_2}\right) \frac{e^{\theta_1} - e^{\theta_2}}{1 + e^{\theta_1 + \theta_2}}\right], \tag{1.31}$$

where $\theta_i = a_i\xi + \eta/a_i + \xi_{0,i}$. The equation (1.31) is the two-kink solution. It can also be found using the Cole-Hopf transformation.

1.1.3 The nonlinear Schrödinger equation

The cubic nonlinear Schrödinger equation has the form

$$i\psi_t + \psi_{xx} + 2|\psi|^2\psi = 0. \tag{1.32}$$

This equation was used to describe the stationary two-dimensional self-focusing [32, 122, 250]; one-dimensional self-modulation of a monochromatic wave [252, 16, 112, 95, 96]; self-trapping phenomena in nonlinear optics [112] and propagation of light pulses in monomode optical fibers [93]; propagation of heat pulses in solids [253] and Langmuir waves in plasma

University of Cape Town

[74, 102, 240]. It also describes boson gas with two-body δ-function attraction and is related to the Ginzburg-Landau equations of superconductivity [54]. It is worth mentioning here that the NLS equation serves as an amplitude equation for small-amplitude breathers of the sine-Gordon equation and therefore they share some applications. In this subsection we will derive the travelling soliton of the NLS equation. For completeness we will review the breather solution and the N-soliton solutions.

The NLS equation can be derived from the Lagrangian density

$$\mathcal{L} = \frac{i}{2}(\psi\psi_t^* - \psi_t\psi^*) + |\psi|^2 - |\psi|^4. \tag{1.33}$$

Here ψ^* denotes the complex conjugate of ψ. Like the SG and KdV, the NLS equation also has an infinite series of polynomial conservation laws. Physically most important are first three of them. The quantity

$$N = \int_{-\infty}^{+\infty} |\psi|^2 dx \tag{1.34}$$

is interpreted as the number of particles in the studies of boson gas and the total power in the nonlinear optical context. The integral

$$P = \frac{i}{2}\int_{-\infty}^{+\infty} \left(\psi_x\,\bar{\psi} - \bar{\psi}_x\psi\right) dx \tag{1.35}$$

is interpreted as the total momentum of the boson system, and

$$E = \int_{-\infty}^{+\infty} (|\psi_x|^2 - |\psi|^4) dx \tag{1.36}$$

is its total energy.

University of Cape Town

Solitons

To obtain solitary wave solutions, we decompose the field ψ into its modulus and phase:

$$\psi = \phi(x,t)\,\mathrm{e}^{i\,\theta(x,t)},$$

where ϕ and θ are real functions. Substituting into eq.(1.32) and dividing through by $\exp(i\theta)$, yields equations for the real and imaginary parts:

$$-\phi\,\theta_t + \phi_{xx} - \phi\,\theta_x^2 + 2\phi^3 = 0, \tag{1.37}$$

$$\phi_t + \phi\,\theta_{xx} + 2\phi_x\,\theta_x = 0. \tag{1.38}$$

We look for solutions of the form $\theta = \theta(x - u_c t)$ and $\phi = \phi(x - u_e t)$. Under this assumption the system of partial differential equations (1.37)-(1.38) reduces to a system of two ordinary differential equations:

$$\phi_{xx} + u_c \phi \theta_x - \phi \theta_x^2 + 2\phi^3 = 0 \tag{1.39}$$

$$\phi \theta_{xx} + 2\phi_x \theta_x - u_e \phi_x = 0. \tag{1.40}$$

One can readily reduce the order of the second equation in this system by multiplying it by ϕ and integrating. This gives $\phi^2(2\theta_x - u_e) = const$. After substituting the expression for θ_x into the first equation and reducing its order by a similar procedure (this time the integrating factor is ϕ_x), we reduce the problem to the evaluation of an elliptic integral

$$\int_{\phi(0,0)}^{\phi(x,t)} \frac{d\phi}{\sqrt{-\phi^4 + (u_e^2/4 - u_e u_c/2)\,\phi^2 + C}}.$$

In case when $C = 0$ and the coefficient in front of the quadratic term under the square root is positive ($u_e > 2u_c$), the integration can be carried out explicitly which results in the expression for the moving soliton:

$$\psi = \phi_0 \,\mathrm{sech}[\phi_0(x - u_e t)]\, \mathrm{e}^{\frac{i}{2}[u_e\,(x - u_c t)]}, \quad \phi_0 = \sqrt{\frac{u_e^2}{4} - \frac{u_e\, u_c}{2}}. \tag{1.41}$$

Defining

$$A = \phi_0, \quad \xi = -u_e/4, \tag{1.42}$$

eq.(1.41) is cast into what is regarded as the standard form of the soliton:

$$\psi = A \,\mathrm{sech}[A(x + 4\xi t)]\, \mathrm{e}^{-i[2\xi x + (4\xi^2 - A^2)t]}. \tag{1.43}$$

Although the quiescent NLS soliton is a time-periodic solution, it is not customary to call it "breather". The reason for this is that the modulus squared of ψ and hence, the amplitude of the soliton, does not change in time.

The name "breather" is reserved, in the context of the nonlinear Schrödinger equation, to another solution which consists of a bound state of two solitons with zero velocities and close amplitudes η_1 and η_2:

$$0 < \eta_1 - \eta_2 \ll 1. \tag{1.44}$$

The NLS breather is given by the formula

$$\begin{aligned} \psi = \; & - \; 2\eta\zeta\sqrt{|\gamma_1\gamma_2|}\,\frac{\gamma_1^* + \gamma_2^*}{|\gamma_1 + \gamma_2|^2 + 2\zeta^2|\gamma_1\gamma_2|\cosh 2\eta x} \times \\ & \times \; \left\{ \left[1 + \frac{\gamma_1^*\gamma_2^*(\gamma_1 + \gamma_2)}{|\gamma_1\gamma_2|(\gamma_1^* + \gamma_2^*)} \right] \cosh \eta x + \left[1 - \frac{\gamma_1^*\gamma_2^*(\gamma_1 + \gamma_2)}{|\gamma_1\gamma_2|(\gamma_1^* + \gamma_2^*)} \right] \sinh \eta x \right\}, \end{aligned}$$

University of Cape Town

where

$$\zeta = \frac{\eta_1 - \eta_2}{\eta_1 + \eta_2}, \quad \eta = \frac{\eta_1 + \eta_2}{2}, \quad \gamma_j(t) = \gamma_j(0)\,\mathrm{e}^{-i\eta_j^2 t}, \quad j = 1,\, 2. \tag{1.45}$$

The positions of the two solitons are given by the quantities $\ln|\gamma_j(0)|/\eta_j$ and the period of the internal oscillations of the breather is $\pi/(2\eta^2\zeta)$. Since the binding energy of the two solitons constituting the breather is equal to zero, this solution is not physically interesting.

Zakharov and Shabat constructed explicit N-soliton solutions [288] using their inverse scattering formalism. The N-soliton solution is given by

$$|\psi(x,t)|^2 = 2(\ln\det|B\,B^* + 1|)_{xx}, \tag{1.46}$$

where B is an $N \times N$ matrix with elements

$$B_{jk} = \frac{\sqrt{c_j c_k^*}}{\kappa_j - \kappa_k^*}\,\mathrm{e}^{i(\kappa_j 0 - \kappa_k^*)x}, \quad \text{with} \quad \kappa_i \quad \text{const}, \tag{1.47}$$

$$c_j(t) = \mathrm{e}^{4i\kappa_j t + \gamma_j}, \quad \text{with} \quad \gamma_j \quad \text{const}. \tag{1.48}$$

1.1.4 The inverse scattering method

The inverse scattering method is certainly the most powerful technique of solution of nonlinear evolution equations — those which are amenable to solution. It turns out that equations integrable by means of the inverse scattering transform possess many remarkable properties such as the Bäcklund transformations, the Painlevé property, the bilinear formulation, an infinite series of conservation laws, and so on.

The inverse scattering method was originally proposed by Gardner, Green, Kruskal and Miura [79], for the case of the KdV. Their approach allowed to solve the initial-value problem for the KdV through a sequence of linear computations. This approach was generalized by Lax [153]. The essence of the approach is as follows.

Consider a general nonlinear evolution equation

$$v_t = K(v), \tag{1.49}$$

where K is a nonlinear operator. Let us associate with this equation the scattering problem

$$L\psi = \lambda\psi, \tag{1.50}$$

where the operator L depends on the solution of the equation (1.49). Assume that the time evolution of the scattering data is given by

$$i\psi_t = A\psi, \tag{1.51}$$

University of Cape Town

where A is assumed a self-adjoined operator. The compatibility condition for the system (1.50)-(1.51) can be written in the form

$$iL_t + LA - AL = 0, \tag{1.52}$$

and hence the eigenvalue λ is time-independent. There is a correspondence between these constant eigenvalues and constant velocities and amplitudes of the solitons which evolve from the initial conditions.

The essence of the inverse scattering method is to avoid the direct solution of equation (1.49). Instead we can find $v(x,t)$ from the initial data $v(x,0)$ using the following procedure:

1) Solve the direct scattering problem, i.e. calculate the scattering parameters (the reflection and transmission coefficient of the operator L) for ψ at $|x| = \infty$ and $t = 0$ from known $v(x,0)$.

2) Find the time evolution of the scattering data using equation (1.51) together with the asymptotic form of A at $x = \infty$.

3) Solve the inverse problem, i.e., construct $v(x,t)$ from the knowledge of the scattering data of the operator L at time $t > 0$.

There are many potential obstacles associated with this approach. First and foremost, it may not be possible to find operators L and A satisfying the compatibility condition (1.52). And even if the Lax representation exists, the method is effective only if the spectral evolution problem and the inverse scattering problem can be solved analytically.

Zakharov and Shabat [288] applied this method to the NLS equation. The inverse scattering method was applied to the modified KdV equation be Wadati [267] and Tanaka [251]. A more general approach has been developed by Ablowitz, Kaup, Newell and Segur [2, 3]. The so-called AKNS formalism was first applied for sine-Gordon equation. They considered the scattering problem

$$Lv = \zeta v, \tag{1.53}$$

where

$$L \equiv \begin{pmatrix} i\partial_x & -iq \\ ir & -i\partial_x \end{pmatrix}, \quad v \equiv \begin{pmatrix} v^{(1)} \\ v^{(2)} \end{pmatrix} \tag{1.54}$$

and the coefficients $q = q(x,t)$ and $r = r(x,t)$ are arbitrary. The operator A in the evolution equation

$$i\partial_t v = Av \tag{1.55}$$

University of Cape Town

has the form

$$A \equiv \begin{pmatrix} a(x,t,\zeta) & b(x,t,\zeta) \\ c(x,t,\zeta) & -a(x,t,\zeta) \end{pmatrix}, \tag{1.56}$$

where coefficients a, b and c are functions to be determined. Differentiating (1.53) with respect to t and (1.55) with respect to x; imposing the eigenvalue ζ to be independent of t and demanding the cross derivatives to be equal, yields three conditions for the matrix elements of A:

$$a_x = qc - rb, \tag{1.57}$$

$$b_x + 2i\zeta b = i\frac{\partial q}{\partial t} - 2aq, \tag{1.58}$$

$$c_x - 2i\zeta c = i\frac{\partial r}{\partial t} + 2ar. \tag{1.59}$$

It can be shown that particular choices of these coefficients make equations (1.57)-(1.59) equivalent to a large class of nonlinear evolution equations. For example, choosing

$$a = 4\zeta^3 + 2qr\zeta + irq_x - iqr_x$$

yields

$$q_t - 6rqq_x + q_{xxx} = 0, \tag{1.60}$$

$$r_t - 6qrr_x + r_{xxx} = 0. \tag{1.61}$$

When $r = -1$, equation (1.60) reduces to the KdV equation. Choosing $r = \pm q$, equation (1.61) gives the modified KdV equation. On the other hand, the choices

$$a = -\frac{1}{4\zeta}\cos\phi, \quad r = -q = \frac{1}{2}\phi_x$$

and

$$a = -\frac{1}{4\zeta}\cosh\phi, \quad r = -q = \frac{1}{2}\phi_x$$

reduce to the sine-Gordon and sinh-Gordon equations, respectively. Next, the choice

$$a = \zeta^2 + rq$$

produces

$$iq_t + q_{xx} - 2q^2r = 0, ir_t - r_{xx} + 2qr^2 = 0.$$

University of Cape Town

Identifying $r = \pm q^*$, these equations reduce to the NLS equation.

The AKNS approach encompasses the KdV, the modified KdV, the sine- and sinh-Gordon, the NLS, coupled KdV and NLS equations, the massive Thirring model and the complex sine-Gordon equation. Another advantage of the AKNS is that it gives a deductive procedure for finding of the evolution operator for a given scattering operator. The modern formulation of the inverse scattering method is based on the Riemann-Hilbert problem [4, 197].

1.2 Solitons in nearly-integrable systems

In this section we will concentrate mainly on the perturbed nonlinear Schrödinger and sine-Gordon equations. In many physical applications the integrable equations arise from some asymptotic expansions, e.g. expansions in powers of the wave's amplitude and/or wavenumber. Therefore, they provide only an approximate description of the underlying physical system. Usually the inclusion of higher-order terms in these expansions destroys the complete integrability. Nonintegrable perturbations may also originate from the interaction of separate normal modes of a nonlinear system in the case when nonlinear self-interaction and linear dispersion of each mode is sufficiently strong, while their mutual interaction is relatively weak. In this situation one deals with coupled systems of nonlinear equations which are integrable in the uncoupled case, while the coupling terms play the role of nonintegrable perturbations. Terms that describe effects of external fields, inhomogeneities of the medium and various dissipative effects are another source of nonintegrable perturbations. All perturbations can be naturally divided into two classes: Hamiltonian perturbations and dissipative ones. Hamiltonian perturbations conserve only finite number of conservation laws (usually the first two or three) and the rest are destroyed.

University of Cape Town

One of the most remarkable properties of completely integrable equations is the availability of exact multi-soliton solutions. Usually a one-soliton solution persists even after small nonintegrable terms were added to a completely integrable equation. However, only integrable equations possess exact multi-soliton solutions which describe purely elastic interaction between individual solitons.

Small *dissipative* perturbations attenuate the moving solitons and damp their oscillations. Effects generated by *conservative* perturbations are more subtle. As a rule, they do not destroy or attenuate nonoscillating solitons but render collisions of solitons inelastic. Inelastic collisions are accompanied by the emission of radiation waves. As we

have already mentioned, perturbation-induced dynamics of solitons is of interest mainly because it models physical phenomena that cannot be described by completely integrable systems. However, if the model is perturbed but remains close to a completely integrable one in some sense, its investigation may be considerably facilitated. Such systems are referred to as *nearly-integrable*, as opposed to *nonintegrable* systems, which do not have any completely integrable limit. Therefore nearly-integrable systems are of special value as they may be treated by a variety of asymptotic and perturbation techniques.

There are several approaches to the analytical description of soliton dynamics in nonintegrable systems. The simplest type of the dynamics reduces to the evolution of the parameters of the soliton (e.g. amplitude, phase and velocity) under the action of dissipation. In this case modified conservation laws can be used. Assuming in the first approximation that the instantaneous shape of the soliton is not changed, one finds the dissipation-induced rates of change of quantities that are integrals of motion of the underlying unperturbed system. Then expressing the integrals of motion in terms of parameters of the unperturbed soliton, one obtains evolution equations for these parameters [211, 220, 50, 31, 158]. In the presence of Hamiltonian perturbations, evolution equations for the soliton parameters can also be obtained in the lowest approximation. To this end one needs to insert the unperturbed soliton solution into the full Hamiltonian of the system and derive the canonical equations of motion. In this approach one group of the soliton's parameters (e.g. amplitude and position) serve as generalized coordinates while the other (e.g. phase and velocity) play the role of the conjugate momenta. Alternatively, one can use the approach based on the Lagrangian. Both techniques originate from the variational method of Whitham [274] in general nonlinear wave theory. The Hamiltonian and Lagrangian approaches were used in [199, 171, 172, 175]. In many cases the techniques based on modified conservation laws, the Lagrangian and Hamiltonian formalisms can be applied to multi-soliton problems as well.

Many physically important effects arise at higher orders of the perturbation theory and cannot be accounted for by the lowest-order approximation discussed above. Among these effects are the perturbation-induced emission of radiation by solitons and significant corrections to the soliton's shape. Such problems can be solved by the direct perturbation theory where the original nonlinear equations are linearized about the unperturbed soliton. An important stage of this method involves finding the eigenfunctions associated with the linearized equation. Then the first-order evolution equations for the soliton's parameters are obtained as a condition for the absence of secular terms. The radiation emitted by the soliton can be accounted for by the higher order terms in the expansion or by using

University of Cape Town

Green's function [166]. Therefore the direct perturbation theory requires the knowledge of exact unperturbed solitons and the eigenfunctions of the linearized equation but does not require the unperturbed equation to be exactly integrable. The direct perturbation theory is applicable to multi-soliton problems only when solitons are slightly overlapped; then the overlapping is also treated as a perturbation. Important contributions to the direct perturbation theory for the NLS equation we made in [120, 101].

A powerful perturbation technique is based on the inverse scattering transform. This technique requires the unperturbed equation to be integrable. It was introduced in [115, 111, 113]. For the NLS equation it was developed in [116].

Some nearly integrable conservative equations can be formally cast in the unperturbed form by an infinite sequence of canonical transformations. This approach has been used in [137, 138, 139, 181, 182].

The perturbation techniques suggest that there are two different levels of problems concerning dynamics of solitons in nearly-integrable systems. Problems that can be solved in the adiabatic approximation can be classified as lower-level perturbation theory problems while those dealing with emitted radiation and perturbation-induced distortions to the soliton's shape can be classified as higher-level ones.

University of Cape Town

Perturbed nonlinear Schrödinger equation

The general form of the perturbed NLS equation is:

$$i\psi_t + \psi_{xx} + 2|\psi|^2 = \epsilon P(\psi, \psi^*). \tag{1.62}$$

It is a universal equation for the description of evolution of wave envelopes in dispersive weakly nonlinear media and therefore it arises in many different areas.

In optics $\psi(x,t)$ has the sense of a complex envelope of the electromagnetic field and the NLS equation describes the self-modulation and self-focusing of light in a Kerr-type nonlinear medium. The interest in this area was first boosted in [95] where the existence of solitons in nonlinear optical fibers was predicted. This equation also has applications in laser physics [190, 97]. In optical context it is natural to consider a perturbation of the form

$$\epsilon P(\psi, \psi^*) = \epsilon|\psi|^4\psi \tag{1.63}$$

which is the higher nonlinear-dispersion term [224, 147, 127, 200]. In application to nonlinear optical fibers an important role is played by perturbative terms

$$i\epsilon_1\psi_{xxx} \tag{1.64}$$

and

$$i\epsilon_2(|\psi|^2\psi)_x \tag{1.65}$$

and combinations of this [176, 94, 55, 10, 281, 136]. The former term accounts for the higher spatial dispersion, while the latter models the *nonlinear* dispersion of group velocity. Another important perturbation in optics is

$$\epsilon\psi(|\psi|^2)_x \tag{1.66}$$

which describes dissipation induced by the Raman scattering [141, 142].

The NLS equation arising in hydrodynamics is perturbed by dissipative terms of the form

$$\epsilon P(\psi, \psi^*) = -i\gamma_1\psi \tag{1.67}$$

and

$$\epsilon P(\psi, \psi^*) = i\gamma_2\psi_{xx} - i\gamma_3|\psi|^2\psi. \tag{1.68}$$

It describes the instability of the Poiseuille flow, also Couette-Taylor flow and the plane-parallel flow [246, 58]. The same dissipative terms appear in some applications in plasma physics as well [85, 67]. They describe the interaction between the Langmuir and ion-acoustic waves. Another source of dissipative terms is the linear and nonlinear Landau damping which produces nonlocal perturbations of the form [195, 103, 59, 101]:

$$P[\psi(x), \psi^*(x)] = -\fint \psi(y)\,(x-y)^{-1}dy, \tag{1.69}$$

$$P[\psi(x)\psi^*(x)] = -\psi(x)\fint |\psi(y)|^2\,(x-y)^{-1}dy. \tag{1.70}$$

It is interesting to note that these nonlocal dissipative terms preserve the number of particles (plasmon number) integral. The nondissipative terms arising in plasma physics are of the form [81]

$$\epsilon\left[|\psi|^2\psi_{xx} + (|\psi^2|)_x\psi_x - |\psi_x|^2\psi\right]. \tag{1.71}$$

As we mentioned before, introducing dissipative terms in integrable systems may lead to the decay of solitons. In order for the localized structures to persist, one needs to compensate the dissipative losses by adding terms which serve as energy sources. This can be done in a variety of ways. For instance, one can supplement the dissipative term by an external AC driving [202]:

$$\epsilon P(\psi, \psi^*) = i\gamma\psi + he^{i\Omega t}.$$

University of Cape Town

Perturbations of this type occur in the theory of charge-density waves when one considers a small-amplitude localized dipolar excitation driven by an AC electric field [117]. Next, the term

$$\epsilon P(\psi, \psi^*) = |\psi|^2 \mathrm{e}^{i(\Omega t - kx)}$$

models the action of an electromagnetic wave on the Langmuir plasma [78] while the perturbation [266]

$$\epsilon P(\psi, \psi^*) = i\gamma_0 \psi + i\gamma_1 \psi_x + i\gamma_2 \psi_{xx}$$

arises in the description of magnetostatic solitons propagating at a ferromagnet-semiconductor surface, driven by a drift flow of charge carriers in the semiconductor.

In chapters 2 and 3 of this thesis we consider the *parametrically* driven NLS equation:

$$i\tilde{\psi}_t + \tilde{\psi}_{xx} + 2|\tilde{\psi}|^2\tilde{\psi} = h\tilde{\psi}^* \mathrm{e}^{2i\omega t} - i\gamma\tilde{\psi}. \tag{1.72}$$

This equation describes a large variety of physical phenomena, including the nonlinear Faraday resonance in water [277, 184, 259, 260, 109, 149, 280, 48, 278, 270, 269]; parametric instabilities of waves in plasma [289, 278]; the parametric generation of spin waves and magnetic solitons in ferro and anti-ferromagnets [287, 36, 17][287, 36, 17, 165, 279] and, finally, the effect of parametric amplifiers on solitons in optical fibers [56, 164, 179]. It also serves as an amplitude equation for small-amplitude, parametrically-driven sine-Gordon breathers [17] and hence its range of applicability includes all systems modelled by the parametrically driven sine-Gordon equation [214, 89, 86].

University of Cape Town

Perturbed sine-Gordon equation

The range of applications of the perturbed sine-Gordon equation

$$\phi_{tt} - \phi_{xx} + \sin\phi = \epsilon P(\phi), \tag{1.73}$$

coincides with the scope of its unperturbed counterpart. We mentioned some applications in subsec. 1.1.2.

The two most commonly met dissipative perturbations to the SG equation are usually of the form:

$$\epsilon P(\phi) = -\gamma\phi_t, \quad \gamma > 0, \tag{1.74}$$

and

$$\epsilon P(\phi) = \beta\phi_{xxt}, \quad \beta > 0. \tag{1.75}$$

In the context of the long Josephson junction eq.(1.74) describes dissipative losses due to the tunneling of electrons across the dielectric barrier. The second type of dissipative perturbation, eq.(1.75), accounts for losses due to the current along the junction [22]. Next, a point-like dissipative defect due to a local narrowing can be modelled by

$$\epsilon P(\phi) = -\gamma\delta(x)\phi_t. \tag{1.76}$$

Experimentally, such a narrowing can be created by subjecting the junction to a focused laser beam [47], imposing a shorter resistor onto the junction [5], or implanting a metallic microshort [128, 130].

As in the NLS case, in order to sustain stationary nondecaying structures, we need to include some driving term to make up for dissipative losses. For example, the forcing term of the form

$$\epsilon P(\phi) = f(t) \tag{1.77}$$

describes the density of the bias current in Josephson junctions (usually f is constant in this application), or any external AC/DC electric or magnetic field. The equation with the external driving of the form

$$\epsilon P(\phi) = f(t)\sin(\phi/2) \tag{1.78}$$

with f constant, is referred to as the double sine-Gordon equation. In magnetism, an external magnetic field perpendicular both to the x-axis and the magnetization vector is described by

$$P(\phi) = f(t)\cos(\phi/2). \tag{1.79}$$

Other perturbations used in studies of magnetic materials are

$$\epsilon P(\phi) = f(t)\sin\phi, \quad \epsilon P(\phi) = \sin 2\phi. \tag{1.80}$$

Another important source of perturbed SG equations are inhomogeneous long Josephson junctions. For example,

$$\epsilon P(\phi) = g(x)\sin u \tag{1.81}$$

describes inhomogeneities of the maximum Josephson current density. Here $g(x) = \delta(x)$ corresponds to the microresistor (the narrowing of the dielectric layer) and $g(x) = -\delta(x)$ to the microshort (widening of the layer). A periodic lattice of point-like inhomogeneities is described by $g(x) = \sum_n \delta(x - n\,a)$ [237, 83], lattices of finite size inhomogeneities are studied in [9]. The inhomogeneities of the inductance generate perturbations of the form

$$\epsilon P(\phi) = g'(x)\phi_x \tag{1.82}$$

University of Cape Town

while the capacity inhomogeneities are described by

$$\epsilon P(\phi) = g(x)\phi_{tt}. \tag{1.83}$$

Point-like inhomogeneities also describe magnetic impurities. In charge-density-wave systems this perturbation can have a more general form:

$$P(\phi) = \delta(x)\,\sin\left(\frac{\phi}{n} + \theta\right), \tag{1.84}$$

where n is integer and θ an arbitrary constant angle. Higher spatial dispersion-induced perturbation has the form

$$\epsilon P(\phi) = \phi_{xxxx}. \tag{1.85}$$

The *parametrically* driven damped SG equation

$$\phi_{tt} - \phi_{xx} + \sin\phi = -\sin\phi\cos(\omega t), \tag{1.86}$$

which will arise as a continuous limit of a chain of parametrically driven pendula in chapter 3 of this thesis, also appears in studies of magnetism [17, 36] and hydrodynamics [214].

1.2.1 Solitons in damped-driven systems

In this section we will consider the effect of introducing of different combinations of dissipative and driving terms.

Adiabatic dynamics of solitons in damped and driven NLS equations

To find adiabatic changes of the soliton parameters due to small perturbations, it is convenient to write the NLS soliton in the form

$$\psi(x,t) = i\,A\,\mathrm{e}^{[-i(2\xi x+\phi)]}\,\mathrm{sech}[A(x-\zeta)], \tag{1.87}$$

where $\phi = (4\xi^2 - A)\,t + \phi_0$ and $\zeta = -4\,\xi\,t + \zeta_0$ are the soliton's phase and position, respectively. Then the general evolution equations for the soliton's amplitude, velocity, position and phase are given by [132]

$$\frac{dA}{dt} = -\mathrm{Re}\left[\epsilon\int_{-\infty}^{+\infty} P[\psi(z)]\,\mathrm{sech}z\,\mathrm{e}^{i(2\xi x+\phi)}dz\right], \tag{1.88}$$

$$\frac{d\xi}{dt} = \frac{1}{2}\mathrm{Im}\left[\epsilon\int_{-\infty}^{+\infty} P[\psi(z)]\,\tanh z\,\mathrm{sech}z\,\mathrm{e}^{i(2\xi x+\phi)}dz\right], \tag{1.89}$$

$$\frac{d\zeta}{dt} = -4\xi - \frac{1}{A^2}\mathrm{Re}\left[\epsilon\int_{-\infty}^{+\infty} P[\psi(z)]\,z\,\mathrm{sech}z\,\mathrm{e}^{i(2\xi x+\phi)}dz\right], \tag{1.90}$$

$$\frac{d\phi}{dt} = 4\xi^2 - A^2 + \frac{1}{A}\mathrm{Im}\left[\epsilon\int_{-\infty}^{+\infty} P[\psi(z)]\,(1 - A\,x\tanh z)\,\mathrm{sech}z\,\mathrm{e}^{i(2\xi x+\phi)}dz\right], \tag{1.91}$$

University of Cape Town

where $z = A(x - \zeta)$.

The main difference between the unperturbed and the damped equation is that in the latter case the amplitude and velocity of the soliton cannot be arbitrary. The majority of dissipative perturbations do not support moving solitons. As an example, consider the following perturbation arising in hydrodynamics and plasma physics [211, 113, 201]

$$\epsilon P(\psi) = i\gamma_1\psi + i\gamma_2\psi_{xx} - i\gamma_3|\psi|^2\psi; \quad \gamma_i > 0. \tag{1.92}$$

Here the second and third terms represent the nonhomogeneous and nonlinear dampings, respectively, and the first term is a (linear) gain. The flat solution $\psi = 0$ is obviously unstable due to the presence of the gain term, and the third term acts to saturate the instability at a finite level $|\psi_0|^2 = \gamma_1/\gamma_3$. The flat nonzero solution is said to arise via *soft* excitation. The evolution equations for the amplitude, A, and the velocity, $V = -4\xi$, of solitons are [211, 113, 201]:

$$\begin{aligned} \frac{dA}{dt} &= -2A\left[-\gamma_1 + \frac{A^2}{3}(\gamma_2 + 2\gamma_3)\right] - \frac{1}{2}\gamma_2 AV^2 \\ \frac{dV}{dt} &= -\frac{4}{3}\gamma_2 A^2 V. \end{aligned}$$

It can be shown [220] that these two ordinary differential equations have only fixed points pertaining to motionless solitons, with the amplitude

$$A^2 = \frac{3\gamma_1}{\gamma_2 + 2\gamma_3}.$$

However, the corresponding soliton is unstable and decays to the unstable zero homogeneous background If $\gamma_2 = 0$, the soliton can have arbitrary velocity. Its amplitude is given by

$$A^2 = \frac{3\gamma_1}{2\gamma_3}.$$

In systems with *hard* excitation the trivial solution is stable. The simplest example is the perturbation [222]:

$$\epsilon P(\psi, \psi^*) = -i\gamma_1\psi + i\gamma_2\psi_{xx} + i\gamma_3|\psi|^2\psi - i\gamma_4|\psi|^4\psi, \quad \gamma_i > 0. \tag{1.93}$$

This time the first, linear,term represents the damping. The flat nonzero solution can be excited if

$$\gamma_3 \geq 2\sqrt{\gamma_1\gamma_4}.$$

University of Cape Town

The quintic term is necessary for global stability. The reason why this type of excitation is called *hard*, is because the nonzero solution does not result simply from the instability of the zero background. As before only zero-velocity solitons exist in this case. The evolution equation for the soliton's amplitude is

$$\frac{dA}{dt} = 2A\left[-\gamma_1 + \frac{A^2}{3}(-\gamma_2 + 2\gamma_3) - \frac{8}{15}\gamma_4 A^4\right],$$

which gives for the amplitude of the static soliton

$$A^2 = \frac{5(2\gamma_3 - \gamma_2) \pm \sqrt{5[5(2\gamma_3 - \gamma_2)^2 - 96\gamma_1\gamma_4]}}{16\gamma_4}.$$

The two solitons exist if $\gamma_3 \geq 2\sqrt{(6/5)\gamma_1\gamma_4}$. The soliton with the larger amplitude corresponding to sign "+" is stable while the soliton corresponding to sign "−" is unstable [173].

A natural generalization is to consider [223] the perturbation where signs are chosen so that higher power terms bring stability:

$$\begin{aligned}\epsilon P(\psi, \psi^*) &= \gamma_1\psi + \gamma_2\psi_{xx} - \gamma_3|\psi|^2\psi - \gamma_4|\psi|^4\psi - \gamma_5\psi_{xxxx} + \\ &+ \kappa_1|\psi|^2\psi_{xx} + \kappa_2\psi^2\psi^*_{xx} - \kappa_3|\psi_x|^2\psi + \kappa_4\psi_x^2\psi^*. \end{aligned} \tag{1.94}$$

NLS equation with such a perturbation arises as the solvability condition for the fifth-order terms in t he expansion describing the singular Hopf bifurcation. The evolution equations for the soliton's amplitude, A, and velocity, V, are:

$$\frac{dA}{dt} = 2A\left[\gamma_1 - \frac{\gamma_2 V^2}{4} - \frac{\gamma_5 V^4}{16} - A^2\left(c_0 + \frac{c_1 V^2}{4}\right) - c_2 A^4\right], \tag{1.95}$$

$$\frac{dV}{dt} = -\frac{4}{3}VA^2\left[\gamma_2 + \frac{\gamma_5 V^2}{2} + c_3 A^2\right], \tag{1.96}$$

where

$$\begin{aligned} c_0 &= \frac{1}{3}\gamma_1 + \frac{2}{3}\gamma_3, \\ c_1 &= \frac{2}{3}(\kappa_1 + \kappa_2 + \kappa_3 + \kappa_4) + 2\gamma_2, \\ c_2 &= \frac{1}{15}[8\gamma_4 + 7\gamma_5 + 6(\kappa_1 + \kappa_2) + 2(\kappa_3 - \kappa_4)], \\ c_3 &= \frac{2}{5}(\kappa_1 - \kappa_2 + \kappa_4 - 7\gamma_5). \end{aligned}$$

University of Cape Town

Apart from the stable trivial solution ($A = 0$, V arbitrary), the system (1.95)-(1.96) admits stable static solitons ($A \neq 0$, $V = 0$) and stable propagating soliton solutions ($A \neq 0$, $V \neq 0$). Static solitons replace the trivial solution when $\gamma_1 = 0, \gamma_2 > 0$. Propagating solitons with

$$V = \sqrt{\frac{|\gamma_2|}{2\gamma_5}} \tag{1.97}$$

are born when $\gamma_1 = -\gamma_2^2/(4\gamma_5)$ and $\gamma_2 < 0$. The transition between the static and propagating soliton occurs when $\gamma_2 = -c_3 A_s^2/4$, where A_s is the amplitude of the static soliton. When $\gamma_2 + c_3 A_s^2/4 < 0$, the static soliton splits into a pair of counter propagating solitons.

A perturbed system comprising of a higher-order dispersion and higher-order dissipation is given by [141, 138, 137]:

$$i\psi_t + \psi_{xx} + 2|\psi|^2\psi = -i\epsilon\left[\beta_1\psi_{xxx} + 2\beta_2(|\psi|^2\psi)_x + (2\beta_3 + i\sigma_3)\,\psi\,(|\psi|^2)_x\right], \tag{1.98}$$

where β_i and σ_3 are positive. When $\sigma_3 = 0$, the transformation

$$q = \psi - \epsilon i(3\beta_1 - \beta_2/2)\psi_x - \epsilon i(6\beta_1 - 2\beta_2 - \beta_3)\psi\int_{-\infty}^{x}|\psi(y)|^2\,dy + \mathrm{O}(\epsilon^2)$$

takes eq.(1.98) to a completely integrable equation

$$iq_t + q_{xx} + 2|q|^2q = -i\epsilon\beta_1(q_{xxx} + 12|q|^2q_x). \tag{1.99}$$

Using the fact that eq.(1.99) has the same scattering problem as the cubic NLS equation, it was shown that the 2-soliton solution splits into two solitons propagating in opposite directions with different velocities. When $\sigma_3 \neq 0$, the evolution equations for the soliton's amplitude and velocity are

$$\frac{dA}{dt} = 0, \quad \frac{dV}{dt} = -\frac{8}{15}\epsilon\sigma_3 A^4. \tag{1.100}$$

Eqs.(1.100) imply the higher-order dissipation acts as a constant force on the soliton without changing its amplitude.

An example of the nonlocal dissipative perturbation is given by the system with nonlinear Landau damping which arises in plasma physics:

$$i\psi_t + \psi_{xx} + 2|\psi|^2\psi = \epsilon\psi\ \fint_{-\infty}^{+\infty}|\psi(y)|^2\,(x-y)^{-1}dy, \tag{1.101}$$

where ϵ is a real parameter. The evolution equations for the soliton parameters are [101]:

$$\frac{dA}{dt} = 0, \quad \frac{dV}{dt} = \frac{\beta\epsilon}{4}A^2, \tag{1.102}$$

University of Cape Town

where $\beta \approx 7.44$. As in the previous example, the damping acts on the soliton as a constant force in this case .

In order to have persistent localized solutions in a system with dissipation, one needs to supply the energy from outside. This can be done in a variety of ways. In optics, for example, the external energy can be pumped into the fiber by the periodically activating stimulated Raman scattering. The perturbed equation is [140]:

$$i\psi_t + \psi_{xx} + 2|\psi|^2 = -i\gamma\psi + i\gamma\, a \sum_{n=-\infty}^{\infty} \delta(x - na)\, \psi, \tag{1.103}$$

where the second term on the right-hand side accounts for the Raman pump. This term compensates the dissipative losses for all values of the soliton's amplitude and velocity.

Another possibility of compensating losses is to add an external AC driving:

$$i\psi_t + \psi_{xx} + 2|\psi|^2\psi = -i\gamma\psi + h\, \mathrm{e}^{i\Omega t}. \tag{1.104}$$

Using equations for the rate of change of the total power (1.34) and total momentum (1.35), it is possible to derive an autonomous system of equations for the amplitude and phase of the quiescent soliton $\psi(x,t) = iA(t)\mathrm{sech}[A(t)x]\, \exp\left[i\Omega t - i\phi(t)\right]$ [116, 117]:

$$\frac{dA}{dt} = -2\gamma A + \pi h \sin\phi, \tag{1.105}$$

$$\frac{d\phi}{dt} = \Omega - A^2. \tag{1.106}$$

The fixed points of this dynamical system are

$$A = (-1)^k\sqrt{\Omega}, \quad \phi = \arcsin\frac{2\gamma\sqrt{\Omega}}{\pi h} + k\,\pi; \quad k = 0,\, 1. \tag{1.107}$$

In eq.(1.105) the damping causes the decay of the soliton's amplitude while the AC-driving can act both as forcing and damping — depending on the instantaneous phase difference between the soliton and the driver. On the other hand, the change of the soliton's phase depends on its amplitude. Therefore the soliton can lock on to the frequency of the AC-driver and draw as much energy as it needs to maintain the constant amplitude given by (1.107). The threshold value of the driving strength for the existence of solitons is

$$h_{thr} = \frac{2\gamma\sqrt{\Omega}}{\pi}. \tag{1.108}$$

An alternative possibility of compensating dissipative losses is through a parametric AC driver. This type of driving is easier to realize in experiments and we will consider it in chapter 2 and 3 of this thesis. The parametrically driven damped NLS is:

$$i\psi_t + \psi_{xx} + 2|\psi|^2\psi = -i\gamma\psi + h\psi^*\mathrm{e}^{i\Omega t}. \tag{1.109}$$

University of Cape Town

The corresponding evolution equations for the soliton's amplitude and phase are [36, 132]:

$$\frac{dA}{dt} = -2\gamma A - 2hA\sin 2\phi \tag{1.110}$$

$$\frac{d\phi}{dt} = \Omega - A^2 - h\cos 2\phi. \tag{1.111}$$

There are two stable solitons in this system; the corresponding amplitudes and phases are given by the fixed points of (1.110)-(1.111):

$$A = (-1)^k\sqrt{\Omega + \sqrt{h^2 - \gamma^2}}, \quad \phi = 2\arcsin\left(-\frac{\gamma}{h}\right) + k\,\pi; \quad k = 0,\, 1. \tag{1.112}$$

Solitons exist when the driving is stronger than the damping, $h > \gamma$. System (1.110)-(1.111) also has a stable trivial solution, ($A = 0$, $\phi = 2\arccos\Omega/h$), which is also stable under the condition

$$h < \sqrt{\Omega^2 + \gamma^2}. \tag{1.113}$$

All these solutions, both the solitons and the zero solution, will reappear in chapter 2 and 3 of this thesis.

Adiabatic dynamics of damped and driven sine-Gordon solitons

As we mentioned in section 1.1.2 the SG equation has two fundamental types of soliton solutions: kinks and breathers. The adiabatic equations, analogous to eqs.(1.88)-(1.91), for the parameters of the SG kink are [166]:

$$\frac{dv}{dt} = \mp\epsilon\frac{(1-v^2)^{3/2}}{4}\int_{-\infty}^{\infty} P[\phi(z)]\,\mathrm{sech}(z)dz \tag{1.114}$$

$$\frac{d\zeta}{dt} = v \mp \epsilon\frac{v\,(1-v^2)}{4}\int_{-\infty}^{\infty} P[\phi(z)]\,z\,\mathrm{sech}(z)dz, \tag{1.115}$$

where $z = (x-\zeta)\,(1-v^2)^{-1/2}$ and $P(\phi)$ is an arbitrary perturbation of the SG equation.

Consider, for example, the SG equation with the dissipative perturbations (1.74) and (1.75) and constant driving

$$\phi_{tt} - \phi_{xx} + \sin\phi = -\gamma\phi_t + \beta\phi_{xxt} - f. \tag{1.116}$$

In this case it is easier to use energy considerations instead of eqs.(1.114)-(1.115) and obtain [166] the following evolution equation for the kink's velocity, v, satisfies:

$$\frac{dv}{dt} = \pm\frac{\pi f}{4}(1-v^2)^{3/2} - \gamma v(1-v^2) - \frac{\beta}{3}v. \tag{1.117}$$

University of Cape Town

When $\beta = 0$, the equilibrium velocity is

$$v_\infty = \pm \left[1 + \left(\frac{4\gamma}{\pi f}\right)\right]^{-1/2}. \tag{1.118}$$

It worth mentioning that from eq.(1.117) it follows that the terms with γ and β indeed will decrease kink's velocity while the term with f will accelerate the kink to the right and the antikink to the left. When a kink moves steadily with velocity v_∞, the dissipation rate of the energy is exactly equal to the rate of the energy supply by the external driver. However, this method does not give the evolution equation of another kink's parameter, its position ζ. To find the perturbation-induced evolution of the kink's position, it is necessary to use eqs.(1.114)-(1.115).

Let us consider the time-periodic driving: $f(t) = \sin \omega t$. It is convenient to decompose ϕ into the kink part, $U(t, x)$, and the background part which is due to the external force and depends only on time [207]:

$$\phi = \bar{\epsilon} \sin \omega t + U, \quad \bar{\epsilon} = \epsilon/(1 - \omega^2). \tag{1.119}$$

Here we have assumed that $|\epsilon| \ll |1 - \omega^2|$.

In the adiabatic approximation, in the low-frequency case $\omega \ll \epsilon^{3/2}$, the position of the kink is given by [174]

$$\zeta(t) = -\frac{1}{\omega} \arcsin \left\{ \left[\left(\frac{4\omega}{\pi \bar{\epsilon}}\right)^2 + 1 \right]^{-1/2} \sin \omega t \right\}. \tag{1.120}$$

The energy of the radiation emitted at the frequency $n\omega$ is equal to

$$W_n = \frac{1}{2} \epsilon \omega^2 \exp\left(-\frac{8}{\pi\epsilon} - \frac{64\omega^4}{3\pi^3\epsilon^3} n\right), \tag{1.121}$$

and the total power is

$$W_{tot} = \sum_{n>1/\omega} W_n \approx \int_{1/\omega}^{\infty} W_n \, dn = \frac{\sqrt{3}\pi^2 \epsilon^{5/2}}{32} \exp\left(-\frac{8}{\pi\epsilon}\right). \tag{1.122}$$

In the high-frequency case, $\omega > 1/2$, the kink is static in the adiabatic approximation [185]. However, if one takes into account the perturbation-induced oscillations of the kink, in the next approximation the kink's position and the radiation power are given by

$$\zeta(t) = -\frac{\epsilon}{2\omega} \sin \omega t, \quad W = \frac{\pi^2 \epsilon^4}{8\omega\sqrt{4\omega^2 - 1}} \operatorname{sech}^2\left(\frac{\pi}{2}\sqrt{4\omega^2 - 1}\right) \tag{1.123}$$

University of Cape Town

and the radiation is emitted at frequency 2ω.

The driving of the form

$$\epsilon P(\phi) = \epsilon \sin(\phi/2) \sin \omega t \tag{1.124}$$

gives rise to the parametric resonance at frequencies $\omega = 2(1+\delta\omega)/2n+1)$, $n = 0, 1, 2, \ldots$ where $|\delta\omega| \ll 1$. When $n = 0$ the emitted power is given by

$$W = (\epsilon - 8\Omega)\sqrt{2(\epsilon - 4\Omega)}. \tag{1.125}$$

Let us now discuss the perturbed dynamics of *breathers*.The unperturbed breathers were derived in sec. 1.1.2. It is convenient to rewrite it as

$$\phi = 4 \arctan\left[\tan A \, \sin(\psi \cos A) \, \mathrm{sech}\left(\frac{x-\xi}{\sqrt{1-v^2}} \sin A\right)\right], \tag{1.126}$$

$$\psi = \frac{t - vx}{\sqrt{1-v^2}}, \quad \xi = vt. \tag{1.127}$$

Here v is the breather's velocity and $\tan A$ is its amplitude. The amplitude is related to the frequency ω in the following way:

$$\sin A = \sqrt{1-\omega^2}, \quad \cos A = \omega. \tag{1.128}$$

(Breather's frequency ω cannot be greater than 1.)

The general perturbation-induced equations for the SG breather's parameters were derived in [144, 114]

$$\frac{dA}{dt} = \epsilon \frac{(1-v^2)^{1/2} I_1}{4 \cos A}, \tag{1.129}$$

$$\frac{dv}{dt} = -\epsilon \frac{(1-v^2)^{3/2} I_2}{4 \cos A}, \tag{1.130}$$

$$\frac{d\xi}{dt} = v + \epsilon \frac{(1-v^2)(I_3 - v \tan A \, I_4)}{(2 \sin A)^2}, \tag{1.131}$$

$$\frac{d\psi}{dt} = \sqrt{1-v^2} \cos A - \frac{\epsilon\sqrt{1-v^2}}{2 \sin A \cos^2 A}[v \cot A \, I_3 + (1-v^2)\cos^2 A \; I_4 - I_5], \tag{1.132}$$

where $\zeta = \sin A z$,

$$I_1 = \int_{-\infty}^{\infty} d\zeta \frac{\cosh\zeta \cos(\cos A\psi)}{\cosh^2\zeta + \tan^2 A \sin^2(\cos A\psi)} P[\phi(\zeta)], \tag{1.133}$$

$$I_2 = \int_{-\infty}^{\infty} d\zeta \frac{\sinh\zeta \sin(\cos A\psi)}{\cosh^2\zeta + \tan^2 A \sin^2(\cos A\psi)} P[\phi(\zeta)], \tag{1.134}$$

University of Cape Town

$$I_3 = \int_{-\infty}^{\infty} d\zeta \frac{\zeta \cosh\zeta \cos(\cos A\psi)}{\cosh^2\zeta + \tan^2 A \sin^2(\cos A\psi)} P[\phi(\zeta)], \tag{1.135}$$

$$I_4 = \int_{-\infty}^{\infty} d\zeta \frac{\zeta \sinh\zeta \sin(\cos A\psi)}{\cosh^2\zeta + \tan^2 A \sin^2(\cos A\psi)} P[\phi(\zeta)], \tag{1.136}$$

$$I_5 = \int_{-\infty}^{\infty} d\zeta \frac{\cosh\zeta \sin(\cos A\psi)}{\cosh^2\zeta + \tan^2 A \sin^2(\cos A\psi)} P[\phi(\zeta)]. \tag{1.137}$$

There are two important limits which are easily treatable using perturbation theory: the small-amplitude breather (assuming $A \ll 1$)

$$\phi = 4A \sin[(1 - A^2/2)\psi] \operatorname{sech}(Az), \tag{1.138}$$

and the low-frequency breather (assuming $\pi/2 - A \ll 1$)

$$\phi = 4 \arctan[\sin(\zeta\psi) \operatorname{sech} z/\zeta]. \tag{1.139}$$

As in the case of NLS soliton, the damping term $(-\gamma\phi_t)$ causes the decay of the amplitude of the small-amplitude quiescent breather [166]:

$$\frac{dA}{dt} = -2\gamma A. \tag{1.140}$$

However, if the driving term $-\rho \sin(\omega t)$ is added, the breather may lock on to the phase of the driver [162], similarly to the phase-lock of the NLS soliton. The threshold driving strength for the phase-lock is

$$\rho_{thr} = \frac{2\gamma(1-\omega^2)\arcsin[(1-\omega^2)^{1/2}]}{K(1-\omega^2) - E(1-\omega^2)}, \tag{1.141}$$

where K and E are complete elliptic integrals of the first and second kind, respectively. For small driving strengths, $\rho < \rho_{thr}$, the breather decays to a spatially homogeneous state. For sufficiently strong drivers, $\rho > \rho_{thr}$, the breather is persistently oscillating and frequency-locked to the external driving. When the driving is very strong $\rho \gg \rho_{thr}$ the breather dissociates into a kink-antikink pair.

The emission power of the small-amplitude breather (1.138) under the action of the combination driving of the form

$$P(\phi) = -\epsilon \sin(\omega t) - \epsilon \sin(\omega t) \sin(\phi/2), \tag{1.142}$$

can be calculated when $n < \omega < n+1, \quad n = 0, 1, 2, \ldots$ [174]. The emission frequency χ and power W are given by

$$\chi = |n - \omega + \frac{1}{2}[1 + 3(-1)^n]|, \quad W = \left(\frac{\pi c_n \bar{\epsilon}}{12}\right)^2 \chi\sqrt{\chi^2-1}(\chi^2-5)^2 \exp\left(-\frac{\pi\sqrt{\chi^2-1}}{A}\right), \tag{1.143}$$

University of Cape Town

where the coefficients c_n may depend on χ but not on A and $\bar{\epsilon} = \epsilon/(1-\omega^2)$.

Some analysis was also done on the low-frequency breather (1.139). Perturbations $f(t) \equiv f_0$ and $f_0 \sin\phi/2$ result in its dissociation into a kink-antikink pair. However, if the internal frequency of the breather, $\omega = \cos A$, is high enough, this does not happen [114]. The threshold value above which the dissociation does not occur, is

$$\omega_{thr}^2 = \frac{\pi\epsilon}{4}\left[\ln\left(\frac{16}{\pi\epsilon}\right) + 1\right]. \tag{1.144}$$

1.2.2 Instabilities and chaotic dynamics of the NLS solitons

We will confine ourselves to reviewing instabilities and chaotic dynamics only of the NLS solitons although we should mention that, chronologically, the chaotic behaviour of SG breathers was discovered first and the literature on this subject is enormous [199, 61, 33].

In perturbed systems the radiation emitted by the soliton cannot be considered independently from the dynamics of the soliton itself. It turns out that the interaction of the soliton with radiation can destabilize the soliton and eventually lead to its chaotic behaviour. The analytical studies of the chaotic dynamics are performed by asymptotic or direct perturbation methods, or by the perturbation theory based on the inverse scattering transform. All these methods result in the derivation of a reduced finite-dimensional system which describes instabilities and a sequence of bifurcations leading to chaos. The analytical techniques are usually complemented by numerical simulations. In general, rich varieties of analytical tools available for integrable and nearly integrable systems are absent for strongly perturbed equations; therefore, numerical techniques become an indispensable tool for studying instabilities and chaotic dynamics.

University of Cape Town

In the section on the adiabatic evolution of the NLS solitons, we mentioned that in the presence of an external periodic force, the soliton locks on to the frequency of the driver. However, if the driving force has multiple frequency components, the phase-locking does not occur. An example of the system driven with multiple frequencies is given by

$$i\psi_t + \psi_{xx} + 2|\psi|^2\psi = i(\epsilon_1 - \epsilon_2|\psi|^2)\psi + \epsilon_3\psi_{xx} - \frac{h_0}{T}\sum_{n=-\infty}^{\infty}\exp(in\omega_0 t), \quad \omega_0 = \frac{2\pi}{T}. \tag{1.145}$$

In this case the evolution equation for the soliton's parameters can be reduced to the following map which iterates corrections to the amplitude, phase, velocity, and position of the soliton [201]:

$$A_{n+1} = \mathrm{e}^{-\tau}(A_n + 2\hat{h}_0 \sin\phi_n), \tag{1.146}$$

$$\phi_{n+1} = \phi_n - \phi_0 T - K\sin\phi_n - 2T\frac{A_0 A_n(1-\exp(-\tau))}{\tau+\nu_0\nu_n}, \tag{1.147}$$

$$\nu_{n+1} = \nu_n - 2\frac{\nu_0}{A_0}\hat{h}_0\sin\phi_n, \tag{1.148}$$

$$X_{n+1} = X_n - 4(\nu_0+\nu_n)T + 8T\frac{\nu_0}{A_0}\hat{h}_0\sin\phi_n. \tag{1.149}$$

Here parameters with the subscript 0 pertain to the unperturbed soliton: $A_0^2 = 3\epsilon_1/(2\epsilon_2)$, $\phi_0 = A_0^2 + 4\nu_0^2$. Other notations stand for $\tau = 4h_0\,T$, $\hat{h}_0 = (\pi/2)\,\epsilon_0\,\mathrm{sech}(\pi\nu_0/A_0)$ and

$$K = 4A_0\,\hat{h}_0\,T\left[\frac{1-\mathrm{e}^{-\tau}}{\tau} + \left(\frac{2\nu_0}{A_0}\right)^2\right]. \tag{1.150}$$

When both $|K|$ and τ are greater than 1, the soliton becomes chaotic in the sense that its phase ϕ is chaotic and its amplitude oscillates chaotically around the fixed point. The chaotic deviation of the soliton's position from the unperturbed trajectory associates with the diffusion in its velocity parameter ν.

If the system is driven by two frequency components:

$$i\psi_t + \psi_{xx} + 2|\psi|^2\psi = i\gamma\psi_{xx} + h_1\mathrm{e}^{i\Omega t} + h_2\mathrm{e}^{2i\Omega t}, \tag{1.151}$$

the phase-locked solitons are replaced by solitons with oscillating amplitude. The corresponding reduced-dimensional system for the soliton's amplitude and phase is [202]:

$$\frac{dA}{dt} = -\frac{2}{3}\gamma A^3 + \pi[h_1\sin(\Omega t-\phi) + h_2\sin(2\Omega t-\phi)], \tag{1.152}$$

$$\frac{d\phi}{dt} = -A^2. \tag{1.153}$$

The limit cycles arising in this system are given by

$$A \approx A_1 - \pi\,h_2\cos(\Omega t+\phi_1), \quad \phi \approx \Omega t - \phi_1 - 2\pi h_2 A_1\sin(\Omega t+\phi_1), \tag{1.154}$$

$$A \approx A_2 + \pi h_1\cos(\Omega t-\phi_2), \quad \phi \approx 2\Omega t - \phi_2 + 2\pi h_1 A_2\sin(\Omega t-\phi_2), \tag{1.155}$$

where

$$A_k = \sqrt{k\,\Omega}, \quad \phi_k = \arcsin\left(\frac{2\gamma}{3\pi h_k}A_k^3\right), \quad k = 1,\,2. \tag{1.156}$$

The existence condition of these attractors is $|h_k| > (2\gamma/3\pi)(k\Omega)^{3/2}$. If either h_1 or h_2 vanishes, one of the limit cycles disappears and the other one shrinks to a fixed point which represents the familiar phase-locked soliton.

University of Cape Town

As h_k are increased, the two attractors start interacting with each other. One of them survives as a limit cycle but its partner undergoes the period-doubling route to chaos. It is confirmed in numerical simulations that a single soliton, a bound state of two solitons and the chaotic attractor are the only possible outcomes of the evolution of the initial condition in the form of the "pure" (i.e. unperturbed) NLS soliton.

In fact, the soliton may become chaotic even in presence of a one-frequency AC driving:

$$i\psi_t + \psi_{xx} + 2|\psi|^2\psi = h\exp(i\omega t) - i\gamma\psi. \tag{1.157}$$

The chaotisation occurs due to the resonance of the soliton with the external field. Some insight into this phenomenon can be gained by utilizing the second-order perturbation theory [203]. As the driving strength is increased, the period-doubling route to chaos take place. The emerging chaotic attractor is characterized by a quadratic return map.

Another approach to eq.(1.157) is based on the assumption that radiations with finite wavenumbers disperse away and only the long-wavelength radiation interacts significantly with the soliton. This allows to derive a finite-dimensional system for soliton's amplitude and phase and the amplitude of the long-wavelength radiation. The technique used involved a combination of the Hamiltonian approach with the perturbation theory based on the inverse scattering. The damping was added in an ad-hoc way [204]:

$$\begin{aligned}
\frac{dA}{dt} &= -\pi|c|A^2\cos\phi - 2\gamma A + 4\pi|c|^2 A\sin 2\phi + \frac{8}{\pi}fA|c\bar{\rho}|\sin(2\phi-\chi) + \\
&+ \gamma f|\bar{\rho}|\sin(\phi-\chi), && (1.158)\\
\frac{d\phi}{dt} &= \omega - A^2 + 2\pi|c|A\sin\phi + 2|c|^2\cos 2\phi - 4|c|^2 + \frac{4}{\pi}f|c\bar{\rho}|\cos(2\phi-\chi) + \\
&+ \frac{(2-\pi)\gamma}{\pi A}f|\bar{\rho}|\cos(\phi-\chi), && (1.159)\\
\frac{d\bar{\rho}}{dt} &= i\omega\bar{\rho} + 4iA|c|\,\mathrm{e}^{2i\phi} + i\pi\gamma\,\mathrm{e}^{i\phi} - \gamma\bar{\rho}, && (1.160)
\end{aligned}$$

where A is the soliton's amplitude, $c = ih/\omega$ is the background to which the soliton decays as $|x| \to \pm\infty$. $\phi = 2\phi_0 + \arg c$, $\bar{\rho} = \rho\exp(i\arg c)$ with ρ amplitude of the long-wavelength radiation and $\chi = \arg\bar{\rho}$. Finally, f is a phenomenological constant determined by comparing to numerical simulations. When the driving h (or $|c|$) and the damping γ are small, the soliton decouples from the radiation:

$$\begin{aligned}
A_t &= -2\gamma A - \pi|c|A^2\cos\phi, && (1.161)\\
\phi_t &= \omega - A^2 + 2\pi|c|A\sin\phi. && (1.162)
\end{aligned}$$

University of Cape Town

The decoupled system (1.161)-(1.162) has two attractors: the homogeneous forced oscillation

$$A = 0 \quad \text{and} \quad \phi = \omega t, \tag{1.163}$$

and the phase-locked soliton

$$A \approx \sqrt{\omega} \quad \text{and} \quad \cos\phi = -\frac{2\gamma}{\pi A|c|} \approx -\frac{2\sqrt{\omega}\gamma}{\pi|h|}, \tag{1.164}$$

where $\sin\phi > 0$. The existence condition of the phase-locked soliton is

$$\frac{2\sqrt{\omega}\gamma}{\pi|h|} < 1. \tag{1.165}$$

The analysis of the reduced system (1.158)-(1.160) was performed for the fixed $\gamma = 0.1$ and $\omega = 1$; h was variable and serve as the bifurcation parameter. When the driving is small, i.e. when condition (1.165) is not in place, the homogeneous oscillation (1.163) is the only attractor in the system. As h is increased, a phase-locked soliton is born. A further increase of the driving amplitude destabilises the soliton and as a result of the Hopf bifurcation, a soliton of periodically oscillating amplitude is born. Increasing the driving strength still further, leads to a chaotic attractor via a sequence of period-doubling bifurcations. For even larger values of h the chaotic soliton suddenly disappears and is replaced by the forced homogeneous oscillation. As the driving strength is further increased, the homogeneous solution looses its stability, and the spatiotemporal chaotic state sets in.

In [257] it is shown that spatiotemporal chaos may also occur via a quasi-periodic route.

The dependence of the finite-dimensional system (1.158)-(1.160) on the damping strength γ was studied in [245, 249]. This study confirmed that the period-doubling scenario of transition to spatiotemporal chaos is rather universal for not very large values of the damping. For large values of γ, there is no period-doubling. In this case the oscillating soliton does not destabilize as the driving strength is increased. My own studies of the externally driven damped NLS (not included in this thesis) reveal that for large values of γ the spatiotemporal chaos sets in through intermittency.

So far, our discussion of the AC-driven, damped NLS equation concerned only the case of small driving strengths and dissipation coefficients. We conclude our review of its solitons by mentioning Ref.[21] where eq.(1.157) was studied for arbitrarily large h and γ. The results include the existence and stability regions on the (h, γ)-plane. It was also

University of Cape Town

shown that irrespective of the value of γ, two (not one as it was assumed before) phase-locked solitons are born in the saddle-node bifurcation — and hence one of them is always unstable. The stability properties of the other soliton depend on γ. For $\gamma \lesssim 0.3$, the soliton is stable for small h but undergoes a Hopf bifurcation as h is increased above a certain threshold value. For $\gamma \gtrsim 0.3$ the soliton is stable in the whole interval of its existence. These properties are very similar to those of the *parametrically* driven NLS, to which chapters 2 and 3 of this thesis are devoted. The interest in the parametrically driven NLS was triggered by the fact that this equation appeared in hydrodynamical context [184] and nonlinear optics [93]. The parametrically driven NLS in *two* spatial dimensions is also attracting a lot of attention. Using a simple phase transformation $\psi(x,t) \to \mathrm{e}^{i(\Omega/2)t}\,\psi(x,t)$, the parametrically driven NLS (1.109) can be cast in the autonomous form:

$$i\psi_t + \psi_{xx} + 2|\psi|^2\psi - (\Omega/2)\psi = -i\gamma\psi + h\psi^*. \tag{1.166}$$

In chapters 2 and 3 of this thesis we set $(\Omega/2)$ to 1 by scaling the time variable. Alternatively, the damping γ can be fixed to unity:

$$i\psi_t + \psi_{xx} + 2|\psi|^2\psi - \sigma\psi = h\psi^* - i\psi. \tag{1.167}$$

In this case, the role of control parameters is played by the amplitude and frequency of the driver. This approach was adopted in [66].

In Ref.[259] explicit stationary constant-phase solutions (*cn*- and *dn*-noidal waves) were constructed and their stability examined. Non-constant-phase solutions were constructed perturbatively. It was shown that *cn*- and *dn*-noidal waves can bifurcate from zero and uniform solutions, respectively. Both types of the noidal waves undergo a Hopf bifurcation. Numerical simulations revealed a variety of periodic, quasi-periodic and chaotic motions. An oscillating soliton is found, numerically, as a special case of an oscillating *cn*-noidal wave.

Existence and stability of solitons in the parametrically driven damped NLS are the topics of Refs.[17] and [149]. In [17] it is shown that similarly to the externally driven NLS (1.157), two solitons are born in a saddle-node bifurcation and one of the two is unstable for all values of the damping and driving, while the other one can be stable in some parameter range. As h is increased, the stable stationary soliton looses its stability to a periodically oscillating soliton in a Hopf bifurcation. The transition between stable solitons and noidal waves was investigated in [75]. When the soliton becomes unstable with respect to the continuous spectrum excitations, it can either transform into a noidal wave or seed the spatiotemporal chaos. An extensive numerical study of possible transitions to chaos was

University of Cape Town

carried out in [38]. It was shown that there are two basic transition scenarios. In the first scenario, the soliton first undergoes the Hopf bifurcation and then a sequence of period-doubling bifurcations leads to a temporally chaotic soliton. As the driving amplitude is further increased, the chaotic soliton undergoes a crisis and the zero solution survives as the only attractor in the system. Increasing h still further, the zero solution is replaced by the spatiotemporal chaos. In the second scenario, the spatiotemporal chaos is ignited directly by the periodic soliton. No period-doubling bifurcations or flat solutions arise in the second scenario.

Refs.[17, 149, 38] do not investigate in detail the nonlinear stage of the instability for h near the Hopf bifurcation curve as well as the oscillatory instability which occurs in the undamped case. These are some of the issues that will be addressed in chapter 2 of this thesis.

University of Cape Town

1.2.3 Soliton-impurity interactions: the sine-Gordon equation

In this section we will discuss the dynamics of the sine-Gordon kinks and breathers in potentials created by δ-function-like terms.

We start with the damped-driven sine-Gordon equation with an impurity term of the form:

$$\phi_{tt} - \phi_{xx} + \sin\phi = -f - \gamma\phi_t - \mu\delta(x)\sin\phi. \tag{1.168}$$

It describes an inhomogeneity of the maximum Josephson current density. When μ is positive, the impurity is interpreted as a microshort, and $\mu < 0$ is a microshunt (microresistor). The above impurity term can be alternatively interpreted as resulting from an external AC magnetic field applied to the edge of a semi-infinite Josephson junction [208].

The motion of the kink in eq.(1.168) can be represented in the adiabatic approximation as a motion of a particle of mass $m = 8$ in the combination potential created by the driving term and the impurity [166]:

$$U(\xi) = \mp 2\pi f\xi + 2\mu\,\mathrm{sech}^2\xi. \tag{1.169}$$

There is also a friction force

$$F = -8\gamma\frac{d\xi}{dt}. \tag{1.170}$$

The potential created by the microshort being repulsive, it repels the kink regardless of its polarity. A microshunt, on the contrary, attracts the kink and antikink.

It can be shown that the velocity and position of the kink of eq.(1.168) satisfy

$$\frac{dv}{dt} = \pm \frac{\pi f}{4}(1-v^2)^{3/2} - \gamma v(1-v^2) + \\ + \frac{\mu}{2}(1-v^2)\,\mathrm{sech}^2\left(\frac{\xi}{\sqrt{1-v^2}}\right)\tanh\left(\frac{\xi}{\sqrt{1-v^2}}\right), \tag{1.171}$$

$$\frac{d\xi}{dt} = v - \frac{\mu}{2}\xi v\,\mathrm{sech}^2\left(\frac{\xi}{\sqrt{1-v^2}}\right)\tanh\left(\frac{\xi}{\sqrt{1-v^2}}\right). \tag{1.172}$$

The stationary point of this two-dimensional system is $v = 0$, $\xi = \xi_0$, where ξ_0 is the root of the equation

$$\frac{\pi f}{2\mu} + \mathrm{sech}^2(\xi_0)\tanh(\xi_0) = 0. \tag{1.173}$$

If the bias current f is sufficiently strong, the microshort slows the kink down but does not capture it. However, if the current is weak, the kink will loose all of its kinetic energy before reaching the repulsive impurity and then, after performing some oscillations, remain at the equilibrium position $\xi = \xi_0$. Equating the kink's kinetic energy $8\sqrt{1-v_\infty^2}$ to the energy stored at the microshort (2μ), one can obtain the threshold value for the bias current f for which the capture of the kink is possible:

$$f_{thr} = \frac{\gamma}{\pi}\sqrt{8\mu+\mu^2} \approx \frac{2\gamma}{\pi}\sqrt{2\mu}. \tag{1.174}$$

The capture of the kink by the *microshunt* ($\mu < 0$) is possible whenever $f < f_c = 4\sqrt{3}/(9\pi)$. To determine the threshold value it is necessary to use dynamical considerations [130, 133] equating dissipative energy loss to the kinetic energy. The threshold value of the bias current and the kink's velocity are given by

$$f_{thr}^2 = \frac{16}{\pi}\gamma^3\sqrt{2|\mu|}, \quad v_{thr} = 2^{21/8}\pi^{1/4}|\mu|^{3/8}\exp\left(-\sqrt{2/|\mu|}\right). \tag{1.175}$$

In the undamped, undriven case it is possible for the kink to be repelled by an attractive impurity if the kink's velocity lies within certain resonance "windows" [124]. If the incoming velocity of the kink is larger than some critical value v_c, the kink will pass through the impurity and escape in positive direction, loosing a part of its kinetic energy through radiation and excitation of an impurity mode. The relation between the incoming velocity v_i and the final velocity v_f is $v_f^2 = \alpha(v_i^2 - v_c^2)$, where α is a constant. However, if the incoming velocity of the kink is smaller than v_c, the kink cannot escape to infinity after the first collision, but will stop at a certain distance away and then return back due to the attraction potential of the impurity. For most velocities the kink will loose energy

University of Cape Town

again in the second collision and finally become trapped by the impurity. However, for some special incoming velocities the kink may escape to the negative infinity after the second collision. The reflection of the kink is possible only if the kink's velocity falls into a certain resonance window. This happens because during the first interaction with the impurity a localized impurity mode is excited and if the kink arrives back to the impurity at the right time, it will extinguish this mode and gain from it enough energy to recover the loss of kinetic energy and escape. (There is no damping in this case, $\gamma = 0$.) The favourable timing in this case means that the second collision coincides with the passage of the impurity oscillation through some phase angle characteristic of the impurity mode extinction. Thus the condition for the restoration of the kink's kinetic energy after the second interaction is found to be

$$T_{12}(v) = nT + \tau, \tag{1.176}$$

where T_{12} is the time between the first and second collisions, T the period of the impurity mode, τ an offset phase, and n is an integer. The resonant windows are given by

$$v_n^2 = v_c^2 - \frac{11.0153}{(nT + 0.3)^2}, \quad n = 1, 2, 3, \ldots. \tag{1.177}$$

Here v_c depends on the impurity strength μ, and coefficients have been calculated numerically. However, the higher-order resonances ($n = 2, 3 \ldots$) are not observed in simulations. (Instead, quasiresonances are found). This may be explained by radiation losses which were ignored in the above qualitative description.

The dissipative defects can be accounted for by adding the term $-\beta\delta(x)\phi_t$ to the right-hand side of eq.(1.168). This term will give rise to an additional friction force acting on the kink:

$$F = -4\beta\dot{\xi}\,\mathrm{sech}^2\xi. \tag{1.178}$$

The threshold value of the bias current for which the capture of the kink is possible, can be obtained in the limit $\beta \gg \sqrt{|\mu|} \gg \gamma$. In the case of microshort, it is given by

$$f_{thr} = \frac{2\gamma\beta}{\pi}, \tag{1.179}$$

while in the case of microshunt the threshold is

$$f_{thr} = \frac{\gamma\beta}{\pi}\left[3 + \left(1 - \frac{4\gamma\beta}{|\mu|}\right)^{1/2}\right]. \tag{1.180}$$

University of Cape Town

A damped-driven long Josephson junction with spatially varying inductance can be modelled by [230, 131]

$$\varphi_{tt} - \phi_{xx} + \sin\phi = -f - \gamma\phi_t + \nu\delta(x)\phi_x. \tag{1.181}$$

The motion of the fluxon can be again represented as a motion of a particle of mass $m = 8$ in the potential

$$U(\xi) = 4\nu \tanh\xi - 2\pi f\xi. \tag{1.182}$$

When the damping is small ($\gamma^2 \ll \nu$), the kink can be captured by this effective potential provided the bias current is smaller than

$$f_{thr} = \frac{4\gamma}{\pi}\sqrt{2\nu}. \tag{1.183}$$

Magnetic nonlinear excitations in a long Josephson junction with a finite size inhomogeneity can be described by

$$\phi_{tt} - [\varepsilon_1(x)\phi_x]_x + \varepsilon_2(x)\sin\phi = f - \gamma\phi_t, \tag{1.184}$$

where

$$\varepsilon_n = 1 + \varepsilon_n[\theta(x) - \theta(x - L)],\ n = 1,\ 2. \tag{1.185}$$

Here $\theta(x)$ is the Heaviside step function and L is the dimensionless length of the inhomogeneity. In this case the kink moves in the effective potential [126]

$$U(\xi) = 2(\varepsilon_1 + \varepsilon_2)[\tanh\xi - \tanh(\xi - L)] \pm 2\pi f\xi. \tag{1.186}$$

For $L \ll 1$, the critical value of the bias current which allows the kink to escape from the impurity is

$$f_c = \frac{4|\varepsilon_1 + \varepsilon_2|L}{3\sqrt{3}\pi}. \tag{1.187}$$

Under the condition $\varepsilon_1^2,\ \varepsilon_2^2 \gg \gamma$, the threshold value of the bias current sufficient for the kink's capture by the repulsive inhomogeneity ($\varepsilon_1 + \varepsilon_2 > 0$), is

$$f_{thr} = \frac{4\gamma}{\pi}\sqrt{(\varepsilon_1 + \varepsilon_2)\tanh\frac{L}{2}}. \tag{1.188}$$

When the inhomogeneity is attractive ($\varepsilon_1 + \varepsilon_2 < 0$), this threshold is given by

$$f_{thr} = \frac{8\gamma^{3/2}}{\pi}\left(|\varepsilon_1 + \varepsilon_2|\tanh\frac{L}{2}\right)^{1/4}\sqrt{K\left(\tanh\frac{L}{2}\right)}, \tag{1.189}$$

University of Cape Town

where $K(z)$ is the complete elliptic integral of the first kind. A point-like attractive impurity cannot capture more than one kink. However, if the inhomogeneity has a finite size, such a capture is possible and the critical length L_c of the inhomogeneity allowing the capture of two kinks in the undamped case, is

$$L_c = \frac{1}{2} \ln \left(\frac{2}{\varepsilon_1 + \varepsilon_2} + 1 \right) \approx \ln \left(\varepsilon_1 + \varepsilon_2 \right)^{-1/2}. \tag{1.190}$$

In the case of the repulsive point-like impurity the capture of two kinks is possible for $f \neq 0$ and the corresponding f_c is less than the threshold value for a single kink.

The SG breathers can be frequency-locked to the impurity [208]. This phenomenon occurs in long Josephson tunnel junction modelled by

$$\phi_{tt} - \phi_{xx} + \sin \phi = -\gamma \phi_t, \tag{1.191}$$

$$\phi_x(0) = 0, \quad \phi_x(l) = a \sin \omega t, \tag{1.192}$$

where l is the junction length. The driving applied at the right boundary of the junction can be interpreted as a $\delta(x - l)$ impurity. The root-mean-square value of the emitted voltage, $\sqrt{\langle \phi_t^2 \rangle}$, plotted versus the impurity strength a forms a hysteresis loop. The quasilinear standing waves sustain one of the branches, while the other is sustained by a breather frequency locked to the frequency of the driver. Similar hysteresis also takes place in a system with the external driving, $\sin \omega t$.

If the breather is not close to the threshold decay into a kink-antikink pair, i.e. when the period of its internal oscillations $\tau = 2\pi / \cos A$ is much smaller than the characteristic time scale induced by the perturbation $\nu \delta(x)$, it is natural to average the full Hamiltonian of the system with respect to the fast internal oscillations and represent the motion of the breather as a motion of a particle of mass $m = 16 \sin A$ moving in the potential [174]

$$U(\xi) = -\frac{8\nu \cot A \cosh \left(\sin A\xi \right)}{\left[1 + \cot^2 A \cosh^2 \left(\sin A\xi \right) \right]^{3/2}}. \tag{1.193}$$

When the internal frequency is large enough: $\cos^2 A > 1/3$, this is a one-well attractive potential with the minimum at the origin. When $\cos^2 A < 1/3$, eq.(1.193) gives a double-well attractive potential. The low-frequency breather will oscillate inside either of the two potential wells and as a result of the resonance between the internal oscillations of the breather and its oscillations in the well, the dynamics may become chaotic.

As a result of the interaction with a localized inhomogeneity the low-frequency breather may dissociate into a kink-antikink pair [170]. This may also happen as a result

University of Cape Town

of the scattering on an Abrikosov vortex (described by the perturbation of the form $\nu\delta'(x)$), when $\cos A < 1/2\nu v$, where v is the initial velocity of the breather [92].

Numerical simulations reveal more scenarios of the breather-impurity interactions [291]. In particular, the outcome of the scattering exhibits a sensitive dependence on the initial phase of the breather. (This result has not received and analytical explanation so far.) For example, a breather with an intermediate frequency slightly greater than $1/\sqrt{3}$ and low velocity can pass through an attractive impurity, be trapped or repelled by it depending on its initial phase. The interaction of a low-frequency ($\omega < 1/\sqrt{3}$) breather with an attractive impurity depends on its initial phase as well. Depending on the phase, the repulsion, attraction, passage through and dissociation into a kink-antikink pair is possible. The most surprising fact is that the breather can split even when its energy is less than 16 (which is double the kink energy at rest). The scattering of low-frequency breathers on *repulsive* impurity is both initial phase- and initial velocity-sensitive. If its velocity is less than $v_{c_1} \approx 3^{-3/4}(\nu/\sqrt{1-\omega^2})^{1/2}$, the breather is repelled for all initial phases. On the other hand, if the breather's velocity is greater than some critical value $v_{c_2} > v_{c_1}$, it will always pass through the impurity. And when $v \in [v_{c_1}, v_{c_2}]$, the breather can be repelled, trapped or can pass through the impurity, depending on its initial phase. Next, the attractive inhomogeneity can support a localized impurity mode which oscillates with the frequency $\omega_{imp} \approx \sqrt{1-\nu^2/4}$. If the breather's frequency is close to ω_{imp}, the impurity mode can be excited as a result of this scattering. Irrespectively of its initial phase, in this case the small-amplitude breather will be trapped, if its velocity is low, or pass through the impurity, if its velocity is high. On the other hand, high-frequency breather behaves like a hard particle when scattered on a repulsive impurity. It passes through the impurity if its velocity is larger than $v_c = (0.5\nu\omega\sqrt{1-8\omega^2})^{1/2}$, and is repelled otherwise.

University of Cape Town

1.2.4 Soliton-impurity interaction in the NLS equation

The interaction of the nonlinear Shrödinger solitons with impurity is not so well documented. The NLS equation with the δ-function term

$$i\psi_t + \psi_{xx} + 2|\psi|^2\psi = \varepsilon\delta(x)\psi \tag{1.194}$$

was introduced as a model of the crystal with impurity [125]. As expected from an impurity, this term changes, locally, the spectrum of linear excitations. The nonstationary

impurity is modelled by the right-hand side of the form [1]:

$$i\psi_t + \psi_{xx} + 2|\psi|^2\psi = \varepsilon\delta[x + \varphi(t)]\psi, \tag{1.195}$$

where $\varphi(t)$ characterises the motion of the impurity on the x-axis. The trajectory can be either periodic: $\varphi(t) = \varphi_0 \cos \Omega t$, or random, where $\varphi(t)$ is the Gaussian δ-correlated random process with properties $\langle\varphi\rangle = 0$ and $\langle\varphi(t)\,\varphi(t')\rangle = 2\sigma_\varphi^2\delta(t - t')$. In either case the evolution equations for the soliton's parameters are [1]

$$\frac{d\xi}{dt} = -\frac{\varepsilon}{2}A^2 \operatorname{sech}^2 z_0 \tanh z_0, \tag{1.196}$$

$$\frac{dx_0}{dt} = -4\xi, \tag{1.197}$$

$$\frac{d\phi}{dt} = 4\xi^2 - A^2 + \ldots, \tag{1.198}$$

and $A = A_0$. In eqs.(1.196)-(1.198),

$$x_0 = -4\int_0^t \xi(t)\,dt, \quad z_0 = -A[x_0 + \varphi(t)]. \tag{1.199}$$

Eliminating ξ between (1.196) and (1.197) gives the equation for the soliton's position:

$$\frac{d^2x_0}{dt^2} = 8\varepsilon \operatorname{sech}^2 z_0 \tanh z_0. \tag{1.200}$$

Defining $y = -z_0$, one obtains the equation

$$\frac{d^2y}{dt^2} = A\varphi''(t) + 2\varepsilon A^3 \operatorname{sech}^2 y \tanh y \equiv f(t) - \frac{\partial U}{\partial y}, \tag{1.201}$$

which describes the motion of a particle of unit mass in the potential field $U(y)$ and under the action of nonconservative force $f(t)$. Assume $\varphi(t)$ is periodic and let ω denote the frequency of the corresponding local mode. Nonlinear resonances in the motion of the particle arise provided

$$(2m + 1)\omega = \Omega. \tag{1.202}$$

The motion can become chaotic if the width of an individual nonlinear resonance is larger than the distance between the consecutive resonances:

$$\frac{32\varphi_0\Omega\sqrt{\pi}}{\omega} \geq 1. \tag{1.203}$$

The envelope solitons of the nonlinear monoatomic chain with the nearest-neighbours interaction can be described in the continuous limit by [134]:

$$i\psi_t + \psi_{xx} + 2|\psi|^2\psi = \frac{\gamma}{2}(\mu\psi - i\nu\psi_t + i\psi_x)\,[\delta(x) + \delta(x - D)]. \tag{1.204}$$

University of Cape Town

The reflection coefficient of a single impurity placed at the origin is

$$R_1 = \frac{\pi\mu\gamma EA^4}{16}\int_{-1/\alpha}^{\infty}(y^2+1)^2\,\mathrm{sech}^2(\pi y/2)\,dy, \tag{1.205}$$

where E is the energy of the soliton's radiation and $\alpha = A/(2\xi)$ the spectral value for which the spectral energy density emitted by the soliton, attains its maximum. The reflection coefficient for two impurities is

$$R \approx 2R_1 + \frac{4\mu\gamma E\alpha}{A}\,\mathrm{e}^{-\pi/\alpha}\cos(2B), \tag{1.206}$$

where $B = 2D\mu\xi^2$. The oscillatory dependence of the reflection coefficients implies that the resonant scattering of solitons takes place.

In [37] stationary localized solutions of equation

$$i\psi_t + \psi_{xx} + \beta|\psi|^2\psi = q\delta(x)\psi \tag{1.207}$$

are investigated for different combinations of signs of β and q. It is shown that solitons exist for the following combinations: ($\beta > 0$, $q < 0$), ($\beta > 0$, $q < 0$) and ($\beta < 0$, $q < 0$). Point-like inhomogeneities with $Q < 0$ form a potential well; therefore for both signs of β solitons are predicted to be stable in this case. When $Q > 0$, solitons are predicted to be unstable.

It would be interesting to find out how the pinned solitons respond to damping and driving terms, as well as to perform a more detailed analysis of arising instabilities. We will return to these topics in chapter 3.

University of Cape Town

1.3 Localized solutions in systems of reaction-diffusion equations

1.3.1 Travelling waves in one spatial dimension

In this section we will consider the other basic type of equations that support solitary waves, namely the dissipative (parabolic) systems. A particular example of dissipative systems are the reaction-diffusion systems where localized solutions arise as a result of the balance between the diffusion (dissipation) and the nonlinearity (reaction forces).

Unlike the linear wave equation (1.2) which is hyperbolic and propagates any wave profile with the same speed c, each travelling wave solution of a reaction-diffusion equation is allowed to propagate only with its own specific velocity. The construction and study

of pulse-like solutions of nonlinear parabolic systems is important not only in connection with the applications of the solitary waves *per se*, but also due to their role in gaining a better understanding of phenomena in large domains, where the arising patterns may resemble (at least locally) travelling waves.

Until recent years the attention was focused on problems concerning plane waves, i.e. waves moving through $\mathbb{R}^n$ in a fixed direction, having translational symmetry in any direction perpendicular to that of the motion. For some time, chemists and others observed many strange wave-like structures in systems that could be modelled via reaction-diffusion equations. Spiral and scroll waves are well documented within certain chemical reactions [276].

In many of the applications of reaction-diffusion systems it is the long-term behaviour of solutions that is important. The interest is focused on equilibrium states which display inhomogeneous spatial patterns. An example of such process is the morphogenesis. During this process embryonic cells must somehow order themselves so as to lay down the differentiated structures (organs, limbs, etc .) which constitute a recognizable individual. One theory put forward to explain this phenomena is that the development follows a kind of map, or prepattern, laid down within the growing cell mass by chemicals called morphogens. These are assumed to react and diffuse through the medium. This theory rests upon the ability of the resulting model to exhibit stable solutions with a high degree of pattern. The morphogen theory is by no means universally accepted by theoretical biologists. The problem is that no real morphogens have been identified, so the models remain phenomenological. Another area where the patterned equilibria are of interest, is the populational biology [157], [193], [206]. The idea that individuals of different species separate out from each other as a result of the interspecific competition, has led to mathematical models consisting of systems of coupled reaction-diffusion equations.

In many of the applications of reaction-diffusion systems, interest is centered upon so-called excitable systems and their wave-like pulse solutions. Excitability may be thought of as a property of the reaction kinetics, and is defined as follows: consider a system of ordinary differential equations

$$\vec{u}_t = \vec{F}(\vec{u}),$$

where $\vec{u} = 0$ is a locally stable equilibrium, i.e. the Jacobian matrix $\partial F_i/\partial u_j$ possesses only eigenvalues with negative real parts. By definition, small perturbations will decay exponentially as $t \to \infty$. Larger perturbations may behave differently depending on the nonlinearity in the reaction terms in $\vec{F}$. The system is called excitable if th ere are in-

University of Cape Town

termediate sized perturbations of the resting equilibrium which result in time-dependent solutions taking a prolonged excursion through the state space before returning to rest. The divide between the two qualitatively different kinds of behaviour is known as a threshold effect. Sub-threshold excitations result in a simple return to the quiescent equilibrium, $\vec{u} = 0$, while super-threshold excitations result in trajectories which sweep the state towards some excited regime before returning back, perhaps via a prolonged cycle of behaviour, towards the quiescent equilibrium.

A simple example of an excitable system is given by the following system of ODEs:

$$u_t = f(u) - v, \tag{1.208}$$

$$v_t = \varepsilon(u - v), \tag{1.209}$$

where $f(u) = u(u-a)(1-u)$ and $a \in (0, 1/2)$. Here $0 < \varepsilon \ll 1$, so that v_t is small compared to u_t. Hence, v is called the slow variable and only dominates the behaviour of the system while $f(u) \approx v$, but even then v_t is small and v changes slowly. By analogy, u is called the fast variable. When $f(u) \neq v$, the fast eq.(1.208) dominates the behaviour of the system until such times as u_t and v_t are both $O(\varepsilon)$.

One can check that the fixed point, $(u, v) = (0, 0)$, is locally stable. Indeed, the eigenvalues of the Jacobi matrix are

$$\lambda_{1,2} = \frac{-(a+\varepsilon) \pm \sqrt{(a-\varepsilon)^2 - 4\varepsilon}}{2}.$$

Small perturbations result in trajectories which will return quickly to the equilibrium. It can be shown numerically that larger perturbations result in much more distinct behaviour.

For most excitable systems the requirement of a locally stable equilibrium is relatively easy to check, but threshold-type phenomena are harder to be found. Sometimes it is possible to prove that solution to a system of reaction diffusion system exists without solving it. In [244] theorems of existence and uniqueness of local and global in time solutions are proved.

Existence and uniqueness theorems

Consider the system of reaction-diffusion equations:

$$\vec{u}_t = D\vec{u}_{xx} + \vec{f}(\vec{u}),\ x \in \mathbb{R},\ t > 0,$$

University of Cape Town

where D is a diagonal matrix. We supplement this system by initial condition

$$\vec{u}(x,0) = \vec{u}_0(x), \quad x \in \Omega \subset \mathbb{R}. \tag{1.210}$$

Assume t hat $\vec{u}_0(x)$ is in a Banach space, B. Then there exists time $t_0 > 0$ that depends only on $||\vec{u}_0(x)||$ and the reaction terms $\vec{f}$, such that the system has a unique smooth solution for $t \in [0, t_0]$. The norm of this solution is bounded: $||\vec{u}|| \leq 2||\vec{u}_0||$. The result of this theorem can be extended if we know a priori that the L_∞-norm of the solution is bounded for all times $0 \leq t \leq T \leq \infty$. In this case the solution exists for all $0 \leq t \leq T$ and is in the same admissible Banach space B as the initial condition. The requirement for the solution to be bounded is a realistic one and does not restrict the applicability of the theorem because most of the rd-systems model some realistic processes and therefore one should expect that solutions will be bounded.

The proof of the global in time existence and uniqueness of solutions uses the notion of invariant regions. The definition is as follows.

Definition. A close subset $\Sigma \subset \mathbb{R}^n$ is called an *invariant region* for the local solution defined by (1.3.1-1.210), if any solution $\vec{u}(x,\, t)$ having all of its boundary and initial values in Σ, satisfies $\vec{u}(x,\, t) \in \Sigma$ for all $x \in \Omega$ and for all $t \in [0,\, \delta)$.

The global existence theorem states that if the initial condition $\vec{u}_0(x) \in B$ and $\vec{u}_0(x) \to 0$ as $x \to \infty$, and if the system admits a bounded invariant region Σ, and $\vec{u}_0(x) \in \Sigma$ for all $x \in \mathbb{R}$, then the solution exists for all $t > 0$. In particular, it can be proved that if D i s the identity matrix, $\mathbf{I}$, than any convex region Σ in which the nonlinearity f points into Σ on $\partial\Sigma$, is invariant for the system.

To illustrate the applicability of this theorem, let us consider the FitzHugh-Nagumo system where diffusion is added to both components:

$$u_t = u_{xx} + f(u) - v, \tag{1.211}$$

$$v_t = \varepsilon v_{xx} + \sigma(u - v). \tag{1.212}$$

Here $\sigma > 0$ and $\varepsilon \geq 0$ are constants. The function $f(u) = u(u-a)(1-u)$ where $0 \leq a \leq 1/2$. To prove that the solution to this system exists, we need to construct a sequence of arbitrary large invariant rectangles. Let us consider a two-component vector field consisting of the reaction terms of each of the equations: $\vec{F} = (f(u) - v,\, u - v)$. Now, consider the plot of nullclines on the $(u,\, v)$-plane (fig.1.2). It is clear that above the curve $f(u) - v = 0$ the first component of $\vec{F}$ will be negative and below the curve it will be positive. The same applies to the nullcline $u - v = 0$. Now we need to construct

University of Cape Town

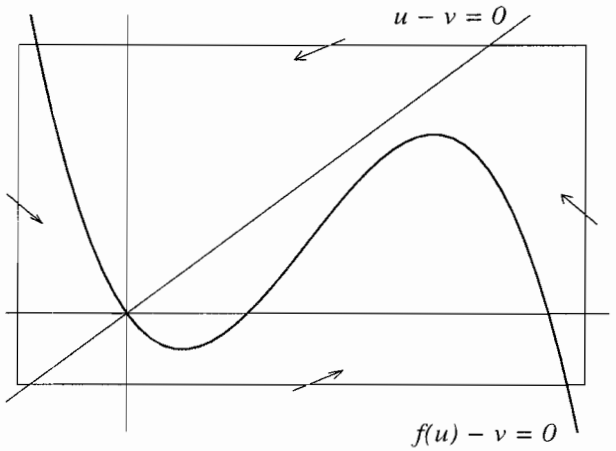

Figure 1.2: Nullclines of the system (1.211)-(1.212).

the rectangles in such a way that $\vec{F}$ points into their internality (these rectangles will be invariant for the system). The invariant rectangle Σ can be constructed as follows: the upper line $v = const$ is chosen so that both components of $\vec{F}$ are negative while on the lower one, they are both positive. On the left line $u = const$ the first component is positive ands the second one negative. On the right line $u = const$ polarity of the components is reversed: the first one negative, the second one positive. Now, as it is clarified by the picture, the vector field consisting of nonlinear terms of the equations points into the rectangle Σ and therefore this rectangle is invariant. Since we can construct an arbitrary large rectangle with the same features, we conclude that the solution exists for all $t > 0$ provided that the initial condition $u_0(x) \to 0$ as $x \to \infty$ and $u_0(x) \in B$.

In the same book, [244], there is a comparison theorem that relates the solution of a system of RD equations and the solution of the associated system of ODEs. This theorem can be used to locate the attracting regions on the phase plane.

Theorem Consider the system:

$$\vec{u}_t = D\Delta\vec{u} + \vec{f}(\vec{u}, t), \quad (x, t) \in \Omega \subset \mathbb{R}^m \times \mathbb{R}_+, \tag{1.213}$$

where Ω is bounded, $\partial\Omega$ is smooth and $\vec{f}$ is a smooth mapping. Here D is a diagonal matrix with constant nonnegative entries. Assume that this system admits bounded invariant region

$$\Sigma = \prod_{i=1}^{n} [a_i, b_i]$$

where $-\infty < a_i < b_i < \infty$. We supplement this system with initial conditions:

$$\vec{u}(x, 0) = \vec{u}_0(x),$$

University of Cape Town

where $\vec{u}_0(x) \in \Sigma$ for all $x \in \Omega$. We assume homogeneous Neumann boundary conditions:

$$\frac{d\vec{u}}{dn} = 0, \text{ on } \partial\Omega \times \mathbb{R}_+,$$

where d/dn denotes differentiation in the outward normal direction on $\partial\Omega$.

We will construct a system of ODEs associated with the initial system of PDEs, so that solutions of the PDEs will be sandwiched between solutions of the associated ODEs.

Consider the partition of the set $\mathbb{Z}_n = 1, \ldots, n$ into two disjoint sets σ_M and σ_m. For such a partition we define functions f_i^+ and f_i^- by

$$f_i^+(\vec{u}, t) = \sup_{\substack{a_j \le \xi_j \le u_j,\ j \in \sigma_M,\ j \ne i \\ u_j \le \xi_j \le b_j,\ j \in \sigma_m,\ j \ne i}} f_i(\xi_1, \ldots, u_i, \ldots, \xi_n),$$

$$f_i^-(\vec{u}, t) = \inf_{\substack{a_j \le \xi_j \le u_j,\ j \in \sigma_M,\ j \ne i \\ u_j \le \xi_j \le b_j,\ j \in \sigma_m,\ j \ne i}} f_i(\xi_1, \ldots, u_i, \ldots, \xi_n).$$

The functions f_i^+ are nondecreasing while f_i^- are nonincreasing. It can be proved that these functions are Lipschitz in $\vec{u}$. Then we set

$$h_i(\vec{v}, t) = \begin{cases} f_i^+(\vec{v}, t),\ i \in \sigma_M \\ f_i^-(\vec{v}, t),\ i \in \sigma_m \end{cases} \tag{1.214}$$

and

$$H_{\sigma_M}(\vec{v}, t) = (h_1(\vec{v}, t), \ldots, h_n(\vec{v}, t)).$$

There are 2^n functions H_{σ_M} for a given integer n. The functions H_{σ_M} will be considered as vector fields, and the orbits of the associated flows will define the "comparison" functions.

Now let $\vec{v}(t)$ be solution of the following problem:

$$\dot{\vec{v}} = H_{\sigma_M}(t), \quad \vec{v}(0) = \vec{v^0} \tag{1.215}$$

$$v_i^0 = \begin{cases} \sup_{x \in \Omega} u_i^0,\ i \in \sigma_M \\ \inf_{x \in \Omega} u_i^0,\ i \in \sigma_n \end{cases}$$

This initial value problem has a unique solution.

The comparison theorem states that the solutions of the PDE (1.213) and ODE (1.215) are related by the following inequalities for all $(x,\ t) \in \Omega \times \mathbb{R}_+$:

$$v_i(t) \ge u_i(x, t),\ i \in \sigma_M$$

$$u_i(x, t) \ge v_i(t),\ i \in \sigma_m.$$

University of Cape Town

Now let us exemplify the above theorem by a system that models predator-prey interaction between species. The equations are of the form:

$$u_t = \alpha\Delta u + uM(u,v), \tag{1.216}$$

$$v_t = \beta\Delta v + uN(u,v). \tag{1.217}$$

Here u and v denote the population densities of the prey and predator, and the functions M and N are the corresponding (nonlinear) growth rates. The predator-prey interaction is defined by the following conditions:

$$M_v < 0, \quad N_u > 0,$$

which state that the prey growth rate decreases as the predator population increases, and that the increase in prey is favourable for the growth rate of the predator. Consider a specific example

$$M(u,v) = -(u-d)(u-1) - cv, \quad N(u,v) = -\mu - \alpha v + cu, \tag{1.218}$$

where d, c, μ, α are constants; $0 < d < 1$, c, $\alpha\mu > 0$, $d < \mu/c < 1$. We consider initial conditions

$$u(x,0) = u_0(x), \quad v(x,0) = v_0(x), \quad x \in \Omega,$$

and homogeneous Neumann boundary conditions

$$\frac{du}{dn} = \frac{dv}{dn} = 0, \quad (x,t) \in \partial\Omega \times \mathbb{R}_+.$$

This system (1.216-1.217) admits arbitrary large bounded invariant rectangles in the first quadrant $u \geq 0$, $v \geq 0$. Thus, if $u_0 \geq 0$, $v_0 \geq 0$ in Ω, then this problem has a unique solution for all $t > 0$ and $u(x,\, t) \geq 0$ and $v(x,\, t) \geq 0$ for all $(x,t) \in \Omega \times \mathbb{R}_+$.

We let $\Sigma = (u,\, v) : 0 \leq u \leq a,\, 0 \leq u \leq b$ be an invariant rectangle. Define the maximal vector field relative to Σ, $(uM^+,\, vN^+)$, as

$$uM^+(u,v) = \sup_{0\leq\xi\leq v} uM^+(u,\xi) = u \sup_{0\leq\xi\leq v} M^+(u,\xi)$$

$$vN^+(u,v) = \sup_{0\leq\xi\leq u} vN^+(\xi,v) = u \sup_{0\leq\xi\leq u} N^+(\xi,v).$$

Denote by $(u^+,\, v^+)$ the solution of

$$\dot{u} = uM^+(u,v), \quad \dot{v} = vN^+(u,v), \quad (u(0),v(0)) = (U,V),$$

University of Cape Town

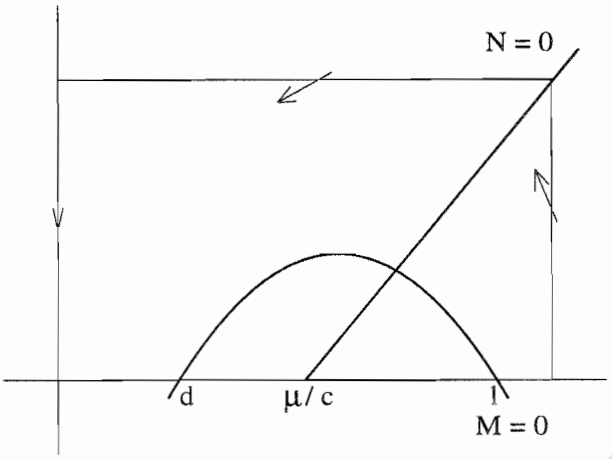

Figure 1.3: Nullclines of the system (1.218).

where

$$(U, V) = \left(\sup_{\bar{\Omega}} u_0(x), \sup_{\bar{\Omega}} v_0(x) \right).$$

Then according to the comparison theorem we have the estimates:

$$0 \leq u(x,t) \leq u^+(t), \quad 0 \leq v(x,t) \leq v^+(t), \quad (x,t) \in \Omega \times \mathbb{R}^+.$$

These enable us to obtain qualitative information concerning the solution (u, v). For example, if $u_0(x) < d$ for all $x \in \Omega$ then we see from fig.1.3 that $(u^+(t), v^+(t))$ tends to $(0, 0)$ as $t \to +\infty$. Furthermore, it is easy to see that the rectangle R is a global attractor for all solutions of the RD-system in the sense that given any neighbourhood of R, there is a $T > 0$ such that if $t > T$, $(u(x,t), v(x,t))$ lies in this neighbourhood for all $x \in \Omega$.

1.3.2 Pulses in the FitzHugh-Nagumo equation

The ideas embodied in the use of fast and slow variables are useful. Simply being able to assume that there are fast variables, u_j, which are almost instantaneously at pseudo-equilibrium ($u_j \approx 0$), means that the system is restricted to a neighbourhood of a lower-dimensional surface where each $u_j = 0$. The slow variables then describe the dynamis of the system over this surface. If the surface is folded over, trajectories may fall off at a fold and then be shifted rapidly by the fast variables on to another branch of the same surface. It can be shown numerically that for the problem at hand this is indeed the case. With the exception of an initial transient, and possibly a subsequent switch between branches, the solution remains near the pseudo-equilibrium curve $v = f(u)$.

University of Cape Town

Clearly, for any given system, if there are any small parameters available, and a consequent fast-slow classification of the state variables, it is much easier to look for threshold behaviour and excitability. The fast-slow construction is equivalent to the techniques of matching asymptotic expansions and two-timing in asymptotic analysis.

When a diffusion term is added to the fast equation, the system reads:

$$u_t = u_{xx} + f(u) - v \tag{1.219}$$

$$v_t = \varepsilon(u - v). \tag{1.220}$$

This system is known as FitzHugh-Nagumo model for the conduction of nerve impulses along unmyelinated nerve axon [225]. We are looking for a wave solutions to this system. The idea is that as the wave passes through a point, the behaviour of the state is similar to the time course of the excited trajectories of the ODE system. The initial excitation is supplied by diffusive interaction with neighbouring points already excited by the earlier arrival of the wave. Thus, the wave propagation goes by successive neighbourhoods stimulating one another, via the diffusion in the fast variables, to become super-threshold. In one dimension this system possesses a travelling wave solution, i .e. a pulse moving with some constant speed, c, without changing its shape.

Unfortunately, when we look for a solution depending on x and t only in combination $z = x - ct$, we are forced to analyze a nonlinear first-order system of ODEs defined on $\mathbb{R}^3$. This is not straightforward as the wave speed, c, is to be determined simultaneously with the wave profile. However, some qualitative insight into behaviour of solutions can be gained by defining fast and slow variables as we describe now.

By exploiting a small parameter present in the system, one can construct travelling wave solution assuming the existence of internal transitional layers. Away from such layers we may solve a system of reduced order, whilst the behaviour of the layer profile must be obtained by a suitable rescaling of the independent travelling variable. We rescale the x-variable in such a way that the diffusion coefficient becomes $O(\varepsilon^2)$, where $\varepsilon > 0$ is very small. Let as also rescale the time by introducing a long time scale $\tau = \varepsilon t$. Then the system (1.219-1.220) becomes:

$$\varepsilon u_t = \varepsilon^2 u_{xx} + f(u) - v, \tag{1.221}$$

$$v_t = u - v. \tag{1.222}$$

Next, we introduce the travelling-wave variable $z = x - ct$ and seek for solutions $u = U(z)$, $v = V(z)$ representing a wave moving to the right with velocity $c > 0$. Eqs.(1.221-

University of Cape Town

1.222) become

$$\varepsilon^2 U_{zz} + \varepsilon c U_z + f(U) - V = 0, \tag{1.223}$$

$$cV_z + U - V = 0. \tag{1.224}$$

We also assume that $c = \mathrm{O}(\varepsilon^0)$ or smaller. Since $0 < \varepsilon \ll 1$, the first equation is in equilibrium provided that the leading terms are in equilibrium, i.e. $V \approx f(U)$. Thus, trajectories on the (U, V)-plane will stay close to this curve except near to one or two points where they may jump from branch to branch. U_{zz} and U_z are large in such events. The solution we are seeking for, has two transition layers, one at $z = 0$, where the fast variable, U, shifts rapidly to the excited regime, and one at $z = z_1 < 0$ where the fast variable jumps before returning to the rest state. The up-jump at the forward transition layer at $z = 0$ is called wave front, whilst the down-jump at $z = z_1$ is called wave back. Both front and back move with velocity $c > 0$ in time with respect to the x-frame.

To construct the pulse solution , we must specify the solution away from the transition layer, and then construct the transition profiles and determine the positive wave speed, c, and the pulses width, z_1, in the process.

Away from neighbourhoods of $z = 0$ and $z = z_1$, we have

$$V \approx f(U), \tag{1.225}$$

$$cV_z + U - V \approx 0, \tag{1.226}$$

since ε is small and U_z, U_{zz} are assumed to be bounded. For $z > 0$ or $z < z_1$ we assume that the inverse of $f(U)$ is defined by its leftmost branch $U = h_-(V)$. For $z \in (z_1, 0)$ U is in the excitable regime and we define the inverse of $f(U)$ as $U = h_+(V)$, where $h_+(V)$ is the rightmost branch of the cubic. Thus, for $z > 0$, we have

$$U = h_-(V), \tag{1.227}$$

$$cV_z = V - h_-(V), \tag{1.228}$$

$$\lim_{z \to +\infty} V = 0, \quad V(0) = V_0, \tag{1.229}$$

where V_0 is a constant to be determined. For $z < z_1 < 0$ we have

$$U = h_-(V), \tag{1.230}$$

$$cV_z = V - h_-(V), \tag{1.231}$$

$$\lim_{z \to -\infty} V = 0, \quad V(z_1) = V_1, \tag{1.232}$$

University of Cape Town

where V_1 is a constant to be determined. Finally, for $z \in (z_1, 0)$ we have

$$U = h_+(V), \tag{1.233}$$

$$cV_z = V - h_+(V), \tag{1.234}$$

$$V(z_1) = V_1, \quad V(z_0) = V_0. \tag{1.235}$$

In (1.228) we require $V \to 0$ as $z \to +\infty$ but $V = 0$ is an unstable equilibrium and, consequently, we must choose $V \equiv 0$ for $z > 0$ and $V(0) = V_0 = 0$. In (1.234) we have $V_z < 0$. By choosing z_1 we fix V_1 and vice verse. If we choose $V(z_1) = V_1 \in (0, V_{max})$, there is a smooth solution that satisfies the boundary conditions. If we fix the constant $V_1 \in (0, V_{max})$, then, since $V = 0$ i s an unstable equilibrium, it is possible to find a smooth solution of (1.231) in the half-line $z < z_1$ satisfying $V(z_1) = V_1$ and $V \to 0$ as $z \to -\infty$.

In this way we have constructed the solution away from z_1 and 0. We need yet to determine the velocity c and the constant V_1 (or z_1). The velocity is fixed by the front of the pulse, at $z = 0$, while V_1 is fixed by the back of the pulse, at $z = z_1$.

Consider a neighbouhood of $z = 0$. Here the slow variable V was matched whilst the fast variable U must have a jump from $U = h_-(V_0) = 0$ to $U = h_+(V_0) = 1$. Introducing a scaled independent variable, $\xi = z/\varepsilon$, and setting $U = \phi(\xi)$, $V = \psi(\xi)$ near $z = 0$, the system (1.221-1.222) becomes

$$\phi_{\xi\xi} + c\phi_\xi + f(\phi) - \psi = 0 \tag{1.236}$$

$$\phi \to 1 \text{ as } \xi \to \infty, \quad \phi \to 1 \text{ as } \xi \to -\infty$$

$$c\psi_\xi + \varepsilon(\phi - \psi) = 0 \tag{1.237}$$

$$\psi \to V_0 = 0 \text{ as } |\xi| \to \infty.$$

Now the term proportional to ε in the second equation is negligible and, consequently, $\psi \equiv 0$. The first equation has a unique solution (ϕ, c). Indeed, $\phi(\xi) = [1 + \exp(\xi/\sqrt{2})]^{-1}$ and $c = \sqrt{2}(1/2 - a)$ are uniquely determined. This can be shown by reducing the order of the ODE by introducing a new variable $p = \phi_\xi$ and then solving for $p = p(\phi)$. Notice that if $a \in (0, 1/2)$, the velocity $c > 0$.

Consider the back of the pulse at $z = z_1$. Set $\varepsilon\xi = (z - z_1)$ and let $U = \phi(\xi)$, $V = \psi(\xi)$ near $z = z_1$. Now the system can be rewritten as

$$\phi_{\xi\xi} + c\phi_\xi + f(\phi) - \psi = 0, \tag{1.238}$$

University of Cape Town

$$\phi \to h_+(V_1) \text{ as } \xi \to +\infty; \quad \phi \to h_-(V_1) \text{ as } \xi \to -\infty, \tag{1.239}$$

$$-c\psi_\xi + \varepsilon(\phi - \psi) = 0, \tag{1.240}$$

$$\psi \to V_1 \text{ as } |\xi| \to \infty. \tag{1.241}$$

As $\varepsilon \to \infty$, t he equation for ψ, (1.240), can be solved explicitly: $\psi \equiv V_1$, and the system reduces to

$$\phi_{\xi\xi} + c\phi_\xi + f(\phi) - V_1 = 0 \tag{1.242}$$

$$\phi \to h_+(V_1) \text{ as } \xi \to +\infty; \quad \phi \to h_-(V_1) \text{ as } \xi \to -\infty. \tag{1.243}$$

Because V_1 takes values between 0 and V_{max} and since there is a value V^* for which $c = 0$, the function $c(V_1)$ is monotonously decreasing with maximum at $V_1 = 0$ and minimum at $V_1 = V_{max}$. Therefore, having found V_1 we fix the value of c. As before, the slow equations

$$cV_2 + h_\pm(V) - V = 0$$

control the behaviour of solutions between the transition layers.

1.3.3 Localized structures in higher dimensions: spirals and scrolls

The main motivation for studying planar and nonplanar wave type solutions to reaction-diffusion equations lies in their applications to problems in physiology, biology and chemistry. For example, the Hodgkin-Huxley equations [99] provide a model for the electrical activity in membranes of living organisms. In one dimension, the Hodgekin-Huxley equations arise as a model for the propagation of action potentials along an unmyelinated nerve axon. The FitzHugh-Nagumo equations constitute a similar but more qualitative model (the Hodgkin-Huxley model can be reduced to the FitzHugh-Nagumo model). In higher than one dimensions the Hodgkin-Huxley model can be employed to model the electrical activity taking place in cells within human heart.

Another example is the oxidation-reduction process known as Belousov-Zhabotinski (BZ) reaction [290], [196], [198]. This reaction is the first experimental evidence of an oscillating chemical process. Before the BZ reaction was discovered, chemists thought that only a homogeneous, time-independent state could emerge from any chemical transformation. A typical BZ reagent consists of such ordinary products as a bromate-generating salt (like $KBrO_3$); an organic reductant [like malonic acid $CH_2(COOH)_2$] and a salt capable

University of Cape Town

of generating a oxidation-reduction couple [like $Ce_2(SO_4)_3$], all dissolved in sulfuric acid. The change of the composition of the system can be followed visually through a change of color and, more quantitatively, by placing electrodes in the solution or measuring the optical absorption caused by a particular substance.

The BZ reaction is controlled by two types of parameters: the concentration of chemicals pumped from outside, and the rate at which they are pumped into the reactor, that is the volume pumped per unit time. The latter quantity, J_i, divided by the volume of the reactor, V, gives the inverse of the residence time, τ_i, of the corresponding chemical within the reactor:

$$\frac{1}{\tau_i} = \frac{J_i}{V}.$$

Under slow pumping conditions (all J_i small) the chemicals will remain in the reactor for a very long time and will, for all practical purposes, reach a state of chemical equilibrium just as if the reactor were closed. However, for large J_i, the chemicals will leave the reactor very quickly, essentially with the concentration of the feed stream and will be unable to react significantly and equilibrate with the bulk. The residence parameter, τ, can be used as a convenient control parameter playing the role of the constraint.

Consider now the principal modes of behaviour of BZ-like reactions in an open well-stirred reactor for a range of values of the residence time between the two above-mentioned extremes [264], [30]. As it turns out, there exists a critical threshold τ_c below which stationary behaviour is no longer possible and sustained oscillations are observed. The amplitude and the period of these oscillations are intrinsically determined once the parameters (temperature, concentrations in the feed stream and residence time) are fixed. The birth of this new regime is associated with the breaking of the translational symmetry in the time domain, since then the phase of the system's variables changes with in an oscillating period. This transition can be represented in the form of a bifurcation diagram in which the oscillatory branch bifurcates out of the stationary state when $\tau = \tau_c$. As τ_c is increased, this transition goes through a sequence of complex periodic oscillations of various types [241]. Further change of the constraints leads to a regime of chemical (temporal) chaos in the form of randomly-looking mixture of small- and large-amplitude oscillations. The chaotic regime can be reached in a variety of different ways including the period-doubling cascade, a transition via quasi-periodic behaviour and an intermittency.

A qualitative explanation of the oscillatory behaviour in the BZ reagent was proposed in [69]. The main point is to realize that the BZ reaction involves two different processes, A and B, which alternatively dominate the kinetics, while a third process, C,

University of Cape Town

is responsible for the switching between A and B. More specifically:

• When Br^- concentration is sufficient, the following reactions take place:

(A.1) $Br^- + BrO_3^- + 2H^+ \rightarrow HOBr + HBrO_2$,

(A.2) $Br^- + HOBr + H^+ \rightarrow Br_2 + H_2O$,

(A.3) $Br^- + HBrO_2 + H^+ \rightarrow 2HOBr$.

• Once Br^- concentration is sufficiently lowered, the oxidation of Ce^{3+} to Ce^{4+} is carried out automatically thanks to the liberation of the free radical $BrO_2\cdot$:

(B.1) $2HBrO_2 \rightarrow HOBr + BrO_3 3^- + H^+$,

(B.2) $HBrO_2 + BrO_3^- + H^- \rightarrow 2BrO_2 \cdot + H_2O$,

(B.3) $BrO_2 \cdot + Ce^{3+} + H^+ \rightarrow Ce^{4+} + HBrO_2$.

Autocatalysis takes place through the bromous acid, since two molecules of this substance are produced by (B.3) for each one consumed in (B.2).

• Finally, Ce^{4+} is reduced back to Ce^{3+} while at the same time it regenerates Br^-, thus allowing the process to start all over again. The global reaction for this transformation is:

(C) $10Ce^{4+} + CH_2(COOH)_2 + BrCH(COOH)_2 + 4H_2O + 2Br_2 \rightarrow 10Ce^{3+} + 5Br^- + 6CO_2 + 15H^+$.

Notice that the mere fact of switching from the process B to the process A is not sufficient to explain oscillations. An additional ingredient cooperativity is needed to sustain a cyclic behaviour and is provided by the positive feedback (autocatalysis) of the bromous acid onto itself.

Being limited to a single feedback, the above mechanism cannot generate more than one relevant time scale. Consequently, it cannot explain the quasi-periodicity, composite periodic oscillations and chaos found in numerous experiments. Richetti [227] and coauthors have proposed an additional negative feedback whereby in the presence of hypobromous acid, (HOBr), $HOBr_2$ is consumed in a manner that is autocatalytic in Br^-. The competition between two mechanisms of cooperativity then brings a second time scale into the problem. This suffices to explain the appearance of complex oscillations, including chaotic behaviour [14], [15].

Refs. [265], [70], [87] consider the behaviour of BZ system in an unstirred reactor. For a long time experiments were limited to closed reactors, typically of the of a shallow layer of solution. In this case the arising patterns are regular in space and time and have the form of propagating wave fronts. The waves appear primarily in two different forms: circular fronts displaying a roughly cylindrical symmetry around an axis perpendicular to the layer, usually referred to as target patterns; and spiral fronts rotating in

University of Cape Town

space clockwise and counterclockwise. It is also possible to obtain, although under rather exceptional conditions, the multiarmed spirals. In each case the wave fronts propagate over macroscopic distances without distortion and at a prescribed speed. The formation of these fronts can be associated with space symmetry breaking: translational symmetry breaking in the target wave case and chiral symmetry in the case of spiral wave.

More recently stationary inhomogeneous patterns arising via symmetry breaking have been observed in a modification of the BZ reaction, the chlorite-iodite-malonic acid reaction, thanks to the design of new open, unstirred chemical reactors which allow the development of spatially inhomogeneous states while avoiding parasitic hydrodynamic motion [46]. At the beginning of the experiment the development of a series of light and dark stripes parallel to the edges of the reactor reveals the emergence of a concentration pattern. Although this pattern is nontrivial, the stripes preserve the symmetry imposed by the feed. If the concentration of the malonic acid is within a well-defined range, some of these stripes ultimately break up into lines of periodic spots. This constitutes a genuine symmetry breaking phenomenon in the direction transverse to the imposed gradient. The pattern can be sustained indefinitely. Moreover, the wavelength seems to be intrinsic and characterized exclusively by nongeometric properties. In particular, it is at least one order of magnitude smaller than any geometric dimension of the reactor. This is different from the stationary patterns in the Bénard problem whose characteristic length is determined by the size of the experimental device.

An alternative possibility is the formation of patterns parallel to the direction of the feed, which is, in turn, chosen to be perpendicular to the reactor's largest side [212]. In this case a variety of patterns such as hexagons, stripes and mixed states are observed. Transition from stationary spatial patterns to spatiotemporal chaos (chemical turbulence) are also observed in conjunction with the formation of defects separating different domains. In addition to their fundamental importance in the laboratory-scale chemistry, chemically mediated nonlinearities provide a natural explanation for a large number of complex phenomena in a wide variety of contexts. For example, much of the chemical industry is based on heterogeneous catalysis. For instance, the oxidation of ammonia or of carbon monoxide is usually carried out in the presence of a platinum catalyst. Similarly, in the decomposition of nitrous oxide, N_2O, a catalytic copper oxide surface is used.

There are two sources of cooperativity in this type of phenomena. First, since the total number of sites in the catalyst is finite, the substances inevitably compete for adsorbing sites; thus they exert a negative feedback on each other. Second, some of the adsorbed substances facilitate a structural change of the catalyst surface, which may

University of Cape Town

further affect the adsorption probability of this very substance or of the other substances. It is therefore not surprising that heterogeneous catalysis provides some of the best-documented examples of nonlinear phenomena. A particular illustration is provided by carbon monoxide oxidation on platinum under ultra-high vacuum pressure conditions [52, 64, 104].

Ref. [119] examines spiral waves on the plane. In three dimensions [273] more esoteric phenomena were documented. Scroll waves, toroidal scroll waves and linked-twisted scroll waves are all apparent to some degree. Over a number of years A.T. Winfree [276] pioneered studies of these phenomena. He was able to discuss the geometry and motion of propagating of oscillatory wave structures. By topological (continuity) arguments it is possible to rule out many configurations of linked and twisted scrolls but we are nevertheless no nearer to any analytical statements concerning solutions to excitable reaction-diffusion systems in 3D.

The basic ideas contained within this approach are as follows. If we were to observe a wave passing by, we would see the state of the reaction being excited away from its quiescent stable regime, then moving through a number of distinct stages before returning to the original unexcited state. The next wave would then pass repeating the same qualitative process. The circular evolution associated with excitable systems gives rise to a natural idea of phase as a measurement of how far through the cycle the local state is. One can then get a snapshot of a wave at any time by investigating points in the real space whose states are of the same phase. Their evolution through the domain in time is representative of the original wave structure. This procedure works for simple wave forms, but for rotating wave phenomena it is not sufficient. At the center of the spirals, for example, we have phaseless points.

In three dimensions the phaseless points can be visualized as forming arcs or curves. Such curves are called singular filaments. By fixing a critical phase one can see how the corresponding constant phase surface propagates around the singular filament as time passes. For example, a simple linear scroll wave can be visualized as a linear filament and a scrolling surface rotating about it. If a linear scroll is bent around in a circle so that the filament and scrolling surface are joint, one obtains a toroidal scroll wave. Such a wave possesses a singular filament in the form of a ring, as well as a point somewhere in the middle where the scrolling surface converges before dividing into two components, one equivalent to a sphere propagating off to infinity and the other restarting the original cycle. If the linear scroll were twisted before being bent round and joined up, one would obtain a twisted toroidal scroll.

University of Cape Town

To study motion of spirals and scrolls one is formally seeking an asymptotic solution to a reaction-diffusion problem. This construction is analogous to Winfree's abstract construction. In spite of the fact that the asymptotic approach formally breaks down at the singular filaments, it is capable to give some qualitative information about the way in which the waves propagate.

The problem of two- and three-dimensional wave propagation can be compared with that for wave propagation in one dimension by demanding that the front of the wave is located on a surface which propagates according to

$$N + \varepsilon K = c, \tag{1.244}$$

where N is the normal velocity, K is twice the mean curvature and ε and c are constants obtained from the original reaction-diffusion equation. Equation (1.244) is usually called the eikonal equation. The basic idea [119, 121, 84, 88] is to represent the wave front by a local transformation layer exploiting a small scaling constant in the original reaction-diffusion system.

One seeks solutions to the FitzHugh-Nagumo equations in the form of a single spiral wave in the plane rotating about the origin. One can apply the eikonal equation and, since it is known that such a wave ought to rotate uniformly about its central core, it is merely a matter of determining the geometry of the spiral. In order to use this approach we must have a single fast variable, u, which dominates the wave-like behaviour of the system. ε is a parameter present explicitly in the equations but the constant c is not so obviously determined. The system may possess many plane periodic waves containing sharp transition-layers each moving with a different speed. As $|\mathbf{r}| \to \infty$, the prospective spiral waves look like plane periodic waves, at least locally, so some means must be found of choosing the correct wave speed c to be inserted into the eikonal equation.

Strictly speaking, this solution will not be valid in some neighbourhood of the center. This core region remains a problem. One shall allow the transition layer to reach as far as the origin about which it rotates uniformly. However, the transition layer requires at least a width of $O(\varepsilon)$ in which to fill the corresponding transition profile. Hence, it is expected that the solution will be valid to within an ε-sphere of the origin. Nevertheless it is possible to obtain some useful information regarding simple spiral waves in the plane.

Consider an anti-clockwise wave rotating clockwise about the origin. We suppose that the wave possesses a transition layer located by such a spiral. Let us parametrize the curve locating the transition layer by $r = \sqrt{x^2 + y^2}$, so that in polar coordinates the

University of Cape Town

geometry and motion of the spiral are given by

$$\theta = g(r) - \omega t. \tag{1.245}$$

Here, the function g is to be determined and must satisfy

$$g_r \geq 0, \tag{1.246}$$

$$\lim_{r\to\infty} g_r = g_\infty = \text{constant}, \tag{1.247}$$

and is bounded at $r = 0$. Without loss of generality we may set $g(0) = 0$. The condition on g as $r \to \infty$ means that for large r the waves are almost outgoing spherical waves with the wavelength $\lambda = 2\pi/g_\infty$. The whole spiral satisfying (1.245)-(1.247) would have a period $2\pi/\omega$, so for large r the transition layer would move a distance λ in radial direction in time $2\pi/\omega$. Thus, an observer moving off to infinity would see waves moving with speed ω/g_∞ asymptotically in the radial direction. For large enough r the curvature of such waves becomes negligible and the local observer would see plane periodic waves with speed ω/g_∞ and wavelength λ. Now, returning to the geometric theory where $c = N + \varepsilon K$, we must have $c = \omega/g_\infty$ since ω/g_∞ is the speed of the plane waves at infinity. Hence,

$$g_\infty = c/\omega \tag{1.248}$$

and

$$\lambda = 2\pi\omega/c. \tag{1.249}$$

Now, for c fixed we must solve the eikonal equation for the pair (g, ω) satisfying (1.246-1.247) and (1.248). This is a nonlinear eigenvalue problem. Finally, we demand that the wavelength λ lies on the dispersion curve, which is assumed to be known. As c varies, we may regard ω as a functional of c and hence require the curve (1.249) in the (c, λ) plane to intersect the dispersion curve. The result is a unique intersection (or at least finite number of intersections), determining c and hence ω.

In order to examine the geometry of the spiral waves we use (1.245) and substitute

$$x(r) = r\cos\left[(g(r) - \omega t)\right] \tag{1.250}$$

$$y(r) = r\sin\left[(g(r) - \omega t)\right] \tag{1.251}$$

into the expressions for N and K for a wave propagating on the plane. We have

$$N = \frac{x_t y_r - y_t x_r}{(x_r^2 + y_r^2)^{1/2}} = \frac{r\omega}{(1 + r^2 g_r^2)^{1/2}} \tag{1.252}$$

University of Cape Town

and

$$K = \frac{y_{rr}x_r - x_{rr}y_r}{(x_r^2 + y_r^2)^{3/2}} = \frac{2g_r + rg_{rr} + r^2g_r^3}{(1 + r^2g_r^2)^{3/2}}. \tag{1.253}$$

If εK is small, the eikonal equation can be solved explicitly:

$$g(r) = \left(\frac{r^2\omega^2}{c^2} - 1\right)^{1/2} - \arctan\left(\frac{r^2\omega^2}{c^2} - 1\right)^{1/2}. \tag{1.254}$$

Clearly, $g_r \to c/\omega$ as $r \to \infty$, but g is unable to satisfy the boundary condition at $r = 0$ since it cannot reach this far. The curve represented by (1.254) is the involute of a circle of radius c/ω. However, there are some deficiencies between such involute spirals and the spiral waves observed in excitable media. In particular the involute spirals fail to reflect the effects of curvature on normal velocity and lack agreement with experiments near the center of the spiral [293].

Involute spirals cannot be considered as a good approximation to the experimentally observed spirals because of three main reasons. First, they fail to provide any explanation of the core geometry and are undefined for small r. Second, they fail to fix the parameter ω in terms of c and this is important to do in order to force the plane waves at infinity to satisfy the dispersion curve and hence to obtain unique spirals. Third, as r tends to c/ω, g_{rr} becomes unbounded and consequently K becomes unbounded as well. Thus, εK term is non-negligible and the full eikonal equation should be solved. However, it should be noticed that since we require $g_r \to c/\omega$ as $r \to \infty$, we will obtain $c = N$ at infinity. So, the solution of the full eikonal equation must be asymptotic to an involute spiral for large r.

One has

$$c = \varepsilon\frac{2g_r + rg_{rr} + r^2g_r^3}{(1 + r^2g_r^2)^{3/2}} + \frac{r\omega}{(1 + r^2g_r^2)^{1/2}}. \tag{1.255}$$

As $r \to 0$, we require $g \to 0$, so we must have $g_r \to c/2\varepsilon$. Setting $h = rg_r$, the eikonal equation can be rewritten in the form

$$rh_r = (1 + h^2)\left(\frac{rc}{\varepsilon}(1 + h^2)^{1/2} - \frac{\omega r^2}{\varepsilon} - h\right) \tag{1.256}$$

supplemented by the boundary conditions:

$$h(0) = 0, \quad \lim_{r\to\infty} h' = \frac{c}{\omega}$$

for a chosen value of c. At $r = 0$ one must have $h_r = c/2\varepsilon$. Equation (1.256) then is solved numerically [121] together with $h(0) = 0$ and $h_r(0) = c/2\varepsilon$. As c is varied, different

University of Cape Town

values of ω are obtained. But only for one value of ω, the derivative h_r remains bounded and tends to c/ω for $r \to \infty$. Then the corresponding orbit is integrated to provide the solution for g. Now, for different choices of c we will have different values for ω. If we sketch the curve $\lambda = 2pi\omega(c)/c$ in the (c, λ)-plane and superimpose on it the dispersion curve, we will obtain an intersection corresponding to a uniquely determined value of c and hence for ω for spiral waves.

The same procedure can be carried out for obtaining toroidal scroll waves but in this case the scroll is parametrized in the coordinate system rotating about the z-axis.

1.4 Objectives of this thesis

In the next, second, chapter of the thesis we will construct a reduced-dimensional model that will allow us to gain some analytical insight into the development of the nonlinear stage of the oscillatory instability and predict which attractors will replace the unstable soliton as a result of this instability.

The objective of the third chapter is to provide an explanation of the stabilizing effect of an impurity introduced in a parametrically driven damped chain of coupled nonlinear oscillators.

In the forth chapter we study pulse solutions to the reaction-diffusion model of an excitable surface reaction between the nitric oxide and the carbon monoxide.

University of Cape Town

Chapter 2

Supercritical dynamics of parametrically driven NLS solitons beyond the onset of oscillatory instability

University of Cape Town

2.1 Motivation

As we emphasized in the introductory chapter, soliton solutions are of paramount importance for nonlinear dispersive systems. Stable solitons dominate the long-term asymptotic behaviour of spatially inhomogeneous initial conditions. Unstable solitons can nucleate collapses [108, 258], spatially localized temporally periodic and chaotic states [61, 34, 35, 213, 201, 202, 259, 260, 109], spatio-temporal chaos [38] and phase transitions [20]. The nonlinear evolution of a linearly unstable soliton can often be predicted from knowing the *mechanism* of its instability. Until the early nineties, the onset of soliton instability in conservative systems was typically associated with the transition of a linearized eigenvalue from the imaginary to positive real axis (see e.g. [148, 217] and references therein). In the case of the nonlinear Schrödinger equations that we will be concerned with in this chapter, the nonlinear evolution of this instability (usually referred to as the *translational* instability) may follow a limited number of scenarios: Unstable *bright* solitons blow up, disperse away, or evolve into a long-lived oscillating structure asymptotically settling to a stable stationary soliton [216, 219]; unstable *dark* solitons dissociate into a couple or inflate [20, 218].

More recently it was realized that there are also different mechanisms of soliton instability; in particular, the soliton can be destroyed as a result of a resonance of two

internal oscillation modes [19, 257, 17, 21, 215]. Our objective in this chapter is to follow the nonlinear development of this new instability (known as the *oscillatory* instability) and describe supercritical dynamical regimes of solitons. As a prototype nonlinear PDE, we adopt the parametrically driven, damped nonlinear Schrödinger equation (NLS):

$$i\psi_T + \psi_{XX} - \psi + 2|\psi|^2\psi = \mathrm{h}\psi^* - i\gamma\psi. \tag{2.1}$$

Here h is the amplitude of the driver and γ the dissipation coefficient; the frequency of the driver has been normalized to unity. Equation (2.1) is obtained from eq.(1.72) by gauging away the time dependence through the transformation

$$\tilde{\psi}(t,x) = \psi(t,x)\mathrm{e}^{i\omega t}, \quad \omega = 1.$$

As we mentioned in the Introduction this equation describes a variety of physical phenomena, including the nonlinear Faraday resonance in hydrodynamics, the parametric generation of spin waves and magnetic solitons in ferro and anti-ferromagnets and, finally, the effect of phase-sensitive amplifiers on solitons propagating in optical fibers. In the next chapter, chapter 3, we will use the fact that it also serves as an amplitude equation for small-amplitude, parametrically-driven sine-Gordon breathers and hence its range of applicability includes all systems modelled by the parametrically driven sine-Gordon equation.

When the driver's amplitude is very large: $\mathrm{h}^2 > 1 + \gamma^2$, the trivial solution $\psi = 0$ of eq.(2.1) is unstable against continuous spectrum perturbations [17]. (This is what physicists call "parametric instability" [259],[277],[36].) In the present chapter we will be concerned with a complementary region, $\mathrm{h}^2 < 1 + \gamma^2$, and so the trivial solution will always be deemed stable. In this region eq.(2.1) has two stationary soliton solutions. One of these is always unstable and will be disregarded in the bulk of this chapter. The other one is stable for small driving strengths but loses its stability as h is increased for the fixed dissipation coefficient. In the undamped case ($\gamma = 0$) the instability arises due to the collision of two pure imaginary eigenvalues of the associated linearized operator, one detaching from the continuous spectrum and the other one originating from the broken $U(1)$ gauge invariance [17]. The two imaginary eigenvalues collide at a critical value $\mathrm{h} = \mathrm{h}_c \approx 0.064$ and then emerge into the complex plane producing the oscillatory instability (and hence the oscillatory-instability bifurcation) of the soliton. The linearized stability problem for the full, dissipative case can be reduced, by a nonlinear eigenvalue transformation [17], to the one for the undamped equation. Roughly speaking, this transformation subtracts γ from all eigenvalues so that the instability occurs for larger values of h, when a pair of

University of Cape Town

complex-conjugate eigenvalues crosses the line $\mathrm{Re}\lambda = 0$. This is now a Hopf bifurcation, typical of dissipative systems.

A natural question is what localized nonlinear structures serve as attractors in the supercritical domain (i.e. beyond the onset of the oscillatory and Hopf bifurcations, respectively). In the dissipative case ($\gamma \neq 0$) this was addressed by means of direct computer simulations of eq.(2.1) [38]. It was observed that in the neighbourhood of the transition curve on the $(\gamma, \mathtt{h})$-plane, the stationary soliton is replaced by a temporally-periodic one. Having fixed some γ in the range $0 < \gamma < 0.37$ and increasing $\mathtt{h}$, the soliton undergoes the period-doubling (for γ smaller than 0.25) or quasiperiodic (for $0.25 \leq \gamma \leq 0.37$) transition to chaos [38]. (For $\gamma > 0.37$ the static soliton is stable in its entire domain of existence.)

In this work we attempt to describe the supercritical dynamics of the soliton analytically. Our analysis is based on the reduced amplitude equations for the soliton's perturbation which we derive for $\mathtt{h}$ in the neighbourhood of the oscillatory and the Hopf bifurcation. We also perform computer simulations of eq.(2.1) in the hamiltonian case ($\gamma = 0$) which has not been previously studied numerically. Results of these simulations are compared to conclusions of the finite-dimensional analysis. Although the $\gamma = 0$ case is clearly nongeneric (in the sense that some small damping is present in all underlying physical settings), it provides insight into, and serves as a starting point for the analysis of the general, dissipative equation.

The plan and a brief summary of this chapter is as follows. First in section 2.2, we consider the *weakly* dissipative regime, $\gamma \ll 1$, and derive a reduced amplitude equation describing the nonlinear evolution of the perturbation to the soliton in the vicinity of the bifurcation point ($\mathtt{h} \sim \mathtt{h}_c$). This amplitude equation is a complex nonlinear ODE of the second order. In some parts of our derivation we have to rely upon numerical solutions of eigenvalue and boundary value problems; we discuss details of the corresponding numerical algorithms in section 2.3. In the *strongly* dissipative regime, i.e. for $\gamma \sim 1$, the above second-order equation is replaced by the (first-order) complex Landau equation. The latter is derived in section 2.4. The subsequent section, Sec.2.5.1, contains a detailed analysis of solutions to the above finite-dimensional system for the vanishing, small and finite γ. The upshot of this study is that no periodic solutions are possible in the $\gamma = 0$ case; all finite-dimensional trajectories escape to infinity. However, adding a small damping gives rise to a stable periodic orbit coexisting with unbounded motions. Finally, only periodic finite-dimensional trajectories survive when γ is made finite. In section 2.6 the conclusions based on the reduced amplitude equation for the undamped case are compared to results

University of Cape Town

of numerical simulations of the full, nonreduced NLS equation (2.1). Consistently with the finite-dimensional predictions, no stably oscillating solitons were observed in these simulations. All localized initial conditions were seen to evolve either into a radiating soliton with the amplitude growing without bound, or into a slowly-decaying, small-amplitude breather-like solution (or possibly into a couple of diverging breathers.) The last section (section 2.7) contains concluding remarks and outlines some open problems.

2.2 Reduced amplitude equations for the oscillatory-instability bifurcation

2.2.1 Soliton solutions and linear corrections

The two stationary soliton solutions of the parametrically driven, damped NLS equation (2.1) are given by [184, 17]:

$$\psi_{\pm} = A_{\pm} e^{-i\theta_{\pm}} \operatorname{sech}(A_{\pm} X), \tag{2.2}$$

where

$$\sin 2\theta_{\pm} = \frac{\gamma}{\mathtt{h}}, \quad \cos 2\theta_{\pm} = \pm\sqrt{1 - \frac{\gamma^2}{\mathtt{h}^2}} \tag{2.3}$$

and

$$A_{\pm}^2 = 1 \pm \sqrt{\mathtt{h}^2 - \gamma^2}. \tag{2.4}$$

The two solitons emerge via a saddle-node bifurcation at $\mathtt{h} = \gamma$. The ψ_+ soliton is stable in some neighbourhood of the bifurcation point while the ψ_- always has a positive linearized eigenvalue and hence is unstable for *all* $\mathtt{h}$ and γ. Since this unstable soliton does not undergo any further bifurcations, we are disregarding it and concentrating on the ψ_+ in what follows. (We will only return to the evolution of the instability of the ψ_- soliton when we present results of our numerical simulations in Section 2.6.)

Since we are interested in solutions which are close to the soliton (2.2) in some sense, it is convenient to rescale variables as

$$X = \frac{x}{A}, \quad T = \frac{t}{A^2}$$

and decompose ψ into its real and imaginary part:

$$\psi = A\{U(x,t) + iV(x,t)\} e^{-i\theta}. \tag{2.5}$$

Here $A = A_+$ and $\theta = \theta_+$; the subscript was omitted. Defining

University of Cape Town

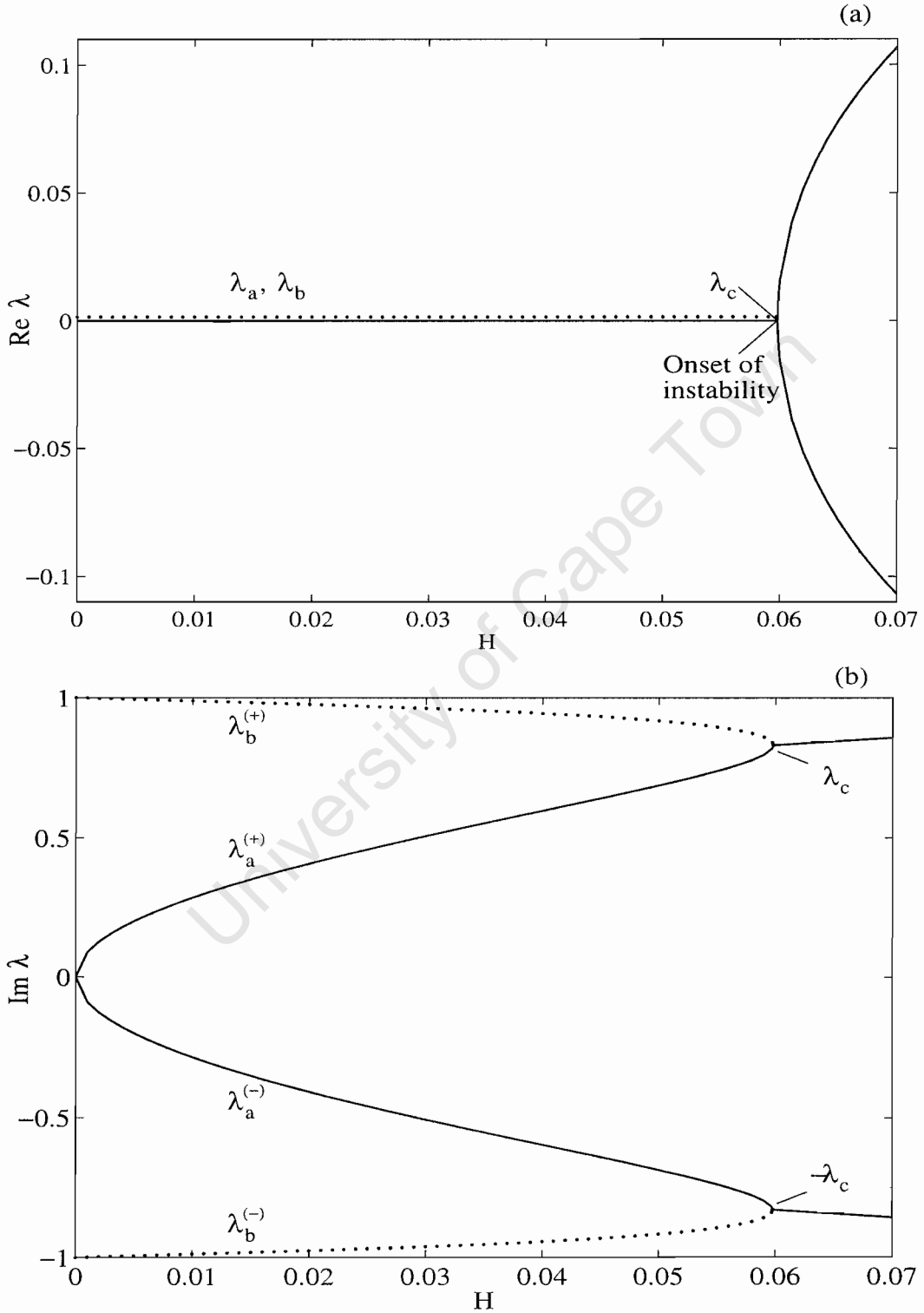

University of Cape Town

Figure 2.1 continues on the next page.

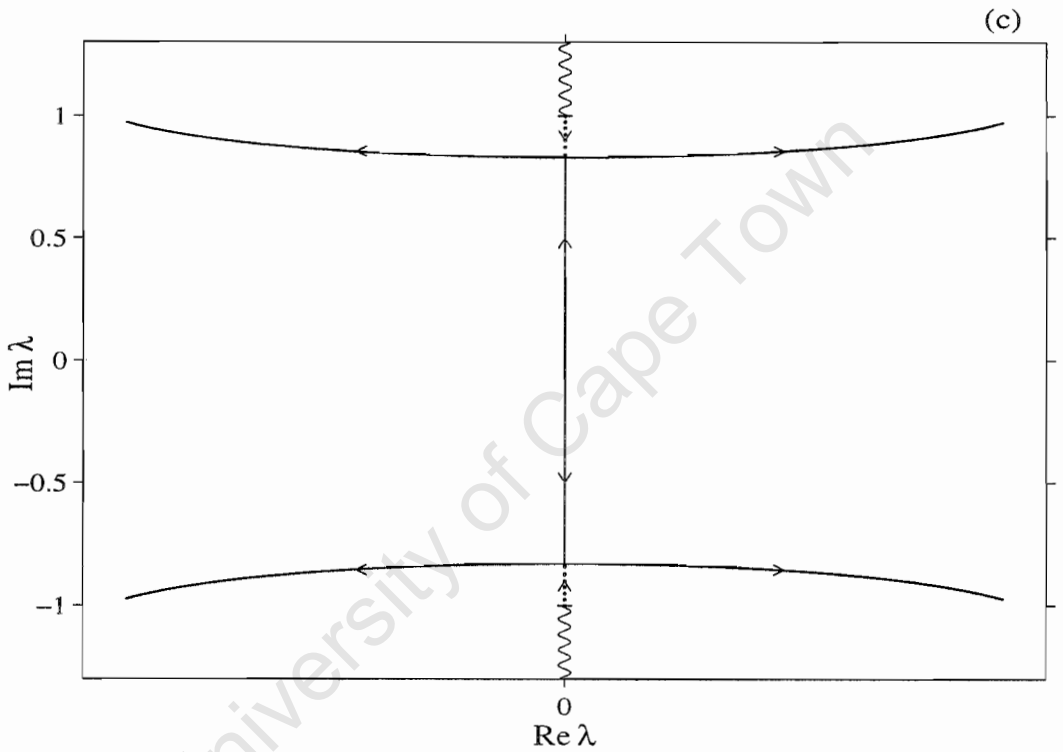

University of Cape Town

Figure 2.1: The bifurcation diagram for $\gamma = 0$. Real (a) and imaginary (b) parts of the eigenvalues $\lambda = i\omega$ are shown as functions of H. The complex plane in (c) results from the combination of (a) and (b). The wavy line on (c) depicts the continuous spectrum and the dotted lines show the imaginary eigenvalues $\lambda_b^{(\pm)} = \pm i\omega_b$ detaching from the continuum. The oscillatory instability sets in when two pairs of imaginary eigenvalues merge at $H = H_c$ ($i\omega_a, i\omega_b \to i\omega_c$) and become a complex quadruplet.

$$H = \frac{(\mathrm{h}^2 - \gamma^2)^{1/2}}{A^2}, \quad \Gamma = \frac{\gamma}{A^2},$$

the equation (2.1) becomes

$$-V_t - 2\Gamma V = -U_{xx} + U - 2(U^2 + V^2)U, \tag{2.6}$$

$$U_t + 2HV = -V_{xx} + V - 2(U^2 + V^2)V. \tag{2.7}$$

The soliton solution of eqs.(2.6-2.7) is now

$$U_0 = \operatorname{sech} x, \quad V_0 = 0.$$

Linearizing eq.(2.6-2.7) about the soliton,

$$U = U_0(x) + \varepsilon f(x)e^{i\Omega t}, \quad V = i\varepsilon g(x)e^{i\Omega t}, \tag{2.8}$$

where ε is a small parameter, gives an eigenvalue problem for f and g:

$$\begin{pmatrix} L_1 & 2i\Gamma \\ 0 & L_2 \end{pmatrix} \begin{pmatrix} f \\ g \end{pmatrix} = \Omega \begin{pmatrix} 0 & 1 \\ 1 & 0 \end{pmatrix} \begin{pmatrix} f \\ g \end{pmatrix}. \tag{2.9}$$

Here

$$L_1 = -\frac{\partial^2}{\partial x^2} + 1 - 6\operatorname{sech}^2 x, \tag{2.10}$$

$$L_2 = -\frac{\partial^2}{\partial x^2} + 1 - 2H - 2\operatorname{sech}^2 x, \tag{2.11}$$

and the eigenvalue Ω is the frequency of the perturbed soliton's oscillations. In studies of stability problems it is more common to deal with the quantity $\lambda = i\Omega$ which is referred to as the "linearized eigenvalue", or "stability eigenvalue". However, the frequency Ω turns out to be more suitable for our present purposes. Occasionally we will make reference to λ as well.

The damped eigenvalue problem (2.9) can be reduced, via a nonlinear eigenvalue transformation [17], to the one with $\Gamma = 0$:

$$\begin{pmatrix} L_1 & 0 \\ 0 & L_2 \end{pmatrix} \begin{pmatrix} u \\ v \end{pmatrix} = \omega \begin{pmatrix} 0 & 1 \\ 1 & 0 \end{pmatrix} \begin{pmatrix} u \\ v \end{pmatrix}, \tag{2.12}$$

or equivalently,

$$\Lambda \begin{pmatrix} u \\ v \end{pmatrix} \equiv \begin{pmatrix} 0 & L_2 \\ L_1 & 0 \end{pmatrix} \begin{pmatrix} u \\ v \end{pmatrix} = \omega \begin{pmatrix} u \\ v \end{pmatrix}. \tag{2.13}$$

University of Cape Town

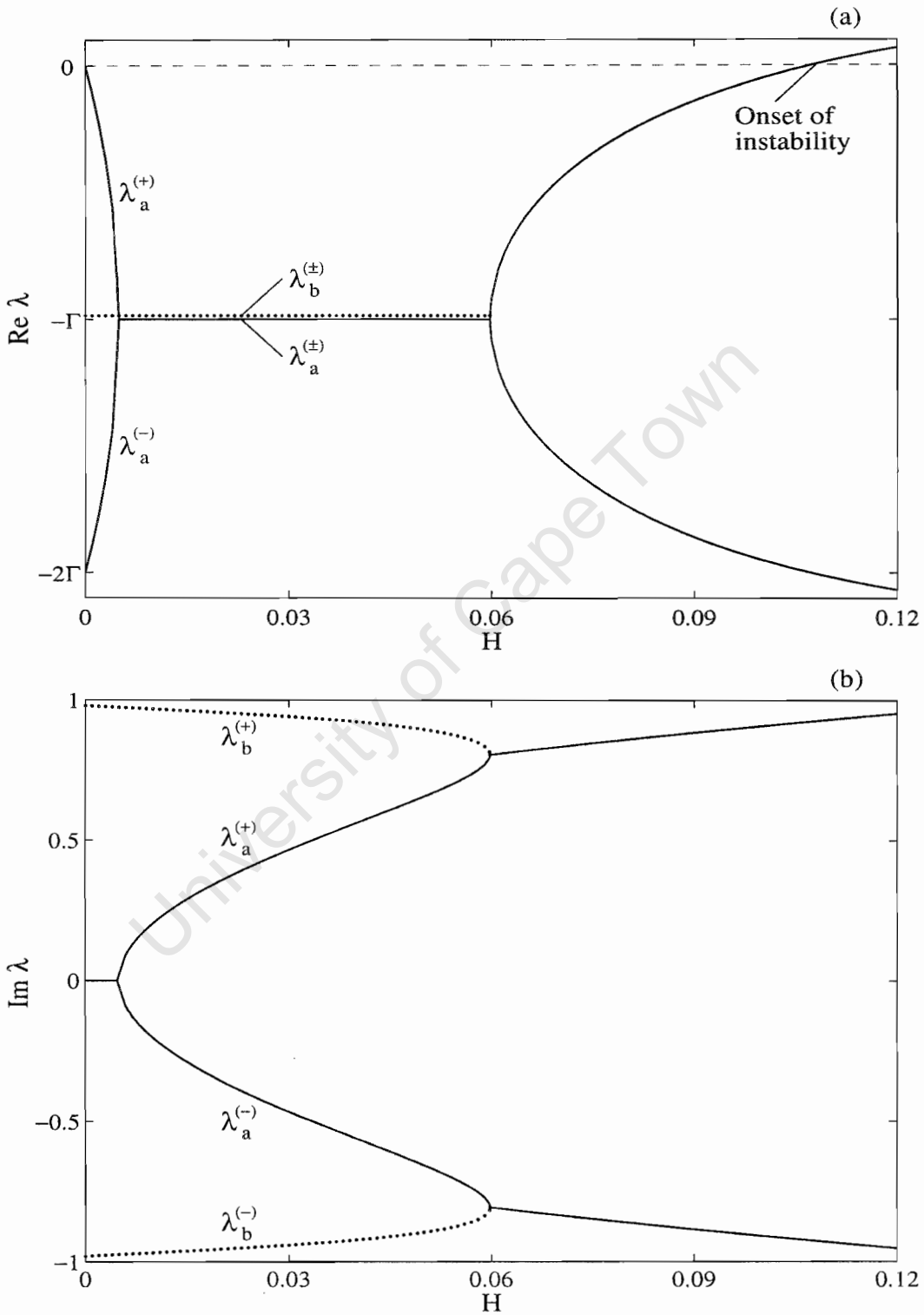

University of Cape Town

Figure 2.2 continues on the next page.

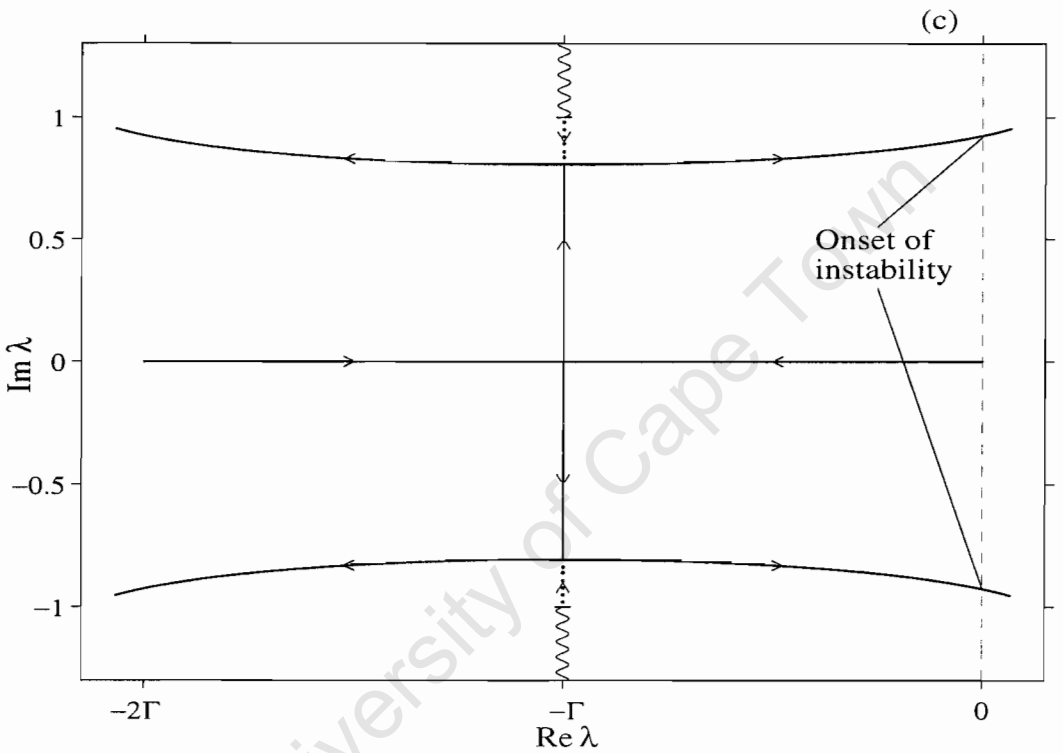

University of Cape Town

Figure 2.2: The bifurcation diagram for $\gamma \neq 0$. (In this plot $\Gamma = 0.2$). This diagram was obtained from the one in fig.2.1 by applying the transformation (2.14): $\lambda = -\Gamma \pm i(\omega^2 - \Gamma^2)^{1/2}$. For small H such that $\omega_a < \Gamma$, there is a pair of real eigenvalues $\lambda_a^{(\pm)} = -\Gamma \pm (\Gamma^2 - \omega_a^2)^{1/2}$ (solid line). When ω_a exceeds Γ, an imaginary part appears while the real part remains fixed: $\lambda_a^{(\pm)} = -\Gamma \pm i(\omega_a^2 - \Gamma^2)^{1/2}$. Another pair of complex-conjugate eigenvalues is $\lambda_b^{(\pm)} = -\Gamma \pm i(\omega_b^2 - \Gamma^2)^{1/2}$ (dotted curve). At $H = H_c$, where $\omega_a = \omega_b$, the λ_a and λ_b eigenvalues merge pairwise, and the real parts start to grow. The instability sets in when Reλ crosses the horizontal zero line (dashed) in (a).

Here

$$\omega = z\Omega, \quad z = \left(1 - \frac{2i\Gamma}{\Omega}\right)^{1/2}, \tag{2.14}$$

and

$$u = f, \quad v = zg. \tag{2.15}$$

As it was shown, numerically, in Ref.[17], the operator Λ has two pairs of nonzero discrete eigenvalues, $\pm\omega_a$ and $\pm\omega_b$. For $H < H_c$, these eigenvalues are real and lie in the gap of the continuous spectrum: $\omega_a, \omega_b < \sqrt{1-2H}$ (see Fig.2.1). As H reaches the critical value $H_c \approx 0.060$, the two eigenvalues merge ($\omega_a, \omega_b \to \omega_c \approx 0.83$), and then immediately split up moving into to the complex plane (Fig. 2.1). In the undamped case ($\Gamma = 0$), this implies the oscillatory bifurcation. For $H > H_c$ the solution is unstable; the nonlinear evolution of this oscillatory instability will result in some other nonlinear attractors. In the next two subsections we develop an asymptotic formalism which captures the essentials of the nonlinear dynamics of the unstable soliton in this supercritical domain.

In the weakly dissipative case (Γ small but nonzero) the instability sets in not at $H = H_c$ but later, when the real part of $\lambda = i\Omega$ becomes positive [see Fig. 2.2(a,c)]. In literature, this would be usually referred to as the *Hopf* bifurcation. However, the asymptotic formalism associated with the *oscillatory-instability* bifurcation provides an adequate description of supercritical dynamics in the weakly dissipative limit as well. More importantly, the resulting amplitude equation is fundamentally different from the normal form of the Hopf bifurcation (see below). For this reason we will be using the term "oscillatory-instability bifurcation" not only when $\Gamma = 0$ but also in the small-Γ case.

University of Cape Town

2.2.2 Asymptotic analysis: Second-order corrections

Now we are prepared to derive a reduced nonlinear model describing the evolution of the perturbations to the stationary soliton (2.8) in the vicinity of the bifurcation value $H = H_c$ in the nearly conservative case, $\Gamma \sim 0$. The derivation is facilitated by factorizing the complex amplitude of the linear part of the perturbation (assumed small) as ϵa. Here $a = \mathrm{O}(1)$ and ϵ is a dimensionless small parameter; the perturbation is also assumed to be slowly varied: $a = a(\tau)$, where $\tau = \epsilon t$. We expand U and V in the asymptotic series in ϵ:

$$U = U_0(x) + \sum_{n=1}^{\infty} \epsilon^n U_n(x,t,\tau), \tag{2.16}$$

$$V = \sum_{n=1}^{\infty} \epsilon^n V_n(x,t,\tau), \tag{2.17}$$

where $U_0 = \operatorname{sech} x$,

$$U_1 = \left[a(\tau)e^{i\omega_c t} + a^*(\tau)e^{-i\omega_c t}\right] u_c(x), \tag{2.18}$$

$$V_1 = i\left[a(\tau)e^{i\omega_c t} - a^*(\tau)e^{-i\omega_c t}\right] v_c(x), \tag{2.19}$$

and u_c, v_c are components of the eigenvector of the operator (2.13) associated with the eigenvalue $\omega = \omega_c$ and parameter value $H = H_c$. These functions are real-valued and exponentially decaying at infinities; we also assume that they are normalized to unity:

$$\int_{-\infty}^{\infty} (u_c^2 + v_c^2)dx = 1. \tag{2.20}$$

Writing

$$H = H_c + \epsilon^2 h, \quad \Gamma = \epsilon\rho, \tag{2.21}$$

we include weak dissipative effects and a small deviation from the bifurcation point into the leading order of the asymptotic analysis. Substituting eqs.(2.16)-(2.19) and (2.21) into the system (2.6)-(2.7), and equating coefficients of like powers of ϵ and equal harmonics, we obtain for the ϵ^2-correction:

$$U_2 = |a|^2 u_0(x) +$$

$$+2\,\mathrm{Re}\left\{i\frac{da}{d\tau}e^{i\omega_c t}\right\} u_1(x) + 2\rho\,\mathrm{Re}\left\{iae^{i\omega_c t}\right\} u_\gamma(x) + 2\,\mathrm{Re}\left\{a^2 e^{2i\omega_c t} u_2(x)\right\}, \tag{2.22}$$

$$V_2 = -2\,\mathrm{Re}\left\{\frac{da}{d\tau}e^{i\omega_c t}\right\} v_1(x) - 2\rho\,\mathrm{Re}\left\{ae^{i\omega_c t}\right\} v_\gamma(x) + 2\,\mathrm{Re}\left\{ia^2 e^{2i\omega_c t} v_2(x)\right\}, \tag{2.23}$$

where the functions u_0, u_1, u_γ, u_2 and v_0, v_1, v_γ, v_2 are to be found by solving the following set of linear nonhomogeneous equations:

$$L_1 u_0 = 4U_0\left(3u_c^2 + v_c^2\right); \tag{2.24}$$

$$M_{\omega_c}\begin{pmatrix} u_1 \\ v_1 \end{pmatrix} \equiv \begin{pmatrix} L_1 & -\omega_c \\ -\omega_c & L_2 \end{pmatrix}\begin{pmatrix} u_1 \\ v_1 \end{pmatrix} = -\begin{pmatrix} v_c \\ u_c \end{pmatrix}; \tag{2.25}$$

$$M_{\omega_c}\begin{pmatrix} u_\gamma \\ v_\gamma \end{pmatrix} = -2\begin{pmatrix} v_c \\ 0 \end{pmatrix}; \tag{2.26}$$

$$M_{2\omega_c}\begin{pmatrix} u_2 \\ v_2 \end{pmatrix} \equiv \begin{pmatrix} L_1 & -2\omega_c \\ -2\omega_c & L_2 \end{pmatrix}\begin{pmatrix} u_2 \\ v_2 \end{pmatrix} = 2U_0\begin{pmatrix} 3u_c^2 - v_c^2 \\ 2u_c v_c \end{pmatrix}. \tag{2.27}$$

University of Cape Town

(Here the operator L_2 is defined by eq.(2.11)with $H = H_c$.)

It is worthwhile to comment on the meaning of each term in eq.(2.22)-(2.23) and the solvability of equations (2.24)-(2.27). First of all, the functions u_0, u_2, and v_2 represent the nonlinearity-induced corrections to the soliton's shape (zeroth and second harmonic, respectively.) The equation (2.24) always admits a solution decaying as $x \to \pm\infty$, since the solution of the associated homogeneous equation is an odd function (the translational zero-frequency mode $f_T(x) = \tanh x \operatorname{sech} x$) and therefore, is orthogonal to the even function on the right-hand side. On the contrary, the solution of the nonhomogeneous equation (2.27) is bounded but does not have to decay at the infinities as there is no reason why the solution of the corresponding homogeneous equation should be orthogonal to the vector-function on the right-hand side of (2.27). The solution of the homogeneous equation is the eigenfunction of the eigenvalue problem (2.13) associated with the eigenvalue $\omega = 2\omega_c \approx 1.66$. This eigenvalue belongs to the continuous spectrum and so the nonhomogeneous solution u_2, v_2 is defined up to the addition of an arbitrary combination of two continuous spectrum eigenfunctions.[1] Physically, the terms proportional to u_2 and v_2 are interpreted as the radiation emitted by the oscillating soliton. The boundary conditions corresponding to the *outgoing* radiation waves read

$$\begin{pmatrix} u_2 \\ v_2 \end{pmatrix} \to \begin{pmatrix} 1 \\ \frac{k_c^2+1}{2\omega_c} \end{pmatrix} \mathcal{R}^{\pm} e^{\mp i k_c x} \quad \text{as } x \to \pm\infty, \tag{2.28}$$

where the wavenumber k_c is positive, with

$$k_c^2 = \sqrt{H_c^2 + 4\omega_c^2} + H_c - 1. \tag{2.29}$$

With the above choice, the radiation terms in eqs.(2.22)-(2.23) reduce, as $x \to \pm\infty$, to the outgoing harmonic waves proportional to $\exp\{i(2\omega_c t \mp k_c x)\}$. The functions u_2 and v_2 are, therefore, complex-valued. The functions on the right-hand side of eq.(2.27) are even; it is not difficult to realize that this fact, together with the radiation conditions (2.28), requires that $u_2(x)$ and $v_2(x)$ should also be even. Hence, $\mathcal{R}^+ = \mathcal{R}^- \equiv \mathcal{R}$.

Before commenting on eqs.(2.25)-(2.26), we need to recall that ω_c is a *repeated* (double) eigenvalue of the operator (2.13) arising from the coalescence of two simple eigenvalues, ω_a and ω_b. The associated eigenvectors, $\{u_a, v_a\}$ and $\{u_b, v_b\}$, are orthogonal in the sense of the following [$SO(1,1)$-invariant] scalar product: $\int_{-\infty}^{\infty}(u_a v_b + u_b v_a)dx = 0$. When ω_a and ω_b coalesce, the associated eigenvectors can either stay linearly independent

[1] Here we use the term "eigenfunction" simply for the sake of brevity; the continuous spectrum "eigenfunctions" are, of course, nonnormalizable.

University of Cape Town

(i.e. the double eigenvalue ω_c is complete) or collapse into one (i.e. ω_c is defective). Our numerical analysis shows that the second possibility occurs in the case at hand: when $H \to H_c$, we have $u_a, u_b \to u_c$ and $v_a, v_b \to v_c$. Consequently, the orthogonality condition at the point $H = H_c$ becomes

$$I_c \equiv 2\int_{-\infty}^{\infty} u_c v_c \, dx = 0. \tag{2.30}$$

In order to illustrate the validity of eq.(2.30), we have plotted the quadratic forms

$$I[u, v] = 2\int_{-\infty}^{\infty} uv \, dx \tag{2.31}$$

for the two eigenvectors of the linearized operator (2.13) (Fig.2.3). The forms I_a and I_b are indeed seen to merge and vanish at $H = H_c$.

Turning to eq.(2.25), we can now identify its solution $\{u_1, v_1\}$ as a rank-2 generalised eigenvector associated with the eigenvalue ω_c of the linearized operator (2.13). The solvability condition for eq.(2.25) is nothing but the orthogonality relation (2.30); the fact that the quadratic form I_c of the eigenvector $\{u_c, v_c\}$ vanishes, guarantees that the generalized eigenvector $\{u_1, v_1\}$ exists and decays as $|x| \to \infty$. The real functions $u_1(x)$ and $v_1(x)$ can be interpreted as resonant ϵ^2-corrections to the linearised perturbation.

Finally, the same eq.(2.30) gives the solvability condition for the system (2.26). The real functions u_γ and v_γ account for the ϵ^2-corrections due to the weak damping.

2.2.3 The reduced finite-dimensional system

Having found the second-order corrections, we proceed to the third order of the asymptotic expansion, which yields the following linear nonhomogeneous system:

$$\begin{pmatrix} L_1 & \partial/\partial t \\ \partial/\partial t & L_2 \end{pmatrix} \begin{pmatrix} U_3 \\ V_3 \end{pmatrix} = \begin{pmatrix} Y \\ Z \end{pmatrix}, \tag{2.32}$$

where

$$Y = 2(U_1^2 + V_1^2)U_1 + 4U_0\,(3U_1U_2 + V_1V_2) - V_{2\tau} - 2\rho V_2, \tag{2.33}$$

$$Z = 2(U_1^2 + V_1^2)V_1 + 4U_0V_1U_2 + 4U_0U_1V_2 + U_{2\tau} + 2hV_1, \tag{2.34}$$

and U_1, V_1, U_2 and V_2 are as in (2.18)-(2.19) and (2.22)-(2.23). The solvability condition for eq.(2.32) involves coefficients of the resonant harmonic; we denote them y and z:

$$\begin{pmatrix} Y \\ Z \end{pmatrix} = \begin{pmatrix} y(x,\tau) \\ z(x,\tau) \end{pmatrix} e^{i\omega_c t} + c.c. + (\text{other harmonics}). \tag{2.35}$$

University of Cape Town

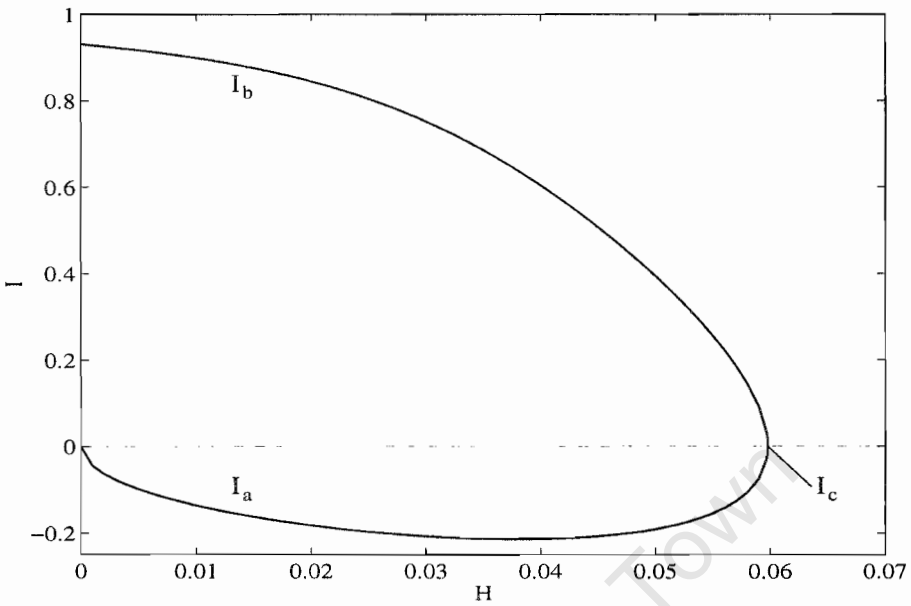

Figure 2.3: The quadratic form $I = 2\int uvdx$, evaluated numerically for two soliton's internal modes, $\{u_a, v_a\}$ and $\{u_b, v_b\}$. When ω_a merges with ω_b, both I_a and I_b vanish ensuring the existence of the generalized eigenvector $\{u_1, v_1\}$ at the point $H = H_c$.

A bounded solution exists only if

$$\int_{-\infty}^{\infty}(yu_c + zv_c)dx = 0. \tag{2.36}$$

After some algebra this solvability condition can be reduced to an equation for the complex amplitude of the soliton's perturbation:

$$\alpha\left(\frac{d^2a}{d\tau^2} + 2\rho\frac{da}{d\tau} + \rho^2 a\right) = \beta h a - \zeta|a|^2 a. \tag{2.37}$$

Here

$$\alpha = -\int_{-\infty}^{+\infty}(u_c v_1 + v_c u_1)\,dx, \tag{2.38}$$

$$\beta = 2\int_{-\infty}^{+\infty} v_c^2 dx, \tag{2.39}$$

$$\begin{aligned}\zeta &= -2\int_{-\infty}^{+\infty}\left(3u_c^4 + 2u_c^2 v_c^2 + 3v_c^4\right)dx \\ &- 4\int_{-\infty}^{+\infty} U_0\left[3u_c^2(u_0 + u_2) + v_c^2(u_0 - u_2) + 2u_c v_c v_2\right]dx.\end{aligned} \tag{2.40}$$

In the derivation of the linear part of eq.(2.37) we used the relations

$$\int_{-\infty}^{+\infty} u_c v_\gamma dx = \int_{-\infty}^{+\infty} v_c u_\gamma dx = \int_{-\infty}^{+\infty} u_c v_1 dx = \int_{-\infty}^{+\infty} v_c u_1 dx;$$

University of Cape Town

these follow from (2.13), (2.25) and (2.26).

The coefficient β is manifestly positive. Since the oscillatory instability is expected to set in for supercritical values of H, i.e. for $h > 0$, we expect the coefficient α to be positive as well. Finally, the coefficient ζ involves complex functions u_2 and v_2 and therefore, is complex-valued. Using eq.(2.27) in eq.(2.40) one can readily find the imaginary part of this coefficient:

$$\mathrm{Im}\zeta = 2k_c \frac{H_c^2 + 4\omega_c^2 + H_c\sqrt{H_c^2 + 4\omega_c^2}}{\omega_c^2} |\mathcal{R}|^2 > 0. \tag{2.41}$$

The eigenvalue problem (2.13) and nonhomogeneous equations (2.24)-(2.27) were solved numerically. (We discuss the details in the next section.) We have found the following values for the coefficients occurring in the reduced amplitude equation (2.37):

$$\alpha = 1.3297, \quad \beta = 1.6447,$$
$$\mathrm{Re}\,\zeta = (7.5555 \pm 0.0005) \times 10^{-2}, \quad \mathrm{Im}\,\zeta = (1.59 \pm 0.04) \times 10^{-3}. \tag{2.42}$$

2.3 Numerical analysis of eigenvalue and boundary-value problems

In this section we outline the scheme of numerical solution of the eigenvalue problem (2.13) and inhomogeneous equations (2.24)-(2.27). Some parts of this scheme are plain applications of the Fourier method; other parts are not so straightforward yet general enough to be useful in the asymptotic analyses of other instances of radiating solitons.

2.3.1 Exponentially localized solutions

Expanding eigenfunctions u and v over cosines,

$$\begin{pmatrix} u(x) \\ v(x) \end{pmatrix} = \frac{1}{\sqrt{L}} \begin{pmatrix} u^{(0)} \\ v^{(0)} \end{pmatrix} + \sqrt{\frac{2}{L}} \sum_{n=1}^{\infty} \begin{pmatrix} u^{(n)} \\ v^{(n)} \end{pmatrix} \cos\left(\frac{\pi n x}{L}\right), \tag{2.43}$$

and truncating the series at $n = N$ reduces eq.(2.13) to an eigenvalue problem for a block matrix:

$$\begin{pmatrix} \mathcal{L}_1 & \mathbf{0} \\ \mathbf{0} & \mathcal{L}_2 \end{pmatrix} \begin{pmatrix} \mathbf{u} \\ \mathbf{v} \end{pmatrix} = \omega \begin{pmatrix} \mathbf{0} & \mathbf{I} \\ \mathbf{I} & \mathbf{0} \end{pmatrix} \begin{pmatrix} \mathbf{u} \\ \mathbf{v} \end{pmatrix}. \tag{2.44}$$

University of Cape Town

Here $\mathbf{u}$ and $\mathbf{v}$ are $(N+1)$-dimensional column vectors: $\mathbf{u} = (u^{(0)}, u^{(1)}, \cdots u^{(N)})^T$, $\mathbf{v} = (v^{(0)}, v^{(1)}, \cdots v^{(N)})^T$ and $\mathcal{L}_1$ and $\mathcal{L}_2$ are $(N+1) \times (N+1)$ matrices with entries

$$\mathcal{L}_2^{(0,0)} = 1 - 2H - \frac{2}{L}, \quad \mathcal{L}_1^{(0,0)} = 1 - \frac{6}{L};$$

$$\mathcal{L}_2^{(0,m)} = \mathcal{L}_2^{(m,0)} = -\frac{\sqrt{2}\pi^2 m}{L^2 \sinh\left(\frac{\pi^2 m}{2L}\right)}, \quad \mathcal{L}_1^{(0,m)} = \mathcal{L}_1^{(m,0)} = 3\mathcal{L}_2^{(0,m)};$$

$$\mathcal{L}_2^{(m,n)} = \mathcal{L}_2^{(n,m)} = -\frac{\pi^2}{L^2}\left(\frac{m+n}{\sinh\left[\frac{\pi^2(m+n)}{2L}\right]} + \frac{m-n}{\sinh\left[\frac{\pi^2(m-n)}{2L}\right]}\right),$$

$$\mathcal{L}_1^{(m,n)} = \mathcal{L}_1^{(n,m)} = 3\mathcal{L}_2^{(m,n)} \quad (m,n = 1,\ldots,N, \quad m \neq n);$$

$$\mathcal{L}_2^{(m,m)} = \left(\frac{\pi m}{L}\right)^2 + 1 - 2H - \frac{2}{L} - \frac{2\pi^2 m}{L^2 \sinh\left(\frac{\pi^2 m}{L}\right)},$$

$$\mathcal{L}_1^{(m,m)} = \left(\frac{\pi m}{L}\right)^2 + 1 - \frac{6}{L} - \frac{6\pi^2 m}{L^2 \sinh\left(\frac{\pi^2 m}{L}\right)}. \tag{2.45}$$

In eq.(2.43) we restricted ourselves to the cosine series since u and v are assumed to be even. The matrices $\mathcal{L}_1$ and $\mathcal{L}_2$ are finite-dimensional approximations for the differential operators L_1 and L_2, respectively. In eq.(2.45) we have also approximated finite-range integrals of the form $\int_0^L \operatorname{sech}^2(x)\cos\left(\frac{\pi m x}{L}\right)dx$ by

$$\int_0^\infty \operatorname{sech}^2(x)\cos\left(\frac{\pi m x}{L}\right)dx = \frac{\pi^2 m}{2L}\sinh\left(\frac{\pi^2 m}{2L}\right).$$

The introduced error is exponentially small in L. The normalization condition (2.20) for the eigenfunctions translates into the normalization condition for the Fourier coefficients:

$$2\left(\mathbf{u}^2 + \mathbf{v}^2\right) = 1. \tag{2.46}$$

The matrix eigenvalue problem (2.44)-(2.46) was solved by a standard numerical routine. Taking $L = 20$ with $N = 100, 200$ and 400, we have found $H_c = 0.0597928, \omega_c = 0.83028$ and $\beta = 1.644676$ in all cases, while increasing the interval twice ($L = 40$) gave $H_c = 0.0597933, \omega_c = 0.830294$ and $\beta = 1.644669$ (both for $N = 200$ and 400). Further increasing the interval ($L = 80$ with $N = 400$) did not bring any change to the last set of numbers.

The need for such a high accuracy stems from the fact that small errors in H_c, ω_c and hence the critical wavenumber (2.29), produce large errors in the asymptotic phase

University of Cape Town

of the radiation-wave solution $u_2(x)$, $v_2(x)$ as $|x| \to \infty$. Since it is exactly the asymptotic phase that selects the particular solution we need (the outgoing wave), an inaccurately determined far-field phase would have resulted in an incorrect near-field behaviour of u_2, v_2 and eventually, in a highly inaccurate value of the integral ζ [eq.(2.40)].

Having found the critical eigenvalue ω_c and the corresponding eigenvector $(\mathbf{u}_c, \mathbf{v}_c)$, we proceed to solution of the nonhomogeneous equation (2.25). Expanding

$$\begin{pmatrix} u_1(x) \\ v_1(x) \end{pmatrix} = \frac{1}{\sqrt{L}} \begin{pmatrix} u_1^{(0)} \\ v_1^{(0)} \end{pmatrix} + \sqrt{\frac{2}{L}} \sum_{n=1}^{\infty} \begin{pmatrix} u_1^{(n)} \\ v_1^{(n)} \end{pmatrix} \cos\left(\frac{\pi n x}{L}\right), \tag{2.47}$$

and substituting into (2.25) gives

$$\mathcal{M}_{\omega_c} \begin{pmatrix} \mathbf{u}_1 \\ \mathbf{v}_1 \end{pmatrix} \equiv \begin{pmatrix} \mathcal{L}_1 & -\omega_c \mathbf{I} \\ -\omega_c \mathbf{I} & \mathcal{L}_2 \end{pmatrix} \begin{pmatrix} \mathbf{u}_1 \\ \mathbf{v}_1 \end{pmatrix} = - \begin{pmatrix} \mathbf{v}_c \\ \mathbf{u}_c \end{pmatrix}, \tag{2.48}$$

with $\mathbf{u}_1 = (u_1^{(0)}, u_1^{(1)}, \ldots, u_1^{(N)})^T$ and $\mathbf{v}_1 = (v_1^{(0)}, v_1^{(1)}, \ldots, v_1^{(N)})^T$. Although the matrix $\mathcal{M}_{\omega_c}$ has a zero eigenvalue, the solvability of this linear system is guaranteed by the fact that the associated eigenvector $\{\mathbf{u}_c, \mathbf{v}_c\}$ satisfies the condition (2.30):

$$\mathbf{u}_c \cdot \mathbf{v}_c = 0. \tag{2.49}$$

In order to factor out the linear subspace spanned by this eigenvector, we decompose the singular matrix as $\mathcal{M}_{\omega_c}\mathcal{E} = \mathcal{Q}\mathcal{R}$, where $\mathcal{R}$ is upper-triangular and $\mathcal{Q}$ orthogonal matrix. Eq.(2.48) is transformed to the upper triangular form:

$$\mathcal{R} \begin{pmatrix} \tilde{\mathbf{u}}_1 \\ \tilde{\mathbf{v}}_1 \end{pmatrix} = -\mathcal{Q}^T \begin{pmatrix} \mathbf{v}_c \\ \mathbf{u}_c \end{pmatrix}, \tag{2.50}$$

where

$$\begin{pmatrix} \tilde{\mathbf{u}}_1 \\ \tilde{\mathbf{v}}_1 \end{pmatrix} = \mathcal{E}^{-1} \begin{pmatrix} \mathbf{u}_1 \\ \mathbf{v}_1 \end{pmatrix} \tag{2.51}$$

and $\mathcal{E}$ is a permutation matrix which is chosen so that to make the zero diagonal element of the matrix $\mathcal{R}$ appear in the lower right corner. The matrix $\mathcal{Q}$ will then contain the vector $\{\mathbf{u}_c, \mathbf{v}_c\}$ as its last column and by virtue of eq.(2.49), the last component of the vector on the right-hand side of eq.(2.50) will be zero. Hence, in order to solve the linear system (2.50) it is sufficient to discard its last equation (which is simply $0 \cdot \tilde{v}_1^{(N+1)} = 0$). The resulting system of $(2N+1)$ equations has a nonsingular matrix and can be solved by a standard routine. After that we put $\tilde{v}_1^{(N+1)} = 0$ and use eq.(2.51) to recover a solution of the original system (2.48). [Choosing any other value for $\tilde{v}_1^{(N+1)}$ amounts to adding

University of Cape Town

$\tilde{v}_1^{(N+1)} \times \{u_c, v_c\}$ to the solution $\{u_1, v_1\}$; in view of the orthogonality relation (2.30) this does not affect the value of α, eq.(2.38).]

The accuracy of the computation can be judged by the values of the integral (2.38). Choosing $L = 20$ with $N = 100, 200$ and 400 we obtained $\alpha = 1.330575$ in all cases; doubling the interval length with $N = 200$ and 400 gave $\alpha = 1.329676$; finally taking $L = 80$ with $N = 400$ produced $\alpha = 1.329675$.

The nonhomogeneous equation (2.24) is solved in a similar way. The only difference is that since the homogeneous solution of eq.(2.24) is an odd function, the matrix $\mathcal{L}_1$ is nonsingular and so there is no need in the diagonalization in this case.

2.3.2 Radiation waves: the two-interval technique

The solution of the boundary-value problem (2.27)-(2.28) turns out to be somewhat more laborious. As we have already mentioned in sec.2.2.2, eq.(2.27) has a bounded homogeneous solution:

$$\begin{pmatrix} L_1 & -2\omega_c \\ -2\omega_c & L_2 \end{pmatrix} \begin{pmatrix} u_h \\ v_h \end{pmatrix} = 0. \tag{2.52}$$

This solution is the eigenfunction of the operator (2.13) associated with the continuous spectrum eigenvalue $\omega = 2\omega_c$. In general, the forcing term on the right-hand side of (2.27) will not satisfy the condition of solvability of eq.(2.27) in the class of square-integrable functions:

$$\int_{-\infty}^{\infty} \{u_h, v_h\} \cdot \begin{pmatrix} 3u_c^2 - v_c^2 \\ 2u_c v_c \end{pmatrix} U_0 \, dx = 0. \tag{2.53}$$

This does not mean, of course, that *nondecaying* nonhomogeneous solutions do not exist. Quite the contrary, from the fact that u_h, v_h undergo nondecaying oscillations as $|x| \to \infty$ one can readily deduce that the nonhomogeneous eq.(2.27) has oscillatory solutions. We need to construct the solution $\{u_2, v_2\}$ satisfying the radiation conditions (2.28) at infinity; the problem, however, is that the Fourier method can only be implemented on *finite* intervals. This difficulty can be circumvented by making use of *two* finite intervals; our method is as follows.

First, we observe that the homogeneous equation (2.52) will not, in general, have solutions with periodic boundary conditions $u_h(L) = u_h(-L)$, $u_h'(L) = u_h'(-L)$ (and similarly for v_h). The periodic solutions will arise only for particular values of L. [Here we assume that L is large enough ($L \gg 1$) so that when $|x| \sim L$, the functions $u_h(x)$

University of Cape Town

and $v_h(x)$ will have settled to their oscillatory asymptotes.] For these *resonant* values of L and for sufficiently large $|x| \sim L$ we will have then

$$u_h \to A\cos\{k_c(|x| - L)\} \tag{2.54}$$

and a similar relation for v_h. Next, since the operator $M_{2\omega_c}$ has a zero eigenvalue with the associated eigenfunction periodic on the interval $(-L,\ L)$, the nonhomogeneous equation (2.27) does not have a periodic solution on this interval. We can, however, solve it on a nonresonant interval $(-\tilde{L},\ \tilde{L})$, where $\tilde{L} \neq L$; we will denote the corresponding solution $\{\tilde{u}_2,\ \tilde{v}_2\}$. The functions on the right-hand side of eq.(2.27) fall with distance[2] as $e^{-|x/x_0|}$, where $x_0 \approx 0.6$; consequently we should choose $\tilde{L} \gg 1$. Then, for sufficiently large $|x| \sim \tilde{L}$ we have

$$\tilde{u}_2 \to B\cos\{k_c(|x| - \tilde{L})\} \tag{2.55}$$

and a similar relation for $\tilde{v}_2$.

Finally, the nonhomogeneous solution satisfying the radiation condition (2.28) can be constructed as a linear combination of the nonhomogeneous solution $\{\tilde{u}_2,\ \tilde{v}_2\}$, periodic with period $2\tilde{L}$, and the even homogeneous solution $\{u_h,\ v_h\}$ periodic with period $2L$:

$$\begin{pmatrix} u_2 \\ v_2 \end{pmatrix} = \begin{pmatrix} \tilde{u}_2 \\ \tilde{v}_2 \end{pmatrix} + C\begin{pmatrix} u_h \\ v_h \end{pmatrix}. \tag{2.56}$$

Substituting (2.54), (2.55) and (2.56) into (2.28) and setting the coefficients of $\exp\{ik_c|x|\}$ to zero, we find the value of C:

$$C = -\frac{B}{A}e^{ik_c(L-\tilde{L})}, \tag{2.57}$$

while comparing coefficients of $\exp\{-ik_c|x|\}$ gives a simple relation between $\mathcal{R}$, the amplitude of the radiation at infinity, and B, the amplitude of the nonhomogeneous solution periodic on the interval $(-\tilde{L}, \tilde{L})$:

$$B = -i\mathcal{R}\frac{e^{-ik_cL}}{\sin\{k_c(\tilde{L} - L)\}}. \tag{2.58}$$

This formula is another manifestation of the fact that the inhomogeneous problem cannot be solved on the resonant interval $(-L,\ L)$ on which the homogeneous solution was found. The smaller is the difference $|\tilde{L} - L|$, the greater will be the amplitude B and, according to (2.57), the larger coefficient C we will have to take in eq.(2.56) in order to offset the

[2]More precisely, $1/x_0 = 1+2\kappa_c$, where κ_c is the decay rate of $u_c(x)$ and $v_c(x)$: $\kappa_c^2 = 1-H_c-\sqrt{H_c^2+\omega_c^2}$.

University of Cape Town

ingoing component of the radiation wave. Consequently, the less accurate will be the resulting solution $u_2(x)$.

¿From the above construction it is also clear why we did not invoke *odd* homogeneous solutions. Adding an odd homogeneous solution to the function $u_2(x)$ given by eq.(2.56) with C fixed by eq.(2.57), would bring an uncompensated ingoing wave $\sim e^{ik_c|x|}$ thereby violating the radiation condition. For this reason we have identified the amplitudes of the right and left outgoing waves in Sec.2.2.2: $\mathcal{R}^+ = \mathcal{R}^- \equiv \mathcal{R}$.

In order to implement the above procedure numerically, we expand

$$\begin{pmatrix} u_2(x) \\ v_2(x) \end{pmatrix} = \frac{1}{\sqrt{L}} \begin{pmatrix} u_2^{(0)} \\ v_2^{(0)} \end{pmatrix} + \sqrt{\frac{2}{L}} \sum_{n=1}^{\infty} \begin{pmatrix} u_2^{(n)} \\ v_2^{(n)} \end{pmatrix} \cos\left(\frac{\pi n x}{L}\right),$$

$$2U_0(x) \begin{pmatrix} 3u_c^2(x) - v_c^2(x) \\ 2u_c(x)v_c(x) \end{pmatrix} = \frac{1}{\sqrt{L}} \begin{pmatrix} s_0 \\ t_0 \end{pmatrix} + \sqrt{\frac{2}{L}} \sum_{n=1}^{\infty} \begin{pmatrix} s_n \\ t_n \end{pmatrix} \cos\left(\frac{\pi n x}{L}\right). \tag{2.59}$$

Truncating the series at $n = N$, eq.(2.27) is converted to a linear algebraic system

$$\mathcal{M}_{2\omega_c} \begin{pmatrix} \mathbf{u}_2 \\ \mathbf{v}_2 \end{pmatrix} \equiv \begin{pmatrix} \mathcal{L}_1 & -2\omega_c \\ -2\omega_c & \mathcal{L}_2 \end{pmatrix} \begin{pmatrix} \mathbf{u}_2 \\ \mathbf{v}_2 \end{pmatrix} = \begin{pmatrix} \mathbf{s} \\ \mathbf{t} \end{pmatrix}, \tag{2.60}$$

where $\mathbf{u}_2, \mathbf{v}_2, \mathbf{s}$ and $\mathbf{t}$ are $(N+1)$-dimensional vectors, e.g. $\mathbf{u}_2 = (u_2^{(0)}, u_2^{(1)}, \ldots, u_2^{(N)})^T$. For resonant interval lengths L the matrix $\mathcal{M}_{2\omega_c}$ will have zero among its $2(N+1)$ eigenvalues $\mu_0, \mu_1, \ldots, \mu_{2N+1}$. The resonant lengths can be found with any desirable accuracy. In particular, taking $L = 20.11725$ with 100 Fourier modes yields the smallest modulus eigenvalue $\mu_\alpha = 1.1 \cdot 10^{-6}$. The choices $L = 38.610176$ with $N = 200$ and $L = 79.295415$ with $N = 400$ result in $\mu_\alpha = 3.7 \cdot 10^{-7}$ and $\mu_\alpha = 3.6 \cdot 10^{-7}$, respectively. The associated eigenvectors give a reasonably accurate approximation for the even homogeneous solution (u_h, v_h) of eq.(2.27), periodic with period $2L$.

Next, by varying intervals slightly, $L \to \tilde{L}$, we can always ensure that the smallest modulus eigenvalue $\tilde{\mu}_\alpha$ is not *very* small. In particular, choosing $\tilde{L} = 19.65$ with $N = 100$ gives $\tilde{\mu}_\alpha = 3.5 \cdot 10^{-2}$; for $\tilde{L} = 38$ with $N = 200$ and $\tilde{L} = 78.65$ with $N = 400$ one obtains $\tilde{\mu}_\alpha = 2.4 \cdot 10^{-2}$ and $\tilde{\mu}_\alpha = 1.2 \cdot 10^{-2}$, respectively. We solved the nonhomogeneous system (2.60) in each of these cases. The resulting even nonhomogeneous solution $\tilde{u}_2$, $\tilde{v}_2$ is, of course, periodic with period $2\tilde{L}$: $\tilde{u}_2'(0) = \tilde{u}_2'(\tilde{L}) = 0; \tilde{v}_2'(0) = \tilde{v}_2'(\tilde{L}) = 0$. These boundary conditions are imposed by making use of the Fourier expansions.

After $\tilde{L}$ has been picked up not very close to L, the dominant error in the numerically found solution u_2, v_2 comes from the *finiteness* of the interval $(-\tilde{L}, \tilde{L})$. The truncation of the infinite interval results in that the δ-function peak in the Fourier transform of

University of Cape Town

$\tilde{u}_2(x), \tilde{v}_2(x)$ is replaced by the *sinc*-function:

$$\mathcal{R}\delta(k-k_c) \longrightarrow \mathcal{R}\frac{\tilde{L}}{\pi}\frac{\sin\{(k-k_c)\tilde{L}\}}{(k-k_c)\tilde{L}} \equiv \mathcal{R}\frac{\tilde{L}}{\pi}\mathrm{sinc}\{(k-k_c)\tilde{L}\}. \tag{2.61}$$

Next, k can only assume a discrete set of values: $k = k_n = \pi n/\tilde{L}$, where $n = 0, 1, \ldots, N$. In general, *two* values of k, say k_m and k_{m+1}, will fall into the central lobe of the *sinc*-function: $k_c - \pi/\tilde{L} < k_m < k_{m+1} < k_c + \pi/\tilde{L}$. Accordingly, the solution $\tilde{u}_2, \tilde{v}_2$ will approach a linear combination of *two* cosines, $\cos(k_m x)$ and $\cos(k_{m+1}x)$, as $x \to \infty$. On the top of that, additional wavenumber components will be introduced by the sidelobes of the *sinc*-function, and thus the asymptotic waveform may substantially deviate from $\cos(k_c x)$.

These undesirable numerical effects can be reduced by increasing the interval length. First, the width of the central lobe of the *sinc*-function is equal to $2\pi/\tilde{L}$; as $\tilde{L}$ is increased, the central lobe narrows and the error in the asymptotic wavenumber reduces as $1/\tilde{L}$. Second, the amplitude of the central lobe grows in proportion to $\tilde{L}$ whereas amplitudes of the sidelobes remain constant. Hence, increasing the interval length suppresses the leakage to the sidelobes as well.

With the solution of the boundary-value problem (2.27)-(2.28) at hand, we can evaluate the coefficient ζ, eq.(2.40). The imaginary part of ζ can be recomputed in a different way: Instead of doing the integral (2.40), we identify the amplitude B from the asymptotic behaviour of $\tilde{u}_2(x)$ [see eq.(2.54)]; then recover the amplitude $\mathcal{R}$ from eq.(2.58) and finally, use eq.(2.41). The discrepancy between the two answers for $\mathrm{Im}\zeta$ provides an estimate for the accuracy of the computation.

We have carried out three series of calculations for the increasing values of L, $\tilde{L}$ and N. Results are presented in the following table.

	$\mathrm{Re}\zeta$	$\mathrm{Im}\zeta$, eq.(2.40)	$\mathrm{Im}\zeta$, eq.(2.41)
$L = 79.295415$, $\tilde{L} = 79.0$, $N = 400$	8.42×10^{-2}	1.92×10^{-3}	2.55×10^{-3}
$L = 119.9807$, $\tilde{L} = 119.75$, $N = 600$	8.15×10^{-2}	1.84×10^{-3}	2.22×10^{-3}
$L = 179.15922$, $\tilde{L} = 178.95$, $N = 600$	7.95×10^{-2}	1.76×10^{-3}	2.00×10^{-3}

When plotted versus $1/L$, the values of $\mathrm{Re}\zeta$ lie on the same straight line. The linear extrapolation to $L = \infty$ gives $\mathrm{Re}\zeta = (7.5555 \pm 0.0005) \times 10^{-2}$. The corresponding values of the imaginary part of the integral (2.40) (second column in Table 1) also change linearly with $1/L$. Extrapolating to infinity we get $\mathrm{Im}\zeta = (1.60 \pm 0.02) \times 10^{-3}$. On the other hand, the linear extrapolation of $\mathrm{Im}\zeta$ obtained by means of the far-field formula

University of Cape Town

(2.41) gives $\mathrm{Im}\zeta = (1.59 \pm 0.04) \times 10^{-3}$ which agrees well with the result of the numerical integration.

2.4 Reduced amplitude equations for the Hopf bifurcation

In this section we derive the reduced amplitude equation governing nonlinear evolutions beyond the Hopf bifurcation. The Hopf bifurcation occurs when a pair of complex-conjugate linearized eigenvalues crosses the imaginary axis at $\lambda = i\Omega_c(\Gamma)$ [see Figs. 2.2(a,c)]. As we have already mentioned, this bifurcation takes place in the *strongly* dissipative case, i.e. for $H = H_c(\Gamma)$ with *finite* Γ. [3] We expand the fields as in eqs.(2.16)-(2.19):

$$U = U_0(x) + \epsilon \left[a(\tau)e^{i\Omega_c t} + a^*(\tau)e^{-i\Omega_c t}\right] f_c(x) + \sum_{n=2}^{\infty} \epsilon^n U_n(x,t,\tau), \tag{2.62}$$

$$V = i\,\epsilon \left[a(\tau)e^{i\Omega_c t} - a^*(\tau)e^{-i\Omega_c t}\right] g_c(x) + \sum_{n=2}^{\infty} \epsilon^n V_n(x,t,\tau), \tag{2.63}$$

with, however, a different time scaling:

$$\tau = \epsilon^2 t.$$

We also assume that

$$H = H_c(\Gamma) + \epsilon^2 \hat{h}.$$

In eqs.(2.62)-(2.63) f_c and g_c are *complex* eigenfunctions of the operator (2.9) associated with the eigenvalue $\Omega = \Omega_c(\Gamma)$ and arising for $H = H_c(\Gamma)$. The second-order correction terms become

$$U_2 = |a|^2 f_0(x) + 2\,\mathrm{Re}\left\{a^2 e^{2i\Omega_c t} f_2(x)\right\},$$

$$V_2 = |a|^2 g_0(x) + 2\,\mathrm{Re}\left\{ia^2 e^{2i\Omega_c t} g_2(x)\right\},$$

where f_0 and g_0 are real functions satisfying the nonhomogeneous system

$$\begin{pmatrix} L_1 & 2\Gamma \\ 0 & L_2 \end{pmatrix} \begin{pmatrix} f_0 \\ g_0 \end{pmatrix} = 4U_0 \begin{pmatrix} 3|f_c|^2 + |g_c|^2 \\ i(f_c^* g_c - g_c^* f_c) \end{pmatrix}, \tag{2.64}$$

[3] In the previous two sections we used the notation H_c for the value of H for which the eigenvalues ω_a and ω_b merge and become complex. That previous H_c would be called $H_c(0)$ in the context of this section.

University of Cape Town

and $\{f_2, g_2\}$ is a complex solution to

$$\begin{pmatrix} L_1 & 2i\Gamma - 2\Omega_c \\ -2\Omega_c & L_2 \end{pmatrix} \begin{pmatrix} f_2 \\ g_2 \end{pmatrix} = 2U_0 \begin{pmatrix} 3f_c^2 - g_c^2 \\ 2f_c g_c \end{pmatrix}. \tag{2.65}$$

Solutions of the nonhomogeneous equations (2.64) and (2.65) decay exponentially as $|x| \to \infty$ because the solutions of the corresponding homogeneous equations are all unbounded — with a single exception of the translational mode $f_T(x) = \tanh x \operatorname{sech} x$, $g_T(x) = 0$ which we have already mentioned in Sec.2.2. As for the continuous spectrum of the operator (2.9), it consists of Ω with $\Omega(\Omega - 2i\Gamma) = \omega^2$, where ω is real and $\omega^2 > 1 - 2H_c$. Consequently, no real Ω belong to the continuous spectrum.

Thus, we proceed to the third-order approximation along the lines of Sec. 2.2 and find the complex Landau equation for the amplitude $a(\tau)$:

$$\hat{\alpha}\frac{da}{d\tau} = \hat{\beta}\hat{h}a - \hat{\zeta}|a|^2 a. \tag{2.66}$$

Here the complex coefficients $\hat{\alpha}$, $\hat{\beta}$, and $\hat{\zeta}$ are expressible through the functions f_c, g_c and f_0 to g_2:

$$\begin{aligned}
\hat{\alpha} &= (\Gamma + i\Omega_c)\int_{-\infty}^{+\infty} f_c g_c dx, \\
\hat{\beta} &= (\Omega_c - 2i\Gamma)\int_{-\infty}^{+\infty} g_c^2 dx, \\
\hat{\zeta} &= -\Omega_c \int_{-\infty}^{+\infty} \left(3|f_c|^2 f_c^2 + |f_c|^2 g_c^2 + |g_c|^2 f_c^2 + 3|g_c|^2 g_c^2\right) dx \\
&+ 2i\Gamma \int_{-\infty}^{+\infty} \left(3|g_c|^2 g_c^2 + 2|f_c|^2 g_c^2 - |g_c|^2 f_c^2\right) dx \\
&- 2\Omega_c \int_{-\infty}^{+\infty} U_0\{3f_c^2 f_0 + 3|f_c|^2 f_2 + (f_c g_c^* + f_c^* g_c)g_2 + g_c^2 f_0 - |g_c|^2 f_2\} dx \\
&+ 4i\Gamma \int_{-\infty}^{+\infty} U_0(g_c^2 f_0 - |g_c|^2 f_2 - i f_c g_c g_0 + f_c^* g_c g_2) dx.
\end{aligned}$$

The amplitude equation (2.66) is a normal form of the Hopf bifurcation occurring in finite-dimensional dissipative systems (see e.g. [91, 177]).

We conclude this section by a comment on the correspondence between "large Γ" and "small Γ" amplitude equations, i.e. eqs.(2.66) and (2.37). Sending $\Gamma \to 0$, we have

$$\begin{pmatrix} f_c \\ g_c \end{pmatrix} = \begin{pmatrix} u_c \\ v_c \end{pmatrix} + i\Gamma \begin{pmatrix} u_\gamma \\ v_\gamma \end{pmatrix} + \mathrm{O}(\Gamma^2) \tag{2.67}$$

University of Cape Town

and the coefficients of eq.(2.66) become

$$\hat{\alpha} = \Gamma\Omega_c\alpha, \quad \hat{\beta} = \frac{\Omega_c}{2}\beta, \quad \hat{\zeta} = \frac{\Omega_c}{2}\zeta. \tag{2.68}$$

On the other hand, when $\rho \to \infty$ the amplitude equation (2.37) becomes overdamped and $a_{\tau\tau}$ term can be discarded. This converts eq.(2.37) into the first-order equation[4]

$$2\alpha\rho a_\tau = (\beta h - \alpha\rho^2)a - \zeta|a|^2 a, \tag{2.69}$$

which coincides with (2.66), (2.68) after we have made the identification $\hat{h} = h - \alpha\rho^2/\beta$, or, equivalently,

$$H_c(\Gamma) = H_c(0) + \frac{\alpha}{\beta}\Gamma^2. \tag{2.70}$$

As an aside remark we note that eq.(2.70) can be rewritten as

$$\mathrm{h}_c(\gamma) = \mathrm{h}_c(0) + \frac{\alpha}{\beta}\frac{\gamma^2}{1+\mathrm{h}_c(0)} = 0.063596 + 0.76013\,\gamma^2, \tag{2.71}$$

which gives a small-γ approximation for the upper boundary of the stationary soliton's stability domain.

2.5 Finite-dimensional supercritical dynamics

2.5.1 Linear stage

The linear stability properties of the stationary soliton of the NLS equations (2.6-2.7) are exactly reproduced by the reduced amplitude equation, eq.(2.37). In terms of eq.(2.37) the linear stage of instability can be described by discarding the cubic term. This yields

$$a(\tau) = a_0 e^{\mu\tau}, \quad \mu = -\rho \pm \sqrt{\frac{\beta h}{\alpha}}. \tag{2.72}$$

In the *undamped* case ($\rho = 0$) eq.(2.72) implies that the oscillatory instability sets in immediately as h becomes greater than zero. This is in exact correspondence with Fig.2.1(a) where the instability is seen to arise when two imaginary eigenvalues $\lambda_a = i\omega_a$ and $\lambda_b = i\omega_b$ merge for $H = H_c$ (or, equivalently, for $h = 0$) and then split up and diverge from the imaginary axis. In the *weakly dissipative* case ($\rho \neq 0$) the coalescing eigenvalues have a negative real part at the point of their merger and so the instability sets in not when they

[4] A more formal way to obtain a first-order equation consists in transforming to $\tilde{\tau} = \tau/\rho$ and then sending $\rho \to \infty$.

University of Cape Town

coalesce but later, when one of the diverging eigenvalues crosses the imaginary axis. This happens at $h = h_c \equiv \alpha\rho^2/\beta$ and again, this threshold value is exactly reproduced by the threshold value of the reduced equation (which is straightforward from (2.72)).

Finally, in the *strongly* dissipative case the merger of the eigenvalues and the imaginary axis crossing occur for two widely separated values of H. Here we deal with the conventional Hopf bifurcation; in this case the second-order amplitude equation does not apply and should be replaced by the complex Landau equation, eq.(2.66).

2.5.2 Energy considerations

The undamped parametrically driven NLS equation (2.1) has two conserved quantities, the field momentum and energy. The eigenfunctions associated with the soliton's internal oscillation modes are symmetric in x and so these oscillations do not affect the value of the momentum. Consequently, energy is the only relevant integral in the present context. Although in the dissipative case ($\gamma \neq 0$) energy is not conserved, it remains a useful characteristic of the wave field in this case as well. For $\gamma \neq 0$ the local energy balance equation follows from eqs.(2.62.7):

$$\frac{\partial \mathcal{E}}{\partial t} + \frac{\partial F_{\mathcal{E}}}{\partial x} = -2\Gamma D_{\mathcal{E}}, \tag{2.73}$$

where

$$\mathcal{E} = \frac{1}{2}\left[U_x^2 + V_x^2 + U^2 + (1-2H)V^2 - (U^2+V^2)^2\right] \tag{2.74}$$

is the energy density,

$$F_{\mathcal{E}} = U_x V_{xx} - U_{xx} V_x + UV_x - (1-2H)VU_x + 2(U^2+V^2)\left(U_x V - UV_x\right) \tag{2.75}$$

the associated flux, and

$$D_{\mathcal{E}} = V_x^2 + (1-2H)V^2 - 2(U^2+V^2)V^2 \tag{2.76}$$

is the density of the dissipative function. Substituting the asymptotic expansion (2.16)-(2.17) in eq.(2.74) and integrating over x gives a total energy of the nonlinear wave field:

$$E = \int_{-\infty}^{+\infty} \mathcal{E}\, dx = E_0 + \epsilon^2 E_2 + \epsilon^3 E_3 + \mathrm{O}(\epsilon^4), \tag{2.77}$$

where E_0 is the energy of the unperturbed soliton ($E_0 = 2/3$), and E_2, E_3, *etc* are corrections due to the small localized perturbation. It follows from eqs.(2.13) and (2.16)-(2.17) that

$$E_2 = \omega_c I_c |a|^2,$$

University of Cape Town

where I_c is the quadratic functional (2.31) evaluated at the critical eigenvector $\{u_c, v_c\}$: $I_c = I[u_c, v_c]$. The quadratic form I is positive for the eigenmode $\{u_b, v_b\}$ which detaches from the edge of the continuous spectrum and negative for the eigenvector $\{u_a, v_a\}$ arising from the broken phase invariance (see Fig.2.3). Therefore, the eigenfunction $\{u_b, v_b\}$ always brings a positive contribution to the energy of the nonlinear field, while the contribution of the mode $\{u_a, v_a\}$ is always negative. At the resonance ($H = H_c$) the two contributions cancel each other and the second-order correction E_2 vanishes according to eq.(2.30). The merger of two modes of the opposite energetic contents produces the oscillatory instability of the stationary soliton (2.2). At the resonance, the asymptotic expansion (2.77) must be extended to include the third-order correction, for which we obtain

$$E_3 = i\alpha\omega_c \left(a\frac{da^*}{d\tau} - a^*\frac{da}{d\tau} \right) \tag{2.78}$$

with α is as in eq.(2.38). Finally, integrating eq.(2.73) over x and keeping terms up to ϵ^3 in the expansion (2.77) we find the rate of change of the energy of the localized wave field:

$$\frac{dE_3}{d\tau} = -2\rho E_3 - 2\omega_c \mathrm{Im}\zeta |a|^4. \tag{2.79}$$

[This equation, with E_3 defined by eq.(2.78), can also be derived directly from the reduced amplitude equation (2.37).] The equation (2.79) shows that the soliton is suffering two types of energy losses: the dissipative losses described by the first term on the right-hand side and losses due to the emission of radiation waves described by the second term.

2.5.3 Effective particle representation

It appears useful to interpret the reduced amplitude equation (2.37) as the equation of motion of a fictitious classical particle. In terms of the vector $\mathbf{r} \equiv \{\mathrm{Re}\, a, \mathrm{Im}\, a\}$, Eq.(2.37) becomes

$$\ddot{\mathbf{r}} + 2\rho\dot{\mathbf{r}} - \eta\mathbf{r} + gr^2\mathbf{r} = qr^2\mathbf{r} \times \hat{\mathbf{z}}, \tag{2.80}$$

where we have defined

$$g = \frac{\mathrm{Re}\zeta}{\alpha} \approx 0.0568, \quad q = \frac{\mathrm{Im}\zeta}{\alpha} \approx 0.0012,$$

and

$$\eta = \frac{\beta}{\alpha}h - \rho^2.$$

(The control parameter η is positive in the supercritical region). Next, $\hat{\mathbf{z}}$ is a unit vector in the vertical direction; $r \equiv |\mathbf{r}|$, and the overdot indicates differentiation with respect to

University of Cape Town

τ. Eq.(2.80) describes a particle in a mexican hat-shaped radially-symmetric potential

$$\mathcal{U}(r) = -\frac{\eta}{2}r^2 + \frac{g}{4}r^4, \tag{2.81}$$

subject to the constant friction with coefficient 2ρ and clockwise r-dependent torque $-qr^4\hat{\mathbf{z}}$. Two quantities useful for the analysis are the angular momentum

$$l = \left[\mathbf{r} \times \dot{\mathbf{r}}\right]\Big|_z = \frac{i}{2}(a\dot{a}^* - a^*\dot{a}), \tag{2.82}$$

and the Hamiltonian

$$\mathcal{H} = \frac{\dot{r}^2}{2} + \frac{l^2}{2r^2} + \mathcal{U}(r). \tag{2.83}$$

In terms of l and $\mathcal{H}$ the vector equation (2.80) can be rewritten as

$$\dot{l} = -2\rho l - qr^4, \tag{2.84}$$

$$\dot{\mathcal{H}} + 2\rho\dot{r}^2 = -2\rho\frac{l^2}{r^2} - qlr^2. \tag{2.85}$$

Notice that l coincides, up to a constant factor, with the third-order correction to the soliton's energy, eq.(2.78):

$$E_3 = 2\alpha\omega_c l. \tag{2.86}$$

Accordingly, eq.(2.84) is simply the equation of the soliton's energy variation, eq.(2.79), rewritten in terms of the angular momentum of the fictitious particle.

2.5.4 Conservative case ($\rho = 0$)

First we consider the case $\rho = 0$. Although the nonlinear Schrödinger equation is conservative in this case (i.e. the total energy (2.77) does not change with time), the motion of the effective particle is not. According to eq.(2.79), in the conservative case the solitary wave evolves in such a way that the energy E_3 is decreasing at all times due to the radiation losses. In the language of the fictitious particle this means that the angular momentum is always growing towards minus infinity due to the nonzero clockwise torque. As we will see, the consequence of this in the unstable region $h > 0$ is that the dynamical system (2.37) has no bounded trajectories and the amplitude a has to grow indefinitely.

If there were no external torque ($q = 0$), both l and $\mathcal{H}$ would be conserved and consequently, the fictitious particle would perform quasiperiodic oscillations in the ring $R_1 < r < R_2$. Here R_1^2 and R_2^2 are the two positive roots of the cubic equation

$$\mathcal{U}_{\text{eff}}(R^2) = \mathcal{H}, \quad \mathcal{U}_{\text{eff}}(R^2) = \frac{l^2}{2R^2} - \frac{\eta}{2}R^2 + \frac{g}{4}R^4. \tag{2.87}$$

University of Cape Town

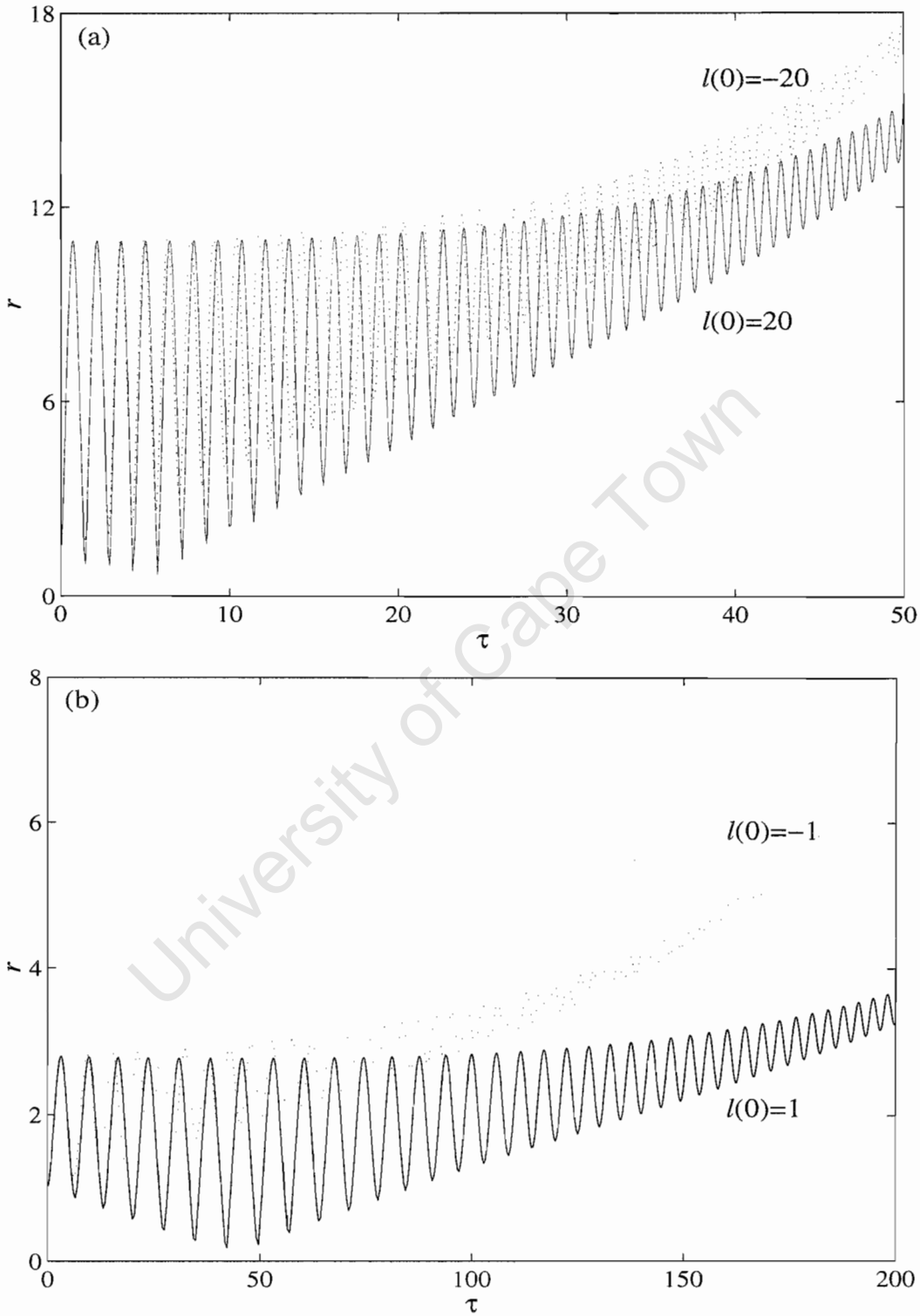

University of Cape Town

Figure 2.4: The motion of the undamped classical particle as obtained by numerical simulations of eq.(2.80): the radial position of the particle (a,b) and the exponent $\sigma = gl^4/\mathcal{H}^3$ (c,d). In these plots $h = 0.1\,(\eta = 0.1237)$; in all four runs the initial radial position was $r(0) = 1$ and the initial radial velocity $\dot{r}(0) = 0$. On (a,c) the initial angular momentum is $l(0) = \pm 20$ which gives $\eta^2/g\mathcal{H}(0) \sim 10^{-3}$ and $\sigma(0) \sim 10^{-3}$ so that the inequalities (2.91)-(2.92) hold true. On the contrary, neither of these inequalities is satisfied for the evolutions shown on (b,d); these start with $l(0) = \pm 1$ which gives $\eta^2/g\mathcal{H}(0) \approx 0.6$ and $\sigma(0) \approx 0.6$.

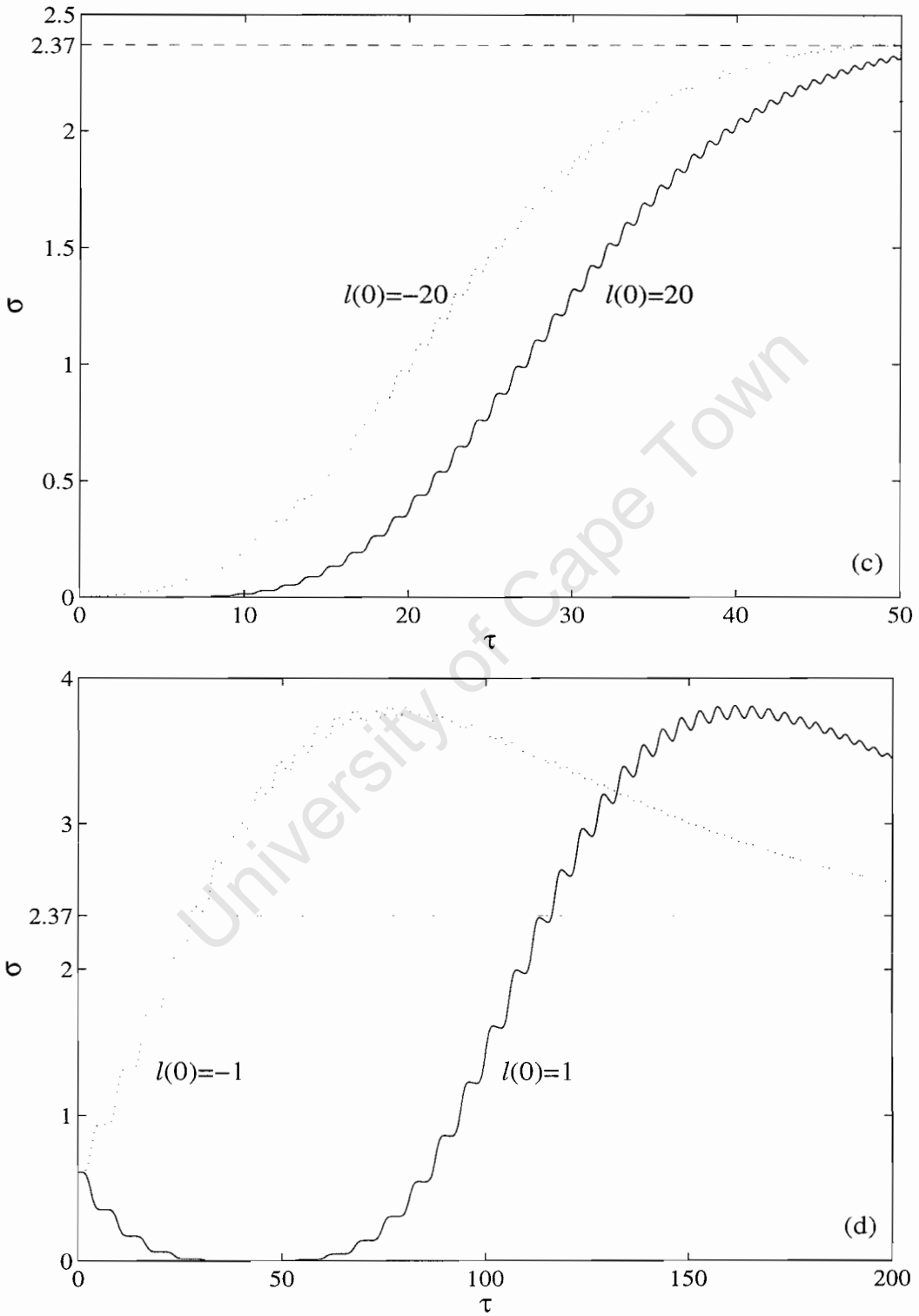

Figure 2.4 continued.

University of Cape Town

Let now q be nonzero but so small that we can still regard the particle as being trapped in an effective radially-symmetric potential well (2.87), with l, the width of the centrifugal barrier, and the energy of the particle slowly changing with time:

$$\dot{l} = -qr^4, \quad \dot{\mathcal{H}} = -qlr^2. \tag{2.88}$$

Assume first that the initial value of the angular momentum is negative: $l(0) < 0$. Then l will grow in magnitude remaining negative all the time, and the energy $\mathcal{H}$ will also grow. It is not difficult to show that as a result of this, the inner and outer radii of the ring (the so-called apsidal distances) will grow as well. Indeed, differentiating the identity $\mathcal{U}_{\text{eff}}(R_i^2) = \mathcal{H}$ and then using eq.(2.88) and the representation

$$\frac{l^2}{2R^2} - \frac{\eta}{2}R^2 + \frac{g}{4}R^4 - \mathcal{H} = \frac{g}{4}\frac{(R^2 - R_1^2)(R^2 - R_2^2)(R^2 + R_3^2)}{R^2}, \tag{2.89}$$

one finds

$$\frac{d}{d\tau}R_i^2 = -\frac{4qlr^2}{g}\frac{|R_i^2 - r^2|}{(R_2^2 - R_1^2)(R_i^2 + R_3^2)}, \quad i = 1, 2, \tag{2.90}$$

which is ≥ 0 for $l < 0$. Intuitively it is quite clear from (2.90) that the inner circle of the ring will grow faster than the outer circle; this claim can be readily justified by comparing the increments incurred by R_1 and R_2 in one half-period of oscillation, i.e. as the particle travels from R_1 to R_2. Consequently, the particle will spin around the origin within an adiabatically expanding and narrowing annular well. (By "narrowing" we mean that the width of the ring will be decreasing.)

Assume now that the initial value of the angular momentum is positive: $l(0) > 0$. In this case both l and $\mathcal{H}$ will initially decrease, and, according to (2.90), the trajectory will be sandwiched between two adiabatically shrinking circles: $dR_{1,2}/d\tau < 0$. Eventually l will become negative, and the evolution will cross over to the previous scenario.

The motion remains adiabatic as long as the width of the ring, $R_2 - R_1$, is much larger than the increments incurred by $R_1(\tau)$ and $R_2(\tau)$ during one half-period of oscillation. To find the region of applicability of this condition, we consider the stage where the Hamiltonian is already so large that

$$\frac{\eta^2}{g\mathcal{H}} \ll \frac{1}{3}. \tag{2.91}$$

We also assume, for simplicity of calculations, that[5]

$$\sigma \equiv \frac{gl^4}{\mathcal{H}^3} \ll \left(\frac{4}{3}\right)^3; \tag{2.92}$$

[5]The particular numerical values on the right hand side of (2.91) and (2.92) are suggested simply by the fact that for $\eta^2/g\mathcal{H} < 1/3$ and $\sigma < (4/3)^3$, the roots of the cubic equation can be found as convergent series in $(\eta^2/g\mathcal{H})$ and σ.

University of Cape Town

then the roots R_i are given by simple expressions

$$R_1^2 \approx \frac{l^2}{2\mathcal{H}}, \quad R_2^2 \approx R_3^2 \approx \left(\frac{4\mathcal{H}}{g}\right)^{1/2}. \tag{2.93}$$

Notice that in view of eq.(2.92), $R_1/R_2 \ll 1$. (More precisely, $R_1^2/R_2^2 \ll 2/\sqrt{27}$). ¿From (2.90) it follows that the velocity of expansion (or contraction) of the inner circle of the ring satisfies

$$|\dot{R}_1| < \frac{2q|l|}{g}\frac{\sqrt{r^2 - R_1^2}}{R_1 R_2},$$

where we have used the fact that $R_3 \approx R_2 \gg R_1$. On the other hand, the radial velocity of the particle is given by

$$|\dot{r}| = \sqrt{\frac{g(r^2 - R_1^2)(R_2^2 - r^2)(r^2 + R_3^2)}{2r^2}},$$

whence the increment in R_1 is

$$|\Delta R_1| = \left|\int_{R_1}^{R_2} \dot{R}_1 \frac{dr}{\dot{r}}\right| < q\left(\frac{g}{2}\right)^{-3/2} \frac{|l|\sqrt{R_2^2 - R_1^2}}{R_1 R_2^2}.$$

Using (2.93), we obtain

$$\frac{|\Delta R_1|}{R_2 - R_1} < \frac{2q}{g},$$

and since our $2q/g \approx 0.04$, we conclude that the adiabaticity condition $|\Delta R_1| \ll R_2 - R_1$ is in place. In a similar way one obtains

$$|\Delta R_2| < \sqrt{2} q g^{-3/2} \frac{|l|\sqrt{R_2^2 - R_1^2}}{R_2^3},$$

and making use of eq.(2.93), this becomes $q|l| < 2(g\mathcal{H})^{3/4}$. Therefore, in order to ensure that $|\Delta R_2| \ll R_2 - R_1$. it is sufficient to require that the dimensionless quantity σ, eq.(2.92), be much smaller than $(2g/q)^4 \sim 8 \times 10^7$. The latter is automatically satisfied if we impose eq.(2.92).

As $\mathcal{H}$ and $(-l)$ grow and the ring expands and its width narrows, the quotient σ will receive a positive increment after each period of oscillation. Quantitatively, the increment incurred in a half-period is

$$\Delta\sigma = \int_{R_1}^{R_2} \dot{\sigma}\frac{dr}{\dot{r}} > \frac{(\sqrt{2} - 1)\pi q}{2g}\sigma. \tag{2.94}$$

University of Cape Town

On the other hand, it takes the particle less than $\frac{\pi}{2}(g\mathcal{H})^{-1/4}$ units of time to travel from R_1 to R_2. Consequently, the average growth rate can be estimated as

$$\langle\dot{\sigma}\rangle \equiv \frac{\int_{R_1}^{R_2} \dot{\sigma}\frac{dr}{\dot{r}}}{\int_{R_1}^{R_2} \frac{dr}{\dot{r}}} \gg \frac{3^{1/4}(\sqrt{2}-1)q}{g} b^{1/2}\sigma^{5/4}, \tag{2.95}$$

where we have used eq.(2.91). This means that σ will grow at least as fast as $1/(\tau_0-\tau)^4$ (with τ_0 determined by the initial value of σ). Eventually the inequality (2.92) will be no longer valid, and oscillations in an adiabatically growing ring will be replaced by a regime of a faster, almost monotonic growth. (What happens is that the annular well becomes so narrow and expands so fast, that it simply "pulls" the particle along.)

It is not difficult to realize that this latter regime is self-similar. Since $\eta/(gr^2) \to 0$, the term with η can be neglected in eq.(2.85) and the growing solution of the resulting system is simply

$$r = \frac{r_1}{\tau_0-\tau}, \quad l = \frac{l_1}{(\tau_0-\tau)^3}, \tag{2.96}$$

where

$$r_1 = \frac{3}{\sqrt{2}}\frac{\sqrt{g}}{q}\left(1+\sqrt{1+\frac{8}{9}\frac{q^2}{g^2}}\right)^{1/2} \approx 3\frac{\sqrt{g}}{q} \approx 6.0\times 10^2, \tag{2.97}$$

and

$$l_1 = \frac{q}{3}r_1^4 \approx 5.0\times 10^7. \tag{2.98}$$

The energy grows as

$$\mathcal{H} = \frac{\mathcal{H}_1}{(\tau_0-\tau)^4}, \quad \mathcal{H}_1 = \frac{q^2}{12}r_1^6 \approx 5.4\times 10^6, \tag{2.99}$$

while the quotient σ remains constant:

$$\sigma = \frac{64g}{3q^2r_1^2} \approx \left(\frac{4}{3}\right)^3 \approx 2.37. \tag{2.100}$$

Figs. 2.4 (a,c) show results of the numerical simulation of the finite-dimensional system (2.37) [equivalently, eq.(2.80)] with the initial conditions satisfying eqs.(2.91) and (2.92). For both negative and positive $l(0)$ the evolution starts with a long transient where the particle performs oscillations in an adiabatically expanding or contracting ring. When $l(0) > 0$, the ring is initially shrinking (this phase is not very clearly seen in the plot) but then starts expanding. When $l(0) < 0$, the shrinking phase is absent and because of that, the evolution in this case is approximately 10 time units ahead of the one for $l(0) > 0$.

University of Cape Town

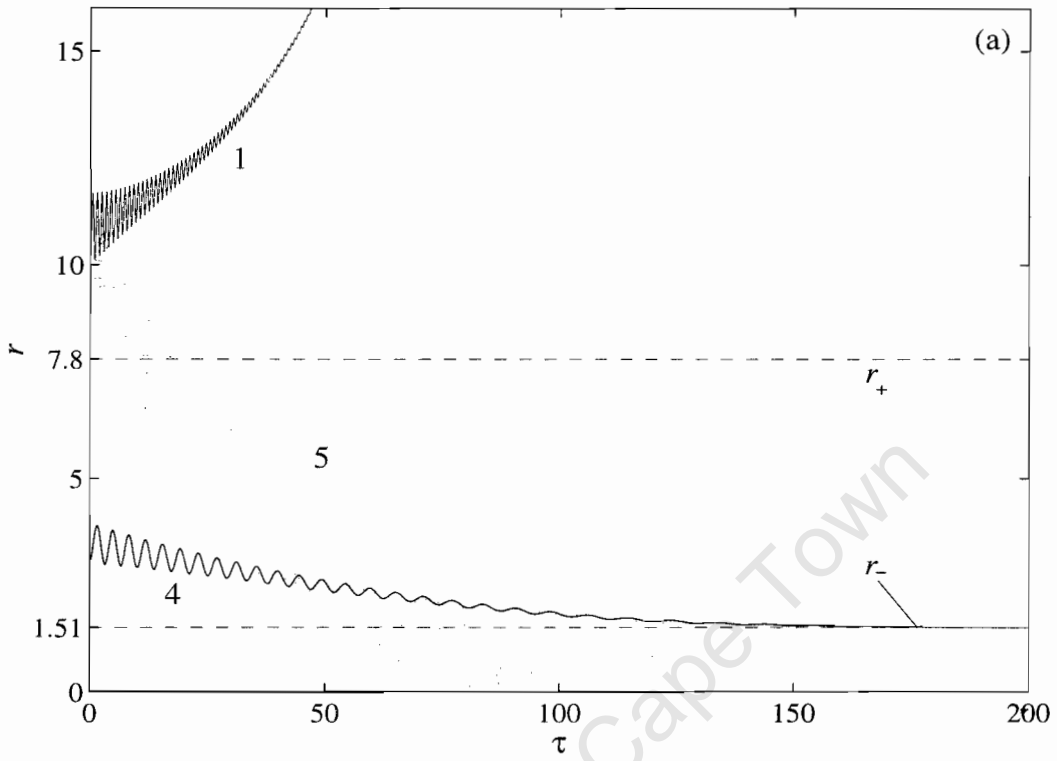

Figure 2.5 continues on the next page.

The exponent σ is seen to tend to the similarity value of 2.37; this indicates that the trajectory is attracted to the self-similar regime (2.96).

It is important to emphasize here that the inequalities (2.91)-(2.92) are sufficient but in no way necessary for the adiabatic transient to occur. (In fact, the only role of eqs.(2.91)-(2.92) was to simplify calculations.) In Figs.2.4 (b,d) we display trajectories of the particle with the initial conditions which do not satisfy (2.91)-(2.92). Similarly to the previous case, initially the particle is oscillating within an adiabatically changing ring (i.e. $\Delta R_i \ll R_2 - R_1$) but then escapes to infinity along a self-similar trajectory ($\sigma \to 2.37$). As in the previous case, the duration of the transient depends on the sign of $l(0)$: for $l(0) < 0$ the ring starts expanding straight away whereas for $l(0) > 0$, the ring first contracts until the sense of rotation of the particle is reversed, and only then starts inflating. In terms of the full, nonreduced nonlinear Schrödinger equation this means that initial perturbations "pushing" the soliton towards smaller values of E will trigger a much faster decay of the unstable soliton than those bringing positive contribution to its energy. Thus we may conclude that in the conservative case, the oscillatory instability bifurcation does not give rise to a stably oscillating soliton. The reason for this is the emission of a strong second-harmonic radiation. Because of the radiation, the trajectory of the soliton's perturbation

University of Cape Town

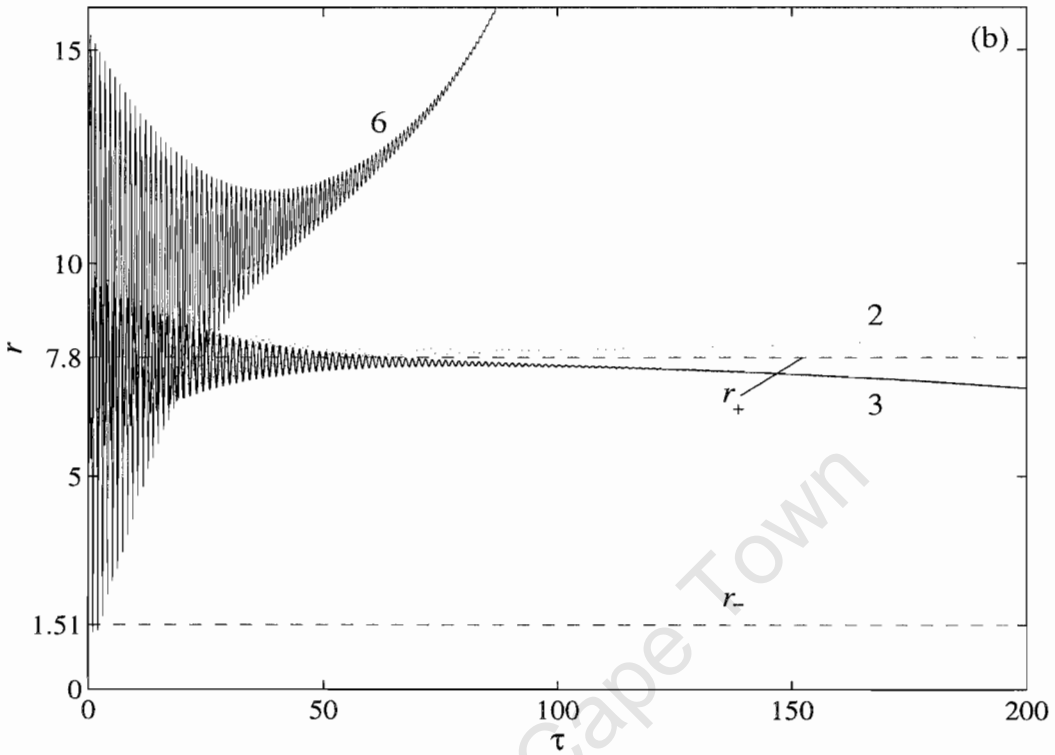

Figure 2.5: Numerical simulations of the damped fictitious particle, eq.(2.80). Here $\rho = 0.02$ and $\eta = 0.1237$; the corresponding stationary orbits are $r_- = 1.51$ (stable) and $r_+ = 7.80$ (unstable). Curve 1 starts with $r(0) = 10$, $l(0) = -300$ and curve 5 has $r(0) = 10$, $l(0) = +300$; in both cases the corresponding $R_1(0) = 10$, and $R_2(0) = 11.7$. Curve 2 has $r(0) = 9.97$, $l(0) = -99.40$; the apsidal distances in this case are $R_1(0) = 5.33$, and $R_2(0) = 9.97$. Curve 3 starts with $r(0) = 9.80$ and $l(0) = 96.04$; the corresponding $R_1(0) = 5.31$ and $R_2(0) = 9.80$. After visiting the unstable orbit r_+, the curve 2 escapes to infinity while the curve 3 settles to the stable orbit r_-. The initial conditions for the curve 4 are $r(0) = 3$ and $l(0) = -9$; hence $R_1(0) = 3$, $R_2(0) = 4$. Curve 6 has $r(0) = 0.5$, $l(0) = +20$, the corresponding $R_1(0) = 0.5$, $R_2(0) = 15.5$.

University of Cape Town

in its internal space is always unbounded. Provided the initial perturbation $|a(0)|$ is not very large, the evolution of instability starts with adiabatically growing oscillations which then transform into a regime of rapid self-similar growth.

2.5.5 Weakly dissipative case (finite ρ)

Adding a weak damping can hinder radiations from freely escaping from the oscillating soliton. According to eq.(2.84) this can result in the angular momentum of the fictitious particle settling to a constant value

$$l_\pm = -\frac{q}{2\rho} r_\pm^4, \tag{2.101}$$

where the radius can adopt one of the two values:

$$r_{\pm}^2 = \frac{2\rho^2}{q^2}\left(g \pm \sqrt{g^2 - \frac{q^2\eta}{\rho^2}}\right). \tag{2.102}$$

The corresponding circular orbits of eq.(2.80) have the form

$$a = r_{\pm}\exp\left(i\nu_{\pm}\tau\right), \tag{2.103}$$

with the angular velocities given by

$$\nu_{\pm} = -\frac{q}{2\rho}r_{\pm}^2. \tag{2.104}$$

Both closed trajectories exist for $g > 0$ which is in place in the case at hand. In terms of the parametrically driven NLS equation, eq.(2.102)-(2.104) describe two periodically oscillating solitons, different in the amplitude and frequency of oscillation.

The soliton with the smaller amplitude of oscillation, $|a| = r_-$, softly bifurcates from the stationary soliton at the onset of the oscillatory instability, $h = h_c = \alpha\rho^2/\beta$. As h is increased, it merges with the second oscillating soliton ($|a| = r_+$) at the turning point

$$\overline{h} = h_c\left[1 + \left(\frac{g}{q}\right)^2\right]. \tag{2.105}$$

The value $\overline{h}$ is the upper boundary of the domain of existence of the two circular orbits (2.102)-(2.104). Intuitively, it is quite clear that the orbit r_- should be stable and r_+ unstable; to verify this conjecture, we add a small perturbation:

$$a(\tau) = \left(r_{\pm} + e^{\mu\tau}\delta a\right)\exp\left(i\nu_{\pm}\tau\right), \quad |\delta a/r_{\pm}| \ll 1. \tag{2.106}$$

Substituting into (2.80) and linearizing with respect to δa yields a characteristic equation for the exponent μ:

$$\mu(\mu^3 + c_1\mu^2 + c_2\mu + c_3) = 0, \tag{2.107}$$

where $c_1 = 4\rho > 0$,

$$c_2 = 4\rho^2 + 2gr_{\pm}^2 + 4\nu_{\pm}^2 > 0,$$

and

$$c_3 = 4\rho\left(gr_{\pm}^2 - 2\nu_{\pm}^2\right) = \mp 4r_{\pm}^2\sqrt{g^2\rho^2 - q^2\eta}.$$

Using the Routh-Hurvitz test, one may readily check that apart from the trivial translational root $\mu = 0$, eq.(2.107) always has two roots with negative real parts. The forth root

University of Cape Town

is positive for $c_3 < 0$ and negative otherwise; that is, we have a stable root for $r = r_-$ and unstable one for $r = r_+$. Thus the oscillating soliton with the larger amplitude of oscillations is unstable and the one with the smaller amplitude is stable within our asymptotic approximation.

All trajectories of the fictitious particle will either be attracted to the stable circular orbit r_-, l_- or escape to infinity along a self-similar trajectory similar to the one arising in the undamped situation. This self-similar solution is given by the same equations (2.96) as in the $\gamma = 0$ case. We are not discussing basins of attraction of the above solutions; this analysis can be performed along the lines of the previous section. In the present work we confine ourselves to displaying only several characteristic transients (Fig.2.5).

In all our experiments the radial component of velocity was initially zero: $\dot{r}(0) = 0$. In the first simulation the initial angular momentum is negative and $|l(0)|$ and $r(0)$ are chosen in such a way that in the first place, $qr^4(0) > 2\rho|l(0)|$, and in the second, the ring of admissible motions is wider than both stationary circular orbits: $R_1(0) > r_+$. [We remind that $R_1(\tau)$ and $R_2(\tau)$ are defined as roots of eq.(2.87).] In this case the angular momentum starts decreasing further ($\dot{l} < 0$) and eq.(2.84) implies that the height of the centrifugal barrier at any fixed point $r = r_0$ grows as

$$\frac{d}{d\tau}\left(\frac{l^2}{2r_0^2}\right) = |l|\frac{qr^4 - 2\rho|l|}{r_0^2}. \tag{2.108}$$

On the other hand, in view of eq.(2.85) the growth rate of the energy of the particle, $\dot{\mathcal{H}}$, is bounded by $|l|(qr^4 - 2\rho|l|)/r^2$ which is smaller than (2.108) provided $r_0 < R_1(\tau)$. Consequently, the centrifugal barrier grows faster than $\mathcal{H}(\tau)$ and the "window" of admissible motions, (R_1, R_2), moves further away from r_+ (curve 1). The particle escapes to infinity.

Initial conditions with $l(0) < 0$ and $qr^4(0) > 2\rho|l(0)|$ do not necessarily give rise to unbounded motions. If the ring of admissible motions is initially smaller than r_+ [i.e. $R_2(0) < r_+$] or contains the orbit r_+ within it [i.e. $R_1(0) < r_+ < R_2(0)$], the expanding ring may lock on to the unstable circular orbit (curves 2 and 3) and then the initial expansion may switch to contraction (curve 3). Finally, such a trajectory will be attracted to the stable orbit r_-.

If $l(0) < 0$ but $qr^4(0) < 2\rho|l(0)|$, both the centrifugal barrier and energy as a whole will decrease and the trajectory will quickly settle to the circular orbit r_- (curve 4).

When the initial angular momentum is positive, the early stage of the evolution will necessarily have to go via the shrinking of the ring, curves 5 and 6. [This is because both l and $\mathcal{H}$ decrease, see eqs.(2.84)-(2.85).] Subsequently, *narrow* rings will shrink to the

University of Cape Town

circle r_- (curve 5) whereas the direction of change of the *large-width* rings may reverse and the trajectory escape to infinity (curve 6).

Returning to solutions of the parametrically driven, damped NLS equation (2.1), we conclude that in the weakly dissipative case the nonlinear evolution of the unstable stationary soliton $\psi_+(X)$ may follow two alternative scenarios. The first one is the formation of a temporally periodic soliton $\psi_\sim(X,T)$; this scenario is in exact agreement with numerical simulations of Ref.[38] where stable oscillating solitons were observed. In the vicinity of the bifurcation the soliton $\psi_\sim(X,T)$ oscillates about the "stationary point" $\psi_+(X)$; that is, the difference $|\psi_\sim - \psi_+|$ is not large. Alternatively, the stationary soliton may undergo a more dramatic transformation described by an unbounded trajectory of the effective particle. The final product of this transformation is beyond the scope of the reduced amplitude equation and the only means to find the resulting attractors seems to be the direct computer simulations of the full, nonreduced NLS (2.1). Some insight can also be gained from studying the undamped limit ($\gamma = 0$), see Section 2.6 below.

2.5.6 Strongly dissipative case ($\rho \gg 1$)

As we have demonstrated in Sec.2.4, for large ρ the second-order amplitude equation simplifies to the normal form of the Hopf bifurcation, eq.(2.69). Any initial condition $a(0)$ of this first-order equation will be attracted to a periodic orbit. The transient (and the resulting orbit) is described by an explicit solution

$$a = Q^{1/2}(\tau) \exp\left[-i\frac{\mathrm{Im}\hat{\zeta}}{\hat{\alpha}} \int_0^\tau Q(\tau')d\tau'\right], \tag{2.109}$$

where

$$Q(\tau) = \frac{Q_\infty}{1 - e^{-\mu(\tau+\tau_0)}} \tag{2.110}$$

for large perturbations of the soliton: $|a(0)|^2 > Q_\infty \equiv \hat{\beta}\hat{h}/\mathrm{Re}\hat{\zeta}$, and

$$Q(\tau) = \frac{Q_\infty}{1 + e^{-\mu(\tau-\tau_0)}} \tag{2.111}$$

for small initial conditions: $|a(0)|^2 < Q_\infty$. Here $\mu = 1/Q_\infty$, and τ_0 is an arbitrary positive constant.

Thus, unlike the weakly dissipative regime, no unbounded trajectories arise for $\gamma \sim 1$. In terms of the full, nonreduced NLS equation this means that in the strongly dissipative case, the unstable stationary soliton ψ_+ will necessarily evolve into a (stable) temporally-periodic soliton $\psi_\sim$. Although the finite-dimensional periodic orbit is stable

University of Cape Town

with respect to arbitrarily large perturbations, this does not guarantee, of course, that the soliton $\psi_\sim$ will be stable against arbitrarily large perturbations within the full NLS equation. We also need to emphasize here that the amplitude equation (2.66) is only valid in the vicinity of the Hopf bifurcation. Numerical simulations showed that for driving strengths further away from $\mathrm{h} = \mathrm{h}_c(\gamma)$, the oscillating soliton loses its stability to a double-periodic or chaotic attractor [38]. These higher bifurcations are not captured by the present asymptotic approach.

2.6 Long-term evolution of the oscillatory instability

2.6.1 Numerical simulations

In the case of finite γ conclusions of our finite-dimensional analysis are in agreement with earlier computer simulations [38] where the unstable stationary soliton ψ_+ was seen to evolve into a temporally-periodic soliton $\psi_\sim$. In the undamped case, on the contrary, our analysis shows that the oscillatory instability should result in a more fundamental transformation of the soliton. This case was not studied numerically before whereas the reduced amplitude equation provides no clue on what the corresponding asymptotic states should be. The case of *small* γ is intermediate; here the instability can give rise both to the oscillating soliton and to some other, yet unknown, asymptotic solutions. With the aim of gaining some insight into the nature of these asymptotic states as well as verifying conclusions of our finite-dimensional analysis, we have performed a series of computer simulations of the full, nonreduced nonlinear Schrödinger equation (2.1).

We restricted ourselves to the undamped case, $\gamma = 0$. Our numerical scheme is a generalization of the split-step pseudospectral method [272] and was previously utilized in Ref.[38]. The method imposes periodic boundary conditions $\psi(L) = \psi(-L), \quad \psi_X(L) = \psi_X(-L)$, where the length of the spatial interval was chosen to be $2L = 152$. Due to the periodic boundary conditions, the emitted radiation waves would re-enter the system and interact with the soliton. This would not happen if the simulations were carried out on an infinite line. In order to emulate the infinite-line situation, a "sound-absorbing" term $-i\gamma(X)\psi$ is added on the right-hand side of eq.(2.1). Here the function $\gamma(X)$ is almost zero within the subinterval $(-60, 60)$ and increases to the value of approximately 0.55 as $X \to \pm 76$:

$$\gamma(X) = 0.3\left[\tanh\left(\frac{X-70}{5}\right) - \tanh\left(\frac{X+70}{5}\right) + 2\right].$$

The effect of this term is to damp small-amplitude radiation waves emanating from the

University of Cape Town

soliton and prevent their reentry back into the system via the periodic boundaries. Typically we used $N = 2^{11} = 2048$ Fourier modes which implied the spatial resolution $\Delta X = 2L/N \approx 7.4 \times 10^{-2}$. Our time increment, $\Delta T = 1.0 \times 10^{-3}$, was chosen so that the stability condition [272] of this numerical scheme be in place: $\Delta T < (\Delta X)^2/\pi = 1.8 \times 10^{-3}$.

We set up the initial condition in the form (2.16)-(2.19), (2.22)-(2.23):

$$\psi(X,0) = A[U(AX) + iV(AX)], \tag{2.112}$$

with

$$U(x) = \mathrm{sech}(x) + 2\epsilon \mathrm{Re} a\, u_c(x) + \tag{2.113}$$

$$+\epsilon^2\{|a|^2\, u_0(x) - 2\mathrm{Im}\dot{a}\, u_1(x) + 2\mathrm{Re}[a^2\, u_2(x)]\},$$

$$V(x) = -2\epsilon \mathrm{Im} a\, v_c(x) - 2\epsilon^2\{\mathrm{Re}\dot{a}\, v_1(x) + \mathrm{Im}[a^2\, v_2(x)]\}. \tag{2.114}$$

Here a, $\dot{a}$ = const; u_c, v_c are the eigenfunctions of the operator (2.13) corresponding to $H = H_c$ and u_0, u_1, v_1, u_2, v_2 are solutions of the nonhomogeneous equations (2.24)-(2.25), (2.27). The link to the reduced amplitude equation (2.37) is provided by setting the two constants, a and $\dot{a}$, equal to the initial values [$a(0)$ and $\dot{a}(0)$, respectively] of eq.(2.37). Finally, A is given by eq.(2.4): $A = (1 + \mathrm{h})^{1/2}$. Our choice of h is related to the value of h used in simulations of the reduced system (2.37) in sec.2.5.4 ($h = 0.1$). Taking $\epsilon = 0.1$, eq.(2.21) gives $\mathrm{h} = 0.06472$. (To get an idea of how close to the bifurcation point we are, recall that the oscillatory instability sets in at $\mathrm{h}_c = 0.06359$.)

For all examined values of a and $\dot{a}$ — provided $|E_3|$ eq.(2.78) is not very large — the evolution starts with a relatively long period of growth of the oscillatory instability. During this transient period the field configuration may be regarded as a ψ_+ soliton with the amplitude and width oscillating about their stationary values (Fig.6). After the amplitude of the growing perturbation has reached a certain critical value, a cross-over occurs and the subsequent evolution settles to one of the two possible asymptotic regimes. Both asymptotic configurations are localised in space and oscillate in time. In contrast to the transient phase, these oscillations are not about the stationary soliton but about $\psi = 0$ [see Fig.6 (c,d)]. In both cases the oscillations of the soliton are accompanied by intensive radiation.

2.6.2 Asymptotic attractors

The first emerging attractor has a *negative* oscillation frequency with the magnitude slightly smaller than 1; it is bell-shaped and its amplitude is very slowly decaying in time

University of Cape Town

[Fig.6(a)]. We will be referring to this solution as the *breather*; it is indeed a relative of the breather solution of the Klein-Gordon equation [145, 53, 238, 40]. [Another, and possibly even closer relative is the soliton of the unperturbed NLS equation with the constant frequency shift, eq.(2.1) with $\gamma = \mathrm{h} = 0$.] Similarly to the Klein-Gordon breather, our breather lives in the gap of the continuous spectrum and can be constructed perturbatively.

To this end, we again decompose eq.(2.1) with $\gamma = 0$ into its real and imaginary part and expand ψ in powers of a small parameter, ε:

$$\psi = U + iV, \quad U = \varepsilon(U_0 + \varepsilon^2 U_2 + \ldots), \quad V = \varepsilon(V_0 + \varepsilon^2 V_2 + \ldots). \tag{2.115}$$

Here U_i and V_i depend on multiple space and time scales: $U_i = U_i(X, T; X_1, T_1)$, $V_i = V_i(X, T; X_1, T_1)$, where $X_1 = \varepsilon X$ and $T_1 = \varepsilon T$. The breather is therefore constructed as a perturbation of the trivial solution $\psi = 0$ with a small (but finite) amplitude. At the first order in ε we have a linear equation

$$M \begin{pmatrix} U_0 \\ V_0 \end{pmatrix} \equiv \begin{pmatrix} -\partial^2/\partial X^2 + 1 + \mathrm{h} & \partial/\partial T \\ -\partial/\partial T & -\partial^2/\partial X^2 + 1 - \mathrm{h} \end{pmatrix} \begin{pmatrix} U_0 \\ V_0 \end{pmatrix} = 0, \tag{2.116}$$

whose solutions are linear waves with the dispersion law $\omega^2 = 1 - \mathrm{h}^2 + k^2$. Since we are primarily interested in nonpropagating structures, we take

$$\begin{pmatrix} U_0 \\ V_0 \end{pmatrix} = \varphi(X_1, T_2) \begin{pmatrix} 1 \\ i\xi \end{pmatrix} e^{i\omega T} + c.c., \tag{2.117}$$

where

$$\omega = \sqrt{1 - \mathrm{h}^2} > 0, \quad \xi = \frac{1 + \mathrm{h}}{\omega} = \left(\frac{1 + \mathrm{h}}{1 - \mathrm{h}}\right)^{1/2}. \tag{2.118}$$

Next, at the order ε^2 we obtain

$$M \begin{pmatrix} U_2 \\ V_2 \end{pmatrix} = \begin{pmatrix} -\partial V_0/\partial T_2 + \partial^2 U_0/\partial X_1^2 + 2(U_0^2 + V_0^2)U_0 \\ \partial U_0/\partial T_2 + \partial^2 V_0/\partial X_1^2 + 2(U_0^2 + V_0^2)V_0 \end{pmatrix}. \tag{2.119}$$

Eq.(2.119) is only solvable if the right-hand side is orthogonal (in the sense of the R_2-scalar product) to the vector $(1, -i\xi)$. This gives the (undriven) NLS equation for φ:

$$-2i\xi \frac{\partial \varphi}{\partial T_2} + (1 + \xi^2)\frac{\partial^2 \varphi}{\partial X_1^2} + 2(3 + 2\xi^2 + 3\xi^4)|\varphi|^2 \varphi = 0, \tag{2.120}$$

with an obvious soliton solution. Returning to the original variable ψ, we can write our breather solution as

$$\psi_\downarrow = \varepsilon b \left(\frac{2(1 - \mathrm{h})}{2 + \mathrm{h}^2}\right)^{1/2} \left\{ \frac{1 + \xi}{2} e^{-i(\omega - \varepsilon^2 b^2/\omega)T} + \frac{1 - \xi}{2} e^{i(\omega - \varepsilon^2 b^2/\omega)T} \right\} \times \mathrm{sech}(\varepsilon b X) + \mathrm{O}(\varepsilon^3), \tag{2.121}$$

University of Cape Town

where ω and ξ are given by eq.(2.118), and the amplitude $b = \mathrm{O}(1)$ is a slowly changing parameter, which is not defined at this order of the expansion. Note that for small $\mathtt{h}$, ξ is close to 1 and the second term in (2.121) is negligible comparing to the first one. It is for this reason that in our numerical simulations the breather appears as a *negative* frequency solution. When $\mathtt{h} = 0$, we have $\omega = 1$ and eq.(2.121) is simply the soliton of the unperturbed NLS equation with the unit frequency shift.

The second localized attractor has *positive* oscillation frequency. Like the decaying soliton $\psi_\downarrow$, it is bell-shaped but its amplitude is growing with time [Fig. 6(b)]. This large-amplitude soliton can also be constructed as a series in small parameter ε; this time we write

$$\psi = \varepsilon^{-1}(\psi_0 + \varepsilon^2\psi_2 + ...), \tag{2.122}$$

where the coefficients of the expansion depend on multiple scales: $\psi_i = \psi_i\,(X_{-1}, T_{-2}; X, T)$. Here $X_{-1} = \varepsilon^{-1}X$ and $T_{-2} = \varepsilon^{-2}T$. Substituting (2.122) into eq.(2.1), the order ε^{-3} yields the unperturbed NLS equation:

$$i\frac{\partial\psi_0}{\partial T_{-2}} + \frac{\partial^2\psi_0}{\partial X_{-1}^2} + 2|\psi_0|^2\psi_0 = 0 \tag{2.123}$$

and so the large-amplitude soliton is given by

$$\psi_\uparrow(X,T) = \frac{B}{\varepsilon}\exp\left(i\frac{B^2}{\varepsilon^2}T\right)\mathrm{sech}\left(\frac{B}{\varepsilon}X\right) + O(\varepsilon), \tag{2.124}$$

where $B = \mathrm{O}(1)$ is a slowly changing function of X and T which is not defined at this level of approximation.

Finding the exact laws of variation of b and B is beyond the scope of this work. We will restrict ourselves to commenting only on *why* the amplitude of the breather $\psi_\downarrow$ has to decay and the amplitude of the soliton $\psi_\uparrow$ to increase. As we mentioned in Sec.2.5.1, in the undamped case the equation (2.1) conserves energy,

$$E = \int\left[|\psi_X|^2 + |\psi|^2 - |\psi|^4 + \frac{\mathtt{h}}{2}(\psi^2 + \psi^{*2})\right]dX. \tag{2.125}$$

Substituting (2.121) into (2.125) yields the energy of the breather:

$$E_\downarrow = E[\psi_\downarrow] = \frac{4(1-\mathtt{h}^2)}{2+\mathtt{h}^2}\varepsilon b + \mathrm{O}(\varepsilon^3), \tag{2.126}$$

while doing the same with eq.(2.124) gives the energy of the large-amplitude soliton:

$$E_\uparrow = E[\psi_\uparrow] \approx -\frac{2}{3}\left(\frac{B}{\varepsilon}\right)^3. \tag{2.127}$$

University of Cape Town

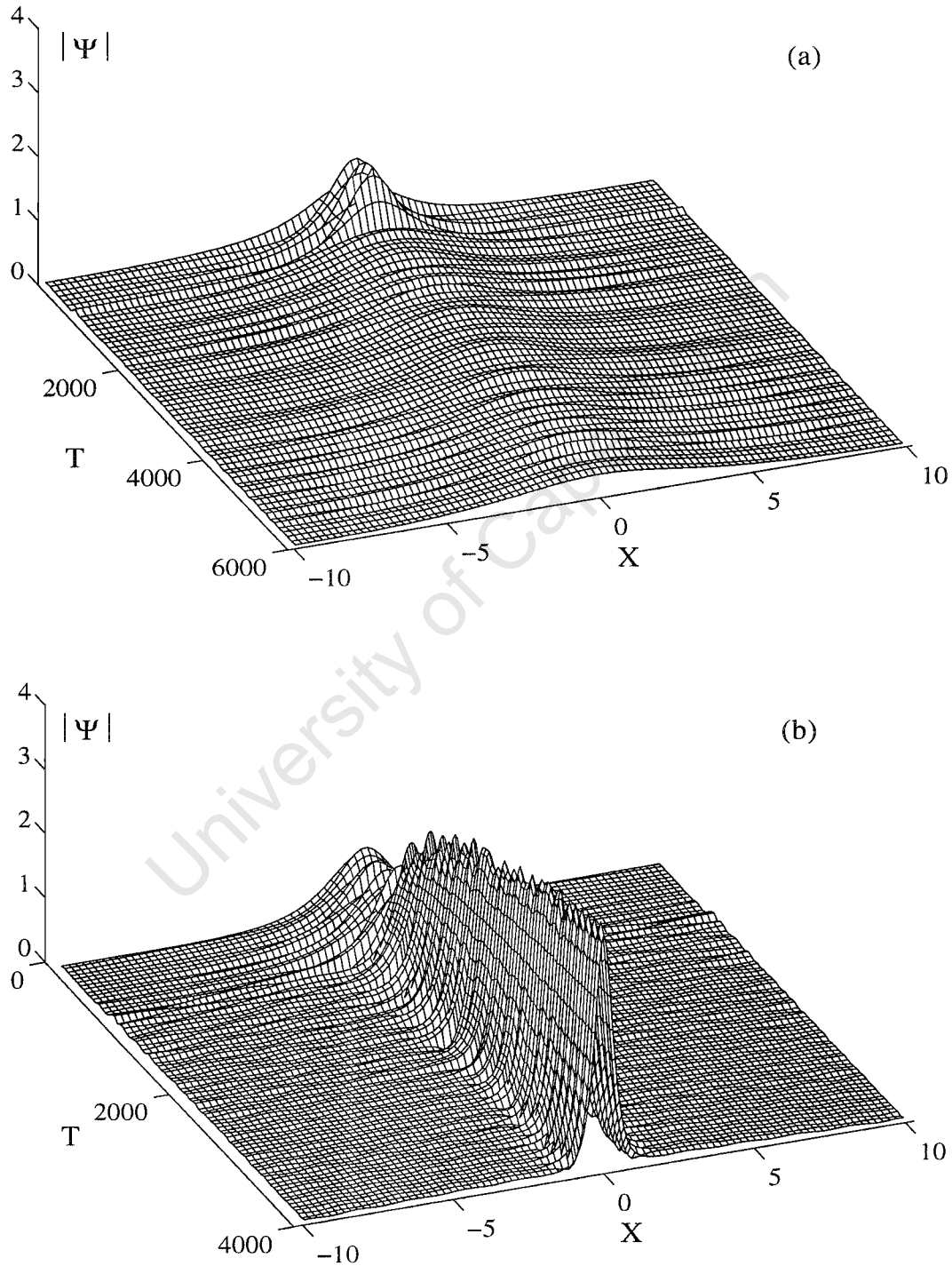

Figure 2.6 continues on the next page.

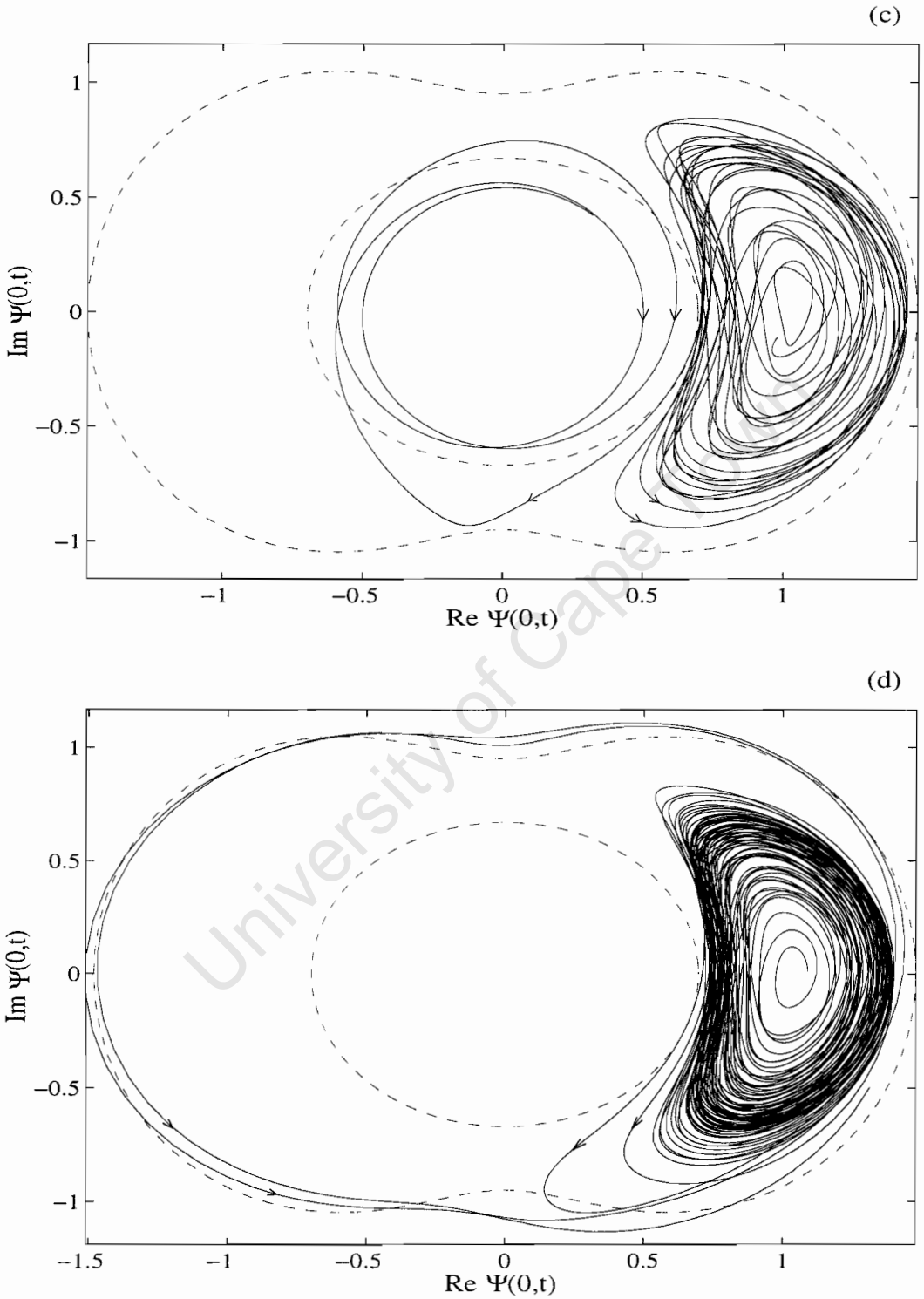

University of Cape Town

Figure 2.6: Evolution of the undamped soliton ($\gamma = 0$) perturbed by a perturbation of the form (2.112) with $|E_3| \sim 1$ [i.e. with $l(0) \sim 1$.] Here (a,c) $a = -1, \dot{a} = i$ and (b,d) $a = 1, \dot{a} = -i$; in both cases $l(0) = -1$. All four pictures are obtained by means of numerical simulations of the full, nonreduced NLS equation (2.1). The simulations were carried out on an interval $[-76, 76]$; on (a,b) the interval has been cut down for graphical clarity. On (c) and (d) plotted is the trajectory of the point $\psi(X = 0, T)$. The dashed lines sketch the boundaries of basins of attraction of (c) $\psi_\downarrow$ and (d) $\psi_\uparrow$ attractor. The arrows indicate the direction of the evolution.

Since the linear radiation waves take away positive energy, the energies $E_\downarrow$ and $E_\uparrow$ have to decay. According to eq.(2.126), this means that the amplitude b of the small-amplitude breather has to decrease. On the contrary, eq.(2.127) implies that the amplitude of the large-amplitude soliton, B, will have to grow.

Thus, from the energy point of view, the difference between the two attractors $\psi_\downarrow$ and $\psi_\uparrow$ is that in the former case the energy of the breather decreases to zero (remaining positive all the time) whereas in the latter case the energy of the soliton is negative and tends to minus infinity.

A natural question is whether the type of the asymptotic regime (decay or growth) can be predicted from the analysis of the finite-dimensional dynamics described by eq.(2.37) with a and $\dot{a}$ featuring in eq.(2.112) taken as the initial values. Surprisingly, the answer is *no*. The evolutions shown in Fig.6 (a,c) and (b,d) correspond to the choices $(a = -1, \dot{a} = i)$ and $(a = 1, \dot{a} = -i)$, respectively. Although these initial conditions evolve into two completely different asymptotic regimes, the corresponding trajectories of the fictitious particle on the plane are identical up to a constant angular shift. In both cases the initial conditions of the particle are $r(0) = 1$, $\dot{r}(0) = 0$ and $l(0) = -1$; the corresponding trajectory is shown in Fig. 2.4(b).

The finite-dimensional system (2.37) is invariant with respect to constant phase shifts $a \to ae^{i\theta_0}$ while it is exactly the initial phase of the perturbation that plays the crucial role in the selection of one or the other asymptotic regime. This is shown symbolically in Fig.6 (c,d). The two dashed closed contours demarcate what can roughly be considered as the boundaries of the basins of attraction of the decaying and growing soliton. Depending on the phase of $a(0)$ (i.e., depending on the initial angular position of the fictituous particle), the spiralling-out trajectory crosses the inner contour (schematically shown as a circle) or the outer one (a dumb-bell). In the first case the trajectory will remain within the inner contour, with the orbits of revolution slowly shrinking to the origin.[6] The corresponding solution of the NLS equation is attracted to the slowly decaying breather, $\psi_\downarrow$. In the second case the trajectory stays outside the dumb-bell, with the orbits slowly expanding. The corresponding NLS solution locks on to the growing soliton

[6]These inner and outer contours should not be confused with the inner and outer circular bounds of the trajectory of the effective particle discussed in Section 2.5.4. The equation of the fictitious particle describes growing oscillations of the field $\psi(X,T)$ about the unstable stationary soliton ψ_+ [i.e. about the point $\psi(0,T) = A$ in Fig.6 (c,d).] On the contrary, the boundaries of the basins of attraction of the solitons $\psi_\downarrow$ and $\psi_\uparrow$ are centered at the origin. Furthermore, the effective-particle description is valid only while the amplitude of the oscillations is still small; it ceases to be applicable *before* the spiral crosses one of the dashed closed contours in Fig.6 (c,d).

University of Cape Town

(2.124).

2.6.3 Large-energy initial conditions; evolution of the soliton ψ_-

The attractors $\psi_\downarrow$ and $\psi_\uparrow$ emerge if the energy $|E_3|$ of the perturbation is not very large (that is, if the initial position and velocity of the fictitious particle are of order 1). We have also studied the evolution of the initial condition corresponding to *large* $|E_3|$. [More specifically, we took $|\dot{a}(0)| \gg 1$ but $|a(0)| = O(1)$.] As we remember from the simulations of the finite-dimensional system (2.37), the growth of $|a|^2$ is much faster in this case. Consistently with the finite-dimensional description, the transient in the evolution of the NLS soliton was indeed seen to be much shorter.

A more significant distinction arises at a later stage, when the unstable soliton splits into a pair of long-lived small-amplitude breathers $\psi_\downarrow$ travelling with constant velocities in opposite directions (Fig.7). The explanation for this phenomenon is suggested by the spatial structure of the perturbation in this case, eq.(2.112). A large initial value of $\dot{a}$ gives rise to a large $\{u_1, v_1\}$-component in the perturbation while both $u_1(x)$ and $v_1(x)$ have a sharp dip in the middle which serves as a nucleus of the future splitting.

Finally, we have simulated the evolution of the soliton ψ_- [eq.(2.2)] which has a *positive* eigenvalue λ in its spectrum of linear excitations (and so is unstable with respect to a *nonoscillatory* mode). The initial condition was taken in the form

$$\psi(X,0) = -iA\mathrm{sech}(AX) - i\epsilon A[u(AX) - v(AX)],$$

where this time A stands for $A_- = (1-\mathrm{h})^{1/2}$, and $\{u(x), v(x)\}$ is the eigenvector[7] of the operator (2.13) associated with the pure imaginary eigenvalue $\omega = -i\lambda$. The subsequent evolution takes the soliton ψ_- to one of the two attractors observed in our simulations of the ψ_+ soliton. Namely, choosing $\epsilon < 0$ results in the slowly decaying breather (2.121) while in the $\epsilon > 0$ case one observes a slowly growing soliton (2.124). Thus, in the undamped case both the oscillatory and the translational, nonoscillatory, instability give rise to the same asymptotic attractors. The peculiarity of the oscillatory instability manifests itself only in the $\gamma \neq 0$ case, where it brings about a stably oscillating soliton.

[7] In the case of the ψ_- soliton the linearized operator has the same form as in the ψ_+ case, eqs.(2.10)-(2.13), where one only needs to replace $H \to -H$ and remember that now $H = -\mathrm{h}/(1-\mathrm{h})$.

University of Cape Town

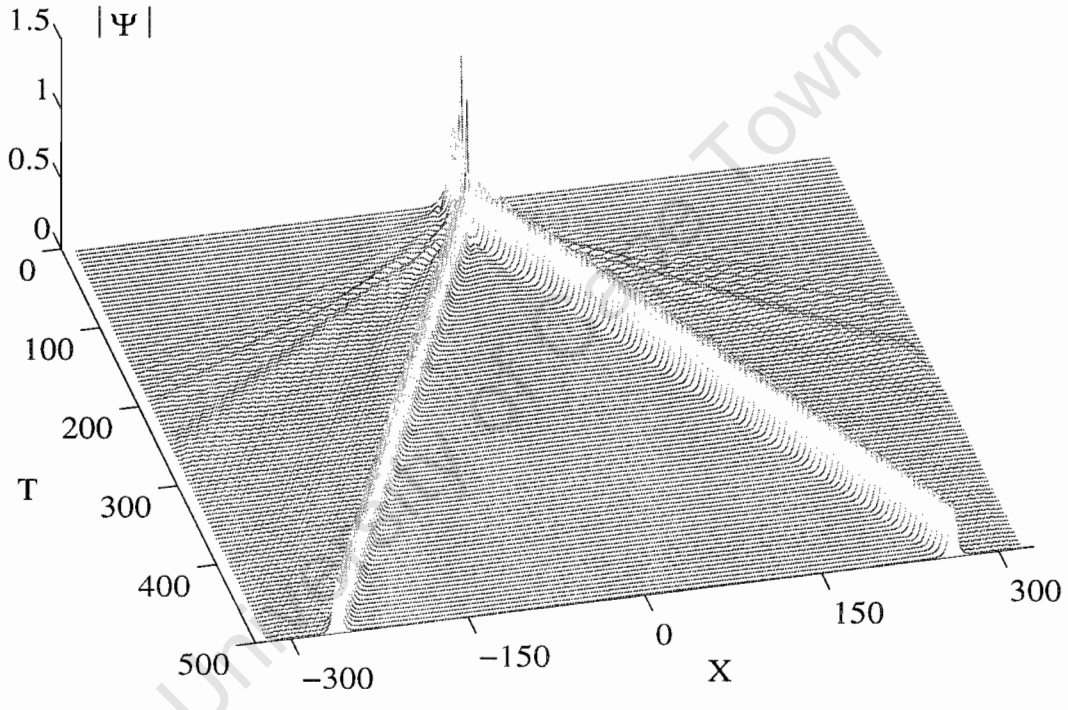

Figure 2.7: Evolution of the undamped soliton ($\gamma = 0$) perturbed by a perturbation of the form (2.112) with *large* negative E_3 (large negative l). Here $a = 1$, $\dot{a} = -18i$ [and so $l(0) = -18$.] The ψ_+ soliton splits into a couple of small-amplitude breathers $\psi_\downarrow$ eq.(2.121), propagating in opposite directions and slowly decaying in time.

2.7 Concluding remarks and open problems

In this chapter we have derived a reduced amplitude equation for the soliton in the vicinity of the oscillatory instability bifurcation. Bifurcations of this type occur in conservative and *weakly* dissipative wave systems. Similarly to the case of the Hopf instability (characteristic of *strongly* dissipative systems), the oscillatory instability sets in when a pair of complex-conjugate linearized eigenvalues crosses the imaginary axis. What makes the oscillatory instability bifurcation fundamentally different from the Hopf bifurcation, however, is the phenomenon of fusion and subsequent dissociation of a pair of stable eigenvalues which takes place just before the eigenvalues have acquired a positive real part. The oscillatory instability may therefore be regarded as a product of the resonance of two internal oscillation modes. As a consequence of the proximity to such resonance, the amplitude equation associated with the oscillatory instability is qualitatively different from the normal form of the Hopf bifurcation. (The former is second-order whereas the latter is a first-order equation.)

The second-order amplitude equation for the unstable perturbation admits a useful mechanical interpretation as an equation of planar motion of a classical particle in a radially-symmetric potential. The particle is also subject to a constant friction and time-independent torque which is induced by radiation waves emitted by the soliton. Exploiting this analogy and the associated classical mechanical formalism, we have demonstrated that in the $\gamma = 0$ case the presence of the torque always makes the trajectory of the fictitious particle unbounded. (The motion starts with quasiperiodic oscillations in an adiabatically changing ring which subsequently transform into a self-similar trajectory rapidly spiralling out.) In terms of the full nonreduced NLS dynamics, this means that the emission of radiation suppresses stably oscillating solitons. The finite-dimensional analysis provides no answer to *what* will be the resulting asymptotic attractors in this case, however.

In the *weakly* dissipative case (γ small but nonzero) the unbounded motions coexist with stable periodic orbits and therefore, the unstable stationary soliton may transform into a new soliton-like attractor which is localized in space and oscillates in time. Finally, in the *strongly* damped case ($\gamma \sim 1$), where the soliton's perturbations satisfy the complex Landau equation, unbounded finite-dimensional trajectories do not arise at all. Any perturbation of the unstable stationary soliton will necessarily have to evolve into a temporally-periodic solitonic attractor.

In the undamped situation ($\gamma = 0$) the conclusions of the reduced finite-dimensional

University of Cape Town

analysis have been verified in direct numerical simulations of the full, nonreduced NLS equation (2.1). In agreement with the effective particle description, no stably oscillating solitons were seen to arise. Our second aim here was to understand what are the infinite-dimensional counterparts of the unbounded finite-dimensional solutions; in other words, what localized or extended NLS attractors are represented by these spiralling-out trajectories. Depending on the initial perturbation, the decay of the unstable stationary soliton was observed to result in one of the two basic products: (a) a slowly decaying breather $\psi_{\downarrow}$, and (b) the soliton $\psi_{\uparrow}$ whose amplitude is increasing, slowly but indefinitely. Initial conditions with larger energy contents can give rise to a *pair* of small-amplitude breathers moving away from each other.

In the damped case ($\gamma \neq 0$) the numerical simulations of the NLS equation (2.1) were reported in [38]. Consistently, with our present conclusions, it was shown there that in some finite neighbourhood $\mathtt{h} > \mathtt{h}_c$ of the bifurcation value $\mathtt{h}_c(\gamma)$ the unstable stationary soliton ψ_+ is replaced by a stable temporally-periodic soliton $\psi_{\sim}$. Here it is important to emphasize the difference between this soliton and what we refer to as the breather ($\psi_{\downarrow}$). Firstly, the soliton $\psi_{\sim}$ oscillates about the stationary soliton ψ_+, with the amplitude of oscillations being close to zero for $\mathtt{h}$ close to $\mathtt{h}_c$. On the contrary, the breather $\psi_{\downarrow}$ oscillates about the trivial solution $\psi = 0$, with the amplitude of oscillations being about one half of the amplitude of the soliton ψ_+. Secondly, the frequency of the $\psi_{\sim}$ soliton is positive whereas the frequency of the breather $\psi_{\downarrow}$ is negative. Lastly and most importantly, the $\psi_{\sim}$ soliton does not decay whereas the breather has a long but finite lifetime.

As we pointed out in Sec.2.5.5, the unbounded trajectories of the reduced amplitude system persist when a small damping is added. Consequently , the small-amplitude breathers (and large-amplitude slowly growing solitons) should occur for small nonzero γ in the nonreduced NLS equation. However, adding even a small damping should drastically reduce the breather's lifetime. In this case the breather should arise only as a transient structure; the corresponding $T \to \infty$ asymptotic state will be trivial: $\psi = 0$. The trivial attractor was indeed observed in numerical simulations of Ref.[38]. It is appropriate to mention here that in Ref.[38] the unstable stationary soliton was perturbed only by the discretization errors, i.e. the perturbation was always very weak. Speaking in the language of the fictitious particle, its initial radial position and velocity were always very small: $|a(0)|$, $|\dot{a}(0)| \sim 0$. The trajectory evolving from these initial conditions will necessarily be attracted to the stable periodic orbit. This explains the existence of a neighbourhood of the bifurcation value $\mathtt{h}_c$ where the evolution of the unstable stationary soliton ψ_+ necessarily results in the periodic solution $\psi_{\sim}$ [38]. The trivial attractor

University of Cape Town

$\psi = 0$ also exists in this neighbourhood but since the above-mentioned initial conditions lie outside its basin of attraction, it did not arise in the numerical simulations of Ref.[38]. The trivial attractor was only observed for those h where the periodic soliton $\psi_\sim$ becomes unstable, along with its double- and higher-periodic descendants.

It would be interesting to find out what is the $\gamma \neq 0$-counterpart of the growing soliton $\psi_\uparrow$. Computer simulations of the damped NLS equation (2.1) with $0.01 \leq \gamma \leq 0.02$ did exhibit a similar object which was seen to perform irregular walks, back and forth, over a strong radiation background [39]. This large-amplitude "wandering" soliton was observed for fairly large values of h (h ≈ 0.35) whereas for h in the immediate vicinity of $\mathrm{h}_c(\gamma) \approx 0.07$, the decay of the unstable stationary soliton ψ_+ was seen to result in the stably oscillating soliton $\psi_\sim$. Interestingly, the "wandering " soliton emerged for h on the borderline between the region where the dominant attractor was trivial, $\psi = 0$, and the region where the unstable stationary soliton ψ_+ would "ignite" a spatio-temporal chaotic state. A natural question is, therefore, on the relation between the large-amplitude soliton $\psi_\uparrow$ (slowly growing, oscillating and/or wandering) and spatio-temporal chaos. We are planning to return to this problem in future publications.

Finally, it is appropriate to mention a recent paper [163] whose author also uses singular perturbation expansions for the analysis of the parametrically driven NLS equation. However, the focus of Ref.[163] is on *stable* solitons and their response to *structural* perturbations (such as external fields, noise, etc) as well as soliton-soliton interactions. The present work deals with completely different parameter range and completely different class of phenomena.

University of Cape Town

University of Cape Town

Chapter 3

Impurity-induced stabilization of solitons in arrays of parametrically driven nonlinear oscillators

University of Cape Town

3.1 Motivation

One of the most exciting developments in studies of collective synchronization of arrays of coupled nonlinear oscillators was the discovery of a dramatic increase of the degree of synchronization achieved by disordering the array [41, 42, 210, 247]. The synchronization in an array of ten disordered, parametrically driven pendula was confirmed experimentally [239]. This raised hopes of the possibility of "taming spatiotemporal chaos with disorder". In an attempt to understand the nature of this phenomenon, a numerical study of the effect of a single impurity on an otherwise homogeneous chain was carried out [80]. Surprisingly, it turned out that a single impurity can produce simple spatiotemporal patterns in place of complex chaotic behaviour for very long chains of oscillators.

The system simulated in Ref.[80] (see also [42]) consisted of a chain of pendula coupled to their nearest neighbours and driven by a periodic torque. All individual pendula in the array were in their chaotic parameter regime while the natural frequency of the central pendulum (the impurity) was out of the chaotic range. Consequently, the suggested mechanism of stabilization was the formation of a nonchaotic cluster around the defect which would subsequently pull the whole chain out of chaos [42, 80].

In this chapter we examine the effect of an impurity on a damped driven system by considering it from the viewpoint of nonlinear waves; that is, we explore *collective* stabilization mechanisms. As in Ref.[80], we study a chain of coupled pendula, alias the Frenkel-Kontorova model. As we mentioned in the Introduction to the thesis, despite

its seeming simplicity, this model provides a fairly accurate description of a number of physical and biological systems and phenomena, including ladder networks of discrete Josephson junctions, charge-density-wave conductors, crystal dislocations in metals, DNA dynamics and proton conductivity in hydrogen-bonded chains [261, 262, 43, 236].

An important distinction of our work from the problem studied in [80] is that we focus on the regime where all individual pendula are nonchaotic — whereas the array as a whole may easily fall into the state of spatiotemporal chaos. Another distinction from Ref.[80] is that our chain is driven parametrically not externally; the reason is the availability of explicit solutions.

Strongly coupled pendula tend to form soliton-like clusters of coherent oscillation. Time-periodic solitons in damped-driven chains are stable for small driving strengths but lose their stability to quasiperiodic clusters as the driver's amplitude is increased [17, 38, 6]. Increasing the amplitude still further, a spatiotemporal chaotic state sets in — with or without intermediate bifurcations [38].

We will demonstrate that "long" impurities may act as centers of *spontaneous* nucleation of solitons and hence in chains with impurities, solitons are even more natural and common structures than in homogeneous arrays. We will prove that pinning of a stationary soliton on a "long" impurity expands its region of stability. In particular, by choosing a sufficiently long impurity pendulum, the soliton can be stabilized in the parameter region where in the absence of the inhomogeneity it would set off the spatiotemporal chaos. Finally, although solitons pinned on "short" impurities will turn out to be more prone to oscillatory instabilities, we will show that such a pinning is an unlikely occurrence due to the repulsion between solitons and the short defects.

University of Cape Town

3.2 The model

The angle of the n-th pendulum in our chain satisfies

$$ml_n^2\ddot{\theta}_n + \alpha l_n\dot{\theta}_n - k(\theta_{n+1} - 2\theta_n + \theta_{n-1}) = -ml_n\left(g + 4\omega^2\rho\cos 2\omega t\right)\sin\theta_n, \qquad (3.1)$$

where we set $g = m = 1$ and assume a strong coupling: $k = \kappa^2\varepsilon^{-1}$, $\varepsilon \ll 1$. The length $l_n = 1$ for all $n \neq 0$ while the central pendulum is slightly longer ($q > 0$) or shorter ($q < 0$) than the rest of the chain:

$$l_0 = 1 + 2q\kappa\sqrt{\varepsilon}.$$

We define the distance between neighbouring pendula as

$$a \equiv \frac{\kappa}{\sqrt{k}} = \sqrt{\varepsilon}$$

and it is very small ($a \to 0$) since the coupling is very strong. Then we can neglect the $O(a^4)$ terms in the Taylor expansion

$$\theta_{n\pm1} = \theta_n \pm \theta'_n a + \frac{1}{2}\theta''_n a^2 + \ldots,$$

so that

$$\theta_{n+1} - 2\theta_n + \theta_{n-1} \approx \theta''(z_n).$$

Therefore for the case $n \neq 0$ in the continuous limit we obtain the parametrically driven, damped sine-Gordon equation:

$$\theta_{tt} + \alpha\theta_t - \theta_{xx} = -(1 + 4\omega^2\rho\cos 2\omega t)\sin\theta. \tag{3.2}$$

Here the function $\theta(z)$ is assumed to be differentiable at sites $z_n = n\,a$, $-N \geq n \geq N$. This is not valid for $n = 0$ where we have, instead,

$$\theta_1 - 2\theta_0 + \theta_{-1} \approx \quad a\theta'\Big|_{z=-0}^{z=+0} + a^2\frac{\theta''(+0) + \theta''(-0)}{2}. \tag{3.3}$$

therefore for the central pendulum we have:

$$\begin{aligned} & a(1 + 4q\kappa\sqrt{\varepsilon} + 4q^2\kappa^2\varepsilon)\,\ddot{\theta}_0 + a\,\alpha(1 + 2q\kappa\sqrt{\varepsilon})\,\dot{\theta}_0 - \\ - \quad & \kappa^2\left\{\theta'_0\Big|_{z=-0}^{z=+0} + a\frac{\theta''_0(+0) + \theta''_0(-0)}{2}\right\} = \\ = \quad & -a(1 + 2q\kappa\sqrt{\varepsilon})(1 + 4\omega^2\rho\cos 2\omega t)\sin\theta_0 \end{aligned} \tag{3.4}$$

It is convenient to choose the square of the inter-pendula distance $a = \sqrt{\varepsilon}$ as a small parameter. For simplicity we confine ourselves to the case when the driving frequency is just below the edge of the continuous spectrum of linear waves, $\omega^2 = 1 - \varepsilon^2$, and assuming that the driving amplitude and friction in the pivots are small: $4\omega^2\rho = 2h\varepsilon^2$, $\alpha = \varepsilon^2\gamma$. In this case the pendula will perform nearly-synchronised small-amplitude librations of the form

$$\theta = 2\varepsilon\psi(T, X)e^{-i\omega t} + c.c. + O(\varepsilon^3), \tag{3.5}$$

where the envelope ψ is only slowly varying in space and time:

$$X = \varepsilon z, \quad T = \frac{\varepsilon^2}{2}t.$$

University of Cape Town

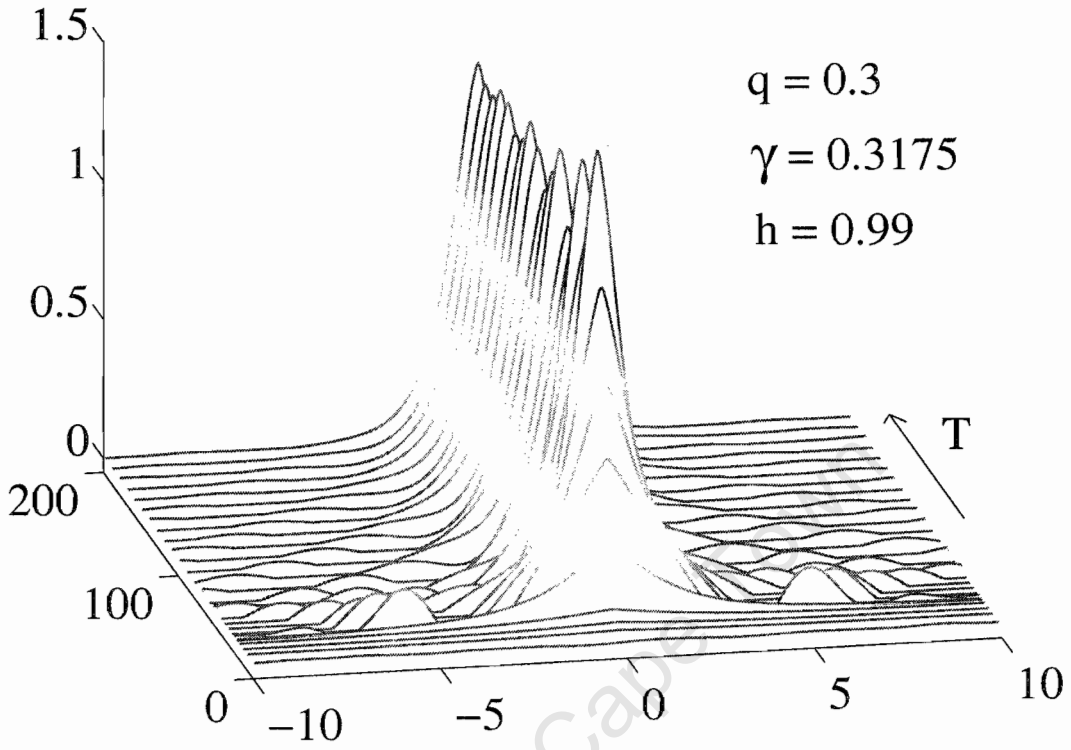

Figure 3.1: A stable pinned soliton spontaneously created from a small-amplitude random spatial distribution.

It is this variable amplitude that contains the information on how disorganized the array is. If ψ were constant, the pendula would be perfectly synchronised; however, ψ will not generally be constant. Substituting (3.5) into eqs.(3.2) with $X \neq 0$ and sending $a \to 0$ we obtain the amplitude equation

$$i\psi_T + \psi_{TT} + 2|\psi|^2\psi - \psi = h\psi^* - i\gamma\psi, \quad X \neq 0. \tag{3.6}$$

Next, let the central pendulum be slightly longer or shorter than the rest of the chain. Then, as $a \to 0$, the equation (3.4) with $X = 0$ gives rise to the boundary condition

$$2q\psi(0) + \psi_X\Big|_{-0}^{+0} = 0. \tag{3.7}$$

Eqs.(3.6) and (3.7) can be combined into the parametrically driven damped nonlinear Schrödinger equation with a δ-function inhomogeneity:

$$i\psi_T + \psi_{XX} + 2|\psi|^2\psi - \psi + 2q\delta(X)\psi = h\psi^* - i\gamma\psi \quad -\infty < X < \infty. \tag{3.8}$$

University of Cape

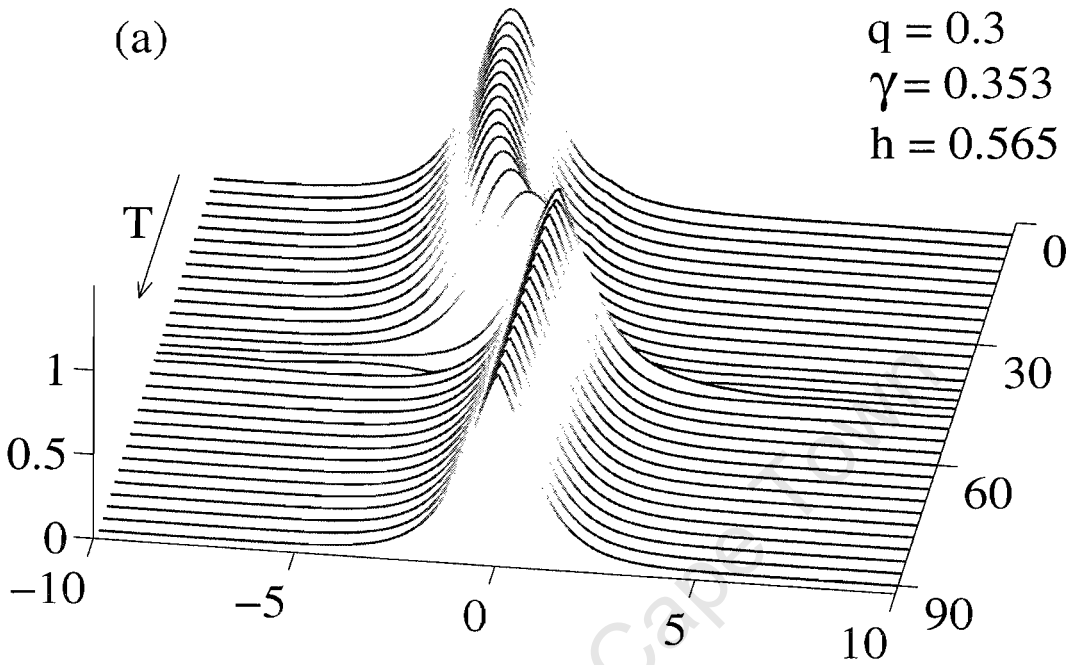

Figure 3.2 continues on the next page

As we mentioned in the Introduction, in the homogeneous case, this NLS equation was used to model the nonlinear Faraday resonance in a long narrow water trough [184, 259, 260, 270]. The impurity term $2q\delta(X)\psi$ represents a local widening (for $q > 0$) or narrowing ($q < 0$) of the trough. We also mentioned that the same equation describes an easy-plane ferromagnet with a combination of a static and hf field in the easy plane [287, 17, 36, 279] and a biaxial ferromagnet. In this context the inhomogeneous term accounts for an impurity spin.

As in the spatially homogeneous case ($q = 0$) [17], for $h > \sqrt{1+\gamma^2}$ the zero solution $\psi = 0$ is unstable against continuous spectrum excitations. *"Long"* impurities ($q > 0$) harbour a discrete mode (here $\epsilon \ll 1$):

$$\delta\psi = \epsilon\left(\cos\Omega T - i\frac{1+h-q^2}{\Omega}\sin\Omega T\right)e^{-\gamma T - q|X|},$$

$\Omega^2 = (1-q^2)^2 - h^2$. When h exceeds the value $\mathtt{h}_{q,\gamma}$,

$$\mathtt{h}_{q,\gamma} = \sqrt{(1-q^2)^2+\gamma^2},$$

this localized mode also produces instability. For positive $q < \sqrt{2}$, in which case $\mathtt{h}_{q,\gamma}$ lies

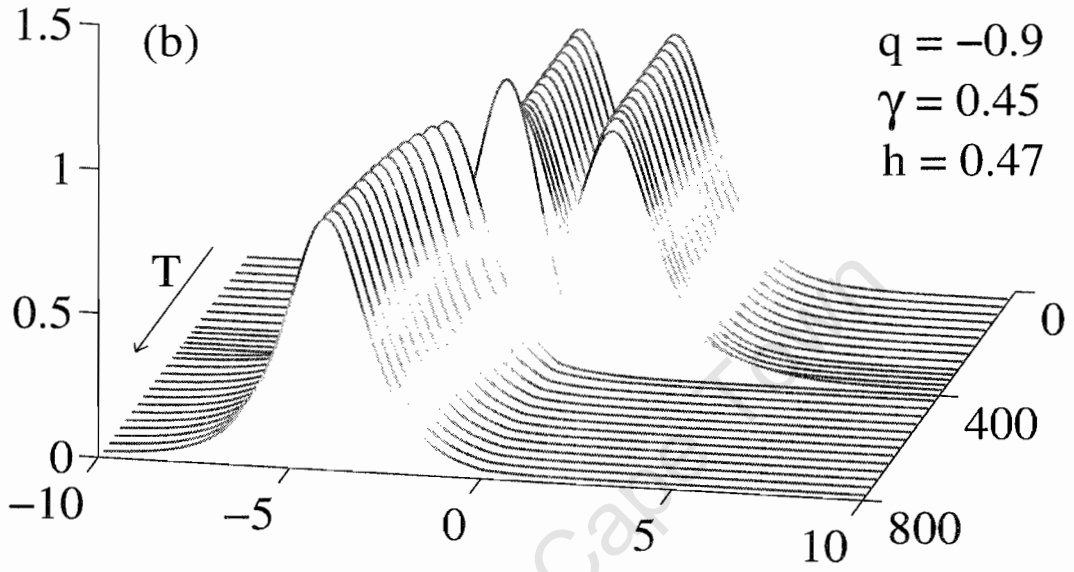

Figure 3.2 continues on the next page

below $\sqrt{1+\gamma^2}$, the nonlinear development of this instability leads to the formation of solitons (fig.3.1), stable or unstable.

3.3 Stationary solitons

Equation (3.8) exhibits *two* stationary soliton solutions, each having a cusp at the origin:

$$\psi_{\pm}(X) = A_{\pm}\mathrm{sech}\,(A_{\pm}|X| + \tilde{x})\, e^{-i\theta_{\pm}}. \tag{3.9}$$

Here

$$\cos 2\theta_{\pm} = \pm\sqrt{1-\gamma^2/h^2}, \quad A_{\pm}^2 = 1 \pm \sqrt{h^2-\gamma^2}, \quad \tilde{x} = \mathrm{arctanh}\,(q/A_{\pm})\,.$$

For weak impurities, $|q| < 1$, the ψ_+ soliton exists for any h and γ satisfying $h > \gamma$, whereas the ψ_- requires, in addition, that $h < \mathrm{h}_{q,\gamma}$. Strong impurities ($|q| > 1$) do not support the ψ_- soliton at all whereas the ψ_+ exists only if $h > \mathrm{h}_{q,\gamma}$.

First we demonstrate that the soliton ψ_- is unstable and can always be disregarded. Taking the linear perturbation in the form

$$\delta\psi_{\pm} = \epsilon(f + ig)e^{-i\theta_{\pm}-\gamma T}$$

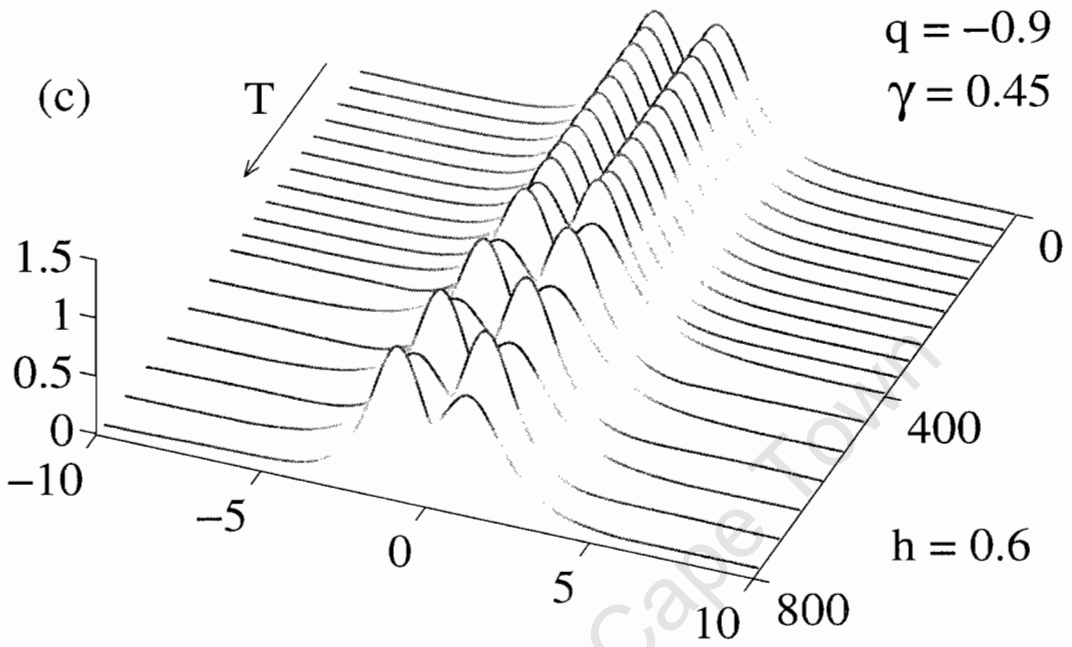

Figure 3.2: (a): The "long" defect attracts a free-standing soliton initially placed at $X_0 = -2.5$. (b,c): The effect of the $q < 0$ impurity. For $h < \mathrm{h}_{q,\gamma}$, the growth of the asymmetric instability leads to the soliton's unpinning and repulsion from the impurity (b), while for $h > \mathrm{h}_{q,\gamma}$, the asymmetric Hopf instability evolves into a two-humped soliton rising and falling in a seesaw motion (c).

gives

$$-g_\tau - \Gamma g = L_1 f, \quad f_\tau - \Gamma f = L_0 g, \tag{3.10}$$

where $\Gamma = \gamma/A_\pm^2$, $\tau = A_\pm^2 T$, and the operators

$$L_1 = -\partial_x^2 + 1 - 6\mathrm{sech}^2(|x| + \tilde{x}) - 2Q\delta(x), \tag{3.11}$$

$$L_0 = -\partial_x^2 + 1 \mp 2H - 2\mathrm{sech}^2(|x| + \tilde{x}) - 2Q\delta(x), \tag{3.12}$$

with

$$Q = q/A_\pm = q\sqrt{1 \mp H}, \quad H = \sqrt{h^2 - \gamma^2}/A_\pm^2,$$

and $x = A_\pm X$. The minimum eigenvalue of the operator L_0 associated with a nodeless eigenfunction $\mathrm{sech}(|x| + \tilde{x})$, is $\nu_0 = \mp 2H$. Consequently, in the case of the ψ_- soliton L_0 is positive definite and Eqs.(3.10) can be rewritten as

$$L_0^{-1} f_{\tau\tau} = \Gamma^2 L_0^{-1} f - L_1 f. \tag{3.13}$$

University of Cape Town

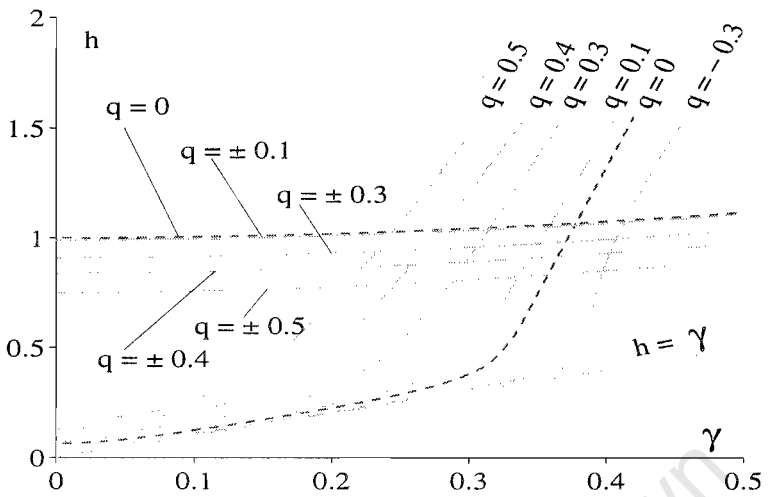

Figure 3.3: An atlas of stability charts on the (γ, h)-plane. Above the dashed "horizontal" curve, $h = \sqrt{1+\gamma^2}$, all localized solutions are unstable w.r.t. continuous spectrum waves. Solid "horizontal" curves are $h = \mathrm{h}_{q,\gamma}$. Below their corresponding $\mathrm{h}_{q,\gamma}$-curves impurities with $q < 0$ repel solitons. The family of "parabolas" depict the onset of (symmetric) instability of the pinned soliton; the greater is q the larger is the stability domain. Finally, in the region between $\sqrt{1+\gamma^2}$ and $\mathrm{h}_{q,\gamma}$ a $q > 0$-impurity will spontaneously nucleate solitons.

The maximum exponential growth rate λ of solutions to Eq.(3.13) is given by [152, 23, 24]

$$\lambda^2 = \Gamma^2 + \sup_f \frac{< f(x)| - L_1|f(x) >}{< f(x)|L_0^{-1}|f(x) >}. \tag{3.14}$$

For any Q the operator L_1 has a negative eigenvalue $\mu_0 = 1 - \kappa^2$ associated with an even eigenfunction

$$y_0(x) = e^{-\kappa\xi}(3\tanh^2\xi + 3\kappa\tanh\xi + \kappa^2 - 1), \tag{3.15}$$

where $\xi = |x| + \tilde{x}$ and $\kappa > 1$ is a root of

$$\kappa^3 + 2\kappa^2 Q + \kappa(3Q^2 - 5Q - 4) + 3Q^3 = 0.$$

Thus the supremum in (3.14) is positive, λ is $> \Gamma$ and the soliton ψ_- is unstable against a symmetric nonoscillatory mode for all q, h and γ.

3.4 Effect of the short impurity

A similar argument can be used to detect the disengagement instability of the other soliton, ψ_+, arising for "short" impurities ($q < 0$). We simply notice that the second

University of Cape Town

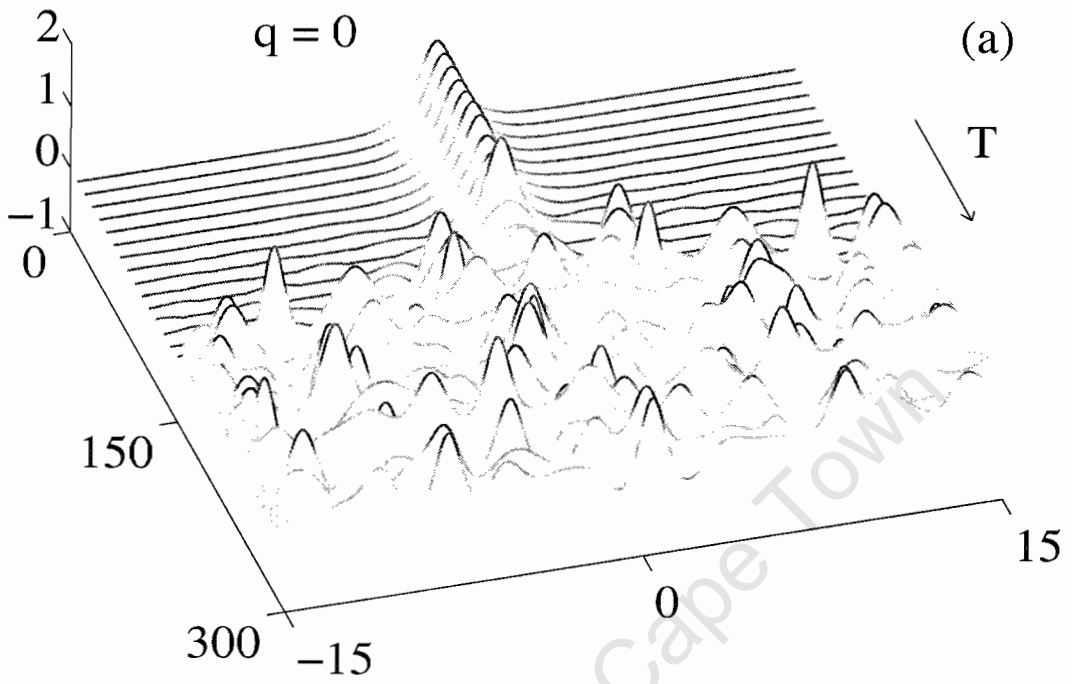

Figure 3.4 continues on the next page.

University of Cape Town

lowest eigenvalue of L_0 which is associated with an odd eigenfunction

$$w_1(x) = \mathrm{sgn}(x) e^{Q(|x|+\tilde{x})} \left\{ \tanh(|x| + \tilde{x}) - Q \right\},$$

is equal to $\nu_1 = 1 - 2H - Q^2$. For $2H < 1 - Q^2$ or equivalently for $h < \mathtt{h}_{q,\gamma}$, the operator L_0 is positive definite on the subspace of odd functions. On the other hand, for $Q < 0$ the operator L_1 has a negative eigenvalue $\mu_1 = 1 - \kappa^2$ associated with an odd eigenfunction $y_1(x) = \mathrm{sgn}x \; y_0(x)$, with y_0 as in (3.15) and $\kappa > 1$ a root of

$$\kappa^2 + 3\kappa Q + 3Q^2 - 1 = 0.$$

Hence the variational principle (3.14) is still applicable, λ is $> \Gamma$ and the ψ_+ is unstable. The interpretation of this instability is straightforward if one notices that in the conservative case ($\gamma = 0$) the inhomogeneous term $-2q\delta(X)|\psi|^2$ produces a local decrease respectively increase of energy for $q > 0$ respectively $q < 0$. Consequently, in the conservative and weakly dissipative cases, the "long" impurity will attract and the "short" one repel small-amplitude tails of *distant* solitons. On the other hand, the energy of the *pinned* soliton is

$$E_Q = \frac{4}{3} A^3 (1 - 3Q + 2Q^3).$$

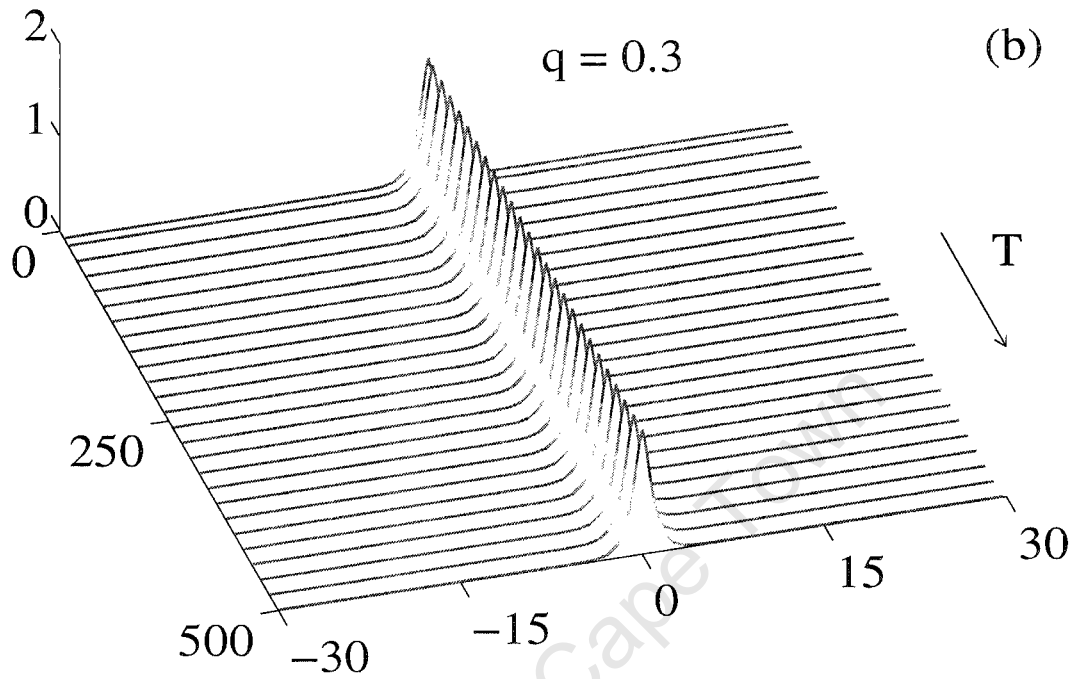

Figure 3.4: In the homogeneous chain with $\gamma = 0.315, h = 0.95$ the unstable soliton seeds spatiotemporal chaos (a). Introducing the impurity with $q = 0.3$ is sufficient to stabilize it (b).

University of Cape Town

For $Q > 0$ ($Q < 0$) this is smaller (greater) than the energy E_0 of the infinitely remote soliton. These two facts indicate that $Q > 0$-impurities should attract and trap solitons (cf.[37, 129, 231, 45]), and numerical simulations confirm this — see fig.3.2(a). In the $Q < 0$ case, conversely, distant solitons will be repelled while an initially pinned soliton will unpin and move away from the impurity regaining its cusp-free shape. This is again confirmed by simulations of Eq.(3.8) (fig.3.2(b)). It is fitting to note here that the unpinning instability is not connected with overdriving the chain; it occurs already in the undriven NLS [37]. We should also mention that all numerical simulations of Eq.(3.8) reported in this paper were verified by computer simulations of the discrete chain (3.1). The two sets of results were always in exact agreement for sufficiently strong couplings of the chain.

In the region $h > \mathtt{h}_{q,\gamma}$ (as well as in the case of symmetric instabilities, and also for long impurities $q > 0$) the variational principle (3.14) is not applicable. Here we let

$$f(x,\tau) = u(x)e^{i\Omega\tau}, \quad g(x,\tau) = -\frac{\omega}{\Gamma + i\Omega}v(x)e^{i\Omega\tau},$$

where $\Omega^2 = \omega^2 - \Gamma^2$. Eq.(3.10) reduces to an eigenvalue problem

$$L_1 u = \omega v, \quad L_0 v = \omega u, \tag{3.16}$$

which we solved numerically. Notice that we have reduced a three- to two-parametric problem. Having found $\omega = \omega(q, H)$, one immediately recovers the instability growth rate $|\mathrm{Im}\,\Omega(q, H)| - \Gamma$ for all q, h, and γ.

For small $h < \mathrm{h}_{q,\gamma}$ there is only one unstable pair of imaginary eigenvalues $\pm\omega_1$, with the associated u and v being odd. As h is increased beyond $\mathrm{h}_{q,\gamma}$, the imaginary eigenvalues move onto the real axis (i.e. the soliton restabilizes) while another real doublet $\pm\omega_2$ detaches from the continuous spectrum. The two collide and emerge as a complex quadruplet after which the real and imaginary parts grow until an asymmetic instability sets in. This is now *not* a disengagement instability; the stationary soliton is replaced by a two-humped structure (still pinned on the impurity) whose left and right wings oscillate 180° out of phase (fig.3.2(c)).

3.5 Effect of the long impurity

When $q > 0$, the motion of eigenvalues ω on the complex plane is similar to the homogeneous case [17]. The soliton ψ_+ is stable for h close to γ but loses its stability to a symmetric oscillating soliton as h is increased. Fig.3.3 shows the Hopf bifurcation curves $h = h_q(\gamma)$ obtained from the relation $|\mathrm{Im}\,\Omega(q, H)| = \Gamma$ for $q = 0.1$, 0.3, 0.4, 0.5 and -0.3. For $q > 0$ the stability domain is wider than without an impurity. For example, in a chain with the coupling $k = 10$ driven at $\omega \approx 0.995$, lengthening the central pendulum by 30% (which gives $q \approx 0.474$) is sufficient to *double* the size of the soliton's stability domain. On the contrary, the $q < 0$ impurity narrows the stability region.

Thus, *long* impurities exert a strong influence on solitons' dynamics. For $h < \mathrm{h}_{q,\gamma}$ they attract and trap solitons; for $h > \mathrm{h}_{q,\gamma}$ pinned solitons are spontaneously formed around the $q > 0$ defects. On the other hand, the soliton with h and γ such that it would ignite spatiotemporal chaos in the homogeneous case [38], is stabilized when pinned on a sufficiently long impurity (fig.3.4). Therefore the $q > 0$ defects should have a stabilizing effect on the chain. One should keep in mind, however, that spatiotemporal chaotic states are not localized and a single stable soliton will clearly be insufficient to suppress chaos in a long chain. The chaos can always be triggered by choosing the initial condition far enough from the soliton. In order to suppress chaos in a larger phase volume multiple

University of Cape Town

impurities should be introduced; one is therefore led to the necessity of examining stability of solitons and periodic waves on finite intervals.

3.6 Discussion

Although we restricted ourselves to the analysis of the effect of a single impurity (and accordingly, stability of a single soliton), our ultimate goal would be to propose a possible mechanism for the "taming chaos" in a chain disordered by a "gas of impurities". The qualitative picture that we have in mind at this stage, involves the formation of a solitonic cluster around each of the long impurities. In each cluster, pendula are synchronised to the common frequency. The solitonic clusters are stable objects; the longer is the impurity, the wider is the range of parameters where the soliton pinned on this impurity is stable. Therefore, each impurity suppresses the spatiotemporal chaos in some neighbourhood around it. Although a single impurity cannot "tame" chaos in a long array, we expect that provided the density of the "soliton gas" is sufficiently high, the probability of synchronisation of the whole chain will be quite significant.

One may argue, however, that in a randomly disordered array, short and long impurities will be met with equal probability. We have shown that short defects promote instability; can they offset the stabilizing effect of long impurities? The answer is no. The fact that short impurities enhance the symmetric instability should not play a destabilizing role since solitons tend to avoid "short" defects. On the contrary, these repulsive inhomogeneities will effectively partition the chain into smaller subintervals and this will generally have a stabilizing effect since long wavelength instabilities will not fit in. (An example of stabilization by the interval shortening is given in Ref.[21].)

The above qualitative picture relies on the assumption that the separation distance between impurities is so large that they virtually ignore each other. It is not unprobable, however, that some defects happen to "live" in the area "controlled" by their neighbours. What happens then? Although the systematic study of the effect of multiple impurities (as well as the related case of short intervals) is beyond the scope of this work, we did make some preliminary analysis of the case of two impurities. As one could expect, when two stable stationary solitons are pinned *very* far away from each other, they do not interact and remain time-independent. However, if the separation is smaller than a certain critical distance, they start exchanging tiny bits of energy in the form of weak radiation waves and develop spontaneous large-amplitude oscillations (fig.3.5). Amazingly, the critical distance turns out to be many times greater than the characteristic width of the solitons.

University of Cape Town

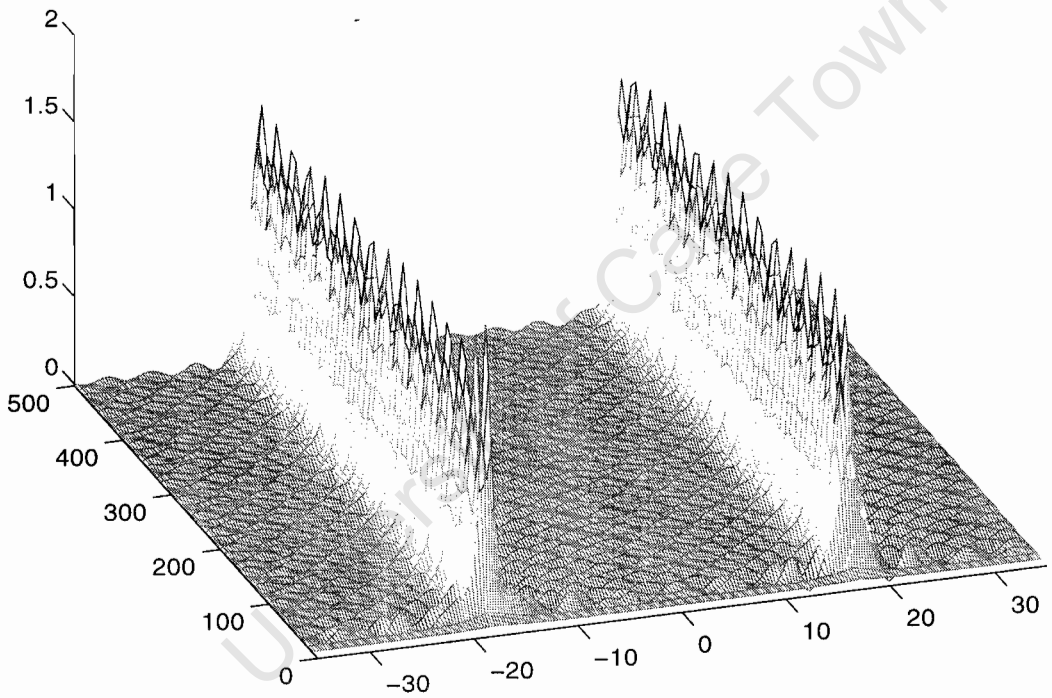

University of Cape Town

Figure 3.5: Two $q > 0$ on impurities placed symmetrically with inter-impurity distance equal to half of the interval.

This means that, contrary to our intuitive assumption, the interaction even between relatively remote defects may play a very significant role in the emerging patterns. The synchronization mechanism that we proposed in this chapter, is sufficient to achieve the synchronization within each solitonic cluster of pendula. The next challenge should be to explain the synchronization of *different* clusters. The encouraging observation coming from our numerical simulations is that the self-induced oscillations of soliton pairs do synchronize. (See fig.3.5.) This suggests that nonlinear disordered arrays may exhibit a hierarchy of synchronisation scales. We are planning to return to this intriguing hypothesis in our future research.

University of Cape Town

Chapter 4

Bound states of pulses in an excitable reaction-diffusion model of the NO + CO reaction on the platinum surface

University of Cape Town

4.1 Motivation

In this chapter we study a system of excitable reaction-diffusion equations. As opposed to equations considered in chapters 2 and 3, these equations are dissipative not dispersive. The system models the isothermal nitric oxide (NO) reduction with carbon monoxide (CO) on platinum [Pt(100)] surface at low pressure ($\sim 10^{-6}$ mbar). To avoid the interaction of the arising chemical patterns with defects of the reacting crystalline surface, it is convenient to study the reaction on the surface of a single Pt crystal. To simplify the problem even further, a ring-shaped reactive domain is used. This is accomplished by superimposing two concentric ring-shaped layers of an inert element (e.g. titanium or titanium dioxide) over the reacting surface. The ring of platinum surface sandwiched between the two rings of Ti, is our reactive domain. Since the outer diameter (110 μm) is much larger that the width (10 μm) of the platinum ring, the problem can be considered as an essentially one-dimensional.

The NO + CO reaction exhibits nonlinear waves such as solitary pulses or wavetrains of pulses. A pulse can be created from the homogeneous state by a suitable excitation; under certain conditions it can propagate with a constant velocity and shape. An important characteristic of the pulse is its dispersion curve, i.e. the dependence of its velocity on the length of the periodic interval. The slope of the dispersion curve is important

for the description of the interaction of widely separated pulses on a ring [228, 62]. The positive slope corresponds to repulsion while the negative slope corresponds to attraction between pulses. The model at hand possesses nonmonotonic dispersion curves in a large region of its control parameters [49]. In sec.4.4 of this chapter, we analyse the shape of the dispersion curve of solitary pulse and on the basis of this analysis uncover transitions between pulses decaying to different homogeneous backgrounds. Next, in sec.4.5 we study stability of equidistant wavetrains and nonequidistant bound states of pulses. We show that the nonequidistant bound states are unstable on large rings. This disagreement with the kinematic theory approach can be explained by the fact that pairs of nonequidistant pulses are strongly overlapping, which violates the main assumption of the kinematic theory.

4.2 The mathematical model

We consider the reaction-diffusion model of the NO-CO chemical reaction introduced in [105]:

$$u_t = k_1 p_{CO}(1-u-v) - k_2 u \exp\left[E(u+v)^2\right] - k_3 uw + Du_{xx}, \tag{4.1}$$

$$v_t = k_1 p_{NO}(1-u-v) - k_4 v \exp\left[E(u+v)^2\right] - k_5 v f(u+v,w) + Dv_{xx}, \tag{4.2}$$

$$w_t = k_5 v f(u+v,w) - k_3 uw, \tag{4.3}$$

where

$$f(u+v,w) = \max\left(1 - \frac{u+v}{0.61} - \frac{w}{0.399}, 0\right)$$

and u, v and w represent CO, NO and O coverage, respectively. The constants k_1, k_2, k_3, k_4, k_5 and E are chosen to be the same as in [65], i.e. they are calculated for the fixed temperature of 424 K. We also fix the diffusion constant D equal to 1 and supplement eqs.(4.1)-(4.3) with periodic boundary conditions on the interval $[0, L]$. The NO and CO pressures, p_{NO} and p_{CO}, are the control parameters of the system.

In order to investigate localized solutions moving with the velocity c, we rewrite eqs.(4.1)-(4.3) in the co-moving frame of reference, where $z = x - ct$:

$$u_t = k_1 p_{CO}(1-u-v) - k_2 u e^{[E(u+v)^2]} - k_3 uw + u_{zz} + cu_z, \tag{4.4}$$

$$v_t = k_1 p_{NO}(1-u-v) - k_4 v e^{[E(u+v)^2]} - k_5 v f(u+v,w) + v_{zz} + cv_z, \tag{4.5}$$

$$w_t = k_5 v f(u+v,w) - k_3 uw + cw_z. \tag{4.6}$$

University of Cape Town

In this frame a wave moving with a constant velocity c appears as a static solution. This stationary solution satisfies a system of ordinary differential equations

$$\dot{y}_1 = y_2, \tag{4.7}$$

$$\dot{y}_2 = -k_1 p_{CO}(1 - y_1 - y_3) + k_2 y_1 \mathrm{e}^{[E(y_1+y_3)^2]} + k_3 y_1 y_5 - c y_2, \tag{4.8}$$

$$\dot{y}_3 = y_4, \tag{4.9}$$

$$\dot{y}_4 = -k_1 p_{NO}(1 - y_1 - y_3) + k_4 y_3 \mathrm{e}^{[E(y_1+y_3)^2]} + k_5 y_3 f(y_1 + y_3, y_5) - c y_4, \tag{4.10}$$

$$\dot{y}_5 = \frac{k_3 y_1 y_5 - k_5 y_3 f(y_1 + y_3, y_5)}{c}, \tag{4.11}$$

where the dot stands for the derivative with respect to z. The static solution is a homoclinic orbit of eqs.(4.7)-(4.11).

We examined the stability of solutions to eqs.(4.7)-(4.11) by solving the following spectral problem which arises from the linearization of eqs.(4.4)-(4.6) about the solutions in question:

$$\begin{pmatrix} \partial_{zz} + c\partial_z + A_{11}(z) & A_{12}(z) & A_{13}(z) \\ A_{21}(z) & \partial_{zz} + c\partial_z + A_{22}(z) & A_{23}(z) \\ A_{31}(z) & A_{32}(z) & c\partial_z + A_{33}(z) \end{pmatrix} \begin{pmatrix} \tilde{u} \\ \tilde{v} \\ \tilde{w} \end{pmatrix} = \lambda \begin{pmatrix} \tilde{u} \\ \tilde{v} \\ \tilde{w} \end{pmatrix}, \tag{4.12}$$

where the coefficients are given by

$$A_{11}(z) = -p_{CO} - k_3 w - k_2[1 + 2Eu(u+v)]\mathrm{e}^{E(u+v)^2},$$

$$A_{12}(z) = -p_{CO} - 2k_2 Eu(u+v)\mathrm{e}^{E(u+v)^2},$$

$$A_{13}(z) = -k_3 u,$$

$$A_{21}(z) = -p_{NO} - 2k_4 Ev(u+v)\mathrm{e}^{E(u+v)^2} + k_5 v/0.61,$$

$$A_{22}(z) = -p_{NO} - k_4[1 + 2Ev(u+v)]\mathrm{e}^{E(u+v)^2} - k_5(1 - (u+2v)/0.61 - w/0.399),$$

$$A_{23}(z) = k_5 v/0.399,$$

$$A_{31}(z) = -k_5 v/0.61 - k_3 w,$$

$$A_{32}(z) = k_5(1 - (u+2v)/0.61 - w/0.399),$$

$$A_{33}(z) = -k_5 v/0.399 - k_3 u$$

University of Cape Town

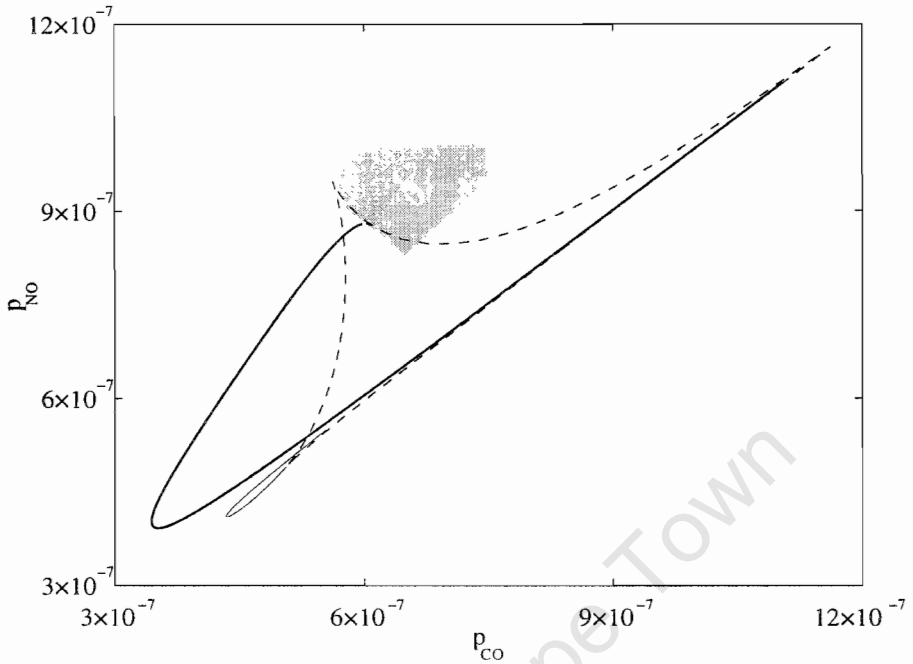

Figure 4.1: The saddle-node and Hopf bifurcation curves on the (p_{CO}, p_{NO})-plane.

University of Cape Town

4.3 Homogeneous solutions and pulses

The main object of this chapter is the solitary pulse — something we would have called soliton in the previous two chapters. By pulses we mean spatially localized solutions propagating with constant velocity without changing their shape. One of the differences between pulses and solitons is that pulses are nonsymmetric solutions. As we mentioned in the Introduction to the thesis, this nonsymmetric shape results in difference in the properties of the front and the back of the pulses. In particular, the front of the pulse decays faster to the homogeneous background. In order to understand the dynamics of pulses, we need to start with the analysis of homogeneous solutions to which the pulses decay. (For large ring lengths this decay is exponential.)

From the point of view of the dynamical systems theory, the homogeneous solutions are fixed points of the system (4.7)-(4.11). The function $f(u+v, w)$ describes the number of vacant sites on the surface available for NO dissociation. Consequently when $f(u+v, w) \equiv 0$, no reaction is possible. In this case the u, v and w components satisfy the following

set of transcendental equations:

$$k_1 p_{CO}(1-u-v) = k_2 u \exp[E(u+v)^2], \tag{4.13}$$

$$k_1 p_{NO}(1-u-v) = k_4 v \exp[E(u+v)^2], \tag{4.14}$$

$$w \equiv 0, \tag{4.15}$$

with an additional constraint $0.61 < u+v < 1$, coming from the expression for f. Such solutions exist only for very large values of the pressures p_{CO} and p_{NO}.

In what follows we will concentrate on the case where $f(u+v,w)$ is positive. (This means there are some vacant sites available for the NO dissociation. In this case the transcendental equations for the components read in this case

$$k_1 p_{CO}(1-u-v) - k_2 u \exp[E(u+v)^2] - k_3 uw = 0 \tag{4.16}$$

$$k_1 p_{NO}(1-u-v) - k_4 v \exp[E(u+v)^2] - k_5 v f(u+v,w) = 0 \tag{4.17}$$

$$k_5 v f(u+v,w) - k_3 uw = 0. \tag{4.18}$$

To study the bifurcation behaviour of the model we used a package of continuation algorithms AUTO97 by Doedel et al [57].

In fig.4.1 we reproduce the 2D-bifurcation diagram where p_{CO} and p_{NO} are the bifurcation parameters. This diagram was first plotted in [105]. The dashed line is the saddle-node bifurcation curve. This curve marks the transition from a single fixed point to multiple fixed points in the space of the control parameters (p_{CO}, p_{NO}). The thick solid line demarcates a supercritical Hopf bifurcation and the faint line a subcritical Hopf bifurcation.

Inside the curvilinear triangle formed by the saddle-node bifurcation curve there are three fixed points and only one outside it. To describe the multiple fixed points it is convenient to use nullcline diagrammes. In fig.4.2 we plot three typical nullcline diagrammes.

Fig.4.2(a) corresponds to the state with a low p_{CO} pressure (which is found to the left of the curvilinear triangle in fig.4.1). In this case there is only one fixed point corresponding to a high NO and low CO coverage. We denote this type of fixed point A. This fixed point is stable beyond the Hopf curve. Periodic chemical waves were observed [65, 105] in the region where the fixed point is unstable. This simple stability analysis explains why the chemical waves exist only on one branch of the Hopf bifurcation curve.

University of Cape Town

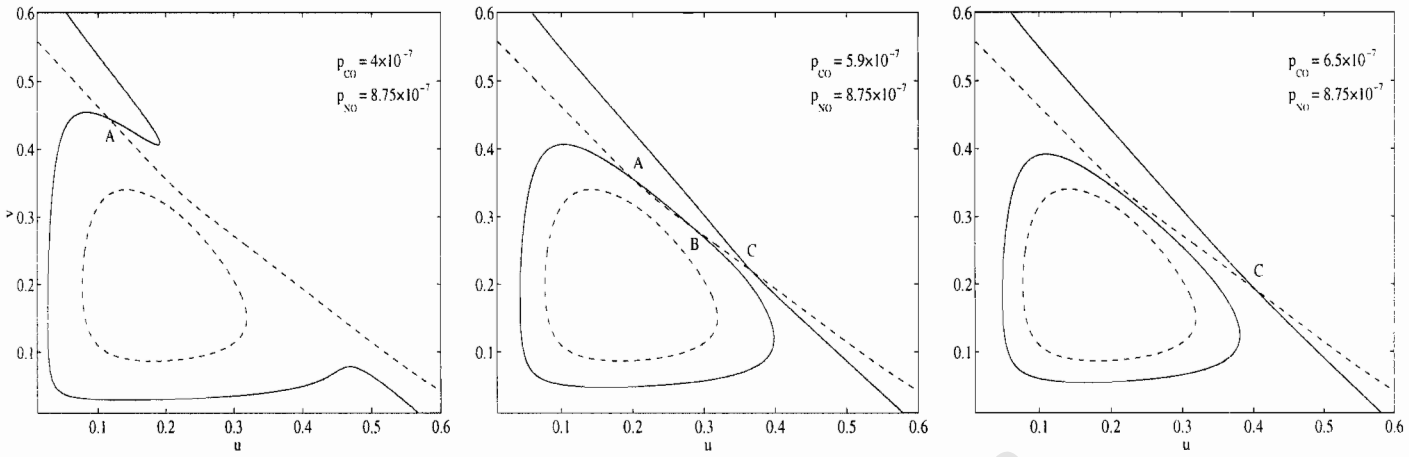

Figure 4.2: Nullclines on the (u, v)-plane The solid line corresponds to the $u_z = 0$ isoclines while the dashed one represents the $v_z = 0$ isoclines.

University of Cape Town

The control parameters in fig.4.2(b) are chosen to be inside the curvilinear triangle where there are three fixed points. We denote these points A, B and C. The fixed point B is always unstable. For this fixed point, the NO and CO coverages are of similar intensity. The fixed point C is stable inside the curvilinear triangle, above it and to the right of it. Unlike the fixed point A, it describes the state with a high CO and low NO coverage. There is a small region of bistability of the fixed points A and B inside the curvilinear triangle, in its upper left corner.

The control parameters in fig.4.2(c) are chosen above the curvilinear triangle of the saddle-node bifurcation curve. The only fixed point that can arise here is the fixed point which we have denoted C.

4.4 Pulses and their dispersion curves

In excitable media, such as the one described by the model under consideration, pulse-like structures can be created from a stable homogeneous state by a suitable perturbation. From the point of view of the system of the travelling wave ODEs, pulses can be considered as homoclinic or heteroclinic orbits. Our model exhibits stable pulses over a wide range of control parameters p_{CO} and p_{NO} [209]. We have found stable pulse solutions decaying to both stable homogeneous states A and C as well as unstable pulses decaying to the unstable homogeneous state B. In fig.4.3 we present typical profiles of pulses decaying to

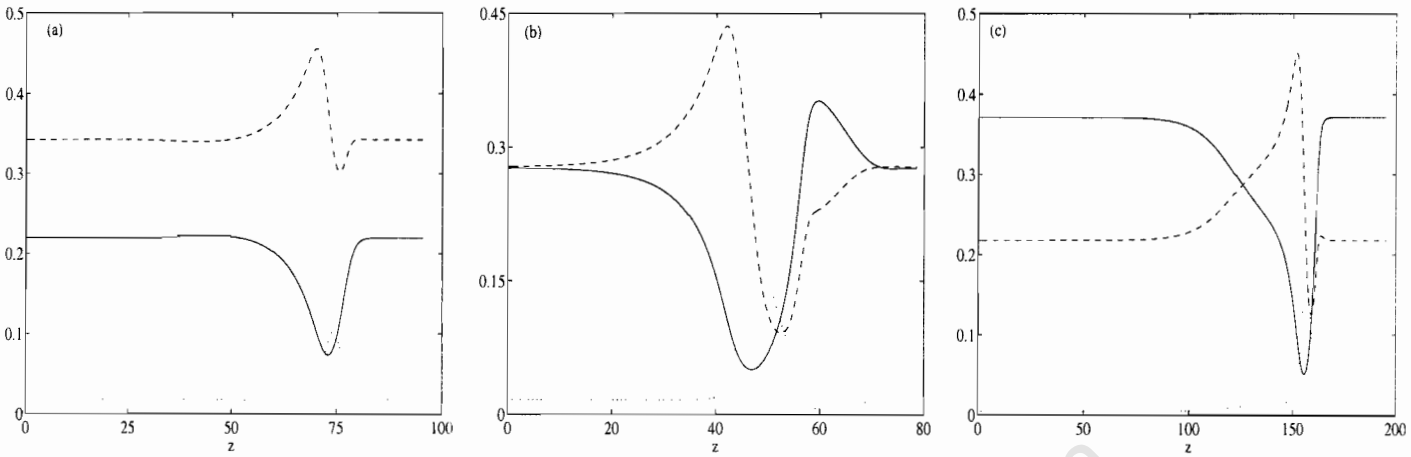

Figure 4.3: (a) The pulse over A with $p_{CO} = 5.8027 \times 10^{-7}$ and $p_{NO} = 9 \times 10^{-7}$. (b) The pulse over B with $p_{CO} = 6.5 \times 10^{-7}$ and $p_{NO} = 8.2754 \times 10^{-7}$. The pulse over C where $p_{CO} = 6 \times 10^{-7}$ and $p_{NO} = 9 \times 10^{-7}$.

University of Cape Town

homogeneous states A, B and C, respectively. The most generic pulses are those decaying to background C. Pulses decaying to A exist only in a small region of bistability of the homogeneous state inside the upper-left corner of the curvilinear triangle formed by the saddle-node bifurcation curve.

The dynamical properties of pulses depend on the way pulses decay to the corresponding homogeneous background. The decay of the front of a right-going pulse can be approximated by the negative eigenvalue with the smallest modulus of the system of ODEs linearized about the corresponding fixed point. In a similar way, the decay of the back of a right-going pulse can be approximated by the smallest positive eigenvalue of the linearized system of ODEs. In fig. 4.4 the four eigenvalues with the smallest absolute values of real parts are plotted as functions of the propagation speed, c. The pressure parameters are chosen to be the same as in fig.4.2. In fig.4.4(a) there are two pairs of complex-conjugate eigenvalues. Fig.4.4(b) explains why pulses decaying to the homogeneous background B look more like left-going pulses: the smallest absolute value belongs to a negative eigenvalue real part. This means that the back of the pulses over background B decays faster than its front.

The velocity of a pulse depends on the spatial interval on which the pulse is considered. This dependence, called the dispersion relation, is constant for large rings and varies rapidly when the length of the ring becomes smaller. For the model at hand it turns out that for all combinations of the control parameters the slope of the dispersion curves is nonmonotonic. For small ring lengths, the dispersion is normal while for large

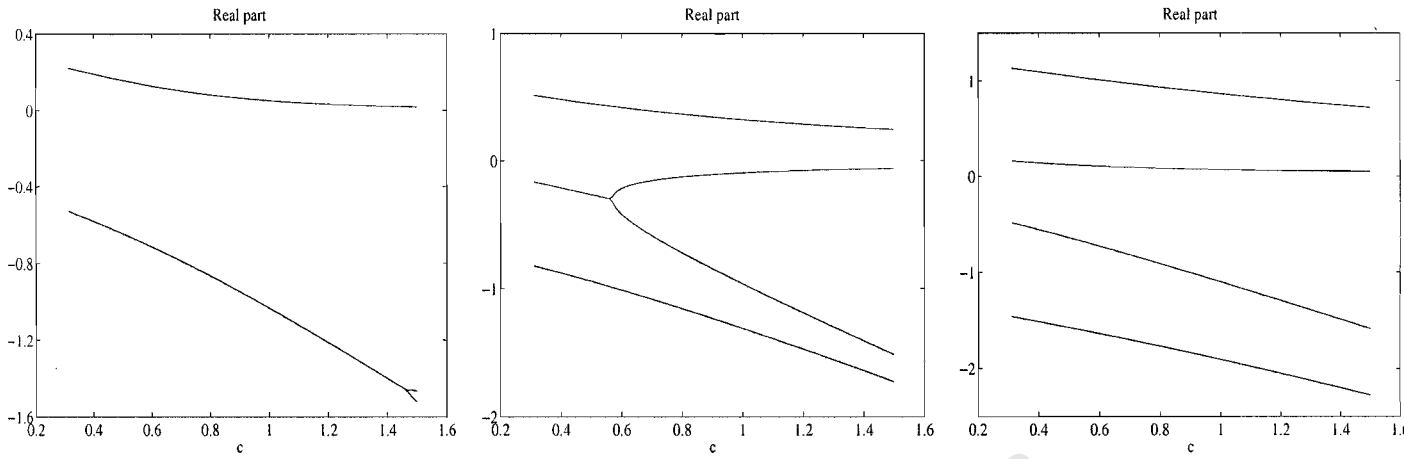

Figure 4.4: Real parts of the four eigenvalues with the smallest absolute values. The linearization was carried out about A, B, and C, respectively.

University of Cape Town

rings it is anomalous. It is important to know the shape of the dispersion curve because, as we mentioned before, it can often explain the interaction between several pulses on a ring.

We found that there are typically two types of dispersion curves for the model at hand. In fig.(4.5) we plot these typical dispersion curves of single-pulse solutions. Both dispersion curves are nonmonotonic, with well pronounced maxima. The difference between them is that one curve has an additional unstable low-velocity branch, while the second one does not. Although the pulses on the unstable branch do not have experimental counterparts, they play an important role in the process of transforming pulses over one homogeneous background to pulse decaying to another homogeneous background.

Roughly speaking, the single-branch dispersion curves are found on the right and lower-right parts of the shaded region where pulses are stable. The two-branch dispersion curves are found on its left and upper-left parts.

If one makes a horisontal slice above the saddle-node bifurcation curve, going in the direction of decreasing CO pressures, The dispersion curves achieve their maximum values for larger spatial intervals. The other tendency is that the maximum itself becomes less pronounced as CO pressure id decreased. In a vertical slice the maxima of the dispersion curves become less pronounced when the NO pressure is increased.

If we make a horizontal cut passing through the region of bistability of homogeneous states A and C, the above-mentioned pattern is preserved. There is a transition from pulses over C to pulses over A. This happens through the formation of a heteroclinic orbit connecting backgrounds B and C. In fig.4.6 we plot the pulse on a large ring for

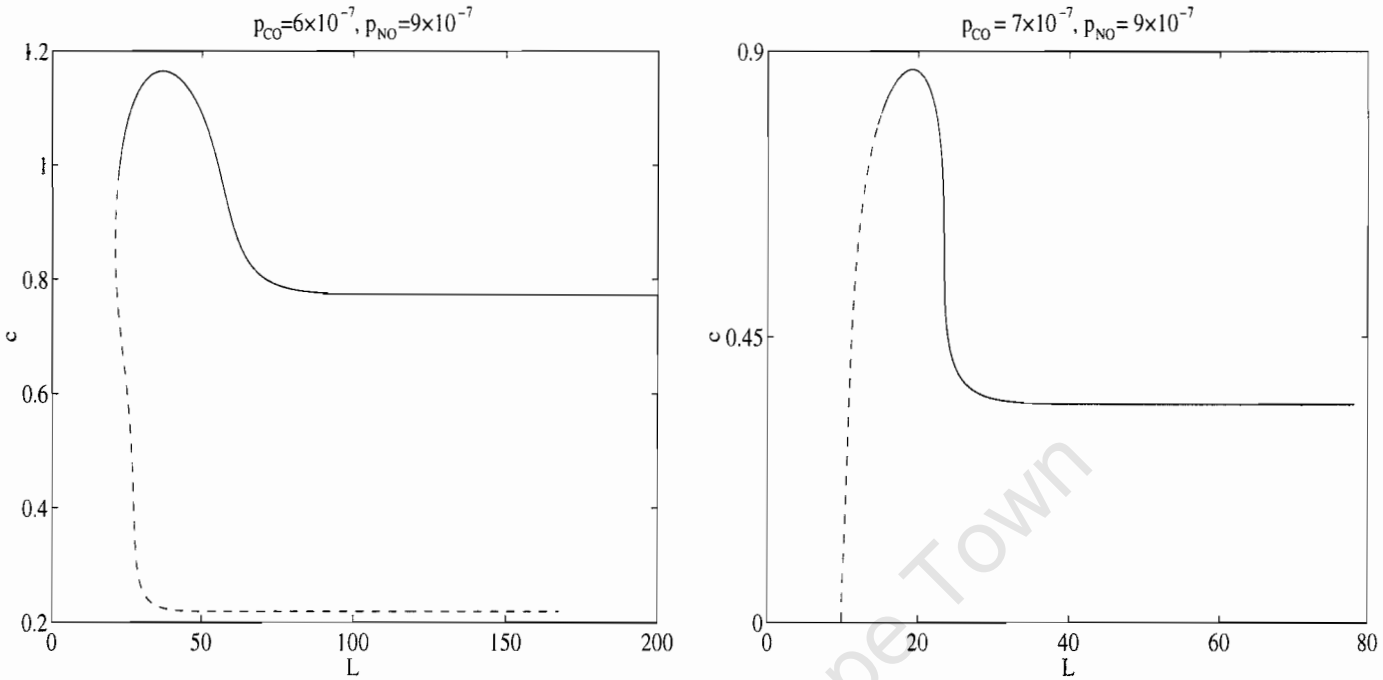

Figure 4.5: Dispersion curves for single-pulse solutions. The solid and dashed lines correspond to stable and unstable pulses, respectively.

University of Cape Town

value of parameters which are close to the T-point (i.e. the point on the control parameters plane where the heteroclinic orbit is formed). In this case the pulse consists of two flat parts connected by steep fronts. The flat parts correspond to two different homogeneous backgrounds. Further transition from pulses over B to pulses over A occurs on smaller rings through the unstable branches of the dispersion curve. Fig.4.7 shows dispersion curves for parameters close to this transition.

In fig. 4.7 the NO pressure is fixed to be 9×10^{-7} mbar while the CO pressure is varied. As the CO pressure is decreased, the dispersion curve starts pinching (fig.4.7(c)) and as a consequence of this, a closed-curve branch detaches from the rest of the semi-infinite dispersion curve on small rings (fig.4.7(b)). The semi-infinite branch continues to pinch and another closed curve branch detaches as the CO pressure is further decreased (fig.4.7(a)). In fig.4.7(a, b) the pulses decay to the homogeneous background A. Fig.4.7(c, d) shows the pulses over all three backgrounds. On the flat part of the dispersion curve at large rings the pulses decay to the homogeneous background C but have a relatively large flat part corresponding to the homogeneous state B. On the steep part of the dispersion curve the pulses decay to the background B. On the flat parts of the dispersion curve the pulses at small rings decay to the background A.

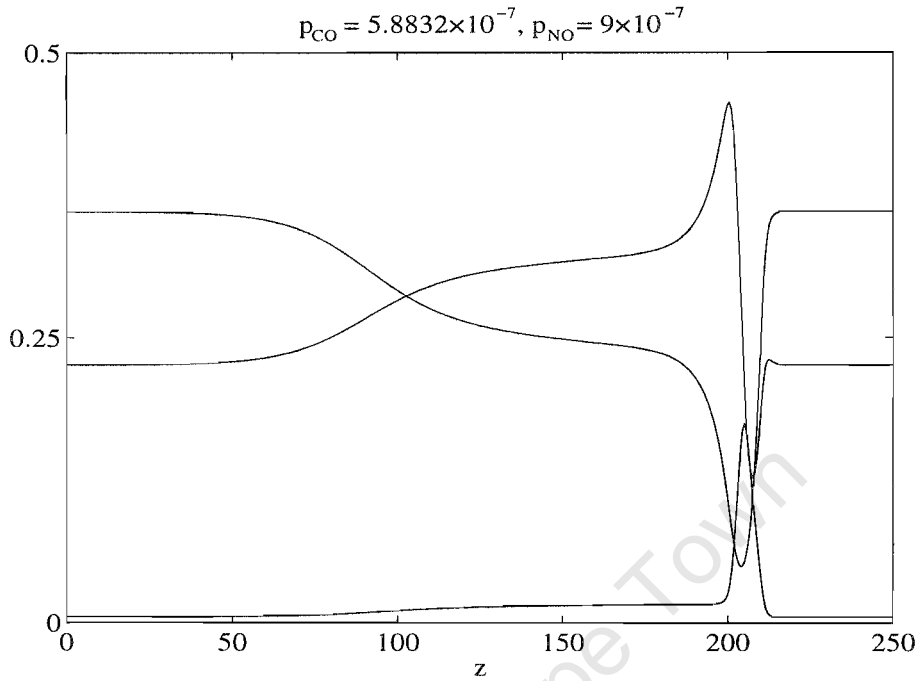

Figure 4.6: The pulse profile for parameter values close to the T-point.

University of Cape Town

There is also another transition of pulses over C to pulses over B in which case an additional semi-infinite dispersion curve is formed, see fig.4.8. Here the CO pressure is fixed while the NO pressure is varied. The pulses decay to the homogeneous background C on the big branch in fig.4.8(a). On the upper branch of the small protrusion, the pulses consist of two flat parts connected by steep fronts. The flat parts correspond to two different homogeneous backgrounds, C and B. On the lower branch of the protrusion, the pulses decay to the homogeneous background C. As the NO pressure is decreased, the protrusion widens (fig.4.8(b, c, d)). Eventually, different branches of the dispersion curve recombine and split into two disconnected semi-infinite curves. In fig.4.8(e, f) pulses on the higher velocity branch decay to the homogeneous background B and those on the lower-velocity branch decay to the background C.

Increasing the CO pressure, all pulses loose their stability. As a result of this instability pulses of periodically oscillating width or more complex (but still regular) patterns may arise as well as degenerate to the homogeneous solution. No chaotic behaviour has been observed in direct numerical simulations of the system (4.1)-(4.3).

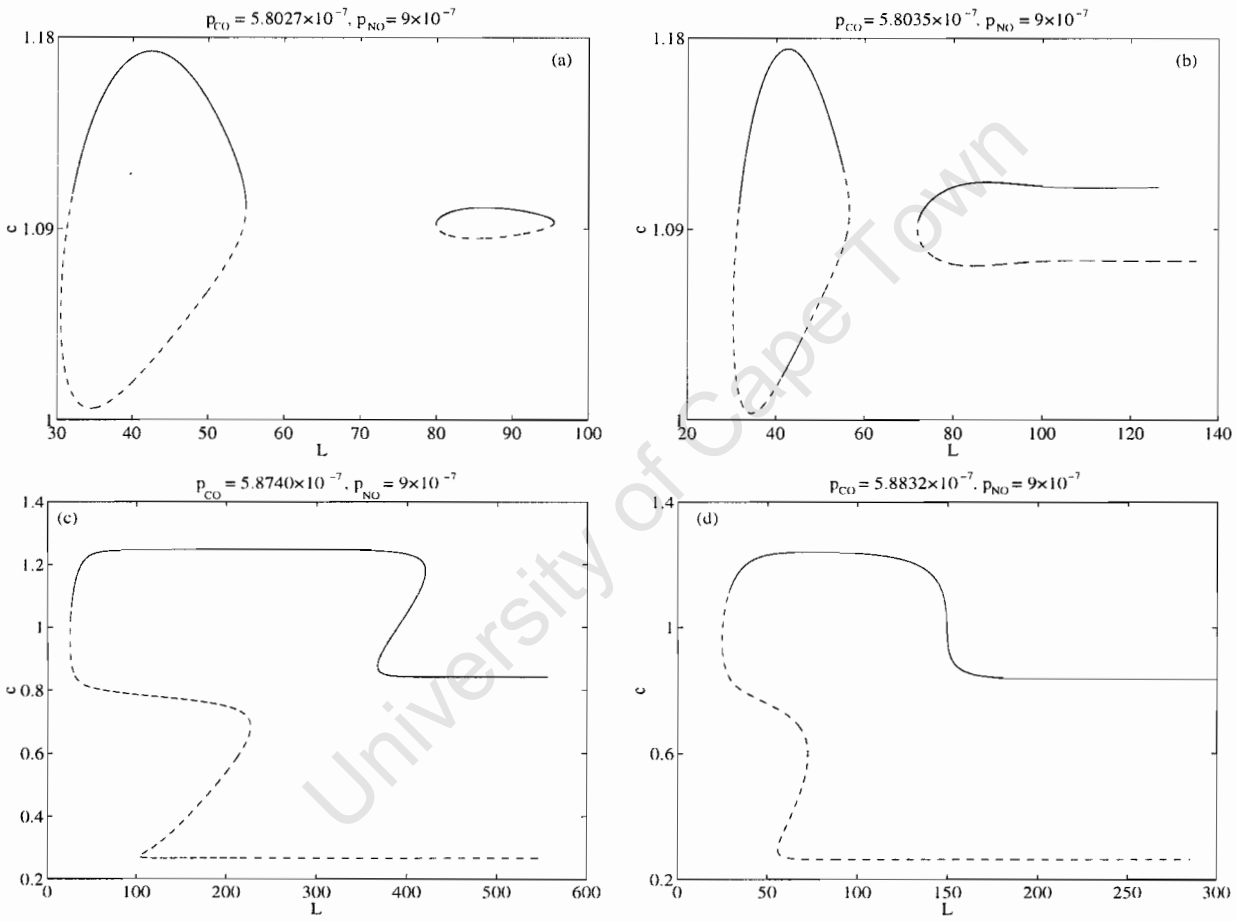

Figure 4.7: Transition of pulses over the background C to pulses over A. The solid (respectively dashed) curves mark the stable (respectively unstable) branches.

University of Cape Town

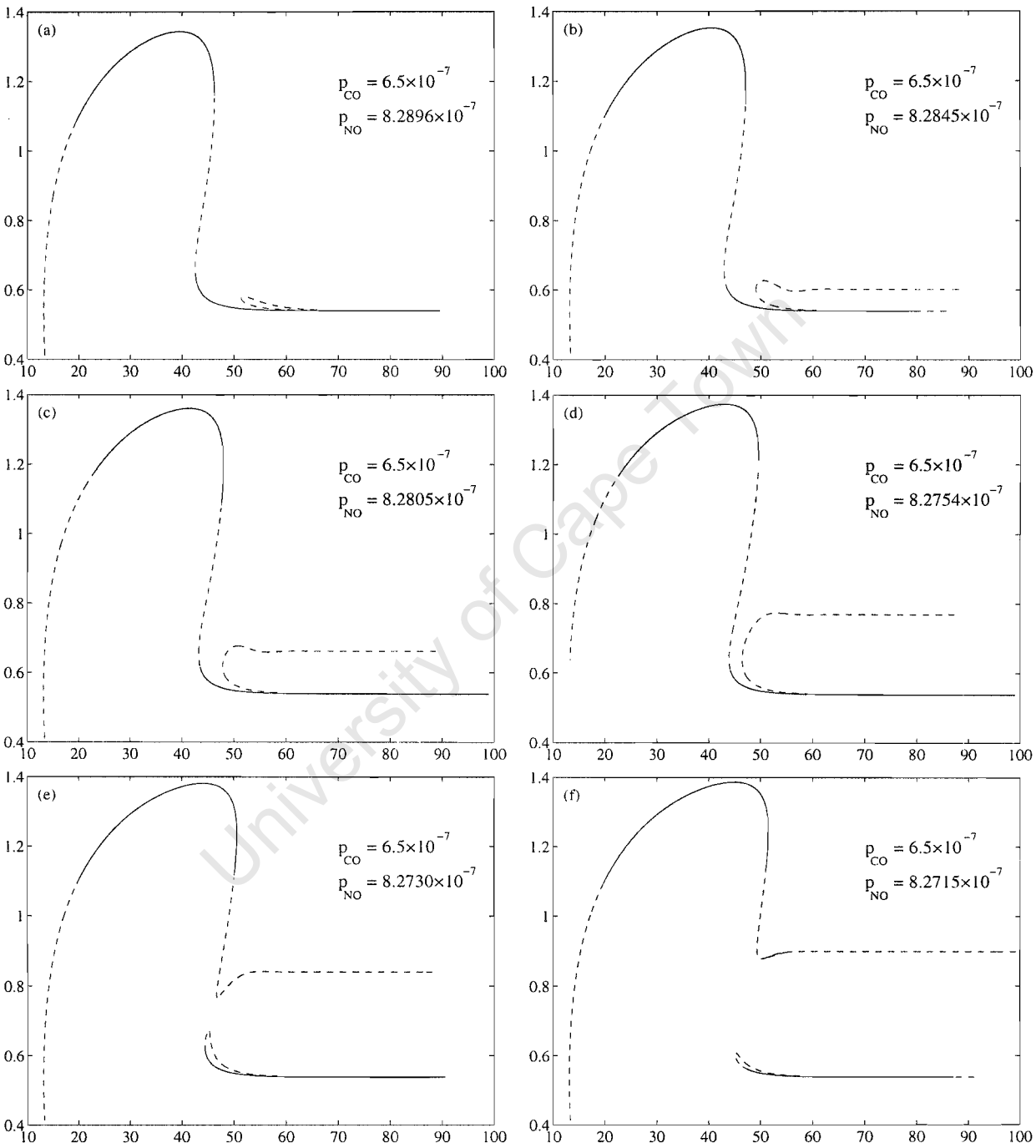

University of Cape Town

Figure 4.8: Transition of pulse over C to pulses over B. As in the previous figures, the solid lines depict sable and dashed lines unstable branches.

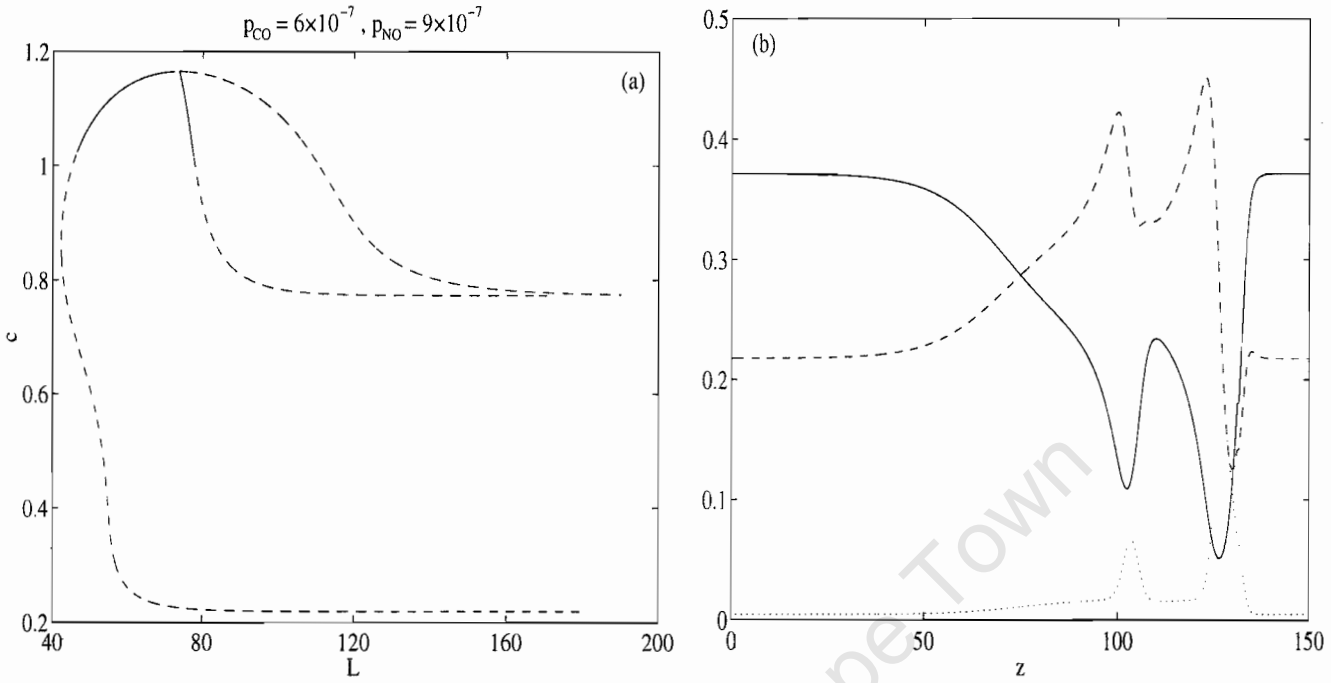

Figure 4.9: Dispersion curve on which stable bound pairs of nonequidistant pulses are possible for small ring lengths.

4.5 Pairs of equidistant and nonequidistant pulses

An important issue in the study of pulses in excitable media is the dynamical behaviour of two or more pulses on a ring. Since we consider our reaction-diffusion system under the periodic boundary conditions, it is clear that the configuration consisting of two identical pulses on a ring of the double length will be a solution to the system. The kinematic theory relates the problem of stability of wavetrains of equidistant pulses to the slope of the dispersion curve of the single-pulse solution.

The essence of this approach is to consider pulses as point-like objects that interact weakly only with their nearest neighbours. Assume that pulses do not change their shape but their positions can deviate from the symmetric configuration. We apply the kinematic approach to study the interaction of only two pulses on a ring Let z_1 and z_2 be the positions of two pulses on a ring of length $2L$. The interaction between the pulses in the frame of reference moving with the velocity $c(L)$ is described by the equations:

$$\dot{z}_1 = c(z_2 - z_1) - c(L), \quad \dot{z}_2 = c(2L - z_2 + z_1) - c(L).$$

Linearizing this dynamical system in small deviations from the symmetric configuration

University of Cape Town

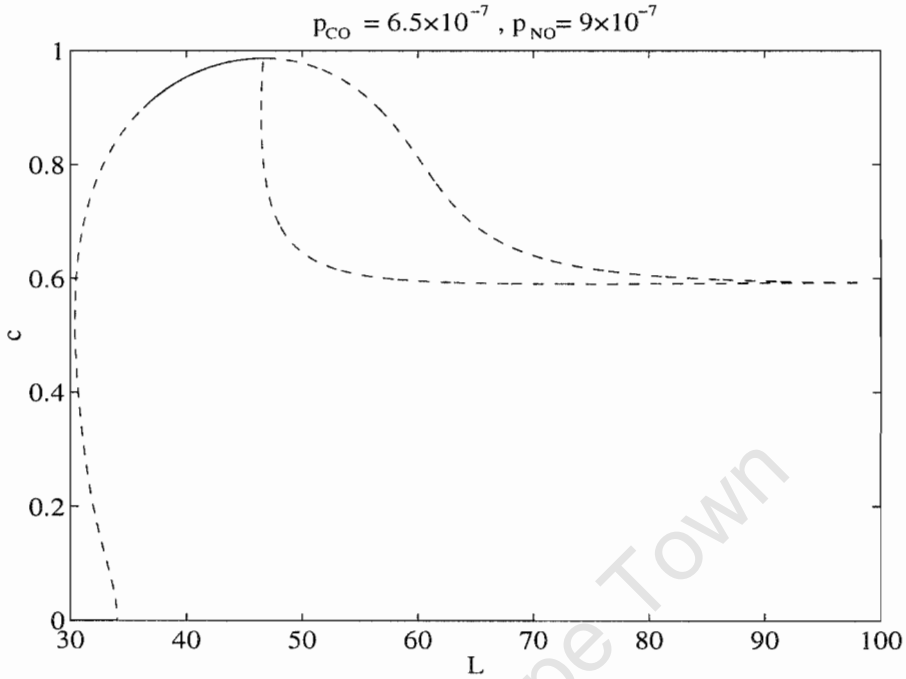

Figure 4.10: Dispersion curve where there are no stable nonequidistant bound states.

$\varepsilon = z_2 - z_1 - L$ we obtain:

$$\dot{z}_1 = c'(L)(z_2 - z - 1 - L), \quad \dot{z}_2 = c'(L)(L - z_2 + z_1),$$

where $'$ denotes the derivative with respect to the inter-pulse separation distance. The eigenvalues of this linear nonhomogeneous system of equations are $\omega_1 = 0$ and $\omega_2 = -2c'(L)$, with the corresponding eigenvectors being (1, 1) and (1, −1) [49]. The zero eigenvalue is due to the translational invariance of the two-pulse solution and the second eigenvalue characterizes the interaction between of the pulses. Thus, the stability of the wavetrain is determined by the slope of the single-pulse dispersion curve, $c'(L)$.

For wavetrains of equidistant pulses this implies that they are stable if the slope of the single-pulse dispersion curve is positive (normal dispersion) and are unstable if the slope is negative (anomalous dispersion).

The nonmonotonic dispersion curve of a single pulse suggests that there are nonequidistant bound pairs of pulses. The nonequidistant branch of the dispersion curve emerges from the maximum of the dispersion for the equidistant wavetrain via a period-doubling bifurcation. By analogy with the equidistant case, the stability of the nonequidistant bound states in the framework of the kinematik theory is determined by the interaction eigenvalue $\omega_2 = -(c'(z_1) + c'(z_2))$. For large rings the sum of the relevant slopes is always

University of Cape Town

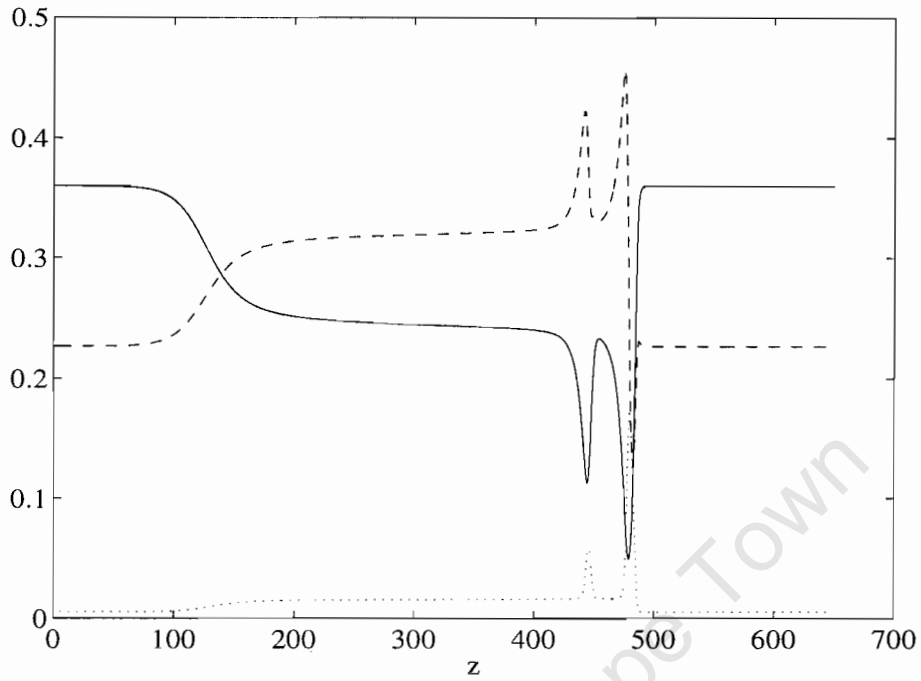

Figure 4.11: Transition of bound states over the background C to bound states over B. Solid line: $u(x)$, dashed line: $v(x)$ and dotted line: $v(x)$.

University of Cape Town

positive and hence implies stability. Surprisingly, the linear stability analysis does not confirm the stability predicted for large rings.

In fig.4.9(a) we present the dispersion curve for a wavetrain of two equidistant pulses and the nonequidistant branch of bound states. The nonequidistant branch is stable for small rings but becomes unstable for large rings through a subcritical Hopf bifurcation. In fig.4.9(b) the profile of a nonequidistant bound pair is plotted. One can see that the pulses are overlapping rather strongly and the second pulse has changed its shape. This can serve as an explanation why the predictions of the kinematic theory are not confirmed.

When the dispersion of the single pulse does not have an additional unstable branch, the emerging nonequidistant bound pair is unstable on rings of all lengths. In fig. 4.10 we display a dispersion curve where the corresponding nonequidistant bound pair is always unstable.

There is a counterpart of the transition of nonequidistant bound pairs over the background C to nonequidistant bound pairs decaying to the background B. This happens in the region of bistability of homogeneous solutions A and C. On the other hand, we were unable to find the transition from B to A.

For all examined values of the control parameters the nonequidistant bound pairs

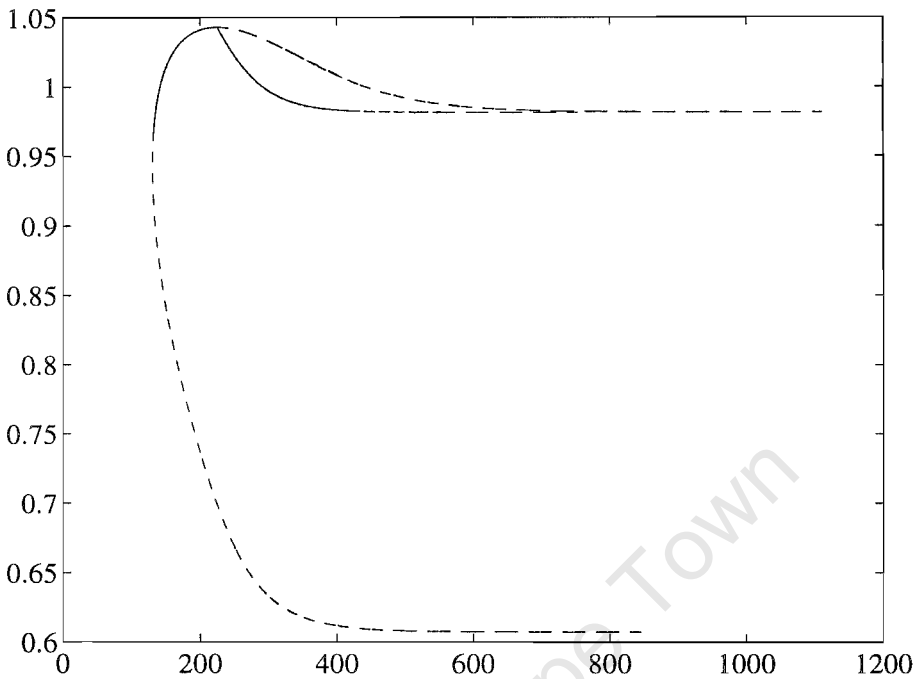

Figure 4.12: Dispersion curve with stable nonequidistant bound states on relatively large rings. Here $p_{CO} = 5.6 \times 10^{-7}$ and $p_{NO} = 9.5 \times 10^{-7}$.

University of Cape Town

are unstable. However, since there are values of the control parameters for which the dispersion curves achieve its maximum for large spatial intervals, we can choose the pressures in such a way that the nonequidistant bound states will be stable on very large rings. Such an example is plotted in fig. 4.12.

4.6 Concluding remarks

In this chapter we studied pulse solutions to an excitable reaction-diffusion system. The transition between pulses decaying to all three homogeneous backgrounds available in the system is uncovered. The stability results obtained within the kinematic theory are shown to be consistent with the linear stability analysis for equidistant pairs of pulses. In the case of strongly overlapping nonequidistant bound states; stablity on large rings suggested by the kinematic theory is not confirmed by the linear stability analysis. The nonequidistant bound states are found to be stable only on finite intervals.

The problem considered in this chapter was effectively one-dimensional. It would be interesting to study its two-dimensional generalisation, and in particular to find two-dimensional pulses and analyse their stability.

Chapter 5

Conclusions

University of Cape Town

1. We have studied the supercritical dynamics of solitons in the parametrically driven, damped NLS equation. Using the multiple-scale asymptotic expansion we derived a reduced amplitude equation for the complex amplitude of the perturbation to the soliton beyond the onset of the oscillatory instability. This fourth-order dynamical system captures the essentials of the supercritical dynamics of the soliton of the full, nonreduced NLS equation and serves as a normal form for the oscillatory instability bifurcation. We have found the relation between this normal form and the normal form of the Hopf bifurcation. From the point of view of the reduced amplitude equation, the bifurcation taking place for small values of the damping, γ, has more in common with the oscillatory instability bifurcation occurring for $\gamma = 0$ than with the Hopf bifurcation characteristic for finite γ. We have thoroughly studied the reduced-amplitude equation by exploiting its classical mechanical interpretation. The key observation here is that the amplitude equation describes the motion of a classical particle in a mexican hat-shaped potential subject to an external torque. We have shown that in the undamped case all trajectories are unbounded and therefore, the oscillatory instability does not give rise to stably oscillating solitons. In the dissipative case the unbounded trajectories coexist with two periodic orbits, of which the stable periodic orbit corresponds to a stably oscillating soliton of the NLS equation. To identify the infinite-dimensional counterparts of the four-dimensional unbounded motions we performed a series of numerical simulations of the full, nonreduced NLS equation and found three different scenarios of the development of the oscillatory instability. The first scenario involves a slowly decaying, small-amplitude breather oscillating about the zero background. In the second scenario we still observe a breather oscillating about the flat background, but this breather has a large amplitude which continues to slowly grow. Asymptotic expansions were derived for both these solutions. We have demonstrated

that the actual selection of the first or second scenario is determined by the phase of the initial perturbation. This explains why the reduced finite-dimensional system (being phase-invariant) cannot predict which of the two scenarios will result from a given initial condition. Finally, the third scenario arises for very strong perturbations in which case the soliton dissociates into a pair of small-amplitude stable solitons propagating in opposite directions with constant velocities.

2. We applied insights gained into the parametrically driven NLS equation to study the synchronization achieved by introducing an impurity into an otherwise homogeneous array of parametrically driven, coupled pendula. We analysed this problem in the small-amplitude regime which can be reduced, in the continuous limit, to the parametrically driven, damped NLS equation with a δ-function term. A positive, respectively negative, coefficient in front of the δ-function term corresponds to a longer, respectively shorter, central pendulum. We have shown that solitons can be nucleated spontaneously in systems with impurities and therefore, solitons are even more generic occurrences in these systems than in homogeneous nonlinear evolution equations. We found two explicit solutions, describing solitons pinned on the impurity one of which was shown to be unstable against a symmetric nonoscillatory mode for all values of the damping coefficient, driver's amplitude and strength of the impurity. Accordingly, the subsequent analysis focussed on the soliton of the second type. The energy-based considerations suggested, and direct numerical simulations confirmed, that long impurity attracts and traps solitons while the short impurity repels them. Similarly to the homogeneous case, solitons pinned on a long impurity may become unstable to a symmetric mode but in the inhomogeneous case the stability region is wider. The stronger the impurity is, the larger is the stability region. As a result, the spatiotemporal chaos arising in the homogeneous system can be suppressed by the introduction of a sufficiently long impurity. Introducing a shortening impurity, on the contrary, contracts the region of stability against a symmetric mode. However, since the soliton is repelled by the short impurity, the symmetric instability will not be able to set in in this case. Thus both types of impurities, the long and the short ones, should act as stabilizers on the chain: the long ones because they suppress instabilities in some neighbourhood around them, and the short ones because they repel solitons and thereby partition the chain into smaller subintervals. (The latter suppresses long-wavelength instabilities.) The effect of closely situated multiple impurities remains an open question however. Our simulations of the chain with two attractive impurities revealed that the two solitons nucleated around the impurities develop spontaneous large-amplitude oscillations — despite the fact that each individual soliton is stable in the

University of Cape Town

parameter range in question.

3. Studies of the reaction-diffusion model of the NO-CO chemical reaction revealed localized pulse solutions decaying to all three homogeneous backgrounds available in the system. Pulses decaying to stable backgrounds are also stable in a large range of control parameters. We have performed a detailed numerical study of dispersion curves associated with the pulses. On the basis of this analysis we uncovered two scenarios of transition between pulses decaying to different backgrounds. In both cases the transition occurs via the formation of a heteroclinic orbit and the dispersion curve splits into two disjoint curves. In the first scenario, the transformation occurs on a large ring while in the second case the transformation occurs on a ring of a small length. We used the kinematic theory to analyse the interaction between two pulses on a ring. The linear stability analysis confirms predictions of the kinematic theory for the case of equidistant pulses. Namely, the equidistant pulses are stable on finite rings if the slope of the single-pulse dispersion curve is positive and unstable if this slope is negative. We also obtained nonequidistant bound states of pulses. The branch of the nonequidistant pulses emerges from the point of maximum of the single-pulse dispersion curve through a period-doubling bifurcation. The stability of nonequidistant bound states suggested by the kinematic theory, was not confirmed by the linear stability analysis and direct numerical simulations of the system of PDEs. We have also found the transition between bound states of pulses over different backgrounds. As opposed to a single-pulse case, bound states decaying to different backgrounds were found to have different velocities on large rings.

Open problems. There are several avenues of further investigation. In particular, it would be of interest to explore whether the parametric driving and damping are capable of "arresting" the collapse in two- and three-dimensional NLS equations. Can a combination of these two perturbations give rise to stable 2D and 3D solitons?

In Chapter 3 we studied the possibility of taming chaos by solitons pinned on impurities. This mechanism does not work for values of control parameters for which the soliton is unstable to continuous spectrum waves. It would be interesting to find out whether chaos can be tamed by using a (pinned) spatially-periodic nonlinear wavetrain instead of a soliton.

As a natural generalisation of our analysis of 1D pulses in the NO + CO reaction-diffusion system, one can consider this reaction in 2D domains. The two-dimensional analogs of the 1D pulses are spiral waves; it would be interesting to study their existence and stability. The influence of the crystal defects on the formation and dynamics of pulses and spiral waves is also worth investigating.

University of Cape Town

University of Cape Town

Bibliography

[1] F.Kh. Abdulaev and A.A. Abdumalikov, Phys. Stat. Sol (b), **167**, 503 (1991)

[2] M.J. Ablowitz, D.J. Kaup, A.C. Newell and H. Segur, Phys. Rev. Lett., **30**, 1262 (1973)

[3] M.J. Ablowitz, D.J. Kaup, A.C. Newell and H. Segur, Phys. Rev. Lett., **31**, 125 (1973)

[4] M.J. Ablowitz and H. Segur, *Solitons and Inverse Scattering Transform*, (SIAM Philadelphia, 1981)

[5] H. Akoh, S. Sakai, A. Yagi and H. Hayakawa, IEEE Trans. Magn., **21**, 737 (1985)

[6] N.V. Alexeeva, I.V. Barashenkov and D.E. Pelinovsky, Nonlinearity **12**, 103 (1999)

[7] N.V. Alexeeva, I.V. Barashenkov and G.P. Tsironis, Phys. Rev. Lett., **84**, 3053 (2000)

[8] N.V. Alexeeva, I.V. Barashenkov and G.P. Tsironis, J. Nonlin. Math. Phys., **8**, 5 (2001)

[9] N.V. Alexeeva and T.L. Boyadjiev, Bulg. J. Phys., bf 24, 63 (1997)

[10] D. Anderson and M. Lizak, Phys. Rev. **A 27**, 1393 (1983)

[11] F.T. Arecchi and R. Bonifacio, IEEE J. Quantum Electron., **1**, 169 (1965)

[12] F.T. Arecchi, V. DeGiorgio and C.G. Someda, Phys. Lett. **A 27**, 588 (1968)

[13] F.T. Arecchi, G.L. Masserini and P. Schwendimann, Riv. Nuovo Cimento, **1**, 181 (1969)

[14] F. Argoul, A. Arnéodo, P. Richetti and J.C. Roux, J. Chem. Phys. **86**, 3325 (1987)

University of Cape Town

[15] A. Arnéodo, F. Argoul, J. Elezgaray and P. Richetti, Physica **D 62**, 134 (1993)

[16] N. Asano, T. Taniuti, and N. Yajima, J. Math. Phys., **10**, 2020 (1969)

[17] I.V. Barashenkov, M.M. Bogdan, and V.I. Korobov, Europhys. Lett., **15**, 113 (1991)

[18] I.V. Barashenkov, Yu.S. Smirnov and N.V. Alexeeva, Phys. Rev. **E 57**, 2350 (1998)

[19] I.V. Barashenkov, T. Zhanlav, and M.M. Bogdan, in *Nonlinear World: IV International Workshop on Nonlinear and Turbulent Processes in Physics* (eds. V.G.Bar'yakhtar et al.), Kiev, 9–22 October 1989, 3 (World Scientific, Singapore, 1990)

[20] I.V. Barashenkov and E.Yu. Panova, Physica **D 69**, 114 (1993)

[21] I.V. Barashenkov ans Y.S. Smirnov, Phys. Rev. **E 54**, 5707 (1996)

[22] A. Barone and G. Paterno, *Physics and Applications of the Josephson Effect*, (Wiley, New York, 1982)

[23] E.M. Barston, Phys. Fluids **12**, 2162 (1969)

[24] E.M. Barston, J. Fluid Mech. **42**, 97 (1970)

[25] V.G. Bar'yakhtar, B.A.Ivanov and M.V. Chetkin, Sov. Phys. Usp., **28**, 564 (1985)

[26] V.G. Bar'yakhtar, B.A. Ivanov and A.L. Sukstanskii, Sov. Phys. JETP, **51**, 757 (1980)

[27] C.P. Bean and R.W. deBlois, Bull. Amer. Phys. Soc., **4**, 53 (1959)

[28] Y.A. Berezin and V.I. Karpman, Sov. Phys. JETP, **19**, 1265 (1964)

[29] Y.A. Berezin and V.I. Karpman, Sov. Phys. JETP, **24**, 1049 (1967)

[30] P. Bergé, Y. Pomeau and C. Vidal, *L'ordre dans le chaos* (Hermann, Paris, 1984)

[31] D.J. Bergman, E. Ben-Jacob, Y. Imri and K. Maki, Phys. Rev. **A 27**, 3345 (1983)

[32] V.I. Bespalov and V.I. Talanov, JETP Lett., **3**, 307 (1967)

[33] A.R. Bishop, K. Fesser, P.S. Lomdahl, W.C Kerr, M.B. Williams and S.E. Trullinger, Phys. Rev. Lett., **50**, 1095 (1983)

University of Cape Town

[34] A. R. Bishop, K. Fesser, P.S. Lomdahl, and S.E. Trullinger, Physica **D 7** 259 (1983)

[35] A.R. Bishop, M.G. Forest, D.W. McLaughlin and E.A. Overman II, Physica **D 23**, 293 (1986)

[36] M.M. Bogdan, A.M. Kosevich and I.V. Manzhos, Sov. J. Low Temp. Phys. **11**, 547 (1985)

[37] M.M. Bogdan, A.S. Kovalev, and I.V. Gerasimchuk, Low Temp. Phys. **23**, 145 (1997)

[38] M. Bondila, I.V. Barashenkov, and M.M. Bogdan, Physica **D 87**, 314 (1995)

[39] M.Bondila, MSc thesis. University of Cape Town, 1995 (unpublished)

[40] J.P. Boyd, Nonlinearity **3**, 177 (1990)

[41] Y. Braiman, W.L. Ditto, K. Wiesenfeld, and M.L. Spano, Phys. Lett. **A 206**, 54 (1995)

[42] Y. Braiman, J.F. Lindner and W.L. Ditto, Nature (London) **378**, 465 (1995)

[43] O.M. Braun, Yu.S. Kivshar, Phys. Rep. **306**, 1 (1998)

[44] R.K. Bullough and P.J. Caudrey, in *Nonlinear Evolution Equations Solvable by the Inverse Spectral Transform*, ed. by F. Calogero, 180, (Pitman, London, 1978)

[45] X.D. Cao, B.A. Malomed, Phys. Lett. **A 206**, 177 (1995)

[46] V. Castets, E. Dulos, J. Boissonade and P. De Kepper, Phys. Rev. Lett., **64**, 2953 (1990)

[47] J.J. Chang, Appl. Phys. Lett., **47**, 431 (1986)

[48] X.-N. Chen and R.-J. Wei, J. Fluid Mech. **259**, 291 (1994)

[49] J. Christoph, M. Eiswirth, N. Hartmann, R. Imbihl, I. Kevrekidis, and M. Bär, Phys. Rev. Lett. **82**, 1586 (1999)

[50] P.L. Christiansen and O.H. Olsen, Wave Motion, **4**, 163 (1982)

[51] P. Coullet and P. Huerre, Physica **D 23**, 27 (1986)

University of Cape Town

[52] M. Cox, G. Ertl and R. Imbihl, Phys. Rev. Lett., **54**, 1725 (1985)

[53] R.F. Dashen, B. Hasslacher and A. Neveu, Phys. Rev. **D 10**, 4130 (1974)

[54] P.G. deGennes, *Superconductivity of metals and alloys*, (New York, Benjamin, 1966)

[55] F. DeMartini, C.H. Townes, T.K. Gustafson and P.L. Kelley, Phys. Rev., **164**, 312 (1967)

[56] I.H. Deutsch and I. Abram, J. Opt. Soc. Am. **B 11**, 2303 (1994)

[57] E.J. Doedel, X.J. Wang, AUTO94: Software for continuation and bifurcation problems in ordinary differential equations, Tech. rep., Center of Research on Parallel Computing, California Institute of Technology, Pasadena, ca 911125, CRPC 95-2

[58] R.C. DiPrima, W. Eckhaus and L.A. Segel, J. Fluid Mech., **48**, 705 (1971)

[59] K.B. Dysthe and H.L. Pécseli, Plasma Phys., **19**, 931 (1977)

[60] J.H. Eberly, Phys. Rev. Lett., **22**, 760 (1969)

[61] J. C. Eilbeck, P. S. Lomdahl, and A. C. Newell, Phys. Lett. **A87** 1 (1981)

[62] C. Elphick, E. Meron, J. Rinzel and E.E. Spiegel, J. Theor. Biol., **146**, 249 (1990)

[63] V. Enz, Helv. Phys. Acta, **37**, 245 (1964)

[64] G. Ertl, Science, **254**, 1750 (1991)

[65] J.W. Evans, H.H. Madden, and R. Imbihl, J. Chem. Phys. **96**(6), 4805 (1992)

[66] A.B. Ezerskii, M.I. Rabinovich, V.P. Reutov and I.M. Starobinets, Sov. Phys. JETP, **64**, 1228 (1986)

[67] A.L. Fabrikant, Sov. Phys. JETP, **59**, 274 (1984)

[68] J.L. Fergason and G.H. Brown, J. Amer. Oil Chemists Soc., **45**, 120 (1968)

[69] R. Field, E. Körös and R. Noyes, J. Am. Chem. Soc. **94**, 8649 (1972)

[70] R. Field and M. Burgers (eds.), Oscillations and travelling waves in chemical systems. (Wiley, New York, 1985)

University of Cape Town

[71] R.M. Fleming, D.E. Moncton, D.B. McWhan and F.J. Disavilo, Phys. Rev. Lett., **45**, 576 (1980)

[72] N.C. Freeman and R.S. Johnson, J. Fluid Mech., **42**, 401 (1970)

[73] J. Frenkel and T.Kontorova, J. Phys. (USSR), **1**, 137 (1939)

[74] B.D. Fried and Y.H. Ichikawa, J. Phys. Soc. Japan, **34**, 1073 (1973)

[75] H. Friedel, E.W. Laedke and K.H. Spachek, J. Fluid Mech, **284**, 341 (1994)

[76] H. Fukushima, J. Phys. Soc. Japan, **45**, 1266 (1978)

[77] T.A.Fulton and R.C. Dynes, Solid State Commun., **12**, 57 (1973)

[78] A.V. Galeev, R.Z. Sagdeev, Yu.S. Sigov, V.D. Shapiro and V.I. Shevchenko, Sov. J. Plasma Phys., **1**, 5 (1975)

[79] C.S. Gardner, J.M. Green, M.D. Kruskal and R.M. Miura, phys. Rev. Lett., **19**, 1095 (1967)

[80] A. Gavrielides, T. Kottos, V. Kovanis and G. P. Tsironis, Phys. Rev. **E 58**, 5529 (1998)

[81] J. Gibbons, Phys. Lett. **A 67**, 22 (1978)

[82] J.D. Gibbons, I.N. James and I.M. Moroz, Phys. Scr., **20**, 402 (1979)

[83] A.A. Golubov, I.L. Serpuchenko and A.V. Ustinov, Sov. Phys. JETP, **67**, 1256 (1988)

[84] J. Gomatam and P. Grinrod, J. Math. Biol., **25**, 611 (1987)

[85] V.V. Gorev, A.S. Kingsep and L.I. Rudakov, Izv. Vyssh. Uchebn. Zav. Radiofiz., **19**, 691 (1976)

[86] R. Grauer and Y.S. Kivshar, Phys. Rev. **E 48**, 4791 (1993)

[87] P. Gray, G. Nicolis, F.Baras, P. Borckmans and S. Scott (eds.), *Spatial inhomogeneities and transient behaviour in chemical kinetics*, (Manchester University Press, Manchester, 1990)

[88] P. Grinrod and J. Gomatam, J. Math. Biol., **25**, 597 (1987)

University of Cape Town

[89] N. Grønbech-Jensen, Y.S. Kivshar and M.R. Samuelsen, Phys. Rev. **B 47**, 5013 (1993)

[90] G. Grüner, A. Zawadowski and P.M. Chaikin, Phys. Rev. Lett., **46**, 511 (1981)

[91] J. Guckenheimer and P. Holmes,*Nonlinear oscillations, dynamical systems and bifurcations of vector fields*, (Springer, Berlin, 1983)

[92] E.V. Gurovich and V.G. Mikhalev, Sov. Phys. JETP, **66**, 731 (1987)

[93] A. Hasegawa, Appl. Opt., **23**, 3302, (1984)

[94] A. Hasegawa and Y. Kodama, Proc. IEEE, **69**, 1145 (1981)

[95] A. Hasegawa and F. Tappert, Appl. Phys. Lett., **23**, 142 (1973)

[96] A. Hasegawa and F. Tappert, Appl. Phys. Lett., **23**, 171 (1973)

[97] H.A. Haus and M.N. Islam, IEEE J Quantum Electron., **21**, 1172 (1985)

[98] R. Hirota, Phys. Rev. Lett., **27**, 1192 (1971)

[99] A.L. Hodgkin, A.F. Huxley, J. Physiol. **117**, 500 (1952)

[100] F.A. Hopf and M.O. Scully, Phys. Rev., **179**, 399 (1969)

[101] Y.H. Ichikawa, Phys. Scr., **20**, 296 (1979)

[102] Y.H. Ichikawa, T. Imamura and T. Tanuiti, J. Phys. Soc. Japan, **33**, 189 (1972)

[103] Y.H. Ichikawa and T. Taniuti, J. Phys. Soc. Japan, **34**, 513 (1973)

[104] R. Imbihl, Physica **A 188**, 34 (1992)

[105] R. Imbihl, Th. Fink, and K. Krischer, J. Chem. Phys., **96**, 6236 (1992)

[106] A. Jeffrey and T. Kakutani, SIAM Rev., **14**, 582 (1972)

[107] B.D. Josephson, Phys. Lett., **1**, 251 (1962)

[108] J. Juul Rasmussen and K. Rypdal. Physica Scripta **33**, 481 (1986)

[109] J. Kambe and M. Umeki, J. Fluid Mech. **212**, 373 (1990)

[110] V.G. Kamenskii, Sov. Phys. JETP, **87**, 1262 (1984)

University of Cape Town

[111] V.I. Karpman, JETP Lett., **25**, 271 (1977)

[112] V.I. Karpman and M.D. Kruskal, Sov. Phys. JETP, **28**, 277 (1969)

[113] V.I. Karpman and E.M. Maslov, Sov. Phys. JETP, **46**, 281 (1977)

[114] V.I. Karpman, E.M. Maslov and V.V. Solov'ev, Sov. Phys. JETP, **57**, 167 (1983)

[115] D.J. Kaup, SIAM J. Appl. Math., **31**, 121 (1976)

[116] D.J. Kaup and A.C. Newell, Proc. R. Soc. London Ser. **A 361**, 413 (1978)

[117] D.J. Kaup and A.C. Newell, Phys. Rev. **B 18**, 5162 (1978)

[118] T. Kawahara, J. Phys. Soc. Japan, **27**, 1331 (1969)

[119] J.P. Keener, SIAM J. Appl. Math., **46**, 1039 (1986)

[120] J.P. Keener and D.W. McLaughlin, J. Math. Phys., **18**, 2008 (1977)

[121] J.P. Keener and J.J. Tyson, Physica, **D 21**, 307 (1986)

[122] P.L. Kelley, Phys. Rev. Lett., **15**, 1005 (1965)

[123] H. Kever and G.K. Morikawa, Phys. Fluids, **12**, 2090 (1969)

[124] Yu.S. Kivshar, Z. Fei and L Vásquez, Phys. Rev. Lett., **67**, 1177 (1991)

[125] Yu.S. Kivshar, A.M. Kosevich and O.A. Chubykalo, Zh. Eksper. Teor. Fiz., **93**, 968 (1987)

[126] Yu.S. Kivshar, A.M. Kosevich and O.A. Chubykalo, Phys. Lett. **A 129**, 449 (1988)

[127] Yu.S. Kivshar and B.A. Malomed, J. Phys. **A 19**, L967 (1986)

[128] Yu.S. Kivshar and B.A. Malomed, Japan J. Appl. Phys., **26**, Suppl. 26-3, 1583 (1987)

[129] Y.S. Kivshar and B.A. Malomed, J. Phys. **A 21**, 1553 (1988)

[130] Y.S. Kivshar and B.A. Malomed, Phys. Lett. **A 129**, 443 (1988)

[131] Y.S. Kivshar and B.A. Malomed, J. Appl. Phys., **65**, 879 (1989)

[132] Y.S. Kivshar and B.A. Malomed, Rev. Mod. Phys., **61**, (1989)

University of Cape Town

[133] Yu.S. Kivshar, B.A. Malomed and A.A. Nepomnyashchii, Sov. Phys. JETP, **67**, 850 (1988)

[134] Yu.S. Kivshar, A. Sánchez, O. Chubykalo, A.M. Kosevich and L. Vazquez, J. Phys. **A 25**, 5711 (1992)

[135] J.K. Kjems and M. Steiner, Phys. Rev. Lett., **41**, 1137 (1978)

[136] Y. Kodama, J. stat. Phys., **39**, 597 (1985)

[137] Y. Kodama, Phys. Lett. **A 107**, 245 (1985)

[138] Y. Kodama, Phys. Lett. **A 112**, 193 (1985)

[139] Y. Kodama, Phys. Lett. **A 123**, 276 (1987)

[140] Y. Kodama and A. Hasegawa, Opt. Lett., **12**, 7 (1982)

[141] Y. Kodama and A. Hasegawa, IEEE J Quant. Elect. **QE 23**, 510 (1987)

[142] Y. Kodama and K. Nozaki, Opt. Lett., **12**, 1038 (1987)

[143] D.J. Korteweg and G. de Vries, Phil. Mag. **39**, 422 (1895)

[144] A.M. Kosevich and yu.S. Kivshar, Sov. J. Low Temp. Phys., **8**, 644 (1982)

[145] A.M. Kosevich and A.S. Kovalev, Zh. Eksper. Teoret. Fiz. **67**, 1793 (1974) [Sov. Phys. JETP, **40**, 891 (1974)]

[146] I.O. Kulik, Sov. Phys. JETP, **24**, 1307 (1967)

[147] A. Kumar, S.N. Sakar and A.K. Ghatak, Opt. Lett., **11**, 321 (1986)

[148] E.A. Kuznetsov, A.M. Rubenchik and V.E. Zakharov, Phys. Rep. **142**, 103 (1986)

[149] E.W. Laedke and K.H. Spatschek, J. Fluid. Mech. **223**, 589 (1991)

[150] G.L. Lamb, Phys. Lett., **A 25**, 181 (1967)

[151] G.L. Lamb, Rev. Mod. Phys., **43**, 99 (1971)

[152] G. Laval, C. Mercier and R. Pellat, Nucl. Fusion, **5**, 156 (1965)

[153] P.D. Lax, Commun. Pure Appl. Math., **21**, 196 (1968)

University of Cape Town

[154] P. Lebwohl and M.J. Stephen, Phys. Rev., **163**, 376 (1967)

[155] S. Leibovich, J. Fluid Mech., **42**, 803 (1970)

[156] S. Leibovich and A.R. Seebass, in *Nonlinear Waves*, (eds. S.Liebovich and A. Seebass), (Cornell Univ. Press, Ithaca, 1974)

[157] S.A. Levin, in *Studies in mathematical biology, Part II*, ed. by S.A. Levin, (M.A.A. Studies in Mathematics, 1978)

[158] O.A. Levring, M.R. Samuelsen and O.H. Olsen, Physica **D 11**, 349 (1984)

[159] L. Lin, C. Shu, J. Shen, P.M. Lam and H. Yun, Phys. Rev. Lett., **49**, 1335 (1982)

[160] L. Lin, C. Shu and G. Xu, J. Stat. Phys., **39** (1985)

[161] P.S. Lomdahl, J. Stat. Phys., **39**, 551 (1985)

[162] P.S. Lomdahl and M.R. Samuelsen, Phys. Rev. **A 34**, 664 (1986)

[163] S. Longhi, Phys. Rev. **E 55**, 1060 (1997)

[164] S. Longhi, Opt. Lett.,**20**, 695 (1995)

[165] V.S. L'vov et al., Fizika Tverdogo Tela **15**, 793 (1973)

[166] D.W. McLaughlin and A.C. Scott, Phys. Rev. **A 18**, 1652 (1978)

[167] S.L. McCall and E.L. Hahn, Phys. Rev., **183**, 457 (1969)

[168] K. Maki, Phys. Rev. **B 11**, 4264 (1975)

[169] K. Maki and P. Kumar, Phys. Rev. **B 14**, 118 (1976)

[170] B.A. Malomed, Physica, **D 15**, 385 (((1985)

[171] B.A. Malomed, Physica, **D 27**, 113 (1987)

[172] B.A. Malomed, Wave Motion, **9**, 401 (1987)

[173] B.A. Malomed, Physica, **D 29**, 155 (1987)

[174] B.A. Malomed, Phys. Lett. **A 120**, 28 (1987)

[175] B.A. Malomed, Phys. Scr., **38**, 66 (1988)

University of Cape Town

[176] D. Marcuse, Appl.Opt., **19**, 1653 (1980)

[177] J. Marsden and M. McCracken, *The Hopf Bifurcation and Its Applications*, (Springer, Berlin, 1976)

[178] O.S. Marsden and C.C. Mei, J. Fluid Mech., **39**, 781 (1969)

[179] A. Mecozzi, L. Kath, P. Kumar, and C.G. Goedde, Opt.Lett. **19**, 2050 (1994)

[180] A. Menikoff, Commun. Pure Appl. Math., **25**, 407 (1972)

[181] C.R. Menyuk, Phys. Rev. **A 33**, 4367 (1986)

[182] C.R. Menyuk and H.H. Chen, Phys. Rev. Lett., **55**, 1809 (1985)

[183] H.I. Mikeska, J. Phys. **C 11**, L29 (1978)

[184] J.W. Miles, J. Fluid Mech. **148**, 451 (1984)

[185] M.B. Mineev and V.V. Shmidt, Sov. Phys. JETP, **52**, 453 (1980)

[186] R.M. Miura, in *Nonlinear Waves*, (eds. S. Leibovich and A. Seebass), (Cornell Univ. Press, New York, 1974)

[187] R.M. Miura, J. Math. Phys., **9**, 1202 (1968)

[188] R.M. Miura, C.S. Gardner and M.D. Kruskal, J. Math. Phys., **9**, 1204 (1968)

[189] R.M. Miura, SIAM Rev., **18**, 412 (1976)

[190] L.F. Mollenauer and R.H. Stolen, Opt. Lett., **9**, 13 (1984)

[191] I.M. Moroz and J. Brindley, Proc. R. Soc. London, **A 377**, 379 (1981)

[192] K.W. Morton, Phys. Fluids, **7**, 1801 (1964)

[193] J. Nagumo, S. Arimoto and S. Yoshizawa, Proc. IRE, **50**, 2061 (1962)

[194] G.A. Nariboli, J. Math. and Phys. Sci., **4**, 64 (1970)

[195] D.R. Nickolson and M.V. Goldman, Phys. Fluids, **19**, 1621 (1977)

[196] G. Nicolis and J. Portnow, Chem. Rev. **73**, 365 (1973)

University of Cape Town

[197] S.P. Novikov, S.V. Manakov, L.P. Pitaevski and V.E. Zakharov, *Theory of Solitons: the Inverse Scattering Method*, (Consultants Bureau, New York, 1984)

[198] R. Noyes and R. Field, Ann. Rev. Phys. Chem. **25**, 95 (1974)

[199] K. Nozaki, Phys. Rev. Lett., **49**, 1883 (1982)

[200] K. Nozaki, Physica **D 23**, 369 (1986)

[201] K. Nozaki and N. Bekki, Phys. Rev. Lett. **50**, 1226 (1983)

[202] K. Nozaki and N. Bekki, Phys. Lett. **A 102**, 383 (1984)

[203] K. Nozaki and N. Bekki, J. Phys. Soc. Japan, **54**, 2363 (1985)

[204] K. Nozaki and N. Bekki, Physica **D 21**, 381 (1986)

[205] A. Okamura and H. Konno, J. Phys. Soc. Japan, **58**, 1930 (1989)

[206] A. Okubo, *Diffusion and ecological patterns: mathematical models*, Biomathematics 10, (Springer-Verlag, New York, 1980)

[207] O.H. Olsen and M.R. Samuelsen, Phys. Rev. **B 28**, 210 (1983)

[208] O.H. Olsen and M.R. Samuelsen, Phys. Rev. **B 34**, 3510 (1986)

[209] M. Or-Guil, I.G. Kevrekidis, and M. Bär, Physica **D 135**, 154 (2000)

[210] G.V. Osipov and M.M. Sushchik, IEEE Trans. Circuits Syst., I: Fundam. Theory Appl. **44**, 1006 (1997)

[211] E. Ott and R.N. Sudan, Phys. Fluids, **12**, 2388 (1969)

[212] Q. Ouyyang and H. Swinney, Nature, **352**, 610 (1991)

[213] E.A. Overman, D.W. McLaughlin, and A.R. Bishop, Physica **D 19** 1 (1986)

[214] S. Pagano, M. Salerno and M.R. Samuelsen, Physica D **26**, 396 (1987)

[215] R.L. Pego, P. Smereka and M.I. Weinstein, Nonlinearity **8**, 921 (1995)

[216] D.E. Pelinovsky, V.V. Afanasjev, and Yu.S. Kivshar, Phys. Rev. **E 53**, 1940 (1996)

University of Cape Town

[217] D.E. Pelinovsky and R.H.J. Grimshaw, in *Nonlinear Instability Analysis* (eds. L. Debnath and S. Choudhury). (Advances in Fluid Mechanics, Computational Mechanics Publications, Southampton, 1997), chapter 8

[218] D.E. Pelinovsky, Yu.S. Kivshar, and V.V. Afanasjev, Phys. Rev. **E 54**, 2015 (1996)

[219] D.E. Pelinovsky, Yu.S. Kivshar and V.V. Afanasjev, Physica **D 116**, 121 (1998)

[220] N.R. Pereira and L. Stenflo, Phys. Fluids, bf 20, 1735 (1977)

[221] J.K. Perring and T.H.R. Skyrme, Nucl. Phys., **31**, 550 (1962)

[222] V.I. Petviashvili and A.M. Sergeev, Sov. Phys. Dokl., **29**, 493 (1984)

[223] L.M. Pismen, Phys. Rev. **A 35**, 1873 (1987)

[224] Kh.I. Pushkarov, D.I. Pushkarov and I.V. Tomov, Opt. Quantum Electron., **11**, 471 (1979)

[225] J. Rauch and J.A. Smoller, Adv. Math., **27**, 12 (1978)

[226] M.J. Rice, A.R. Bishop, J.A. Krumhansl and S.E. Trullinger, Phys. Rev. Lett., **36**, 432 (1976)

[227] P. Richetti and A. Arnéodo, Phys. Lett. **A 109**, 359 (1985)

[228] J. Rinzel and K.J. Maginu, in *Non-equilibrium dynamics in chemical systems*, (eds. C. Vidal and A. Pacault), (Springer-Verlag, Berlin, 1984)

[229] N. Rosen and H.B. Rosenstock, Phys. Rev., **85**, 257 (1952)

[230] S. Sakai, M.R. Samuelsen and O.H. Olsen, Phys. Rev. B 36, 217 1987

[231] R. Scharf, A.R. Bishop, Phys. Rev. **A 43**, 6535 (1991)

[232] A.C. Scott, Bull. Amer. Phys. Soc., **12**, 308 (1967)

[233] A.C. Scott and W.J. Johnson, Appl. Phys. Lett., **14**, 316 (1969)

[234] A.C. Scott, Am. J. Phys., **37**, 52 (1969)

[235] A.C. Scott, Nuovo Cimento, **B 69**, 241 (1970)

University of Cape Town

[236] A.C. Scott, *Nonlinear Science. Emergence and Dynamics of Coherent Structures.* (Oxford Univ. Press, 1999)

[237] I.L. Serpuchenkov and A.V. Ustinov, JETP Lett., **46**, 549 (1987)

[238] H. Segur and M.D. Kruskal, Phys. Rev. Lett. **58**, 747 (1987)

[239] W.L. Shew, H.A. Coy and J.F. Lindner, Am. J. Phys., **67**, 703 (1999)

[240] K. Shimizu and Y.H. Ichikawa, J. Phys. Soc. Japan, **33**, 789 (1972)

[241] R. Simoyi, A. Wolf and H. Swinney, Phys. Rev. Lett. **49**, 245 (1982)

[242] T.H.R. Skyrme, Proc. Roy. Soc., **A 247**, 260 (1958)

[243] T.H.R. Skyrme, Proc. Roy. Soc., **A 262**, 237 (1961)

[244] J. Smoller, *Shock Waves and Reaction-Diffusion Equations*, (Springer- Verlag, New York, 1983)

[245] K.H. Spatschek, H.Pietsch, E.W. Laedke and Th. Eickermann, in Proceedings of the international conference on singular behaviour and nolinear dynamics, Samos, p. 555, (World Scientific, 1988)

[246] K. Stewartson and J.T. Stuart, J. Fluid Mech., **48**, 529 (1971)

[247] S.H. Strogatz, Nature (London) **378**, 444 (1995)

[248] C.S. Su and C.S. Gardner, J. Math. Phys., **10**, 536 (1969)

[249] M. Taki, K.H. Spatschek, J.C. fernandez, R. Grauer and G. Reinisch, Physica **D 40**, 65 (1989)

[250] V.I. Talanov, JETP Lett., **2**, 138 (1965)

[251] S. Tanaka, Proc. Japan Acad., **48**, 466 (1972)

[252] T. Taniuti and H. Washimi, Phys. Rev. Lett., **21**, 209 (1968)

[253] F.D. Tappert and C.M. Varma, Phys. Rev. Lett., **25**, 1108 (1970)

[254] F.D. Tappert and N.J. Zabusky, Phys. Rev. Lett., **27**, 1774 (1971)

[255] F.D. Tappert and C.N. Judice, Phys. Rev. Lett., **29**, 1308 (1972)

University of Cape Town

[256] F.D. Tappert, Phys. Fluids, **15**, 2446 (1972)

[257] G. Terrones, D.W. McLaughlin, E.A. Overman and A.J. Pearlstein, SIAM J. Appl. Math. **50**, 791 (1990)

[258] S.K. Turitsyn, in: *Singularities in fluids, plasmas and optics*, NATO ASI Series, ed. by R. Caflisch (Kluwer Academic Publishers, Dordrecht, 1992)

[259] M. Umeki, J. Phys. Soc. Jpn. **60**, 146 (1991)

[260] M. Umeki, J. Fluid Mech. **227**, 161 (1991)

[261] A.V. Ustinov, B.A. Malomed, S. Sakai, Phys. Rev. **B 57**, 11691 (1998)

[262] H.S.J. van der Zant *et al*, Physica **D 119**, 219 (1998)

[263] L. van Wijngaarden, J. Fluid Mech., **33**, 465 (1968)

[264] C. Vidal and A Pacault (eds.), *Nonlinear phenomena in chemical systems*, (Springer, Berlin, 1981)

[265] C. Vidal and A Pacault (eds.), *Nonequilibrium dynamics in chemical systems*, (Springer, Berlin, 1984)

[266] N.E. Vigdorchik and I.V. Ioffe, Sov. Tech. Phys. Lett., **14**, 479 (1988)

[267] M. Wadati, J. Phys. Soc. Japan, **32**, 1681 (1972)

[268] X. Wang and R. Wei, Phys. Lett. A **192**, 1 (1994)

[269] X. Wang and R. Wei, Phys. Lett. A **227**, 55 (1997)

[270] X. Wang and R. Wei, Phys. Rev. Lett. **78**, 2744 (1997)

[271] H. Washimi and T. Taniuti, Phys. Rev. Lett., **17**, 996 (1966)

[272] J.A.C. Weideman and B.M. Herbst, SIAM J. Numer. Anal. **23**, 485 (1986)

[273] B.J. Welsh, J. Gomatam and A. Burgess, Nature, **304**, 611 (1983)

[274] G.B. Whitham, *Linear and nonlinear waves*, (Wiley, New York, 1974)

[275] G.B. Whitham, Proc. Roy. Soc. Lond., **A 299**, 6 (1967)

University of Cape Town

[276] A.T. Winfree, *When time breaks down*, (Princeton Univ. Press, 1987)

[277] J. Wu, R. Keolian, and I. Rudnick, Phys. Rev. Lett., **52**, 1421 (1984)

[278] N. Yajima and M. Tanaka, Prog. Theor. Phys. Suppl., **94**, 138 (1988)

[279] H. Yamazaki and M. Mino, Prog. Theor. Phys. Suppl., **98**, 400 (1989)

[280] J.R. Yan and Y.P. Mei, Europhys. Lett., **23**, 335 (1993)

[281] C. Yang and Y.R. Shen, Opt. Lett., **9**, 510 (1984)

[282] N.J. Zabusky and M.D. Kruskal, Phys. Rev. Lett., **15**, 240 (1965)

[283] N.J. Zabusky, in *Nonlinear Partial Differential equations*, W. Ames (ed.), (Academic Press, New York), 223 (1967)

[284] N.J. Zabusky, Phys. Rev., **168**, 124 (1968)

[285] N.J. Zabusky, J. Phys. Soc. Japan, **26**, 196 (1969)

[286] N.J. Zabusky, Comput. Phys. Commun., **5**, 1 (1973)

[287] V.E. Zakharov, V.S. L'vov and S.S. Starobinets, Sov. Phys. Uspekhi, **17**, 896 (1975)

[288] V.E. Zakharov and A.B. Shabat, Sov. Phys. JETP, **34**, 62 (1972)

[289] V.E. Zakharov, S.L. Musher and A.M. Rubenchik, Phys. Rep., **129**, 285 (1985)

[290] A. Zhabotinski, Dokl. Akad. Nauk SSSR, **157**, 701 (1964)

[291] F. Zhang, Phys. Rev. **E 58**, 2558 (1998)

[292] A.K. Zvezdin, JETP Lett., **29**, 553 (1979)

[293] V.S. Zykov, *Modelling of wave processes in excitable media*, (in Russian), (Nauka, Moscow 1984)

University of Cape Town

University of Cape Town